



**SYNTHESIS AND CHARACTERIZATION OF MESO-
TETRAPHENYLPORPHYRIN DERIVATIVES AND
THEIR COPPER(II) COMPLEXES**

BY

MR. TOSSAPON PHROMSATIT

**A THESIS SUBMITTED IN PARTIAL FULFILLMENT OF
THE REQUIREMENTS FOR THE DEGREE OF
MASTER OF SCIENCE (CHEMISTRY)
DEPARTMENT OF CHEMISTRY
FACULTY OF SCIENCE AND THEHNOLOGY
THAMMASAT UNIVERSITY
ACADEMIC YEAR 2015
COPYRIGHT OF THAMMASAT UNIVERSITY**

**SYNTHESIS AND CHARACTERIZATION OF MESO-
TETRAPHENYLPORPHYRIN DERIVATIVES AND
THEIR COPPER(II) COMPLEXES**

BY

MR. TOSSAPON PHROMSATIT

**A THESIS SUBMITTED IN PARTIAL FULFILLMENT OF THE
REQUIREMENTS FOR THE DEGREE OF
MASTER OF SCIENCE (CHEMISTRY)
DEPARTMENT OF CHEMISTRY
FACULTY OF SCIENCE AND TECHNOLOGY
THAMMASAT UNIVERSITY
ACADEMIC YEAR 2015
COPYRIGHT OF THAMMASAT UNIVERSIT**



THAMMASAT UNIVERSITY
FACULTY OF SCIENCE AND TECHNOLOGY

THESIS

BY

MR. TOSSAPON PHROMSATIT

ENTITLED

SYNTHESIS AND CHARACTERIZATION OF
MESO-TETRAPHENYLPORPHYRIN DERIVATIVES AND
THEIR COPPER(II) COMPLEXES

was approved as partial fulfillment of the requirements for
the degree of master of science (chemistry)

on July 4 , 2016

Chairman



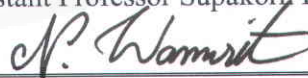
(Assistant Professor Kittipong Chainok, Ph.D.)

Member and Advisor



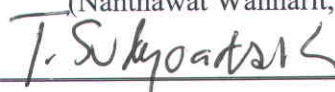
(Assistant Professor Supakorn Boonyuen, Ph.D.)

Member and Co-advisor



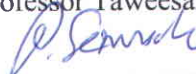
(Nanthawat Wannarit, Ph.D.)

Member



(Assistant Professor Taweesak Sudyoadsuk, Ph.D.)

Dean



(Associate Professor Pakorn Sermsuk)

Thesis Title	SYNTHESIS AND CHARACTERIZATION OF MESO-TETRAPHENYLPORPHYRIN DERIVATIVES AND THEIR COPPER(II) COMPLEXES
Author	Mr. Tossapon Phromsatit
Degree	Master Degree
Major Field/Faculty/University	Chemistry Science and Technology Thammasat University
Thesis Advisor	Assistant Professor Supakorn Boonyuen, Ph.D.
Thesis Co-Advisor	Nanthawat Wannarit, Ph.D.
Academic Years	2015

ABSTRACT

Porphyrins play a vital role in biological systems. Porphyrins and their metal complexes are used in many applications including catalyst, dye-sensitized solar cell, photo dynamic therapy, due to their outstanding properties such as high chemical and thermal stability, strong absorption in visible region, and flexible architectural modification. Moreover, the β -functionalization of *meso*-tetraphenylporphyrin is of great interest since the electronic properties of the porphyrin macrocycle can be altered by small change in the substituents. The β -nitration of the porphyrin ring is of special interest since the nitro group are versatile and can converted into several other functional group.

This study focus on the process of synthesis and properties of *meso*-aryl long chain porphyrin and their metal complexes. The *meso*-aryl long chain porphyrin and their derivative were synthesized by Alder-Longo method between the long chain alkyl substituents aldehyde and pyrrole. The long chain alkyl aldehyde substituents derivatives were synthesized by refluxing 4-hydroxybenzaldehyde with bromoalkane and K_2CO_3 in propionic acid. Then, the *meso*-aryl long chain porphyrin, including Tetraphenylporphyrin (TPP), Tetrakis(4-methoxyphenyl) porphyrin (TOMPP), Tetrakis(4-butyloxyphenyl)porphyrin (TOBPP), Tetrakis(4-octyloxyphenyl)porphyrin

(TOOPP), and Tetrakis(4-decyloxyphenyl)porphyrin (TODPP) were prepared. The copper (II) porphyrin complexes have been synthesized by refluxing the *meso*-alkyl long chain porphyrin with copper acetate in DMF. The results provide the following products: CuTPP, CuTOMPP, CuTOBPP, CuTOOPP, and CuTODPP, respectively. Finally, The β -nitro substituted porphyrin were prepared *via* nitration reaction of copper porphyrin complexes with $\text{Cu}(\text{NO}_3)_2$ and acetic anhydride in chloroform. The CuTPP- NO_2 , CuTOMPP- NO_2 , CuTOBPP- NO_2 , CuTOOPP- NO_2 , and CuTODPP- NO_2 were obtained, respectively. The structure of all synthesized compounds were confirmed by ^1H NMR ^{13}C NMR UV-Vis, fluorescence, FT-IR spectroscopy, CHN elemental analysis, and mass spectrometry. The characterization shows that nitro group is attached on to a β -pyrrolic position of porphyrin. The thermal stability of all complexes were studied by thermal gravimetric analysis. The all complexes were also tested for antibacterial activity using disc diffusion technique. The all synthesized compounds were found to be effective for the inhibition of bacterial growth. Furthermore, the CuTPP- NO_2 was fabricated as film for the detection of alcohol vapours. The sensing properties was investigated by using “electronic nose (e-nose)”. The Principle Component Analysis (PCA) usually chosen for presenting the patterns observed from e-nose. Thus the result confirm that the CuTPP- NO_2 has the capability of performing as an alcohol sensor.

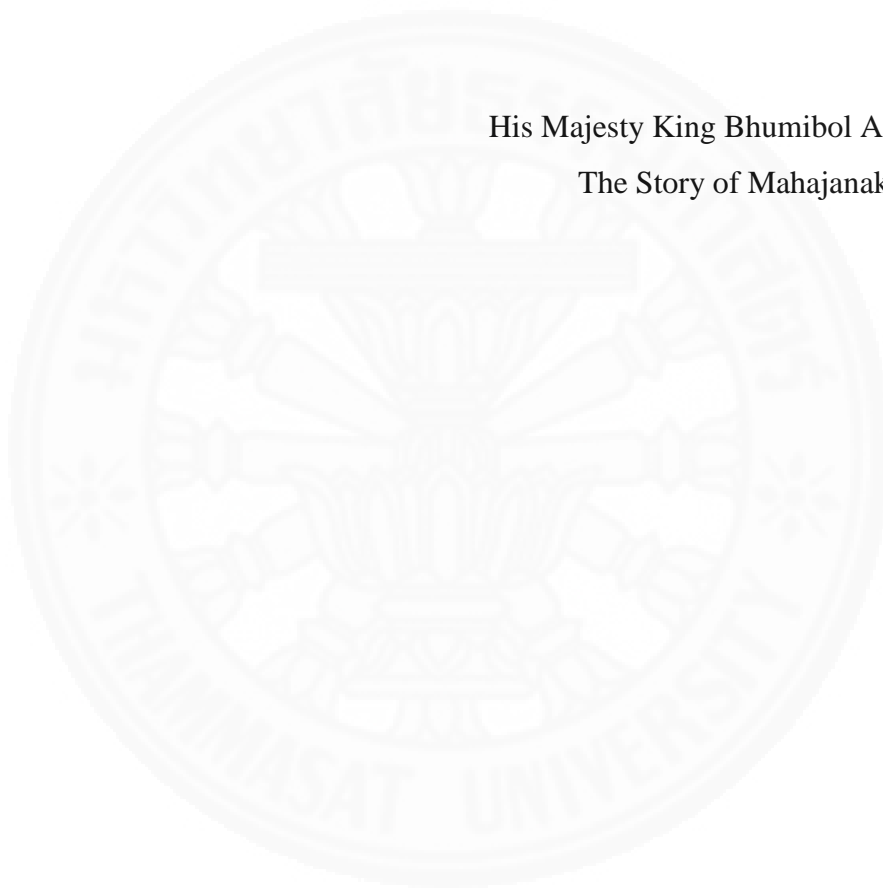
Keywords: Porphyrin long chain, β -Nitro substituted porphyrin, Gases sensor

At this point, the goddess addressed the Great Being with this staza :

“Any enterprise that is not achieved through perseverance, is fruitless; obstacles will occur. When any enterprise undertaken with such misdirected effort result in Death showing his face, what is the use of such enterprise and misdirected effort?”

His Majesty King Bhumibol Adulyadej

The Story of Mahajanaka



ACKNOWLEDGEMENTS

First and foremost, I would like to express my gratitude to my supervisor, Asst. Prof. Dr. Supakorn Boonyuen for his continued support, guidance, polish, and encouragement during the research study and the preparation of this thesis. For their generous assistance in this research, I would like to thank Asst. Prof. Dr. Kittipong Chainok, Dr. Nanthawat Wannarit and Asst. Prof. Dr. Taweesak Sudyoasuk for suggestion along with the technical staffs at Thammasat and Chulalongkorn Universities. I would like to thank Asst. Prof. Dr. Pariya Na Nakron for her suggestion and supported for studied the biological activity. I would to thank Dr. Sumana Kladsomboon for opportunity to test the gas sensing application. My thanks also to my scholarship, science achievement scholarship of Thailand for financial support, Faculty of Science and Technology, Thammasat University, for instruments.

I wish to thank all of my friends, all of my research group lab C404 member for helpful and encourage during the preparation this thesis. I would be thankful to my parents for love and support. I couldn't have done it without all of you, thank you. Finally, the authors acknowledge the Department of Chemistry, Faculty of science and Technology, Thammasat University.

Mr. Tossapon Phromsatit

TABLE OF CONTENTS

	Page
ABSTRACT	(1)
ACKNOWLEDGEMENTS	(4)
LIST OF TABLES	(8)
LIST OF FIGURES	(9)
LIST OF ABBREVIATIONS	(13)
CHAPTER 1 INTRODUCTION	1
1.1 Overview of porphyrin and metalloporphyrin	1
1.2 Natural porphyrin	3
1.3 Synthetic porphyrin	5
1.4 Application of porphyrin	6
1.5 Research objective	7
1.6 Scope and limitations of study	8
1.7 Expected results	9
CHAPTER 2 REVIEW OF LITERATURE	10
2.1 Synthesis of porphyrins and metal complexes	10
2.2 Synthesis of porphyrins long chain and metal complexes	11
2.3 Synthesis of β -functionalize porphyrins and metal complexes	24
2.4 Application of porphyrin and metal complexes	27
2.5 Gas sensing application	31

CHAPTER 3 RESEARCH METHODOLOGY	34
3.1 Materials	34
3.1.1 Reagents	34
3.1.2 Apparatus	35
3.1.2.1 NMR spectroscopy	35
3.1.2.2 FT-IR spectroscopy	35
3.1.2.3 Mass spectroscopy	35
3.1.2.4 The elemental analysis	35
3.1.2.5 Absorption and fluorescence emission spectroscopy	36
3.1.2.6 Thermal analysis	36
3.2 Methods	36
3.2.1 Synthesis of alkyloxybenzaldehydes	36
3.2.2 Synthesis of free base porphyrin	38
3.2.3 Synthesis of copper(II) porphyrin	40
3.2.4 Synthesis of β -nitro substituted porphyrin	42
3.2.5 Biological activity	44
3.2.6 Gases sensing application	44
CHAPTER 4 RESULTS AND DISCUSSION	46
4.1 Aldehyde synthesis and characterization	46
4.1.1 Mass spectrometry	47
4.1.2 NMR spectroscopy	49
4.1.3 Infrared spectroscopy	52
4.2 Porphyrins, copper(II) porphyrin, and β -nitro substituted porphyrin synthesized and characterization	54
4.2.1 CHN elemental analysis	61
4.2.2 Mass spectrometry	61
4.2.3 NMR spectroscopy	63

	(7)
4.2.4 Infrared spectroscopy	67
4.2.5 UV-vis spectroscopy	70
4.2.6 Fluorescence spectroscopy	73
4.2.7 Thermalgravimetric analysis (TGA)	75
4.2.8 Biological activity	78
4.2.9 Gases sensing application	81
CHAPTER 5 CONCLUSIONS AND RECOMMENDATIONS	84
REFERENCES	86
APPENDICES	
APPENDIX A	96
APPENDIX B	102
APPENDIX C	108
APPENDIX D	112
APPENDIX E	120
APPENDIX F	128
BIOGRAPHY	135

LIST OF TABLES

Tables	Page
1 The photovoltaic characteristics of cell using the zinc porphyrins sensitizers	27
2 Characteristic data of aldehydes 1-3	46
3 ¹ H and ¹³ C NMR spectroscopic data for aldehydes 1-3	51
4 The IR data of aldehydes 1-3	53
5 The characteristic data for free base porphyrins, copper(II) porphyrin, and β -nitro substituted porphyrin	60
6 ¹ H and ¹³ C NMR spectroscopic data for free base porphyrins	66
7 The IR data of free base porphyrins	68
8 The absorption data of all compounds	72
9 The absorption-emission wavelength and the estimated energy gap of free base porphyrins in dichloromethane	74
10 Temperatures of decomposition of free base porphyrins, copper(II) porphyrins, and β -nitro substituted porphyrin complexes	76
11 Antibacterial screening data for the synthesized porphyrins 4 – 18	79
12 The MIC and MBC value of copper(II) porphyrin complexes 9 – 13	81

LIST OF FIGURES

Figures	Page
1 Structure of porphyrin and the IUPAC numbering system.	1
2 Delocalized 18 π -electron conjugation pathways of the porphyrin ring system.	1
3 Types of porphyrins: (a) <i>meso</i> -substituted porphyrin and (b) β -substituted porphyrin.	2
4 Structure of heme	3
5 Structure of chlorophyll	4
6 Structure of Vitamin B12	4
7 Synthesis of TPP using Rothemund's method	10
8 Synthesis of TPP using Alder-Longo's method	10
9 Synthesis of TPP using Lindsey's method	11
10 The x-ray structure of complexes 1a and 2a	12
11 Structure of <i>meso</i> -substituted porphyrin	13
12 Structure of tetrakis(2-hydroxy-5-nitrophenyl)porphyrin	14
13 Synthesis of <i>meso</i> -aryl-substituted porphyrins 19a – 22a	14
14 Synthesis of tetrakis-[4-(hexadecyloxy)phenyl]porphyrin and its copper(II) complex	15
15 The synthetic route of the palladium porphyrin complex	16
16 The structure of novel porphyrin 23a and 24a	16
17 The structure of <i>meso</i> -tetra (4-alkylamidophenyl)porphyrin	17
18 <i>meso</i> -nitration of tetraphenylporphyrin 25a – 29a	17
19 Structure of mixed <i>meso</i> -substituted porphyrin	18
20 The structures of the silver porphyrin complex	18
21 The synthetic route of NCPS	19
22 X-ray structure of <i>meso</i> -tetrakis (2,6-dimethyl-4-triflyloxyphenyl) porphyrin	20

LIST OF FIGURES (CONT.)

Figures	Page
23 Preparations of tetra (Schiff-base substituted phenyl) porphyrins and their complexes	20
24 Structure of carboxylic porphyrin 41a and 42a	22
25 The synthetic route of TANPH2 43a , TANPZn 44a and TANPCu 45a	23
26 The structure of porphyrin 46a , 47a , and zinc complex 48a	24
27 Structure of TPPNO ₂ , TPPβNO ₂ , and its metal complexes	25
28 The amination of porphyrin complexes	26
29 Structure of porphyrin sensitizer	27
30 Structure of PZn-BIA-COOH, and PZn-COOH	28
31 Structure of fluorinated porphyrin, 69a and its metal complexes 70a – 74a	29
32 Structure of investigated compound	30
33 The structure of 5,10,15,20-tetrakis[3,4-bis(2ethylhexyloxy)phenyl] 21H,23H-porphine (EHO) and p-tert-butylcalix[8]arene (C8A)	31
34 Schematic view of the e-nose measuring system	32
35 The structure of 5, 10, 15, 20-tetrakis(4-aminophenyl)porphyrin zinc	33
36 Synthesis of alkyloxybenzaldehydes	36
37 Synthesis of porphyrin	38
38 Synthesis of copper(II)porphyrin	40
39 Synthesis of β-nitro substituted porphyrin	42
40a The modified UV-Vis spectrophotometer “electronic nose”	45
40b the diagram of the electronic nose system set up	45
41 Synthesis of butyloxybenzaldehyde 1	46
42 The structure of aldehyde 1 – 3	47
43 Mass spectrum of butyloxybenzaldehyde 1	48
44 ¹ H NMR spectrum of butyloxybenzaldehyde 1	49
45 ¹³ C NMR spectrum of butyloxybenzaldehyde 1	50
46 IR spectrum of butyloxybenzaldehyde 1	53
47 Synthesis of tetrakis(4-butyloxyphenyl)phenylporphyrin (TOBPP 6)	54

LIST OF FIGURES (CONT.)

Figures	Page
48 The structure of TPP 4 , TOMPP 5 , TOBPP 6 , TOOPP 7 , and TODPP 8	55
49 Synthesis of Tetrakis(4-butyloxyphenyl)phenylporphyrinatocopper(II) (CuTOBPP 11)	56
50 The structure of CuTPP 9 , CuTOMPP 10 , CuTOBPP 11 , CuTOOPP 12 , and CuTODPP 13	57
51 The synthesis of 2-nitro-tetrakis(4-butyloxyphenyl) phenylporphyrinatocopper(II) (CuTOBPP-NO ₂ 16)	58
52 The structure of CuTPP-NO ₂ 14 , CuTOMPP-NO ₂ 15 , CuTOBPP-NO ₂ 16 , CuTOOPP-NO ₂ 17 , and CuTODPP-NO ₂ 18	59
53 The mass spectrum of TOMPP 5	61
54 The mass spectrum of CuTOMPP 10	62
55 The mass spectrum of CuTOMPP-NO ₂ 15	63
56 The ¹ H NMR spectrum of TOBPP 6	64
57 The ¹³ C NMR spectrum of TOBPP 6	65
58 IR spectrum of TOMPP 5 , CuTOMPP 10 , and CuTOMPP-NO ₂ 15	69
59 UV-Vis absorption spectra of all free base porphyrin in CH ₂ Cl ₂	70
60 The UV-Vis absorption spectra of TOMPP 5 , CuTOMPP 10 and CuTOMPPNO ₂ 15 in CH ₂ Cl ₂	71
61 The emission spectra of free base ligands in dichloromethane	73
62 Thermogravimetric analysis (TGA) curves of TOBPP 6 , CuTOBPP 11 , and CuTOBPP-NO ₂ 16	75
63 Correlation between decomposition temperatures with number of carbon in alkyl chain porphyrins	77
64 Comparison of the antimicrobial activities of the synthesized porphyrins 4 – 18	80
65 SEM images of a cross section of CuTPP-NO ₂ film (×30,000), and b surface of CuTPP-NO ₂ film (×10,000)	81
66 The CuTPP-NO ₂ film	82

LIST OF FIGURES (cont.)

- 67 The dynamic responses of CuTPP-NO₂ film of UV-vis spectra
under exposure to methanol 82
- 68 PCA plot of the optical response of the CuTPP-NO₂ film to alcohol:
(a) methanol (100%), and ethanol (100%), and
(b) methanol (100%), ethanol (100%), and methanol/ethanol (1:1) 83



LIST OF ABBREVIATIONS

Symbols/Abbreviations	Terms
1a	<i>meso</i> -Tetra(<i>p</i> -cyanophenyl)porphyrinato-mercury(II)
2a	Chloro(<i>N</i> -methyl- <i>meso</i> tetraphenylporphyrinato)-mercury(II)
3a	Acetate-[<i>meso</i> tetra(<i>ρ</i> -chlorophenyl)porphyrinato]thallium(III)
4a	Acetato-[<i>meso</i> -tetra(<i>ρ</i> -chlorophenyl)porphyrinato]indium(III)
5a	Acetate-[<i>meso</i> -tetra(<i>ρ</i> -bromophenyl)porphyrinato]indium(III)
6a	Mesotetraphenylporphyrin
7a	Mononitroporphyrin
8a	di-nitrophenylporphyrins
9a	di-nitrophenylporphyrins
10a	5,10,15-Tris(4-nitrophenyl)-20-phenylporphyrin
11a	5-(4-Aminophenyl)-10,15,20-triphenylporphyrin
12a	5,15-Bis(4-aminophenyl)-10,20-diphenylporphyrin
13a	5,10-bis(4-aminophenyl)-15,20-diphenylporphyrin
14a	5,10,15-Tris(4-aminophenyl)-20-phenylporphyrin
15a	4-Tetradecyloxybenzaldehyde
16a	4-Tetradecanoyloxybenzaldehyde
17a	<i>meso</i> -Tetradecyloxyphenyl)dipyrromethane
18a	<i>meso</i> -Tetradecanoyloxyphenyl)dipyrromethane
19a	5,10,15,20-Tetra(4-tetradecyloxyphenyl)porphyrin

20a	5,10,15,20-Tetra(4-tetradecanoyloxyphenyl)porphyrin
21a	5,15-Bis(4-tetradecyloxyphenyl)-10,20-diphenylporphyrin
22a	5,15-Bis(4-tetradecyloxyphenyl)-10,20-diphenylporphyrin
23a	5,10,15,20-Tetra[4-(3-phenoxy)-propoxy]phenyl porphyrin
24a	5,10,15,20-Tetra[2-(3-phenoxy)-propoxy]phenyl porphyrin
25a	Mononitroporphyrin
26a	di-nitrophenylporphyrins
27a	di-nitrophenylporphyrins
28a	tri-nitrophenylporphyrins
29a	5,10,15,20-tetrakis(4-nitrophenyl)-21H,23H-porphyrin
30a	<i>meso</i> -tetra(p-benzylideneamino) phenyl porphyrin (TBDAPP)
31a	<i>meso</i> -Tetra[p-(p-benzylideneamino)] phenyl porphyrin
32a	<i>meso</i> -tetra[p-(p-carboxy benzylideneamino)] phenyl porphyrin
33a	<i>meso</i> -tetra[p-(p-methoxy benzylideneamino)] phenyl porphyrin
34a	<i>meso</i> -tetra(p-benzylideneamino) phenyl porphyrinatozinc(II)
35a	<i>meso</i> -Tetra[p-(p-benzylideneamino)] phenyl porphyrinatozinc(II)
36a	<i>meso</i> -tetra[p-(p-carboxy benzylideneamino)] phenyl porphyrinatozinc(II)

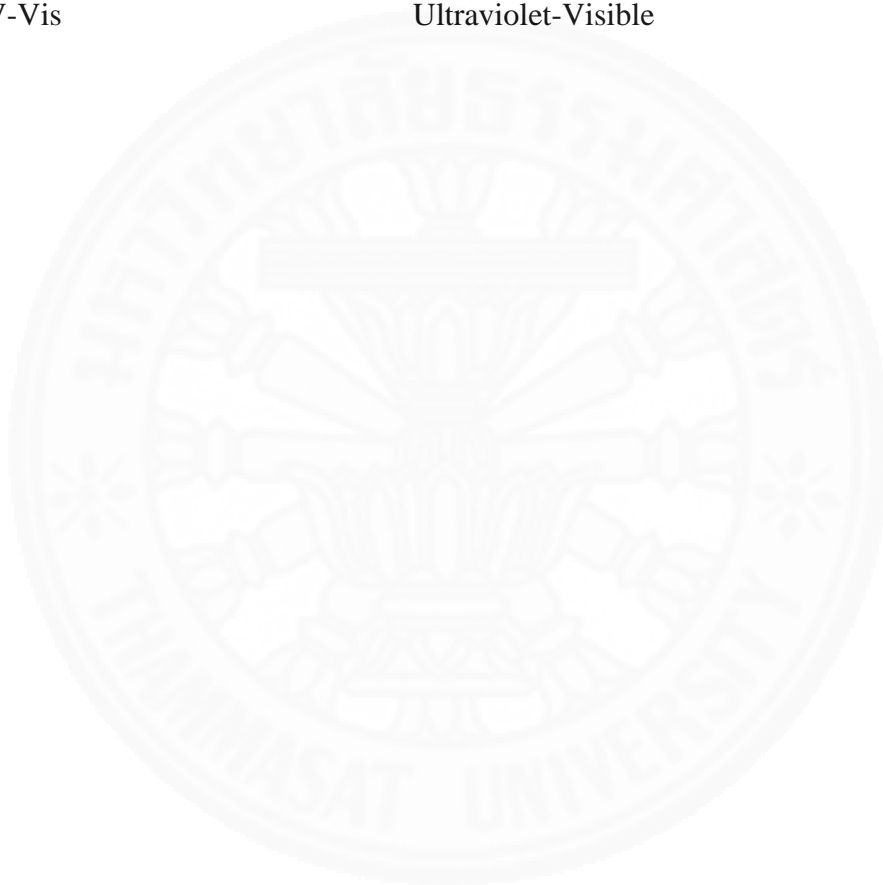
37a	<i>meso</i> -tetra[p-(p-methoxy benzylideneamino)] phenyl porphyrinatozinc(II)
38a	4-chlorobenzoate-(5,10,15,20- <i>meso</i> - tetraphenylporphyrinato)-oxo-tungstan(V)
39a	hydroxo-(5,10,15,20- <i>meso</i> - tetraphenylporphyrinato)-oxo-tungstan(V)
40a	methoxo-(5,10,15,20- <i>meso</i> - tetraphenylporphyrinato)-oxo-tungstan(V)
41a	-
42a	-
43a	porphyrin–naphthalimide pentamer
44a	TANPZn
45a	TANPCu
46a	5,10,15,20-tetrakis(4-ferrocenylethynylphenyl)- porphyrin
47a	5,10,15,20-tetrakis(3-ferrocenylethynylphenyl) porphyrin
48a	(5,10,15,20-tetrakis(3- ferrocenylethynylphenyl)porphyrinatozinc(II))
49a	nickel(II) 2,7,8,13-tetraethyl-3,12- dimethylporphyrin
50a	<i>meso</i> -nitroporphyrin
51a	β -nitroporphyrin
52a	TPPNO ₂
53a	TPP β NO ₂
54a	CuTPPNO ₂
55a	CuTPP β NO ₂
56a	2-amino-3-nitro-substituted
57a	[2-amino-3-nitro-5,10,15,20-tetrakis(3- fluorophenyl)porphyrinato]copper(II)

58a	[2-amino-3-nitro-5,10,15,20-tetrakis(3-chlorophenyl)porphyrinato]copper(II)
59a	[2-amino-3-nitro-5,10,15,20-tetrakis(3-methylphenyl)porphyrinato]copper(II)
60a	[2-amino-3-nitro-5,10,15,20-tetrakis(3-methoxyphenyl)porphyrinato]copper(II)
61a	-
62a	-
63a	-
64a	-
65a	-
66a	-
67a	5-(4-Carboxyl) phenyl-10,15,20-tris(3,4,5-trimethoxyphenyl)porphyrin
68a	5-[p-(4-Carboxyl benzyl idene amino)] phenyl-10,15,20-tris(3,4,5-trimethoxyphenyl)porphyrin zinc
69a	5,10,15,20-tetrakis-(4-trifluoromethylphenyl)-porphyrin
70a	5,10,15,20-tetrakis-(4-trifluoromethylphenyl)-porphyrinatoiron(II)
71a	5,10,15,20-tetrakis-(4-trifluoromethylphenyl)-porphyrinatonickele(II)
72a	5,10,15,20-tetrakis-(4-trifluoromethylphenyl)-porphyrinatocopper(II)
73a	5,10,15,20-tetrakis-(4-trifluoromethylphenyl)-porphyrinatozinc(II)
74a	5,10,15,20-tetrakis-(4-trifluoromethylphenyl)-porphyrinatoplatinum(II)
75a	Tetrakis-(3-hydroxyphenyl)porphyrin

- 76a 5-(4-Hexadecyloxyphenyl)-10,15,20-tris(3-hydroxyphenyl)porphyrine
- 77a Tetrakis-5,10,15,20-(4-hydroxyphenyl)-porphyrine
- 78a Tetrakis-5,10,15,20-(4-hydroxy-3-methoxyphenyl)porphyrine
- 79a Tetrakis-(4-hydroxy-3,5-dimethoxyphenylene)porphyrine
- 80a 5-(4-Hexadecyloxyphenyl)-10,15,20-tris(4-hydroxyphenyl)porphyrine
- 81a 5-(3-Hexadecyloxyphenyl)-10,15,20-tris(3-hydroxyphenyl)porphyrine
- 82a [5-(4-Oxyphenyl)-10,15,20-tris(4-hydroxyphenyl)porphyrine]palmitate
- 83a [5-(3-Oxyphenyl)-10,15,20-tris(3-hydroxyphenyl)porphyrine]palmitate
- 84a 5-(4-Hexadecyloxy-3-methoxyphenyl)-10,15,20-tris(4-hydroxy-3-methoxyphenyl)-porphyrine
- 85a [5-(3-Methoxy-4-oxyphenyl)-10,15,20-tris(4-hydroxy-3-methoxyphenyl)porphyrine]palmitate
- 86a 5-(4-Hexadecyloxy-3,5-dimethoxyphenyl)-10,15,20-tris(4-hydroxy-3,5-dimethoxyphenyl)-porphyrine
- 87a [5-(3,5-Dimethoxy-4-oxyphenyl)-10,15,20-tris(4-hydroxy-3,5-dimethoxyphenyl)porphyrine]palmitate
- 88a 5-(4-Acetylamino-phenyl)-10,15,20-tris(4-methoxyphenyl)porphyrine
- 89a 5-(4-Amino-phenyl)-10,15,20-tris(4-methoxyphenyl)porphyrine

90a	N-[5-(para-phenylene)-10,15,20-tris(4-methoxyphenyl)porphyrine] palmitylamide
91a	N-[5-(para-phenylene)-10,15,20-tris(4-hydroxyphenyl)porphyrine] palmitylamide
¹ H NMR	Proton Nuclear Magnetic Resonance Spectroscopy
¹³ C NMR	Carbon Nuclear Magnetic Resonance Spectroscopy
Δ	Chemical shift
Calcd	Calculated
CuTOBPP	Tetrakis(4-butyloxyphenyl)phenylporphyrinatocopper(II)
CuTODPP	Tetrakis(4-decyloxyphenyl)phenylporphyrinatocopper(II)
CuTOMPP	Tetrakis(4-methoxyphenyl)phenylporphyrinatocopper(II)
CuTOOPP	Tetrakis(4-octyloxyphenyl)phenylporphyrinatocopper(II)
CuTPP	Tetraphenylporphyrinatocopper(II)
CuTOBPP-NO ₂	2-nitro-tetrakis(4-butyloxyphenyl)phenylporphyrinatocopper(II)
CuTODPP-NO ₂	2-nitro-tetrakis(4-decyloxyphenyl)phenylporphyrinatocopper(II)
CuTOMPP-NO ₂	2-nitro-tetrakis(4-methoxyphenyl)phenylporphyrinatocopper(II)
CuTOOPP-NO ₂	2-nitro-tetrakis(4-octyloxyphenyl)phenylporphyrinatocopper(II)
CuTPP-NO ₂	2-nitro-tetraphenylporphyrinatocopper(II)
E-nose	Electronic nose
ESI-MS	Electrospray Ionization Mass Spectrometry
IR	Infrared

K	Kelvin
TGA	Thermogravimetric Analysis
TOBPP	Tetrakis(4-butyloxyphenyl)porphyrin
THPP	Tetrakis(4-hydroxyphenyl)porphyrin
TODPP	Tetrakis(4-decyloxyphenyl)porphyrin
TOMPP	Tetrakis(4-methoxyphenyl)porphyrin
TOOPP	Tetrakis(4-octyloxyphenyl)porphyrin
UV-Vis	Ultraviolet-Visible

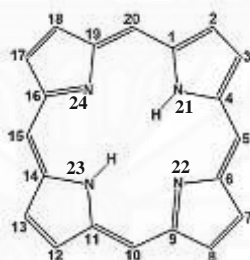


CHAPTER 1

INTRODUCTION

1.1 Overview of porphyrin and metalloporphyrin

Porphyrin are a group of heterocyclic macrocyclic organic compound, composed of four modified pyrrole subunits interconnected at their carbon atom via methane bridges (=CH-). The word porphyrin originated from the Greek word porphura, which was represented the purple color [1]. The basic porphyrin is call porphin, the structure of porphin is show in **Fig. 1**, and the substituted porphins are call porphyrin. The compound of porphyrin is a dark purple solid that dissolves in non-polar solvent.



α -positions (1, 4, 6, 9, 11, 14, 16, 19)

β -positions (2, 3, 7, 8, 12, 13, 17, 18)

meso-positions (5, 10, 15, 20)

Fig. 1 Structure of porphyrin and the IUPAC numbering system [2].

The porphyrin ring is aromatic, as it is planar and obeys Huckel's Rule [$4n + 2$]. **Fig. 2** shows the porphyrin macrocycle with 22- π conjugated electron, 18- π electron of which are in any one delocalized pathway, as a result of the extended conjugation, the HOMO – LUMO gap shrinks and light absorption is seen in the visible region. The visible absorption spectrum shows an intense soret band around 400 nm [3].

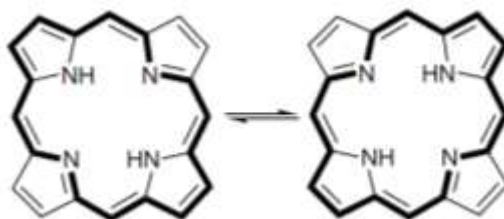


Fig. 2 Delocalized 18 π -electron conjugation pathways of the porphyrin ring system.

Porphyrin are one of the vital chemical units essential for several life processes on the earth. Porphyrin play a vital role in biological system, and their synthesis arouses containing interest in biological, material, and inorganic chemistry [4]. Porphyrin ring provides a vacant site at its center, the acidic character have been process at the NH protons inside the ring of porphyrin and hance can get deprotonated to give porphyrinato ion. These dianion are able to coordinated may result in the distortion of the planar macrocyclic in order to maximize the binding strength towards the metal fragment. Thus metalloporphyrin have been synthesized. The normal coordination geometry around the metal ion in the former species would be square planar. The natural of bonding between a central metal and the porphyrin ligand is found to be originating essentially from the following two type of primary interaction: σ -coordination of nitrogen lone pairs directed towards the metal atom and π -interaction of metal $p\pi$ or $d\pi$ orbital [5].

The structure of a porphyrin exhibits two major points' four *meso*-positions and eight β -positions, that porphyrin can be classified into two main categories base on the pattern of substituents attached to the porphyrin ring namely *meso*-substituted porphyrin and β -substituted porphyrin (**Fig. 3**). The synthetic *meso*-substituted porphyrin offer a great advantage to study the physical and chemical properties of the substituents that may be attached to the periphery. The substituents at *meso*-positions can be readily adjusted utilizing alkyl, aryl, heterocyclic or organometallic group as other porphyrin [6].

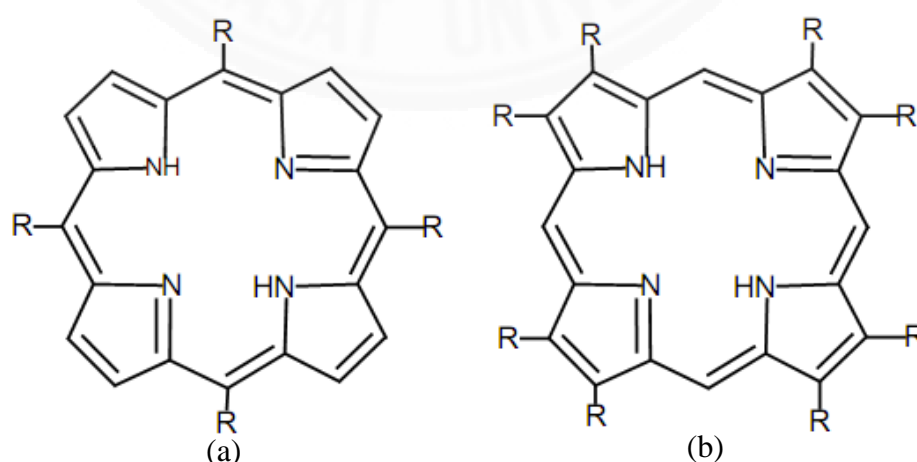


Fig. 3 Types of porphyrins: (a) *meso*-substituted porphyrin and (b) β -substituted porphyrin.

1.2 Natural porphyrin

A large number of natural metalloporphyrin play a vital role in biological system including heme, chlorophyll, vitamin B12, and enzyme etc. There are the most important in biological processes such as respiration, photosynthesis, ion transfer, and other applications in living system.

Heme is a cofactor consisting of a ferrous ion (Fe^{2+}) contained in the center of a porphyrin ring. Hemes are most commonly recognized as components of hemoglobin, the red pigment in blood, but are also found in a number of other biologically important hemoproteins such as myoglobin and cytochrome. The heme is an asymmetric molecule and consist a porphyrin ring and iron atom in central hole (**Fig. 4**). Heme groups contain iron(II) ion molecules, which can reversibly bind to oxygen molecule and transport them to various areas of the body. Hemoglobin and myoglobin are high molecular weight protein systems containing iron(II) porphyrin four unit. They are responsible for oxygen transport and storage in higher animal. Cytochrome are electron transferring protein, containing iron porphyrin too, found in aerobic cell. Some cytochrome found in endoplasmic reticulum, play a role in specialized hydroxylation reaction [7 – 8].

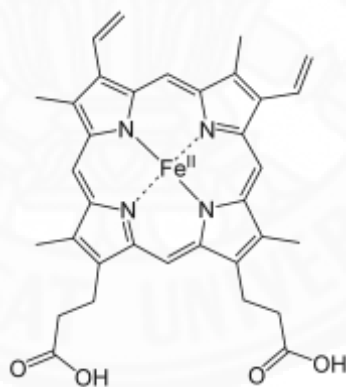


Fig. 4 Structure of heme

Chlorophyll is the green coloring matter of leavers and green stem, and it presence is essential for photosynthesis. The word “chlorophyll” come from two Greek words, ‘chloros’ represent green color, and ‘phyllon’ represent leaf. Chlorophyll is an extremely important biomolecule critical in photosynthesis, which allows plants to absorb energy from light energy. Chlorophyll is a magnesium derivative of porphyrin (**Fig. 5**). The magnesium containing porphyrin is a square planar structure. Attached to the porphyrin is a long chain hydrocarbon, insoluble which interacts with the protein of thylakoids and

serves to hold the molecule in the internal membranes of the chloroplast. All of the chlorophylls absorb light very intensely, particularly at relatively long wavelength regions. The light energy absorbed by a chlorophyll molecule become delocalized and spread throughout the entire electronic structure of the excited molecule [9 – 10].

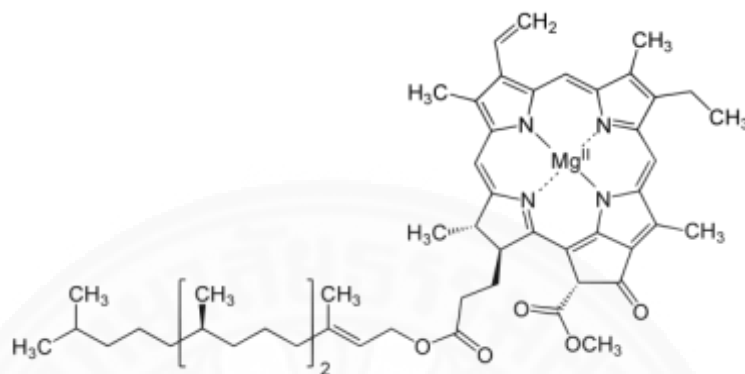


Fig. 5 Structure of chlorophyll

Vitamin B12 or cobalamin is a water soluble vitamin with a key role in the normal functioning of the brain and nervous system, and for the formation of blood. The structure of Vitamin B12 consists of four pyrrole joined on methane bridges from three of these likes and with the two of the pyrrole joined directly. It is similar to a porphyrin, but with one of the bridging methylene groups removed. The structure of vitamin B12 presents a corrin ring with cobalt, positioned right in the center of the structure (**Fig. 6**). Biosynthesis of the basic structure of these vitamin is accomplished only by bacteria and Achaea, but conversion between different forms of the vitamin can be accomplished in the human body [11 – 12].

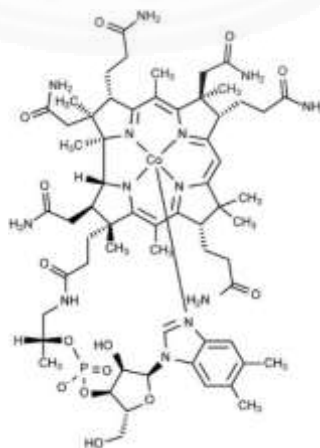


Fig. 6 Structure of Vitamin B12

Enzyme are biological catalysts that govern, initiate and control biological reactivity important for the life process. All known enzyme are proteins, and some contain non-protein moieties termed prosthetic groups that are essential for the main festation of catalytic activities. In several natural enzyme, metalloporphyrins constitute these prosthetic group such as Oxygenases and Peroxidases etc. The most important oxygenase is cytochrome P-450 found in the microsomes of liver cell [13].

1.3 Synthetic porphyrin

In the earlier part of this century, synthetic studies of porphyrin have been dramatically developed and modified with in the synthesis of a large class of pyrrole. The initial works of synthesis porphyrin began in 1935 when Rotemund first developed a method for the synthesis of *meso*-tetramethylporphyrin from heating acetaldehyde and pyrrole in methanol at 95°C [14]. In present, there are several routes that that can be followed to get the *meso*-substituted porphyrin. As mentioned, porphyrin have been group in two categories by the substituent. The *meso*-substituted have been more interested because the *meso*-substituted porphyrins have wide applications such as catalysis, electron transfer, photodynamic therapy, and molecular recognition etc. Although, *meso*-substituted porphyrin are not naturally occurring compound they have provide chemists and other scientist with a multitude of applications and fundamental studies. On the other hand the β -substituted porphyrin closely resemble naturally occurring porphyrin, but natural porphyrins are asymmetric and therefore cannot be prepared via simple method [15]. Since Rothmund reported his work, a series of both symmetric and asymmetric porphyrin has been dramatically studies. Symmetrical porphyrins are more easily synthesized than an asymmetrical porphyrins. Their synthesis is based on condensation of pyrrol and aldehyde with various reaction conditions. On the other hand, the asymmetrical porphyrins are much less synthetically accessible and regarded more processes. The structure of porphyrin contains 22 conjugated π -electron, but 18 π -electron required for conjugated aromatic network. So, porphyrin can undergo addition reaction without loss the aromatic properties. The variety of functionalized porphyrin, that continue to find multiple application in biology, medicine, and materials. The *meso*-position are the most electronically

reactive position of porphyrin, and generally preferential sites for substitution and addition [16]. Although, the β -positions are the most satirically accessible, but there can also undergo the same reaction. One of interesting reaction is “nitration” of porphyrin [17]. The nitration of porphyrins can be achieved with nitric acid, nitrate salt (usually of copper, zinc, and silver), with N_2O_4 , or nitrite ion via the corresponding porphyrin π -cation radicals. *meso*- and β - nitroporphyrins undergo *ipso*- substitution of the nitro group to produce a variety of functionalized porphyrin.

1.4 Application of porphyrins

In the past decade, porphyrin has attracted great research attention as versatile synthetic base for various material. Porphyrin have been widely studied due to their spectroscopy, electrochemical luminescence properties and their biological activity. Porphyrin and their metal complexes were used in many applications, such as catalysis, dye-sensitized solar cell (DSSC), molecular sensor, anticancer, antimicrobial agent, and applications for photosensitizing drugs in photodynamic therapy (PDT) etc. For the applications of porphyrin and their metal complexes, the DSSC have been interested for a past few years. Porphyrin have been intensively studied as artificial light harvesting system over years, because they usually exhibit strong absorption in UV and visible regions with high absorption coefficients. For the light harvested application, the dye must be considered the geometric structure, molecular orbital energy, absorption profile, and aggregation. The photophysical properties were affected when the molecular orbital have been disturbed by substitution with electron-withdrawing or electron-donating group at *meso*- or β - position of the porphyrin ring. Among the novel developed antibacterial agents, porphyrin complexes have been attracted much. The several report shown that the porphyrin analogous can take cytotoxic singlet oxygen directly in tumor cells (causing cell death when irradiate, photosensitization). The photosensitization can represent a useful approach to kill microbes due to their ability to act as photosensitizers when irradiated by visible light. Photodynamic therapy is emerging as an important treatment for many diseases. Many applications of PDT involve killing undesirable disease-causing cells such as malignant cancer cells or pathogenic microorganisms [18]. PDT is also used to destroy unwanted tissues such as

tumors, new blood vessels, and atherosclerotic plaques. In addition, the several report said that the porphyrin analogous can take cytotoxic singlet oxygen directly in tumor cells (causing cell death when irradiate, photosensitization). The photosensitization can represent a useful approach to kill microbes due to their ability to act as photosensitizers when irradiated by visible light [19]. Moreover, porphyrin have been widely investigated because of their photophysical and photochemical properties, which are based on rich π -electron system that make them able to interact with gases [20]. For decades there has been a growing interest in the development of gas sensor with high sensitivity and selectivity. The porphyrin film based can be considered as excellent gas sensing devices at ambient temperature, since the change of electrical conductivity takes place rapidly as a result of the interaction between the surface complexes of porphyrin and the gas molecules detected.

1.5 Research objective

1.5.1 To synthesis and characterized various aldehyde with long chain alkane.

1.5.2 To synthesis and characterized the free base porphyrin with long chain alkane form various aldehyde.

1.5.3 To synthesis and characterized the metalloporphyrin by adding copper ion (Cu^{2+}) in to center of porphyrin ring.

1.5.4. To synthesis and characterized the copper porphyrin with added nitro ($-\text{NO}_2$) group at β -pyrrolic position.

1.5.5. To study and compare the chemical, and physical properties of porphyrin, copper porphyrin, copper porphyrin with nitro group, and their derivative which various techniques.

1.5.6. To study the biological activity of all synthesized porphyrins.

1.5.7. To investigate the gas sensing application of β -nitro substituted porphyrin.

1.6 Scope and limitations of study

1.6.1. The various aldehyde were prepared by refluxing a mixture of 4-hydroxybenzaldehyde with alkyl bromide such as *l*-bromobutane, *l*-bromooctane and *l*-bromodecane.

1.6.2 The long chain porphyrin and its derivatives with different peripheral substitutions ligands by refluxing pyrrole with various aldehyde such as *p*-anisaldehyde, butyloxybenzaldehyde, octyloxybenzaldehyde and decyloxybenzaldehyde were synthesized by a modified Adler-Longo method due to its easy procedure with medium yields.

1.6.3 The metalloporphyrin with various porphyrin were prepared by adding copper ion (Cu^{2+}) in long chain free base porphyrin.

1.6.4 The β -nitro substituted porphyrin were prepared by nitration reaction between metalloporphyrin and $\text{Cu}(\text{NO}_3)_2$ in CH_2Cl_2 .

1.6.5 The NMR, IR, mass spectrometry, and elemental analysis technique and were applied to confirm the synthesized structure.

1.6.6 The photochemical properties of the macrocyclic structures with different peripheral substitutions, a group of long chain porphyrins and metalloporphyrins, were characterized by UV-vis, fluorescence spectrophotometer in different solvent. The thermal properties were studied by the thermal gravimetric analysis (TGA).

1.6.7 The biological activity of all compound were tested by using disc diffusion technique.

1.6.8 The gas sensing application were studied by using CuTPP- NO_2 as sensor, and test to detected alcohol vapors (methanol and ethanol) by using electronic nose.

1.7 Expected results

1.7.1. The synthesis and characterization of aldehydes, free base porphyrins, copper(II) porphyrins and β -nitro substituted porphyrin complexes were achieved with good yield by suitable method.

1.7.2 the properties of porphyrins, copper(II) porphyrins, and β -nitro substituted porphyrin complexes can be compared by using UV-Vis spectroscopy, fluorescence spectroscopy, and TGA.

1.7.3 Porphyrins long chain and metal complexes were used to apply in several applications such as coating on ITO glass.

1.7.4 All compounds was found to be effective for the inhibition of bacterial growth.

1.7.5 The CuTPP-NO₂ can be detected, and clearly separated alcohol vapors.

CHAPTER 2

REVIEW OF LITERATURE

2.1 Synthesis of porphyrins and metal complexes

In 1936, the first studied of synthesis *meso*-tetraphenylporphyrins have been reported by Rothemund. This porphyrin was synthesized by using condensation reaction between benzaldehyde and pyrrole under acidic condition. This method were used hardness conditions (high temperature and high concentration) for refluxing 24 hours. Various aldehydes like propionaldehyde, n-butyraldehyde, and α -furaldehyde with pyrrole were utilized to obtain porphyrin by using this method (**Fig.7**). However, this method were obtain low yields [21].

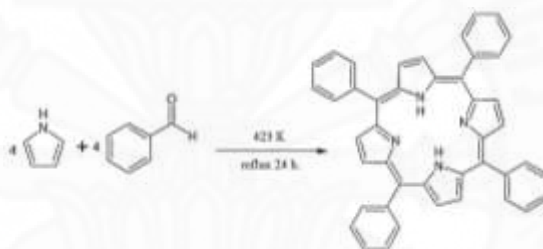


Fig. 7 Synthesis of TPP using Rothemund's method

In 1960, the modification method for synthesized *meso*-substitution porphyrin was reported by Alder and Longo. The synthesis that was achieved by refluxing the mixture of pyrrole and benzaldehyde in propionic acid for 30 minutes under open an atmosphere, as show in **Fig. 8**. The yield from this method was obtained better than previous report. This reaction conditions were relatively mild, which afforded higher yield and gave faster reaction rate, when the current condition was compared with Rothemund conditions [22].

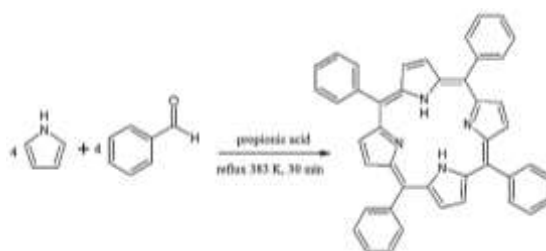


Fig. 8 Synthesis of TPP using Alder-Longo's method

In 1980, Lindsey *et al.* report a new synthetic method that set the standard for *meso*-aryl substituted porphyrin. This method involved a condensation between benzaldehyde and pyrrole. Under this method the synthesis product was obtained after two step reactions, first step is deal with acid catalyzed ($\text{BF}_3\text{-Et}_2\text{O}$ or TFA) condensation to form the intermediate porphyrinogen, followed by the second step, which is the addition of an external oxidant (DDQ or chlorinal) to form the porphyrin (**Fig.9**). This method is producible with typical yield in rang 30 – 40% [23].

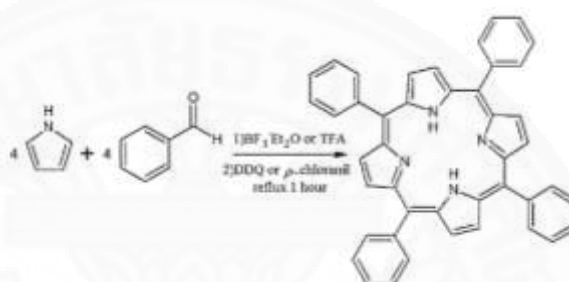


Fig. 9 Synthesis of TPP using Lindsey's method

In 2009, Temelli B, and Unaleroglu C. report the new synthetic route for synthesis 5,10,15,20-tetraphenylporphyrin. These porphyrin was also synthesied in two step. Firstly, the porphyrinogen intermediate were prepared by using metal triflate catalyst with condensation reaction of dipyrrolemethanes and N-tosyl imines. The second reaction is oxidation reaction of porphyrinogen to porphyrin. The convenient availability of these intermidates makes possible to extend this methodology also to the synthesis of tetraphenylporphyrin with difference aryl group [24].

2.2 Synthesis of porphyrins long chain and metal complexes

In 1993, Hermam K.H. and Stefan O. report a very convenient synthetic method for the preparation of alkyl long chains porphyrin. Methylithium (MeLi) or n-butyllithium (n-BuLi) were added in to long chain alcohol in THF solvent for synthesized alkoxide. Then, porphyrin ester was added in the reaction after the alkoxide were completly synthesized. The synthetic products were purified by column

chromatography. Then all compounds were characterized by NMR spectroscopy and mass spectrometry [25]

In 2001, Ming-Cheng W. *et al.* synthesis mercury complexes of *meso*-tetra-(ρ -cyanophenyl) porphyrin (Hg(ρ -(N)₄tpp) **1a** and N-methylporphyrin (Hg(N-Me-tpp)Cl) **2a**, both were prepared by using mercury with Hg(OAc)₂ and HgCl₂ respectively in MeOH. The structure of all compound were characterized by mass, ¹H NMR, ¹³C NMR spectroscopy and UV- Vis spectroscopy. Furthermore, the crystal structure of complexes **1a** and **2a** were observed and shown in **Fig. 10**. Both complexes show P1 space group and triclinic crystal system. [26].

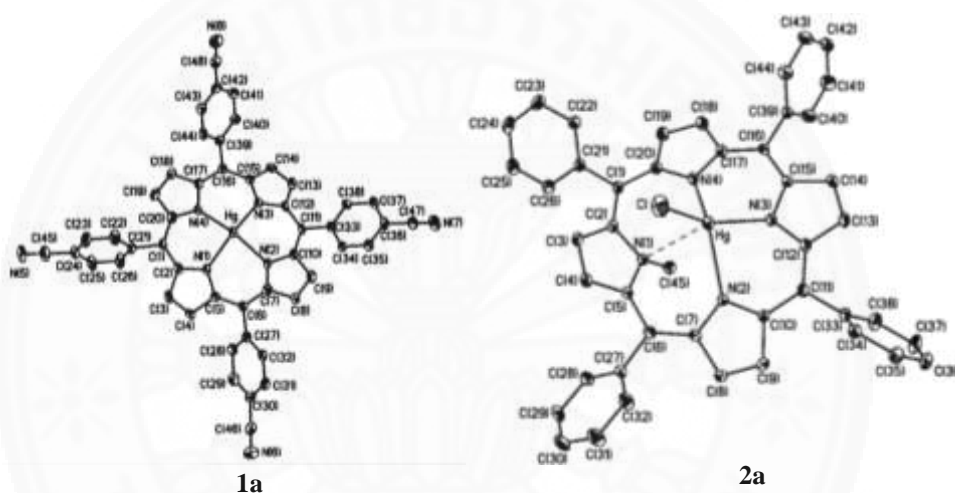
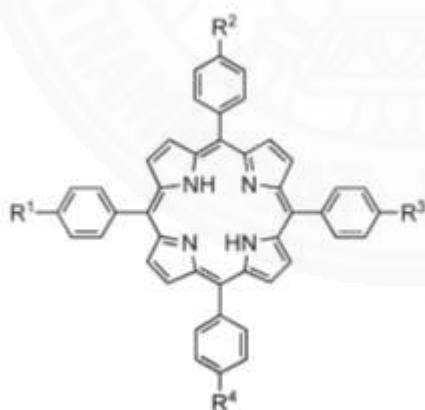


Fig. 10 The x-ray structure of complexes **1a** and **2a**

In 2003, Yu- Yi L. *et al.* report crystal structure of acetate- [mesotetra(ρ -chlorophenyl porphyrinato)]thallium(III)**3a** acetato-[*meso*-tetra(ρ -chlorophenyl)-porphyrinato] indium(III) **4a**, and acetate- [*meso*- tetra(ρ - bromophenyl) porphyrinato] -indiu,(III) **5a**. All porphyrins have been synthesized by refluxing porphyrin ligand with metal salts (Tl(OAc)₂ and In₂O₃), and the products were obtained in 87%, 84%, and 66% yield, respectively. The porphyrin complexes have been characterized by using ¹H NMR, ¹³C NMR, IR and mass spectroscopy. The X-ray structure of all complexes have been determined. All complexes have the P1 space group. The coordination sphere around the Tl³⁺ ion in complex **3a** is a six-coordinate, whereas the In³⁺ ion in complexes **4a** and **5a** is a five coordinate.[27]

In 2003, Iti G. and Mangalampalli R. synthesis a series of *meso*-furyl porphyrin with four different porphyrin cores (N_4 , N_3S , N_2S_2 and N_3O). All compounds have been characterized by 1H NMR, mass spectroscopy and elemental analysis. The comparison of NMR, UV-Vis, and fluorescence properties of all *meso*-furyl porphyrins derivative indicates that electronic properties of porphyrin were changed drastically on the introduction of furyl groups at *meso* position. The furyl groups causes downfield shifts of inner NH protons in 1H NMR, bathochromic shifts at absorption spectra, and large red shifts with reduction in quantum yields of fluorescence band. [28]

In 2004, Raymond L. *et al.* synthesis *meso*-(*p*-nitrophenyl)porphyrin by using $NaNO_2$ and TFA. The regioselective para-phenyl nitration of TPP was developed for and alternative route to nitro-substituted porphyrin. The equivalent amount of $NaNO_2$ and reaction time were used for control the degree of nitration. High yields of nitrated benzene and substituted have been reported under these condition. 1H NMR, UV-Vis spectroscopy, and mass spectroscopy were used for confirmed the structure of porphyrin product. The structure of free base porphyrins are shown in **Fig. 11**. Although, the nitroporphyrins are reduced to the corresponding aminoporphyrins under standard $SnCl_2/HCl$ conditions, and the structure of compound **11a**, **12a**, and **13a** were analyst by single crystal X-ray diffraction [29].



- 6a** $R^1, R^2, R^3, R^4 = H$
7a $R^1 = NO_2, R^2, R^3, R^4 = H$
8a $R^1, R^3 = NO_2, R^2, R^4 = H$
9a $R^1, R^2 = NO_2, R^3, R^4 = H$
10a $R^1, R^2, R^3 = NO_2, R^4 = H$
11a $R^1 = NH_2, R^2, R^3, R^4 = H$
12a $R^1, R^3 = NH_2, R^2, R^4 = H$
13a $R^1, R^2 = NH_2, R^3, R^4 = H$
14a $R^1, R^2, R^3 = NH_2, R^4 = H$

Fig. 11 Structure of *meso*-substitutedporphyrin

In 2004, the synthesis of hydroxyl nitrophenylporphyrins by Adler's method have been reported by Ana P. J. *et al.* The synthesis of tetrakis(2-hydroxy-5-nitrophenyl) porphyrin are involved the condensation of pyrrole and 2-hydroxy-5-nitrobenzaldehyde in propionic acid, at 414 K. The product was obtained in 72% yield

and the structure is shown in **Fig. 12**. ^1H NMR, UV-Vis absorption and fluorescence spectroscopy were used to characterization. The results demonstrate that these hydroxyl nitrophenyl porphyrins can be considered as promising photosensitizers in PDT [30].

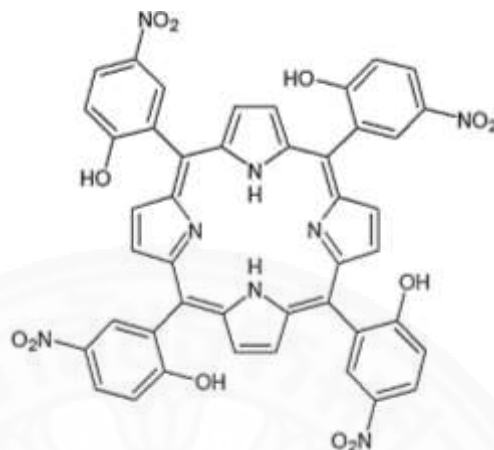


Fig. 12 Structure of tetrakis(2-hydroxy-5-nitrophenyl)porphyrin

In 2007, Irina N.F. *et al.* report the synthesis of symmetrical *meso*-aryl substituted porphyrins with long chain hydrophobic. The lipoporphyrins can be used to design supramolecular lipid ensembles of nanometer size. The reaction of *p*-hydroxy benzaldehyde with tetradecyl bromide and myristic acid chloride were obtained substituted benzaldehydes **15a** and **16a** in 71 and 82% yield, respectively. In addition, the *meso*-aryl substituted dipyrrolylmetanes **17a** and **18a** were prepared and obtained in 75 and 55% yield, respectively. The synthetic route for porphyrins are shown in **Fig. 13**. However, the concentration of both benzaldehyde and pyrrole are gave an optimal yields. The long chain porphyrins were obtained from the substituted benzaldehydes in 33 to 54% yields. Synthesized porphyrins were characterized by IR, MS, ^1H NMR spectroscopy, and CHN elemental analysis [31].

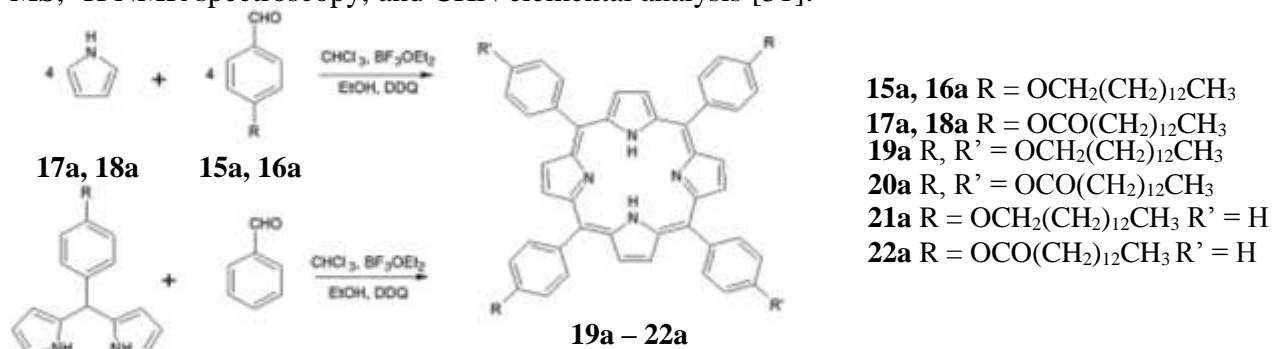


Fig. 13 Synthesis of *meso*-aryl-substituted porphyrins **19a – 22a**

In 2007, Amrita G. *et al.* report the synthesis of tetrakis-[4-(hexadecyloxy)phenyl]porphyrin and its copper(II) complex. The condensation of alkyl alcohol and thionyl chloride in chloroform have been used to synthesize alkyl long chain chloride. It was obtained in 72% yield. Long chain aldehyde derivative was synthesized by reacting alkyl chloride with the *p*-hydroxy benzaldehyde in presence of K_2CO_3 as base catalyst. The product was obtained in 74% yield. This porphyrin was obtained from reaction of aldehyde derivative and pyrroles. Then Cu(II) porphyrin complex was obtained (**Fig. 14**). The controlled aggregation of all compounds were studied in mix-solvent system at room temperature. Structure of the compound was characterized by scanning electron microscopy (SEM), transmission electron microscopy (TEM), powder X-ray diffraction (XRD), and UV-Vis spectroscopy [32].

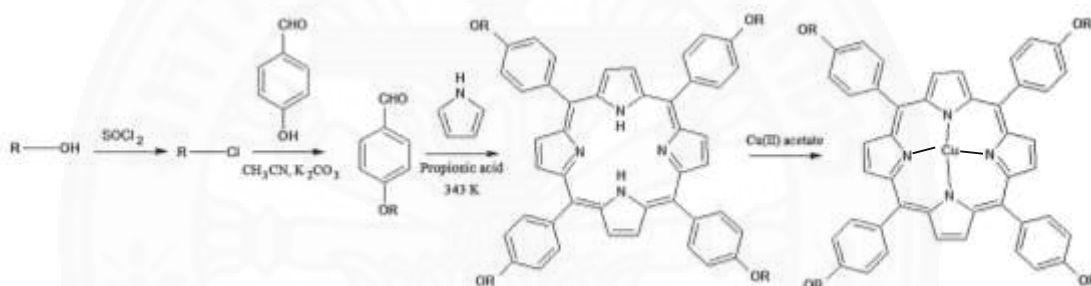


Fig. 14 Synthesis of tetrakis-[4-(hexadecyloxy)phenyl]porphyrin and it copper(II) complex

In 2007, Ioannis D. K. *et al.* report the catalytic properties at a palladium complex with porphyrin ligand. The structure of the palladium complex show in **Fig. 15**. All compound have been characterized by ¹H NMR, ¹³C NMR spectroscopy and Mass spectroscopy. The final product was obtained dark red solid in 97% yield. This complexes can used as a catalyst precursor for the Susuki-Miyaura cross-coupling of aryl bromide under mind condition, and leading to yields of coupling products in range 80-100%. This catalyst can recycled, but loss in activity. [33]

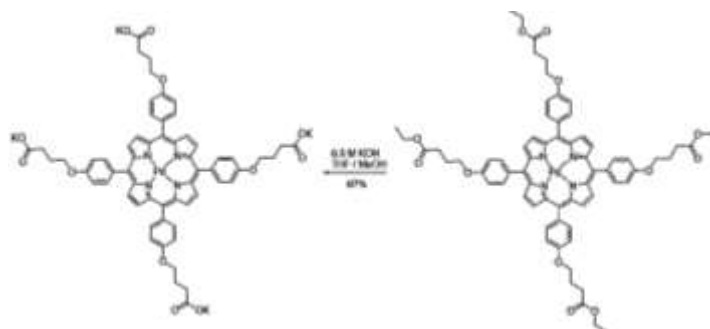


Fig. 15 The synthetic route of the palladium porphyrin complexes

In 2008, Jianzhong L. *et al.* synthesis five novel, *meso*-tetra[4-(3,4,5-trialkoxybenzoate) phenyl porphyrin and their metal complexes. (M=Zn, Ni). Their molecular structures were confirmed by ^1H NMR, FT-IR spectroscopy and elemental analysis. The DSC, X-ray diffraction and polarizing optical microscope have been used to investigate the mesomorphic behavior of the porphyrin derivatives. The mesomorphic properties of the compounds indicate the wanly potential usage in photoelectric fields [34].

In 2009, Chen W. *et al.* synthesized two series of novel *meso*-substituted porphyrins. 5,10,15,20-tetra[4-(3-phenoxy)-propoxy] phenyl porphyrin **23a**, and 5,10,15,20 – tetra[2-(3-phenoxy) propoxybenzaldehyde **24a**, respectively. They were observed less than 15% yield. (**Fig. 16**). Moreover, their Co(II), Cu(II), and Zn(II) complexes were synthesized. All complexes were obtained more than 90% yield. The CHN elemental analysis, FT-IR, ^1H NMR, mass, and UV-vis spectroscopy have been used for characterization the structure of all compounds. Futhermore, their molecular structure was proposed, based on DFT calculation. The photocatalytic activities in degradation of 4-nitrophenol were investigated using polycrystalline TiO_2 impregnated with the porphyrins and metalloporphyrins. [35]

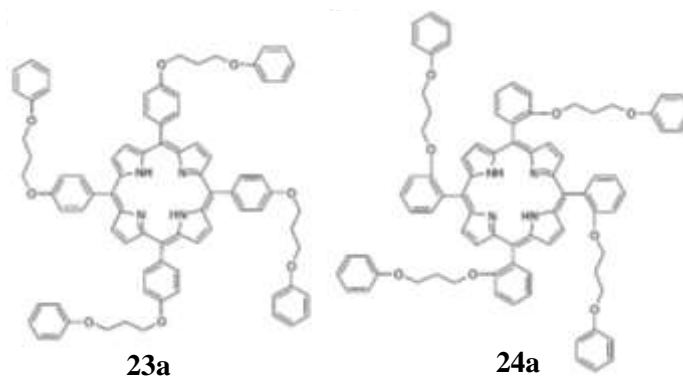


Fig. 16 The structure of novel porphyrin **23a** and **24a**

In 2009, Er-Jun S. *et al.* synthesis a series of novel, long-chain-substituted, porphyrin derivatives, *meso*-tetra (4-alkylamidophenyl)porphyrin ligands (**Fig. 17**) and their Zn complexes (alkyl = 8, 10, 12, 14, 16,18). This porphyrin series were prepared by acylation of the amini group of 5,10,15,20-tetra(4-aminophenyl)porphyrin by alkyl chloride. All compounds have been characterized by using elemental anlysis, cyclic voltametry, ^1H NMR, IR, UV-vis, and fluorescence spectroscopy. Moreover, the mesomorphism was investigated by DSC, POM, XRD, SPS, and EFISPS. This ligand that containing long chain carbon (more 12 atom) exhibited liquid crystalline behavior, while Zinc complexes are not.[36].

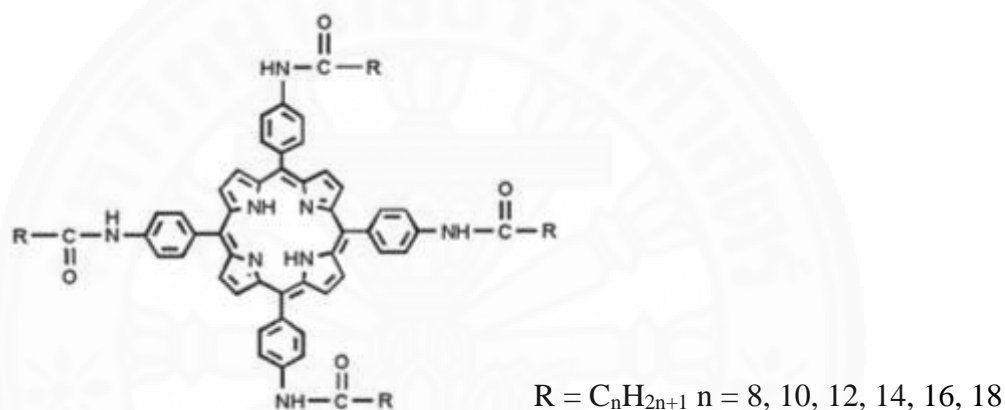


Fig. 17 The structure of *meso*-tetra (4-alkylamidophenyl)porphyrin

In 2011, Zhi X. *et al.* report an in-depth study on *meso*-aryl nitration of tetraphenylporphyrin. The synthetic route is shown in **Fig. 18**. The tetra-substituted derivative have been confirmed that is in fact a major product rather than being degraded in the process. The nitration of tetra-arylporphyrins leading to highly substituted derivatives is of great importance particularly in view of its simplicity, yield and well regiospecific control [37].

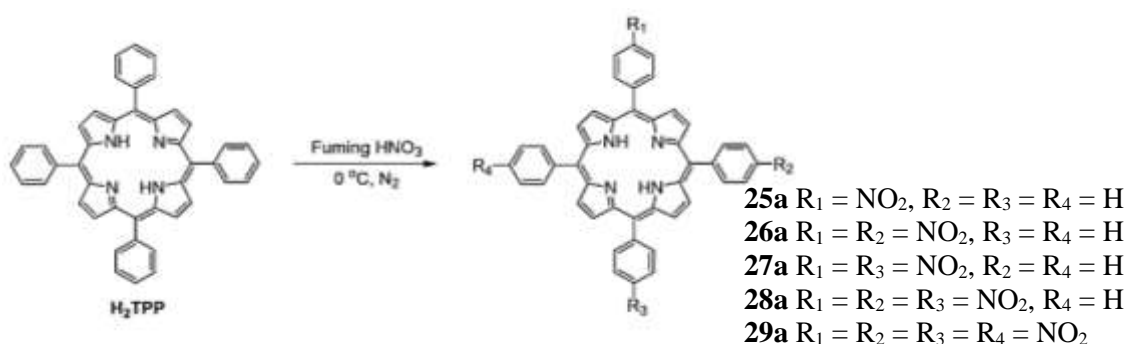


Fig. 18 *meso*-nitration of tetraphenylporphyrin **25a – 29a**

In 2011, Vinich P. *et al.* report the simple method for identification of a series of six *meso*-substituted porphyrins by using ^1H NMR spectroscopy. The series of six porphyrin derivatives were synthesized by mixed two aldehyde (3,5-di-*tert*-butylstyrylbenzaldehyde (**A**) and 4-iodobenzaldehyde (**B**)) in 1:1 ratio, pyrrole and zinc acetate in propionic acid and reflux for 3 hours. The structure of synthesized porphyrins are show in **Fig. 19**. The mixed porphyrin were purified by using column chromatography over silica gel, and eluting with mixture solvent of hexane and dichloromethane. The signal pattern of ^1H NMR of β -pyrrolic proton have been used for identified the structure mixed porphyrin [38].

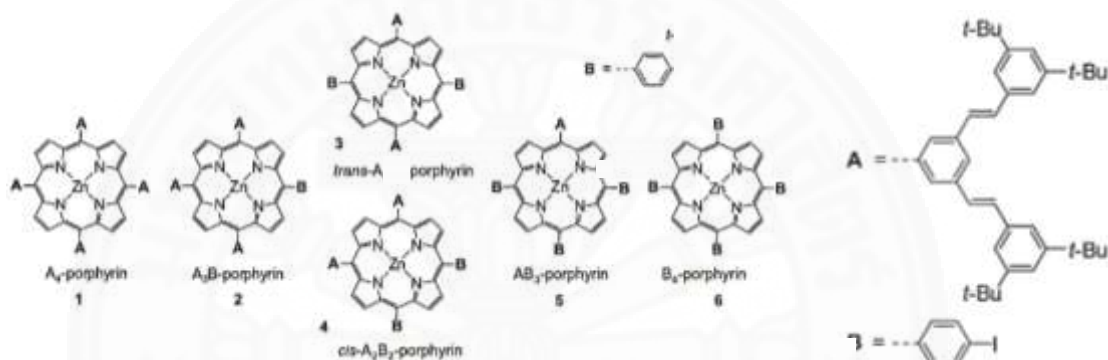


Fig. 19 Structure of mixed *meso*-substituted porphyrin

In 2011, Jun-Xu L. *et al.* report the crystal structure and their crystal data of *meso*-tetrakis[*p*-(heptyloxy)phenyl]porphyrinato]silver(II) **Fig. 20**. This compound have been synthesized by refluxing *meso*-tetrakis[*p*-(heptyloxy)phenyl]porphyrin and AgNO_3 in chloroform for 6 hours. The product was obtained in 23% yield. This compound have characterized by single X-ray diffraction technic. The single crystal was obtained from recrystallization from dichloromethane at room temperature [39].

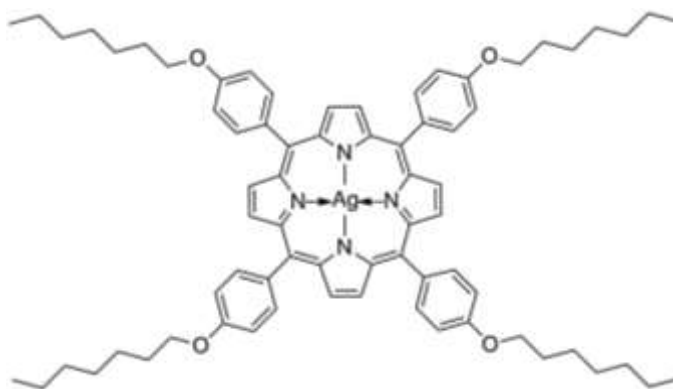


Fig. 20 The structures of the silver porphyrin complex

In 2012, Marcin R. *et al.* synthesis a series of mono-alkylcarboxylic acid derivatives of tetraphenylporphyrin. The carboxyl groups are attached to one of the phenyl rings of TPP via alkyl chains of different lengths. Mass spectrometry, ^1H NMR, UV-Vis, and fluorescence spectroscopy have been used to characterize the structure. Additionally, the lipophilicity was determined, it represent in partition coefficient ($\log P$). TLC method were used to determined $\log P$ value, that calculate by used this equation $\log P = \frac{\log P_{\text{Rekker}}}{2(R_{F1} + R_{F2})}$ were R_{F1} and R_{F2} are retardation factor for methanol:chloroform 8:2 and 7:3 (v/v), respectively, as mobile phase. These porphyrins are potential photosensitizers in photodynamic therapy [40].

In 2012, Ajesk P.T. *et al.* synthesis the water-soluble at N-confused porphyrin (NCP). The *meso*-tetrakis (p-sulfonatophenyl) N-confused porphyrin tetrasodium salt (NCPS) has been synthesized. The synthetic route show in **Fig. 21**. The product was obtained in 56% yield and characterized by using by ^1H NMR, ^{13}C NMR, MALDI-70F, and IR spectroscopy. Moreover, the photodynamic therapeutic (PDT) application was investigated by photophysical and in vitro studies. The cytotoxicity of NCPS in cell lines was investigated both in the presence and absence of light using MTT assay. The IC_{50} value was found as low as 6 μM . [41]



Fig. 21 The synthetic route of NCPS

In 2012, Julien T. *et al.* report the synthesis of a *meso*-tetrakis (2,6-dimethyl-4-triflyloxyphenyl) porphyrin and its X-ray structure (**Fig. 22**). This porphyrin was synthesized by using Lindsey condition with 2,6-dimethyl-4-(triflyloxy) benzaldehyde). This porphyrin could directly be engaged in Suzuki cross-coupling reactions, to be further tetra functionalized with 3-pyridyl ligands. The result porphyrin was matalate

with Zinc(II) and the molecular structures of all compound were determined by using X-ray crystallography. [42]

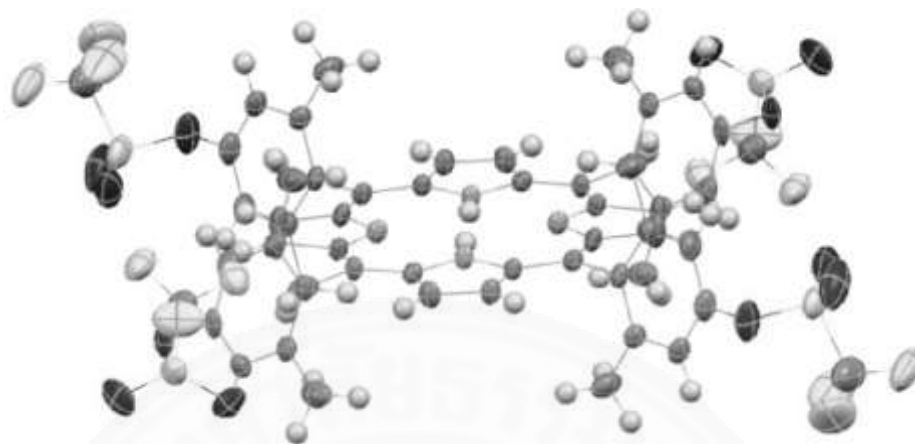


Fig. 22 X-ray structure of *meso*-tetrakis (2,6-dimethyl-4-triflyloxyphenyl)porphyrin

In 2013, Ya-hong W. *et al.* reported a series of novel *meso*-tetra (Schiff-base substituted phenyl) porphyrin and its zinc(II) complexes. The reduction of *meso*-tetra(*p*-nitrophenyl)porphyrin to form *meso*-tetra(*p*-aminophenyl)porphyrin **30a**. The Schiff-base porphyrin were prepared by condensation of porphyrin **30a** with different substituted benzaldehyde. Then zinc(II) porphyrin complex were synthesized (**Fig. 23**) All compounds were successfully characterized by UV-Vis and fluorescence spectroscopy, FT-IR, and EPR determination. The second substituents in Schiff-base groups provide weakly electronic effects on π -electron system. These weak electronic effects are also observed in the electronic spectra of their zinc complex [43].

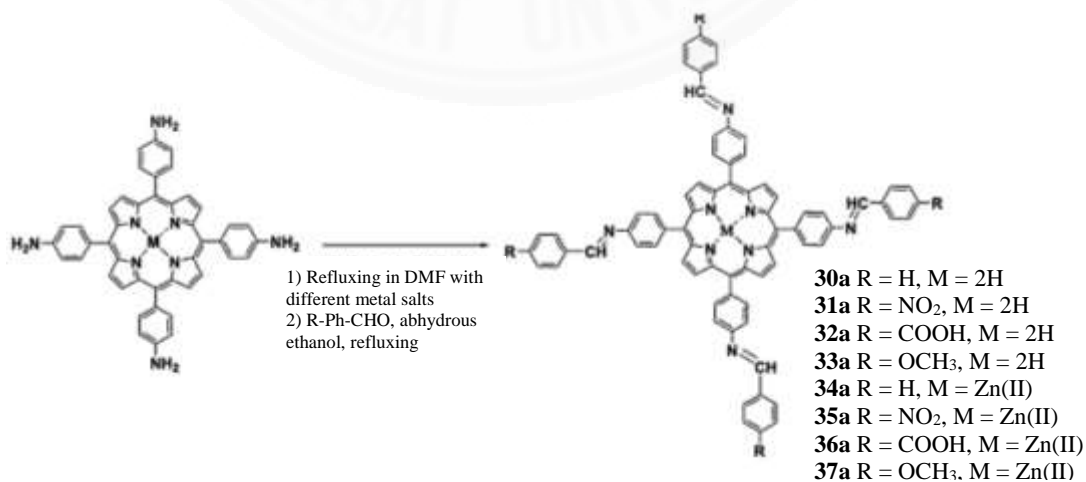


Fig. 23 Preparations of tetra (Schiff-base substituted phenyl) porphyrins and their complexes

In 2013, Yu Jing Z. *et al.* synthesized the novel 5,10,15,20-tetra[n-C_nH_{2n+1}-alkyl (n=12,14,16) Aarbazole] porphyrin and their lanthanide complexes (Dy Hs Er Gd). All compound have been characterized by UV-Vis, IR, ¹H NMR spectroscopy, TGA-DTA, and electrochemical properties. The synthetic ligand was observed in low %yield (18%). Moreover the luminescence of the ligands and complexes have been studied. The results show the intensity of fluorescence emission spectra and the quantum yield were increased when the alkyl group was longer. The Gd porphyrin complexes gives the strongest intensity fluorescence. Lastly, in the electrochemical property was studied. The redox behavior shows that lanthanide porphyrin complexes counts of two redox peaks while ligand has four peaks [44]

In 2013, Victor H. A. P *et al.* studied the thermal stability of the Mn(III) *meso*-tetrakis(N- ethylpyridium- 2- yl) porphyrin chloride(MnTE- 2- PyPCl₅. UV- Vis spectroscopy, ESI- MS and TLC were used to characterize this porphyrin. The thermogravimetric, derivative thermogravimetric, and differential thermal analyses were selected used to study the thermal stability of porphyrin under dynamic air at 1 atm. Three thermal processes were observed by TG/DTG. The first is dehydration in 26-130 °C range, second is dealkylation in the 134-279 °C range and finally in the porphyrin decomposition in the 279-901 °C with multiple step. [45]

In 2014, Gontam N. *et al.* reported the 4-chlorobenzoate-(5,10,15,20-*meso*-tetraphenylporphyrinato)-oxo-tungstan(V) **38a**. Thermal reaction of [W(NO)₂(py)₂(Cl)₂] and *meso*-tetraphenylporphyrin were used to synthesized complex **38a**. Then the complex **38a** derivative, hydroxo-(5,10,15,20-*meso*-tetraphenylporphyrinato)-oxo-tungstan(V) **39a** and methoxo-(5,10,15,20-*meso*-tetraphenylporphyrinato)-oxo-tungstan(V) **40a** were prepared. All complexes were characterized by UV-Vis, IR and ESI-mass spectroscopy. The electrochemical information were reported. Complexes **39a** and **40a** are structurally characterized by single crystal X-ray diffraction [46].

In 2014, Zhijie X. *et al.* synthesized a novel porphyrin-naphthalimide pentamer and their metal(Zn²⁺, Cu²⁺, Mn²⁺, Fe³⁺, Co²⁺) complexes The porphyrin was synthesized by linking four linking four light- harvesting naphthalimide units to a porphyrin via ether bridges and obtain in 61% yield. Then the metal complexes had been synthesized by reaction between porphyrin and metal chloride or metal acetate. The structure at all compound were characterized by ¹H NMR, ¹³C NMR, FT- IR, MALDI- TOF and

elemental analysis UV-Vis and Fluorescence spectroscopy had been used to investigate the photophysical properties. The result show that the excitation energy transfer occurs from the naphthalimide unit to porphyrin core. Moreover, the electrochemical properties of all compound were studied by cyclic volthametry. All compounds show a similar ring oxidation and reduction behavior. [47]

In 2015, Zengqi Z. *et al.* synthesized the novel porphyrin 5,10,15,20-tetra(4-(4-acetateethyl)phenyl)porphyrin and its two metal complexes (Zn(II), and Cu(II)) for act as catalyst in the ethylbenzene oxidation process. All compounds were characterized by spectroscopic techniques. Single crystal X-ray diffraction had been used to analyze the structure of all metal complexes. The zinc and copper complexes display 3D supramolecular structure constructed by $\pi \cdots \pi$ interaction of porphyrin ring and C-H \cdots O hydrogen bond. Then, both of these complexes exhibit highly selectivity to acetophenone(>99%) with the conversion of 23% and 76%, respectively. [48].

In 2015, Ahmad J. *et al.* prepared two new polycarboxylic photosensitizer. The 2,4,5-tris(tert-butoxycarbonylmethoxy)benzaldehyde and two derivative of *meso*-dipyrrromethane had been synthesized. Then both compound were used to synthesize porphyrin under Lindsey's conditions and get porphyrin in 20% and 10% yield, respectively. Then carboxylic porphyrin **41a** and **42a** were obtained (Fig. 24), when porphyrin react with formic acid. The ^1H NMR and ^{13}C NMR spectroscopy and mass spectrometry (MALDI-TOF) were used to characterize structure of all compound. The photophysical properties was studied by UV-Vis spectroscopy. Compound **41a** and **42a** were tested for a photo-antimicrobial agents against *S. aureus* and *B. cereus*. The porphyrin **41a** is shown a significant antimicrobial activity for tested bacteria at 50 μM or higher [49].

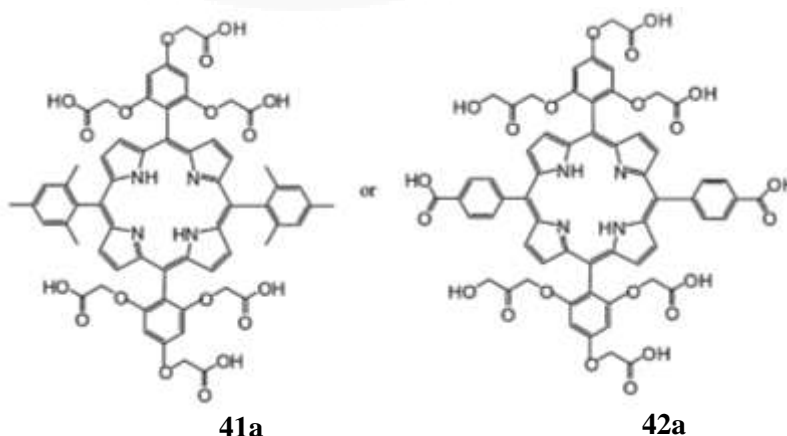


Fig. 24 Structure of carboxylic porphyrin **41a** and **42a**

In 2015, Zhijie X. *et al.* reported the synthesis of a novel ethynyl bridge naphthalimide-functionized porphyrin TANPH₂ **43a** and its metal (Zn and Cu) complexes (TANPZn **44a** and TANPCu **45a**). The 4-((2-(4-(octyloxy)phenyl)-1,3-dioxo-2,3-dihydro-1H-benzo[de]isoquinolin-6-yl)ethynyl)benzaldehyde had been synthesized by Sonogushira coupling condition from 4-bromo-N-(4-(octyloxy)phenyl)-1,8-naphthalimide and 4-ethynylbenzaldehyde, using Pd(PPh₃)₄ and CuI as catalyst. The porphyrin **43a** was synthesized from reaction of pyrrole with the synthesized aldehyde in mixed solvent of propionic acid and nitro benzene, then obtained in 94% and 93%, respectively. The structure of all compound were characterized by using ¹H and ¹³C NMR spectroscopy, FT-IR, MALDI-TOF-MS and elemental analysis. Both UV-Vis and fluorescence spectroscopy had been used to investigate the photophysical properties. The introduction of ethynyl bridges compound **43a** and **45a** can emit intense red light with high fluorescence quantum yields. The excitation energy can transfer occurred from the naphthalimide units to porphyrin core [50].

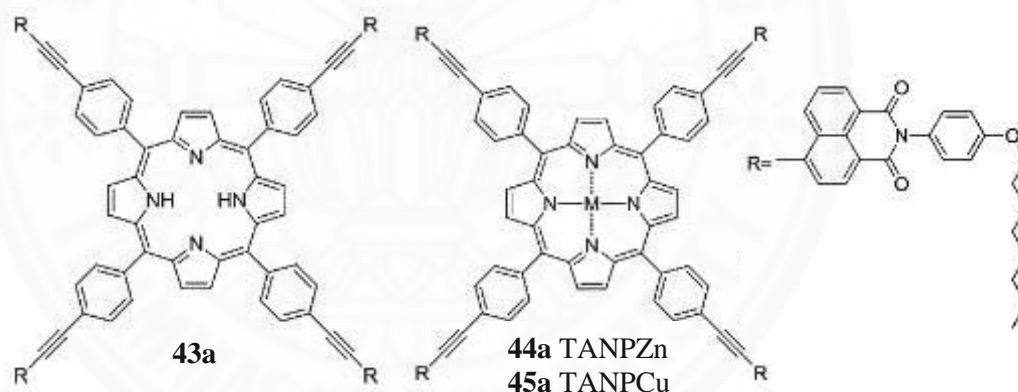


Fig. 25 The synthetic route of TANPH₂ **43a**, TANPZn **44a** and TANPCu **45a**

In 2015, Rajneesh M. and Prabhat G. prepared the *meso*-tetrakis(ferrocenylethynylphenyl)porphyrin P1 **46a** and P2 **47a** and zinc derivative ZnP2 **48a** (**Fig. 26**). The ferrocenylethynylphenyl substituted aldehyde and pyrrole in dry CH₂Cl₂ were used to synthesized porphyrin **46a** and **47a** under Lindsey's condition. TGA, photophysical and electrochemical properties were studied. The ¹H NMR was used to characterize. The porphyrin **47a** and **48a** showed better thermal stability than porphyrin **46a** [51].

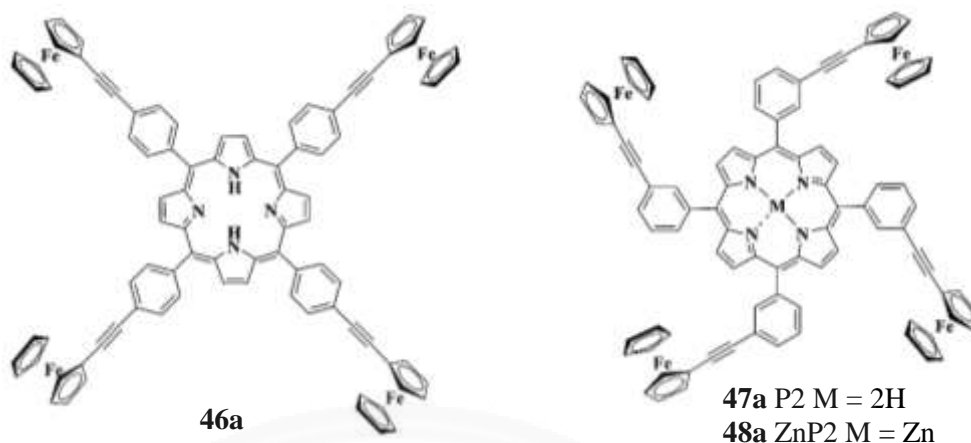


Fig. 26 The structure of porphyrin **46a**, **47a**, and zinc complex **48a**

In 2015, Guan H. *et al.* studied the cyclohexane oxidation by using zinc oxide promoted catalysis of tetrakis(pentafluorophenyl)porphyrin iron chloride [Fe(TPFPP)]. This catalysis have been prepared by immobilized Fe(TPFPP) on to Zinc oxide. The UV-Vis and FT-IR spectroscopy, XRD, TGA, TEM, FE-SEM and SSA had been used to characterization both of FE(TPFPP) and FE(TPFPP)/ZnO. Furthermore, the zinc oxide doped porphyrin catalyst had been used in the oxidation reaction of cyclohexane compound with Fe(TPFPP). The results show ZnO increased the catalytic activity of Fe(TPFPP) for cyclohexane oxidation. [52]

2.3 Synthesis of β -functionalize porphyrins and metal complexes

In 2000, Oliver S. prepared nickel(II) 2,7,8,13-tetraethyl-3,12-dimethylporphyrin **49a** and its nitro substituted. The reaction of porphyrin **49a** with solution of N_2O_4 in petroleum ether afforded the *meso*-nitroporphyrin **50a** and β -nitroporphyrin **51a** in 32 and 20% yield, respectively. On the other way, it using iodine/silver nitrite as catalyst in CH_2Cl_2/CH_3CN , compounds **50a** and **51a** were obtained in 10 and 52% yield, respectively. The structure of all compounds were characterized by 1H NMR IR and UV-Vis spectroscopy. The β -nitration of porphyrin could be completed with *meso*-nitration porphyrin due to the strong π -acceptor properties of the nitro group [53].

In 2001, two isomer of nitro *meso*-tetraphenylporphyrin were reported, one have nitro group at the *para* position of a phenyl ring (TPPNO₂ **52a**) and the other have the same group at β -pyrrolic position (TPP β NO₂ **53a**). Moreover, the copper complexes

(CuTPPNO₂ **54a** and CuTPPβNO₂ **55a**) had been differentiated by Olga V.N. and Michael L.G. The Tandem mass spectroscopy had been used to identify of each species. The porphyrin **52a**, **53a** and their copper complexes **54a**, **55a** had been produce the [M + H]⁺ and M⁺ peak at m/z 660 and 720, respectively by using fast-atom bombardment (FAB) ionization. Although, those two isomer of nitro *meso*-porphyrin exhibit main peak at same position, but the fragment ion of other isomer were not the same position. That can used to identify this isomer. The same result was observe in copper porphyrin isomer to [54].

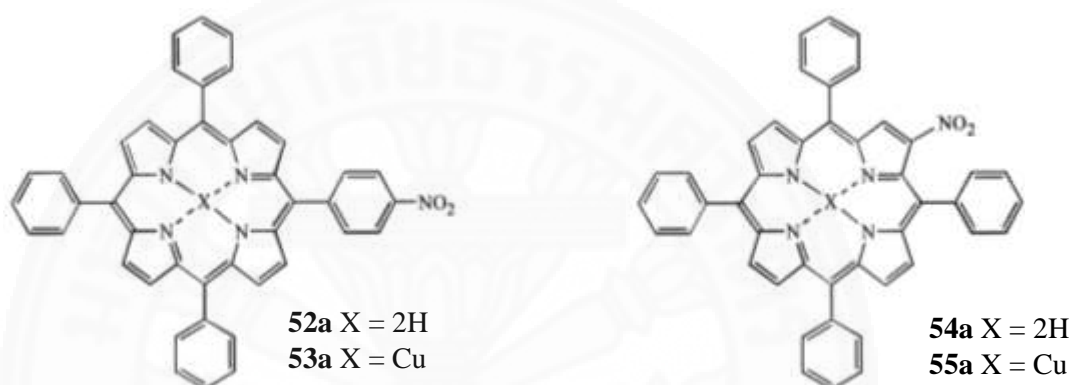


Fig. 27 Structure of TPPNO₂, TPPβNO₂, and its metal complexes

In 2002, Yuichi T. *et al.* studied the synthesis of Zinc(II) complexes of antipodal β-tetrasubstituted *meso*-tetraphenylporphyrin with trifluoromethyl [Zn(TPP(CF₃)₄)], bromine [Zn(TPPBr₄)], and methyl groups [Zn(TPP(CH₃)₄)]. The single crystal X-ray diffraction of mentioned complexes were analyzed. UV-Vis, NMR spectroscopy, and cyclic voltammetry were used to characterize the structure of synthesized complexes. Five coordinate complexes had been observed the revealed distorted macrocyclic core where significant difference in the Zn-N distance between β- and non-β- substituted side [55].

In 2003, Hu J. *et al.* reported the FT-Raman and FT-IR spectrum of 2-nitro-tetraphenylporphyrin (2-NO₂-TPP), nickel-2-nitro-tetraphenylporphyrin (Ni-2-NO₂-TPP), zinc-2-nitro-tetraphenylporphyrin (Zn-2-NO₂-TPP) and copper-2-nitro-tetraphenylporphyrin (Cu-2-NO₂-TPP). All compound had been synthesized and confirmed their structure by using elemental analysis, NMR, and mass spectroscopy. Moreover, the FT-Raman and FT-IR of all compound have been measured in their solid state, and carefully assigned. The β-NO₂ group and their influence of the central metal

ion have an effect on the molecular symmetry and vibration spectra of the porphyrin macrocycle [56].

In 2012, Stanisław O. and Sebastian Grzyb proposed the simple route to synthesize the ρ -amino porphyrin directly. The ρ -nitroporphyrin was used as the starting material. The N,N,N-trimethylhydrazinium iodide (TMHI) was used to react with 2-Nitro-meso tetraphenyl porphyrin (Zinc and Nickel complex) in base (KOH)/DMSO system the synthetic route is shown in **Fig. 28**. The amination of all porphyrin complexes gave good yield of the expected product. ^1H NMR have been used to confirm the amino substitution [57].

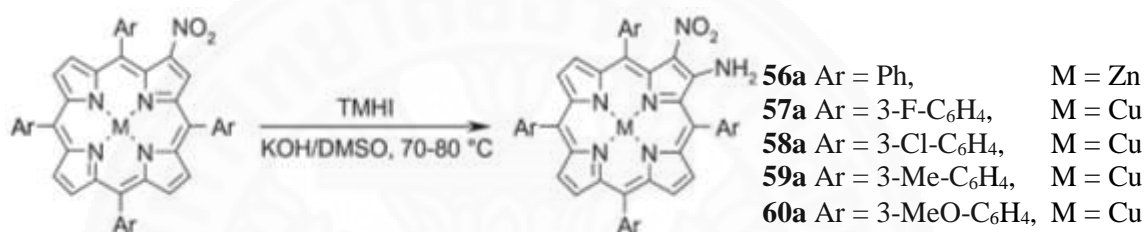


Fig. 28 The amination of porphyrin complexes

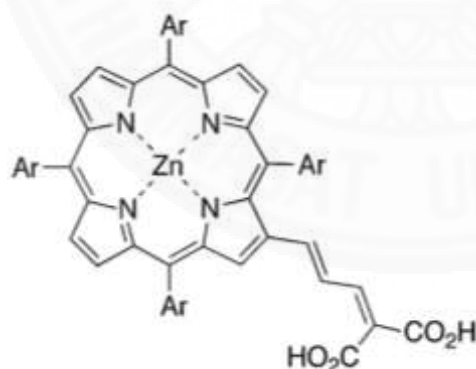
In 2013, Kanokorn S. *et al.* report the synthesis and characterization of new β -pyrrolic functionalized porphyrin with donor- π -accepter character. Both (E)-3-[4-{5,10,15,20-tetrakis(3',5'-di-tert-butylphenyl)-porphyrin-1-yl}phenyl]-2-cyanoacrylic acid, and (E)-3-[5-{5,10,15,20-tetrakis(3',5'-di-tert-butylphenyl)-porphyrin-1-yl}thiophen-2-yl]-2-cyanoacrylic acid had been synthesized, with 86% and 72% yield respectively. Two type of π -conjugated spacers (benzene and thiophene ring) with cyanoacrylic acid as an acceptor were linked to the β -pyrrolic position of porphyrin ring. The structure of these compounds were confirmed by ^1H NMR, ^{13}C NMR, UV-Vis spectroscopy, and high-resolution mass spectrometry. The high thermal and electrochemical stability were found in these porphyrin. The applications as sensitizer in DSSC had been reported. The porphyrin with thiophene ring gave better cell performance with the overall conversion efficiency (η) of 1.94% [58].

2.4 Application of porphyrin and metal complexes

In 2007, Wayne M.C. *et al.* studied the synthesis, electronic, and photovoltaic properties of novel green porphyrin sensitizers **Fig. 29**. The porphyrins were synthesized by using Lindsey's condition, giving a better yield. All compounds were fully characterized by ^1H NMR, UV-Vis spectroscopy, and high-resolution mass spectrometry (HRMS). The photovoltaic characteristics of cells using the zinc porphyrin sensitizers are summarized in **Table 1**. [59]

Table 1. The photovoltaic characteristics of cells using the zinc porphyrin sensitizers

Dye	V_{oc} , mV	J_{sc} , mA/cm ²	FF	η , %
61a	638	12.1	0.66	5.1
62a	680	14.0	0.74	7.1
63a	642	14.8	0.63	5.8
64a	701	13.4	0.68	6.4
65a	649	13.4	0.61	5.3
66a	685	13.3	0.68	6.1



- 61a** Ar = Ph
62a Ar = 4-methylPh
63a Ar = 4-ethylPh
64a Ar = 4-n-butylPh
65a Ar = 4-n-octylPh
66a Ar = 3,5-dimethylPh

Fig. 29 Structure of porphyrin sensitizer

In 2011, Hongshan H. *et al.* synthesized 2-(1-acetyl-2-oxopropyl)-5,10,15,20-tetraphenylporphyrin and its transition metal complexes (Cu^{2+} and Zn^{2+}). The 1-acetyl-2-oxopropyl group is attached to the β -pyrrolic position via substitution reaction of 2-nitro-5,10,15,20-tetraphenylporphyrin and acetylacetone in DMSO. The yields were

obtained more than 70%. The single crystal X-ray diffraction had been used to analyst structure of synthesized compounds. All compounds exhibit strong absorption band at UV and visible region. However, the energy conversion efficiencies of three porphyrin sensitized solar cells are low, that is 0.021, 0.015, and 0.14%, respectively [60].

In 2013, Qinglong T. *et al.* reported the synthetic of the novel zinc porphyrin sensitizes for dye sensitized solar cell. The P_{Zn} -COOH **67a**, and P_{Zn} -BIA-COOH **68a** were synthesized by several steps. Firstly, they synthesized 5-(4-nitro)phenyl-10,15,20-tris(3,4,5-trimethoxyphenyl)-porphyrin by Alder's method. Then the product has been reacted with several reagents. Finally complex **67a** and **68a** were obtained (**Fig. 30**). The 1H NMR, IR spectroscopy, and MOLDI-TOF mass spectrometer were used to confirmed the complexes structure. Two complexes exhibit maximum power of conversion efficiency for 1.75% and 1.06%, respectively [61].

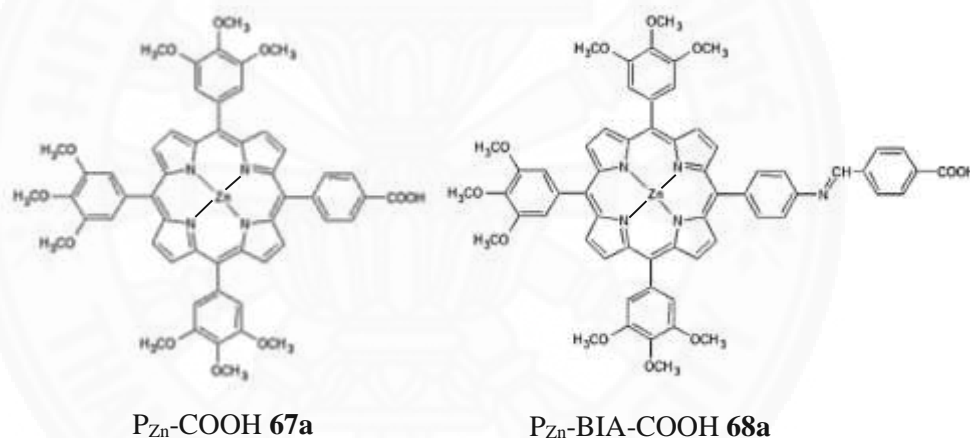
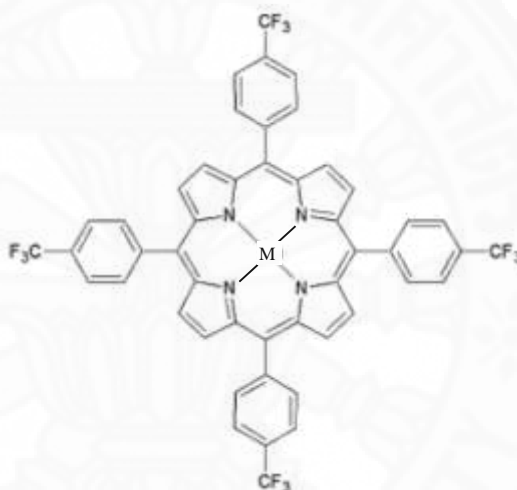


Fig. 30 Structure of P_{Zn} -BIA-COOH, and P_{Zn} -COOH

In 2015, Chirawat C. *et al.* studied the performance of a series of zinc-porphyrins based sensitizer in DSSC by DFT and TD-DFT calculations. The zinc-porphyrin analogues were fully optimized by B3LYP/6-31G(d) method. The effect of π -linker, anchoring group, and capped carbazole a *meso*-substituted porphyrin on the energy conversion efficiency were evaluated. The result show that the increased conjugation length in π -linker and used cyanoacrylic acid as a anchoring group that can increase the conversion efficiency but capped cabazole doesn't affect [62].

In 2015, Fasal R.K. *et al.* reported the synthesis, and spectral studies of 5,10,15,20-tetrakis(4'-trifluoromethylphenyl)porphyrin **69a** and their metal complexes (Fe(II) **70a**, Ni(II) **71a**, Cu(II) **72a**, Zn(II) **73a**, and Pt(II) **74a**). The

pyrrole and 4-(trifluoromethyl)benzaldehyde were used for prepared porphyrin in dichloromethane under nitrogen atmosphere following Lindsey method. All compounds were characterized by UV-Vis and ^1H NMR spectroscopy, and mass spectrometry. Especially compounds **69a**, **71a**, **72a**, and **73a** were successfully characterized by single crystal X-ray diffraction. The crystals were growth at room temperature by the vapor diffusion method, and THF was used as a solvent. Finally, the antimicrobial activity had been reported. All of the synthesized compounds were tested by using well diffusion method at difference concentration (50, 75, and 100 $\mu\text{g/ml}$). Free ligand **69a** was showed the high effective compared to its metal complex [63].



M = 2H **69a**, Fe(II) **70a**, Ni(II) **71a**, Cu(II) **72a**, Zn(II) **73a**, and Pt(II) **74a**

Fig. 31 Structure of fluorinated porphyrin, **69a** and its metal complexes **70a – 74a**

In 2008, Xu X. *et al.* reported the antibacterial activity of Mn(II), tetraphenylporphyrin, ebselen-porphyrin conjugate, and its manganese complex. the stop-flow microcalorimetry were used to study the antibacterial effect of all compound. The *S. aureus* was used as a testing bacteria. The result shows that all compounds had potential to antibacterial reagent, especially the tetraphenylporphyrin has IC_{50} value of 100 $\mu\text{g/ml}$ less than other compound [64].

In 2013, Marein R. *et al.* synthesized the tetrakis-(hydroxyphenyl)porphyrins with long alkyl chain. The summaries of all synthesized structure are shown in **Fig. 32**. Compounds **75a – 79a**, **88a** and **91a** were synthesized by condensation of appropriate

aldehyde with pyrrole and propionic acid. Other porphyrins were obtained from further modified synthetic route. All compounds were characterized by using mass spectrometry, UV-Vis and fluorescence spectroscopy. Lipophilicity and photostability were observed. These data were further assessed in terms of the synthesized compounds usefulness as potential photosensitizers in anticancer photodynamic therapy [65].

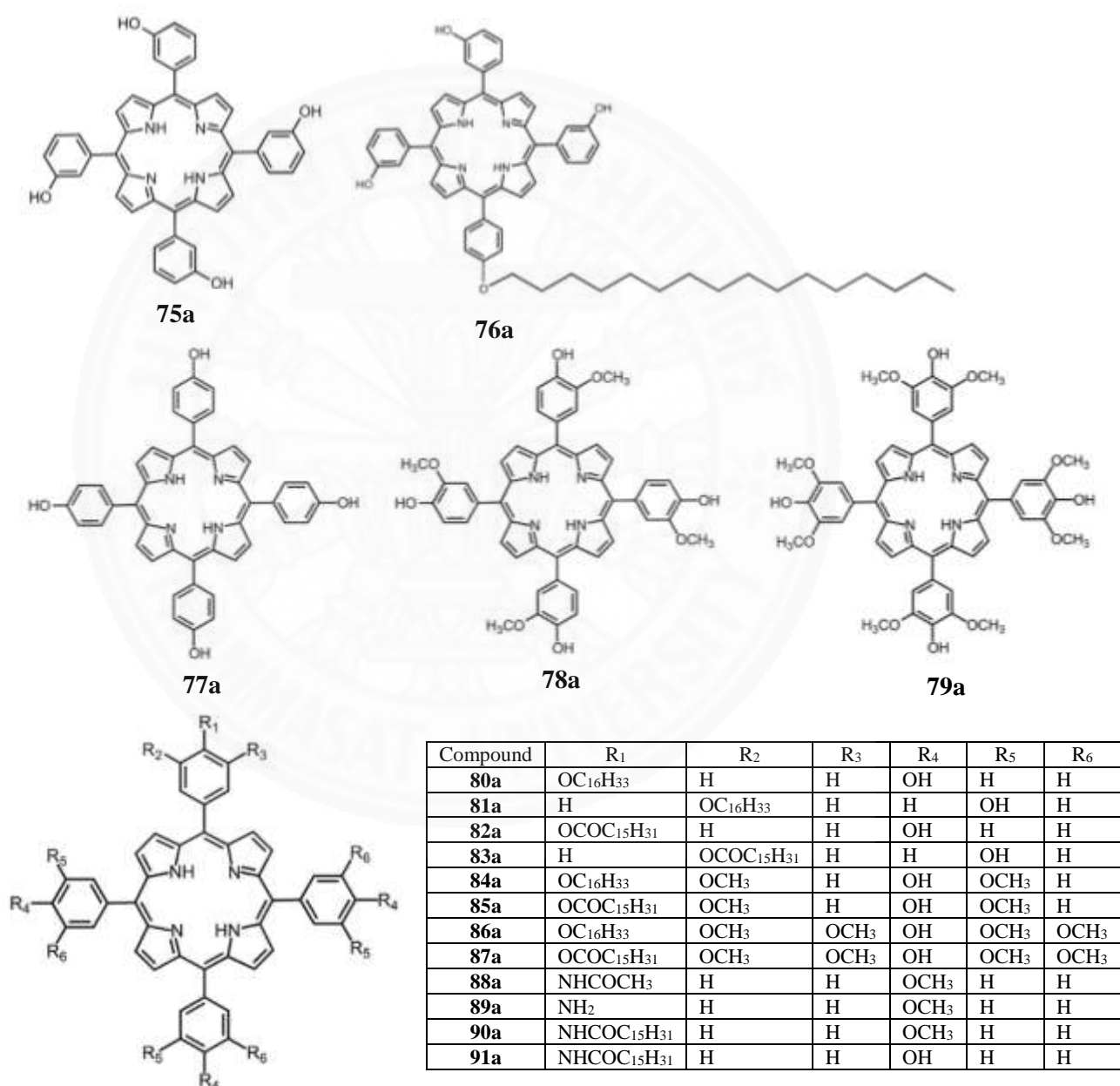


Fig. 32 Structure of investigated compound

2.5 Gas sensor

In 2011, Javier R. *et al.* reported the optimization of Langmuir-Blodgett films by using the mixture of 5,10,15,20-tetrakis[3,4-bis(2ethylhexyloxy)phenyl]-21H,23H-porphine (EHO) and p-tert-butylcalix[8]arene (C8A) **Fig. 33**. This mixed monolayer were prepared on pure water with a molar ratio of 3:2 (C8A:EHO). The properties of the surface of the mixed films had been analyzed through AFM analysis. The result show that, the mixed films architecture leads to a fast response NO₂ sensor, batter than only EHO. [66]

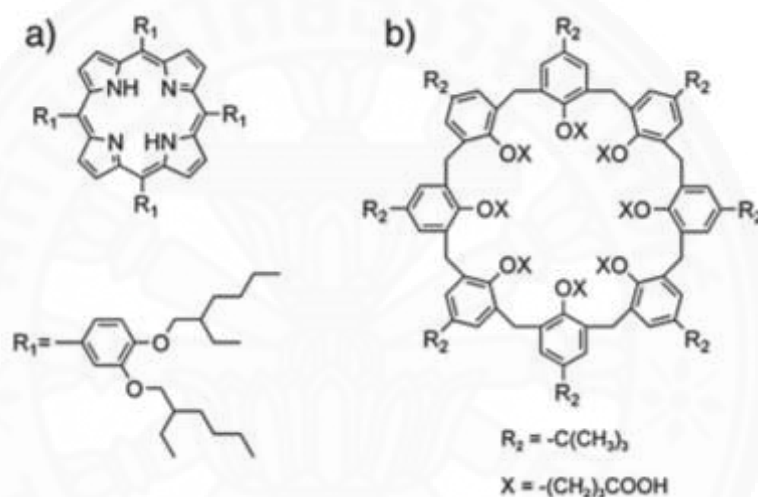


Fig. 33 The structure of 5,10,15,20-tetrakis[3,4-bis(2ethylhexyloxy)phenyl] 21H,23H-porphine (EHO) and p-tert-butylcalix[8]arene (C8A)

In 2012, Sumana K. and Teerakiat K. reported a method for detection of alcohol vapors by using magnesium 5,10,15,20-tetraphenyl porphyrin (MgTPP) thin films as an optical sensing. The thin films were prepared by spin-coated the solution of MgTPP in CHCl₃ (5 mg/mL) on clean glass substrates. This films was subjected to thermal annulling at 280°C under argon atmosphere. The MgTPP sensor have been responded with methanol, ethanol, and isopropanol at the same mol% of each alcohol concentration. Furthermore, Density Functional Theory (DFT) calculations were performed to model the underlying mechanism of this selectivity [67]

In 2014, Carlos H.A.E. *et al.* reported a new kind of composite gas sensors in which the conducting polymer doped with free base or metallated porphyrin including

3,4,5,6-pentafluorophenyl)porphyrin (H_2TPFP), *meso*-Tetra(phenyl)porphyrin (H_2TPP), and their Zinc, Nickel, Cobalt complexes instead of organic Lewis acid. The sensor have been prepared by spin-coating the solution of Poly(2-phenyl-1,4-xylylene) (PPPX) and each free base or metallated porphyrin onto metallic (chrome) interdigitated electrodes. Ethyl acetate, ethanol, propanone, and toluene have been used to the test sample. The **Fig. 34** shows a schematic representation of the e-nose system for used to test these sensor. Both of sensor (doped with free-base and metallated porphyrin) were successfully tested in the identification of four volatile solvent. [68]

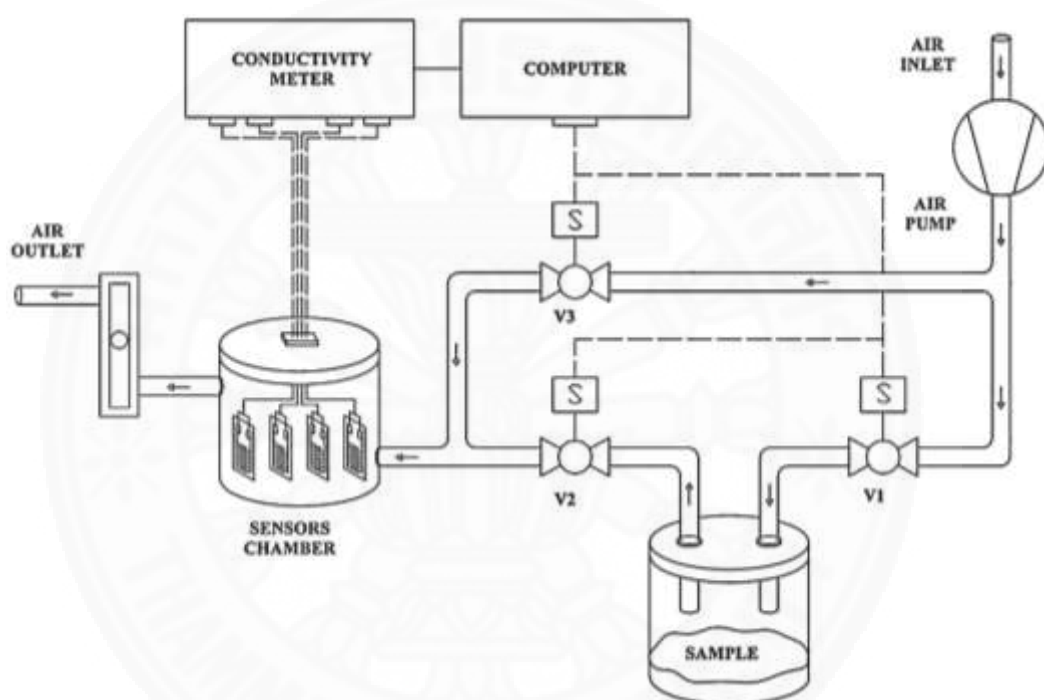


Fig. 34. Schematic view of the e-nose measuring system

In 2016, Feifei S. *et al.* proposed the NO_2 gas sensor by using the porphyrin nanotubes. The nanoporous anodized aluminum oxide (AAO) membrane were to the template to fabricated the highly ordered nanotube of 5, 10, 15, 20-tetrakis(4-aminophenyl)porphyrin zinc (ZnTAP). The porphyrin nanotube had been characterized by electrical absorption spectra, fluorescence spectra TEM, SEM, and XRD techniques. This nanotube showed a good conductivity and can applied as NO_2 gas sensor. The proposed sensor exhibit fast response and recovery behavior, high sensitivity, and good reproducibility moreover, this sensor can achieve a detection limit as low as 1 ppm. [69]

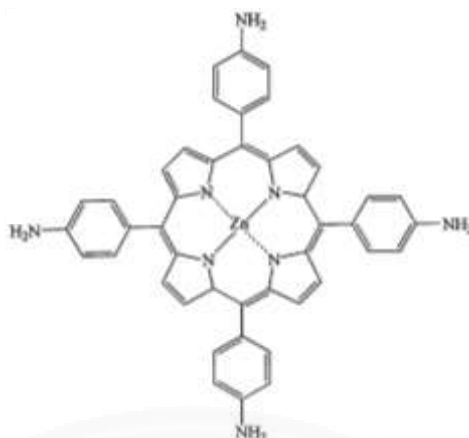


Fig. 35 The structure of 5, 10, 15, 20-tetrakis(4-aminophenyl)porphyrin zinc

In 2016, Lizhi Z. *et al.* prepare the optical sensor membrane for sorption and detection of cadmium in aqueous solution. These optical sensor have been fabricated by immobilized 5,10,15,20-tetrakis(4-N-methylpyridyl) porphyrin *p*-toluenesulfonate (TMPyP) onto the poly(sodium 4-styrenesulfonate), grafted on chloromethylated polysulfone (PSF-PNaSS). The field emission scanning electron microscopy (FESEM) have been used to characterize the PNaSS-grafted membrane. The prepared membrane exhibit a fast response to Cd(II), including apparent spectral and color change. The optical sensor membrane exhibited good stability and reusability which made it efficient for various sorption removal and detection application. [70]

CHAPTER 3

RESEARCH METHODOLOGY

3.1 Materials

3.1.1 Reagents

- *l*-Bromobutane (C₄H₉Br, Assay 99%, Sigma-aldrich, USA)
- *l*-Bromooctane (C₈H₁₇Br, Assay 99%, Sigma-aldrich, USA)
- *l*-Bromodecane (C₁₀H₂₁Br, Assay 98%, Sigma-aldrich, USA)
- 4-Hydroxybenzaldehyde (C₇H₆O₂, Assay 99%, Sigma-aldrich, USA)
- Potassium carbonate anhydrous (K₂CO₃, Assay 99%, Unilab, Australia)
- *N,N*-Dimethylformamide (C₃H₇NO, Analytical grade, MAY&BAKER, England)
- Pyrrole (C₄H₅N, A.R. grade, Aldrich, Steinheim, Germany)
- *p*-Anisaldehyde (C₈H₈O₂, Assay 99%, Sigma-aldrich, USA)
- Propionic acid (C₃H₆O₂, Assay 95%, Poison, Australia)
- Copper acetate (C₄H₆CoO₄, synthesized by Prohmsatit T.)
- Copper nitrate (Cu(NO₃)₂·3H₂O, Carlo Erba, Italy)
- Ethanol (C₂H₅OH, Assay 98%, RCI Labscan, Thailand)
- Methanol (CH₃OH, Assay 98%, RCI Labscan, Thailand)
- Methanol (CH₃OH, HPLC grade, Merck, Germany)
- Dichloromethane (CH₂Cl₂, Assay 98%, RCI Labscan, Thailand)
- Dichloromethane (CH₂Cl₂, HPLC grade, Merck, Germany)
- Acetone (C₃H₆O, Assay 98%, RCI Labscan, Thailand)
- Acetic anhydride (CH₃CO)₂O, Assay 98%, AnalaR, USA)
- Ethyl acetate (C₄H₈O₂, Assay 98%, RCI Labscan, Thailand)
- Toluene (C₇H₈, Assay 98%, RCI Labscan, Thailand)
- Hexane (C₆H₁₄, Assay 98%, RCI Labscan, Thailand)
- Chloroform (CHCl₃, Assay 98%, RCI Labscan, Thailand)
- Chloroform-*d* (CDCl₃-*d*, A.R. grade, Cambridge Isotope, USA)

- DMSO ((CH₃)₂SO)
- Magnesium sulphate anhydrous (MgSO₄, QP Panreac Quimica Sa, Barcelona)
- Distilled water (H₂O)
- Thin layer chromatography (Macherey-nagel, Germany)

3.1.2 Apparatus

Nuclear magnetic resonance spectra were recorded at 400 MHz for ¹H NMR and at 100 MHz for ¹³C NMR using a Bruker (FT-NMR advance 400 MHz) spectrometer. The FT-IR (4000-400 cm⁻¹) spectra were recorded on Perkin Elmer infrared spectrophotometer (spectrum GX). Mass spectra were obtained on Thermo Finnigan mass spectrometer (LCQ Advantage). The elemental analysis was carried out on Perkin Elmer (2400) elemental analyzer. UV-Vis absorption and fluorescence spectroscopic measurements were carried out on a Shimadzu UV-spectrometer (UV-1700) and a Jasco spectrofluorometer (FP-6200), respectively. Thermal analysis were recorded on Perkin Elmer (TGA7).

3.1.2.1 NMR spectroscopy

For ¹H NMR and ¹³C NMR, 2 mg of free base porphyrins and metalloporphyrins were dissolved in chloroform-*d*. The amount of solvent was 1 mL whereas the sample depth was at least 4 cm in the NMR tube.

3.1.2.2 FT-IR spectroscopy

FT-IR spectra of free base porphyrins, copper(II) porphyrins and nitro porphyrin were recorded in KBr in the 4000-400 cm⁻¹ region.

3.1.2.3 Mass spectrometry

The solution of free base porphyrins, copper(II) porphyrins and nitro porphyrin were prepared by dissolved 10 mg in dichloromethane (HPLC grade) and made up to 5 mL.

3.1.2.4 The elemental analysis

The sample under test is weighed in using a tin capsule. The required amount is 5-10 mg of free base porphyrins, copper(II) porphyrins and β-nitro substituted porphyrin complexes. After folding the capsule (looking rather like wrapped tin foil) the sample is placed in the auto sampler.

3.1.2.5 Absorption and fluorescence emission spectroscopy

For the preparation of 0.1 mM solution, 10 mg of free base porphyrins, copper(II) porphyrins and nitro porphyrin were dissolved and made up to 50 mL volumetric flask by dichloromethane. Properties of free base porphyrins, copper(II) porphyrins and β -nitro substituted porphyrin complexes and their derivatives characterized by UV-Vis spectroscopy in the wavelength range of 200 to 800 nm.

3.1.2.6 Thermal analysis

The thermal behaviors including the possible phase transition of free base porphyrins, copper(II) porphyrins, and β -nitro substituted porphyrin complexes were studied during the heating process at temperature of 300 to 1,173 K. The dye of 10 mg porphyrins were used and heating under nitrogen flow with scan rate 10 K/min.

3.2 Methods

3.2.1 Synthesis of alkyloxybenzaldehydes

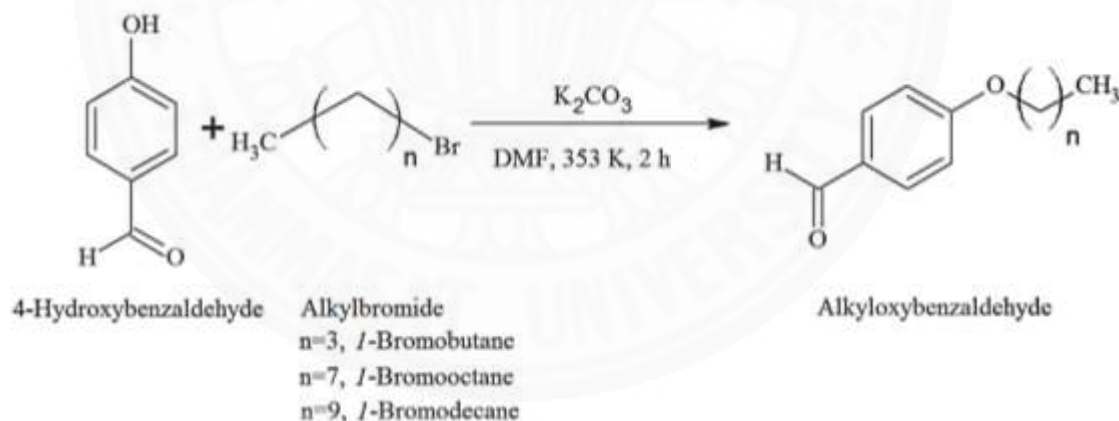


Fig. 36 Synthesis of alkyloxybenzaldehydes

1-Bromoalkane 0.05 mole (1-bromobutane 6.8510 g, 1-bromooctane 8.6368 g, and 1-bromodecane 11.0590 g) were added into the mixture of 4-hydroxybenzaldehyde 0.05 mole (6.1060 g) and K_2CO_3 0.05 mole (6.9601 g) in DMF. The resulting reaction mixture was refluxed at 353 K for 2 hours. After refluxing, the reaction mixture was cooled down to room temperature, and then the salt were filtrated. Then DMF solvent was removed to dryness. The reaction products was re-dissolved in CH_2Cl_2 (100 mL), and washed with distilled water

(4×50 mL). Magnesium sulfate anhydrous was used for drying agent. The product as yellow oil was afforded by filtration and evaporation. The reaction product was used without any farther purification. Butyloxybenzaldehyde **1** was obtained in 60% yield (5.35g). ¹H NMR (400 MHz, CDCl₃): δ 9.9 (1H, *CHO*), 7.8 (2H, Phenyl, *o*-H), 6.9 (2H, Phenyl, *m*-H), 4.0 (2H, *OCH*₂), 1.7 (2H, *-OCH*₂*CH*₂), 1.4 (2H, *-CH*₂*CH*₃), 0.9 (3H, *-CH*₃). ¹³C NMR (100 MHz, CDCl₃): δ 191, 164, 133, 115, 68, 32, 20, 14 ppm. IR (NaCl, nujol) 3072, 2960, 2873, 2737, 1690, 1603, 1509, 1466, 1389, 1161, 1023, 834 cm⁻¹. Mass m/z (ESI) calcd for C₁₁H₁₄O₂: 178.23. Found 178.8 [M]⁺

The similarly method was used to prepare both of Octyloxybenzaldehyde **2** and Dectyloxybenzaldehyde **3** with 71% yield (8.41g) and 72% yield (9.57g), respectively.

Octyloxybenzaldehyde **2** was obtained as yellow oil. ¹H NMR (400 MHz, CDCl₃): δ 9.9 (1H, *CHO*), 7.8 (2H, Phenyl, *o*-H), 6.9 (2H, Phenyl, *m*-H), 4.0 (2H, *OCH*₂), 1.8 (2H, *-OCH*₂*CH*₂), 1.4 (2H, *-CH*₂*CH*₃), 1.2 (8H, *-CH*₂*CH*₂*CH*₂), 0.8 (3H, *-CH*₃). ¹³C NMR (100 MHz, CDCl₃): δ 190, 164, 133, 114, 68, 32, 29, 23, 14 ppm. IR (NaCl, nujol) 3073, 2927, 2856, 2732, 1691, 1602, 1509, 1467, 1395, 1160, 1020, 833 cm⁻¹. Mass m/z (ESI) calcd for C₁₅H₂₂O₂: 234.33. Found 235.3 [M]⁺

Dectyloxybenzaldehyde **3** was also obtained as yellow oil. ¹H NMR (400 MHz, CDCl₃): δ 9.8 (1H, *CHO*), 7.7 (2H, Phenyl, *o*-H), 6.9 (2H, Phenyl, *m*-H), 3.9 (2H, *OCH*₂), 1.8 (2H, *-OCH*₂*CH*₂), 1.4 (2H, *-CH*₂*CH*₃), 1.2 (12H, *-CH*₂*CH*₂*CH*₂), 0.9 (3H, *-CH*₃). ¹³C NMR (100 MHz, CDCl₃): δ 190, 164, 132, 115, 68, 32, 30, 23, 14 ppm. IR (NaCl, nujol) 3074, 2926, 2855, 2732, 1693, 1602, 1509, 1467, 1393, 1160, 1017, 833 cm⁻¹. Mass m/z (ESI) calcd for C₁₇H₂₆O₂: 262.49. Found 261.2 [M]⁺

3.2.2 Synthesis of free base porphyrins

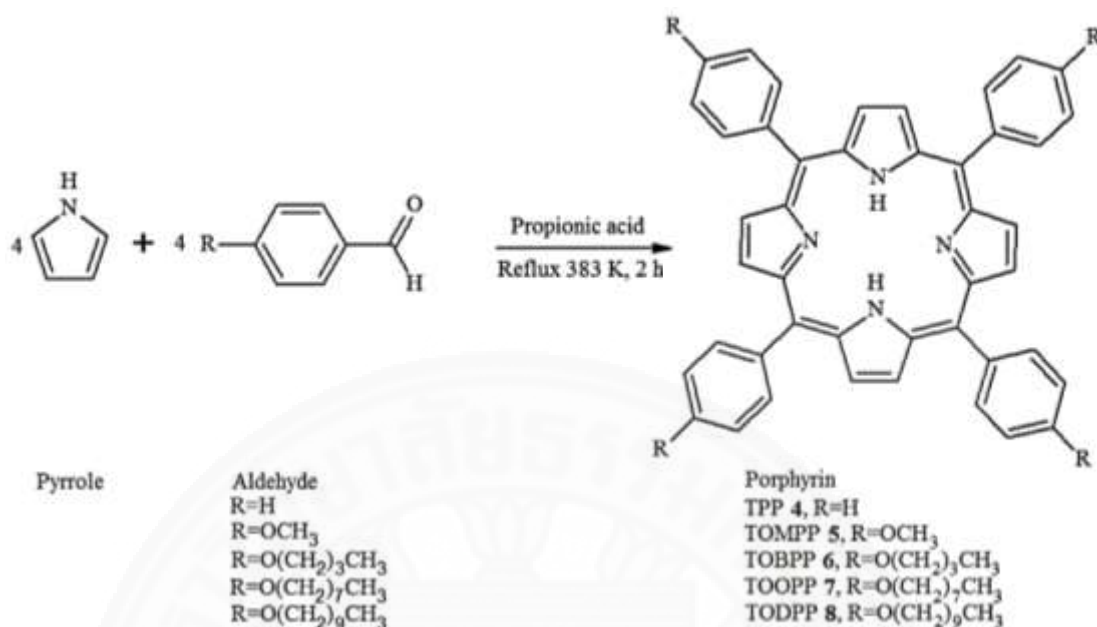


Fig. 37 Synthesis of porphyrin

Free base porphyrin and their derivatives were synthesized by following a published procedure with slight modification [22] Pyrrole 0.028 mole (2 mL) and benzaldehyde 0.03 mole (3.18 g) were taken in a 100 mL round bottom flask containing 40 mL of propionic acid. The reaction mixture was stirred and refluxed at 383 K for 2 hours. After refluxing, the reaction mixture was cooled to room temperature and added 40 mL of ethanol. Then kept it in the refrigerator overnight. The purple crystals were filtered, washed, and dried by vacuum filtration with cold ethanol to removed traces of propionic acid. The crude products were purified by silica gel column chromatography and eluted with the increasing polarity by the mixture of dichloromethane and hexane to afford TPP **4** as a purple crystal in 22% yield (0.4834 g). ¹H NMR (400 MHz, CDCl₃): δ 8.8 (8H, Pyrrole, β-H), 8.2 (8H, Phenyl, o-H), 7.7 (8H, Phenyl, m-H) ¹³C NMR (100 MHz, CDCl₃): 127.70, 134.56, 131.12, 142.22, 120.15, 126.67 ppm. IR (KBr): 3310, 3053, 3024, 1597, 1469, 1212, 1177, 966, 794 cm⁻¹. Elemental analysis; calcd (%) for C₄₄H₃₀N₄: C 86.0, H 4.9, N 9.1; found: C 85.9, H 4.9, N 9.1. Mass m/z (ESI) calcd for C₄₄H₃₀N₄ : 614.7 Found 615.0 [M+H]⁺. UV-vis (CH₂Cl₂): (λ_{abs}(nm), ε (10³M⁻¹cm⁻¹)): S-band; (417, 327.5), Q-band; (514, 14.1), (548, 6.1), (590, 4.6), (649, 3.9).

The TOMPP **5**, TOBPP **6**, TOOPP **7**, and TODPP **8** were prepared similarly to

TPP **4**, with changed benzaldehyde to *p*- anisaldehyde, butyloxybenzaldehyde, octyloxybenzaldehyde, dectyloxybenzaldehyde respectively. It were obtained in 26%, 9%, 12%, and 9% yield, respectively. The tetrakis(4-methoxyphenyl)porphyrin (TOMPP **5**) was obtained in 26% yield (0.5988 g) as purple crystal. ^1H NMR (400 MHz, CDCl_3): δ 8.8 (8H, Pyrrole, β -H), 8.1 (8H, Phenyl, *o*-H), 7.2 (8H, Phenyl, *m*-H), 4.1 (12H, -OCH₃). ^{13}C NMR (100 MHz, CDCl_3): 158.75, 134.68, 133.99, 129.97, 127.89, 118.83, 111.44, 54.65 ppm. IR (KBr): 3316, 2931, 2834, 1607, 1509, 1248, 1174, 966, 804 cm^{-1} . Elemental analysis; calcd (%) for $\text{C}_{48}\text{H}_{38}\text{N}_4\text{O}_4$: C 78.45, H 5.21, N 7.62; found: C 76.42, H 5.75, N 7.42. Mass m/z (ESI) calcd for $\text{C}_{48}\text{H}_{38}\text{N}_4\text{O}_4$: 734.84 Found 735.4 $[\text{M}+\text{H}]^+$. UV-vis (CH_2Cl_2): ($\lambda_{\text{abs}}(\text{nm})$, ϵ ($10^3\text{M}^{-1}\text{cm}^{-1}$)): S-band; (421, 296.9), Q-band; (518, 11.9), (555, 8.2), (595, 3.9), (650, 5.2).

The tetrakis(4-butyloxyphenyl)porphyrin (TOBPP **6**) was obtained as purple crystal in 9% yield. ^1H NMR (400 MHz, CDCl_3): δ 8.9 (8H, Pyrrole, β -H), 8.1 (8H, Phenyl, *o*-H), 7.4 (8H, Phenyl, *m*-H), 4.2 (-OCH₂), 1.9 (-OCH₂CH₂), 1.3 (-CH₂CH₃), 0.9 (-CH₃). ^{13}C NMR (100 MHz, CDCl_3): 159.09, 135.32, 134.74, 130.70, 128.76, 119.7, 112.84, 68.14, 31.49, 23.98, 13.84 ppm. IR (KBr): 3320, 2931, 2868, 1607, 1509, 1245, 1174, 966, 802 cm^{-1} . Elemental analysis; calcd (%) for $\text{C}_{60}\text{H}_{62}\text{N}_4\text{O}_4$: C 79.79, H 6.92, N 6.20; found: C 79.44, H 6.55, N 5.83. Mass m/z (ESI) calcd for $\text{C}_{60}\text{H}_{62}\text{N}_4\text{O}_4$: 903.16. Found 903.6 $[\text{M}+\text{H}]^+$. UV-vis (CH_2Cl_2): ($\lambda_{\text{abs}}(\text{nm})$, ϵ ($10^3\text{M}^{-1}\text{cm}^{-1}$)): S-band; (422, 530.6), Q-band; (519, 22.9), (556, 17.3), (595, 8.6), (651, 11.6).

The tetrakis(4-octyloxyphenyl)porphyrin (TOOPP **7**) was obtained in 12% yield as purple crystal. ^1H NMR (400 MHz, CDCl_3): δ 8.8 (8H, Pyrrole, β -H), 8.2 (16H, Phenyl, *o*-H and *m*-H), 4.2 (-OCH₂), 1.9 (-OCH₂CH₂), 1.3 (-CH₂CH₃), 1.2 (-CH₂CH₂CH₂), 0.9 (-CH₃). ^{13}C NMR (100 MHz, CDCl_3): 159.07, 135.54, 134.57, 131.78, 128.74, 119.79, 112.82, 68.45, 31.84, 29.64, 29.53, 29.45, 26.22, 22.64, 14.00 ppm. IR (KBr): 3318, 2927, 2852, 1607, 1509, 1243, 1174, 965, 804 cm^{-1} . Elemental analysis; calcd (%) for $\text{C}_{76}\text{H}_{94}\text{N}_4\text{O}_4$: C 80.95, H 8.40, N 4.97; found: C 81.10, H 8.25, N 4.93. Mass m/z (ESI) calcd for $\text{C}_{76}\text{H}_{94}\text{N}_4\text{O}_4$: 1125.57. Found 1127.9 $[\text{M}+\text{H}]^+$. UV-vis (CH_2Cl_2): ($\lambda_{\text{abs}}(\text{nm})$, ϵ ($10^3\text{M}^{-1}\text{cm}^{-1}$)): S-band; (422, 611.7), Q-band; (519, 30.9), (556, 24.7), (595, 15.7), (651, 17.4).

The tetrakis(4-decyloxyphenyl)porphyrin (TODPP **8**) was obtained as purple crystal in 9% yield. ^1H NMR (400 MHz, CDCl_3): δ 8.8 (8H, Pyrrole, β -H), 8.0 (16H,

Phenyl, *o*-H and *m*-H), 4.2 (-OCH₂), 1.9 (-OCH₂CH₂), 1.3 (-CH₂CH₃), 1.2 (-CH₂CH₂), 0.8 (-CH₃). ¹³C NMR (100 MHz, CDCl₃): 159.10, 135.51, 134.51, 130.68, 128.76, 119.77, 112.86, 68.48, 31.88, 29.60, 29.55, 29.53, 29.46, 29.28, 26.20, 22.60, 13.93 ppm. IR (KBr): 3317, 2924, 2852, 1607, 1509, 1244, 1174, 967, 803 cm⁻¹. Elemental analysis; calcd (%) for C₈₄H₁₁₀N₄O₄: C 81.37, H 8.94, N 4.52; found: C 81.24, H 8.99, N 4.58. Mass m/z (ESI) calcd for C₈₄H₁₁₀N₄O₄: 1237.17. Found 1239.0 [M+H]⁺. UV-vis (CH₂Cl₂): (λ_{abs}(nm), ε (10³M⁻¹cm⁻¹)): S-band; (422, 440.5), Q-band; (519, 20.8), (556, 15.7), (595, 8.4), (652, 10.6).

3.2.3 Synthesis of copper(II)porphyrins

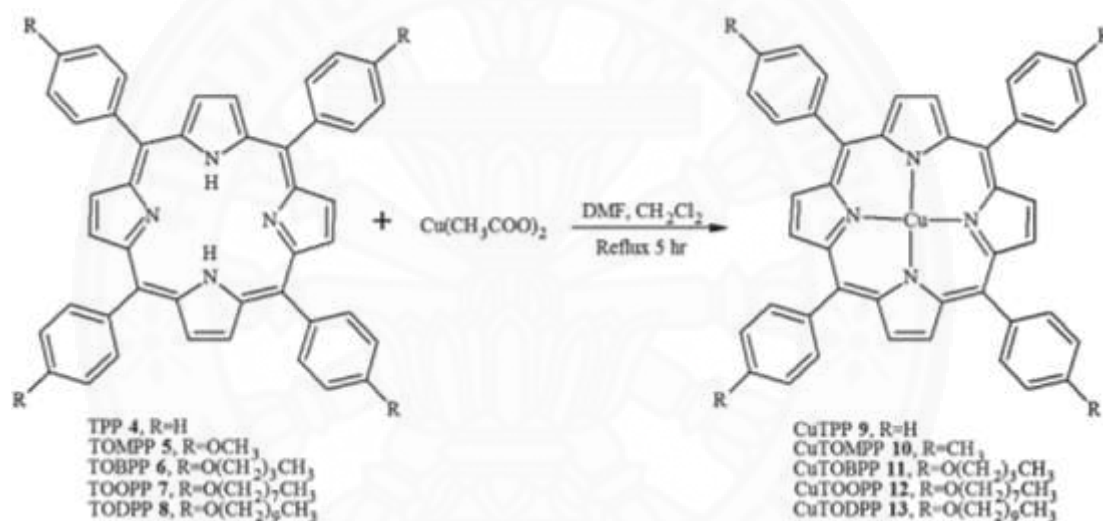


Fig. 38 Synthesis of copper(II)porphyrin

The copper(II) was inserted into each free base porphyrin by following the modification of published procedure [ref]. The copper (II) derivative of tetraphenylporphyrin (CuTPP **9**) was obtained in 93%yield (0.4672 g) by refluxing tetraphenylporphyrin (TPP **4**) 0.3 mole (0.1842 g) with an excess copper acetate [Cu(OAc)₂·3H₂O] in mixed solvent between DMF (15 mL) and dichloromethane (15 mL) for 5 hours. After refluxing, the reaction mixture was cooled to room temperature. The mixture was kept in refrigerator overnight after adding distilled water. Finally, the purple crystals were filtrate, washed, and dried by vacuum filtration with cold methanol. The reaction products were purified by silicagel column chromatography and eluted with the increasing polarity by the mixture of dichloromethane and hexane to afford CuTPP **9**

as a purple crystal. IR (KBr): 3052, 3023, 1600, 1441, 1345, 1165, 793 cm^{-1} . Elemental analysis; calcd (%) for $\text{CuC}_{44}\text{H}_{28}\text{N}_4$: C 78.15, H 4.17, N 8.28; found: C 76.90, H 3.94, N 8.18. Mass m/z (ESI) calcd for $\text{CuC}_{44}\text{H}_{28}\text{N}_4$: 676.27. Found 677 $[\text{M}+\text{H}]^+$. UV-vis (CH_2Cl_2): ($\lambda_{\text{abs}}(\text{nm})$, ϵ ($10^3\text{M}^{-1}\text{cm}^{-1}$)): S-band; (415, 415.9), Q-band; (540, 13.8), (647, 1.3). Other copper porphyrin derivative of CuTOMPP **10**, CuTOBPP **11**, CuTOOPP **12**, and CuTODPP **13** have been synthesized by using similarly method same CuTPP, and they can obtained in 92%, 71.%, 96%, and 63% respectively.

The tetrakis(4-methoxyphenyl)phenylporphyrinatocopper(II) (CuTOMPP **10**) was synthesized by reaction between TOMPP **5** and copper acetate. The product was obtained as purple crystal in 92% yield. IR (KBr): 2929, 2835, 1607, 1499, 1248, 1173, 804 cm^{-1} . Elemental analysis; calcd (%) for $\text{CuC}_{48}\text{H}_{36}\text{N}_4\text{O}_4$: C 72.42, H 4.52, N 7.03; found: C 60.42, H 4.17, N 6.22. Mass m/z (ESI) calcd for $\text{CuC}_{48}\text{H}_{36}\text{N}_4\text{O}_4$: 796.38. Found 797.4 $[\text{M}+\text{H}]^+$. UV-vis (CH_2Cl_2): ($\lambda_{\text{abs}}(\text{nm})$, ϵ ($10^3\text{M}^{-1}\text{cm}^{-1}$)): S-band; (419, 402.5), Q-band; (541, 18.9), (653, 3.6).

The tetrakis(4-butyloxyphenyl)phenylporphyrinatocopper(II) (CuTOBPP **11**) was synthesized by reaction between TOBPP **6** and copper acetate. The product was obtained as purple crystal in 71% yield. IR (KBr): 2930, 2869, 1607, 1502, 1246, 1174, 799 cm^{-1} . Elemental analysis; calcd (%) for $\text{CuC}_{60}\text{H}_{60}\text{N}_4\text{O}_4$: C 74.77, H 6.23, N 5.82; found: C 74.51, H 6.25, N 5.76. Mass m/z (ESI) calcd for $\text{CuC}_{60}\text{H}_{60}\text{N}_4\text{O}_4$: 964.70. Found 965.6 $[\text{M}+\text{H}]^+$. UV-vis (CH_2Cl_2): ($\lambda_{\text{abs}}(\text{nm})$, ϵ ($10^3\text{M}^{-1}\text{cm}^{-1}$)): S-band; (419, 415.4), Q-band; (541, 24.5), (578, 9.6), (618, 7.2).

The tetrakis(4-octyloxyphenyl)phenylporphyrinatocopper(II) (CuTOOPP **12**) was synthesized by reaction between TOOPP **7** and copper acetate. The product was obtained as purple crystal in 96% yield. IR (KBr): 2926, 2852, 1607, 1506, 1244, 1174, 804 cm^{-1} . Elemental analysis; calcd (%) for $\text{CuC}_{76}\text{H}_{92}\text{N}_4\text{O}_4$: C 76.83, H 7.75, N 4.73; found: C 68.65, H 6.95, N 4.40. Mass m/z (ESI) calcd for $\text{CuC}_{76}\text{H}_{92}\text{N}_4\text{O}_4$: 1187.11. Found 1187.0 $[\text{M}+\text{H}]^+$. UV-vis (CH_2Cl_2): ($\lambda_{\text{abs}}(\text{nm})$, ϵ ($10^3\text{M}^{-1}\text{cm}^{-1}$)): S-band; (419, 380.4), Q-band; (541, 29.0).

The tetrakis(4-decyloxyphenyl)phenylporphyrinatocopper(II) (CuTODPP **13**) was synthesized by reaction between TODPP **8** and copper acetate. The product was obtained as purple crystal in 63% yield. IR (KBr): 2923, 2852, 1607, 1504, 1246, 1174, 800 cm^{-1} . Elemental analysis; calcd (%) for $\text{CuC}_{84}\text{H}_{108}\text{N}_4\text{O}_4$: C 77.60, H 8.31, N 4.31;

found: C 66.91, H 7.30, N 3.80. Mass m/z (ESI) calcd for $\text{CuC}_{84}\text{H}_{108}\text{N}_4\text{O}_4$: 1299.32. Found 1303.7 $[\text{M}+\text{H}]^+$. UV-vis (CH_2Cl_2): ($\lambda_{\text{abs}}(\text{nm})$, ϵ ($10^3 \text{ M}^{-1}\text{cm}^{-1}$)): S-band; (419, 311.1), Q-band; (541, 14.2), (578, 4.5), (616, 3.2).

3.2.4 Synthesis of β -nitro substituted porphyrins

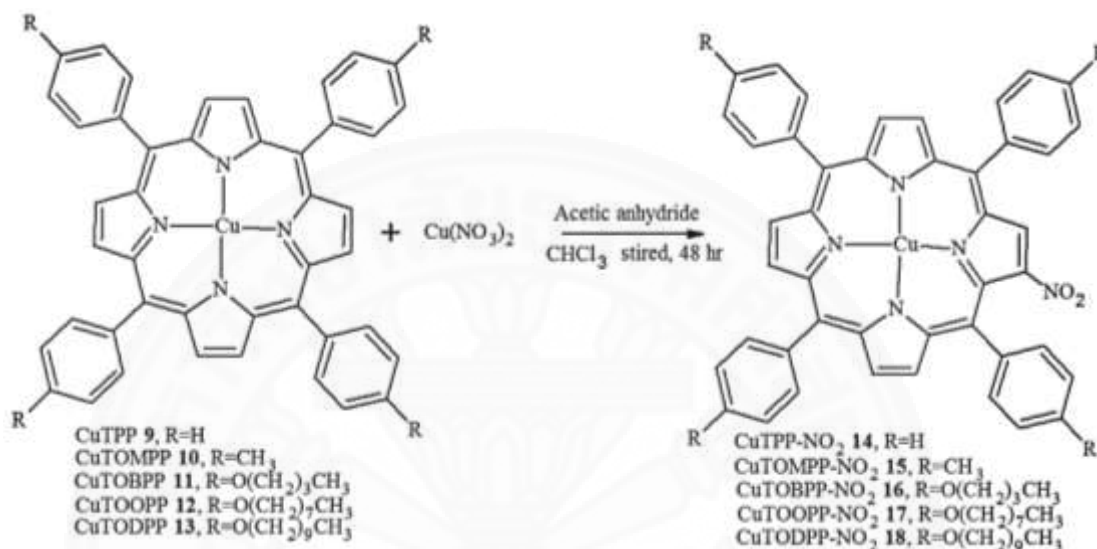


Fig. 39 Synthesis of β -nitro substituted porphyrin

The β -nitro porphyrin derivative have been synthesized via nitration reaction of copper porphyrin following a previous method [60]. The copper tetraphenyl (CuTPP **9**) 0.3 mmole (0.2028g) was dissolved in 100 mL of chloroform solvent in 250 mL round bottom flask. The copper nitrate $[\text{Cu}(\text{NO}_3)_2 \cdot 3\text{H}_2\text{O}]$ 0.5 mmole (0.1208g) and acetic anhydride 9 mL were added in the solution. The synthetic mixture was magnetically stirred for 48 hours at room temperature. After that the mixture was washed with water 4×50 mL. The organic solvent was removed. Then, the final products were purified by silica gel column chromatography and eluted with the increasing polarity by the mixture of dichloromethane and hexane to afford 2-nitro-tetraphenylporphyrinatocopper(II) (CuTPP- NO_2 **14**) as a purple crystal in 31% yield. IR (KBr): 1618, 1442, 1328, 1516, 1342, 799 cm^{-1} . Elemental analysis; calcd (%) for $\text{CuC}_{44}\text{H}_{27}\text{N}_5\text{O}_2$: C 73.33, H 3.75, N 9.72; found: C 73.30, H 3.81, N 9.46. Mass m/z (ESI) calcd for $\text{CuC}_{44}\text{H}_{27}\text{N}_5\text{O}_2$: 721.27. Found 722.3 $[\text{M}+\text{H}]^+$. UV-vis (CH_2Cl_2): ($\lambda_{\text{abs}}(\text{nm})$, ϵ ($10^3 \text{ M}^{-1}\text{cm}^{-1}$)): S-band; (422, 295.3), Q-band; (548, 23.2), (590, 15.4). The similarly reaction was used to synthesized

CuTOMPP-NO₂ **15**, CuTOBPP-NO₂ **16**, CuTOOPP-NO₂ **17**, and CuTODPP-NO₂ **18**. They can be obtained in 13%, 8%, 17%, and 28% yield respectively.

The 2-nitro-tetrakis(4-methoxyphenyl)phenylporphyrinatocopper(II) (CuTOMPP-NO₂ **15**) was prepared by nitration reaction of CuTOMPP **10**. The product was obtained as purple crystal in 92% yield. IR (KBr): 2928, 2830, 1607, 1502, 1249, 1174, 1510, 1340, 801 cm⁻¹. Elemental analysis; calcd (%) for CuC₄₈H₃₅N₅O₆: C 65.93, H 4.07, N 7.92; found: C 66.04, H 4.17, N 7.68. Mass m/z (ESI) calcd for CuC₄₈H₃₅N₅O₆: 841.38. Found 841.8 [M+H]⁺. UV-vis (CH₂Cl₂): (λ_{abs}(nm), ε (10³ M⁻¹cm⁻¹)): S-band; (428, 188.9), Q-band; (551, 15.0), (594, 11.5).

The 2-nitro-tetrakis(4-butyloxyphenyl)phenylporphyrinatocopper(II) (CuTOBPP-NO₂ **16**) was prepared by nitration reaction of CuTOBPP **11**. The product was obtained as purple crystal in 8% yield. IR (KBr): 2927, 2870, 1607, 1506, 1256, 1174, 1521, 1340, 800 cm⁻¹. Elemental analysis; calcd (%) for CuC₆₀H₅₉N₅O₆: C 71.43, H 5.85, N 6.94; found: C 72.79, H 8.27, N 4.38. Mass m/z (ESI) calcd for CuC₆₀H₅₉N₅O₆: 1009.7. Found 1009.6 [M+H]⁺. UV-vis (CH₂Cl₂): (λ_{abs}(nm), ε (10³ M⁻¹cm⁻¹)): S-band; (429, 238.1), Q-band; (552, 20.6), (596, 16.5).

The 2-nitro-tetrakis(4-octyloxyphenyl)phenylporphyrinatocopper(II) (CuTOOPP-NO₂ **17**) was prepared by nitration reaction of CuTOOPP **12**. The product was obtained as purple crystal in 14% yield. IR (KBr): 2927, 2855, 1607, 1505, 1247, 1174, 1509, 1341, 800 cm⁻¹. Elemental analysis; calcd (%) for CuC₇₆H₉₁N₅O₆: C 74.03, H 7.39, N 5.68; found: C 74.12, H 7.28, N 5.54. Mass m/z (ESI) calcd for CuC₇₆H₉₁N₅O₆: 1232.11. Found 1234.2 [M+H]⁺. UV-vis (CH₂Cl₂): (λ_{abs}(nm), ε (10³ M⁻¹cm⁻¹)): S-band; (430, 304.6), Q-band; (554, 24.0), (595, 19.0).

The 2-nitro-tetrakis(4-decyloxyphenyl)phenylporphyrinatocopper(II) (CuTODPP-NO₂ **18**) was prepared by nitration reaction of CuTODPP **13**. The product was obtained as purple crystal in 28% yield. IR (KBr): 2923, 2853, 1606, 1506, 1247, 1173, 1509, 1341, 800 cm⁻¹. Elemental analysis; calcd (%) for CuC₈₄H₁₀₇N₅O₆: C 75.00, H 7.96, N 5.21; found: C 74.95, H 7.95, N 5.10. Mass m/z (ESI) calcd for CuC₈₄H₁₀₇N₅O₆: 1344.32. Found 1344.8 [M+H]⁺. UV-vis (CH₂Cl₂): (λ_{abs}(nm), ε (10³ M⁻¹cm⁻¹)): S-band; (430, 364.3), Q-band; (552, 28.2), (596, 21.5).

3.2.5 Biological activity

The antibacterial activities were evaluated against *Staphylococcus aureus* (ATCC 25923) and *Escherichia coli* (ATCC 25922) by Disc diffusion method [63]. The compounds were dissolved in DMSO (solvent control) to obtain concentration of 1 mg/mL. Nutrient agar medium was prepared by using nutrient broth 4.00 g and agar 7.50 g in water. The disc of Whatmann No.1 filter paper having the diameter 5 mm, autoclave priors used. The compound solution 30 μ L (1,000 ppm) are applied on disc then placed over the media. The DMSO was served as control solvent, while penicillin (1 mg/mL) was selected for standard drug. The samples were incubated for 24 hours at 37 ± 2 °C. The inhibition zone was carefully measured in mm. Furthermore, the minimum inhibitory concentration (MIC) and the minimum bactericidal concentration (MBC) have been determined. The minimum inhibitory concentration (MIC) was observed by microbroth dilution method [67]. Stock solution (1,280 ppm) of all synthesized porphyrins were prepared in DMSO. The test solution were dilute with nutrient broth medium to reduce the haft of concentration in 96-well microplate. Then 50 μ L of bacterial cell was added in each well. The final volume is 100 μ L. The microplate were incubated for 18 hours at 37 ± 2 °C. After that 10 μ L of 0.18% resazurin were added in all well and incubated for 2 hours at 37 ± 2 °C. The MIC value is the lowest concentration of a chemical that prevents visible growth of a bacteria, which can observed by the color in the last well change to purple. After that the minimum bactericidal concentration (MBC) value were investigated by streak result solution from MIC tested that didn't found the bacterial growth (purple solution) on nutrient broth medium, incubated for 18 hours at 37 ± 2 °C. The minimum bactericidal concentration (MBC) is the concentration that results in microbial death.

3.2.6 Gases sensing application

The 2-nitro-tetraphenylporphyrinato copper (II) complex was fabricated as film for test as gas sensor. This film was prepared similarly with previous reported [66]. The CuTPP-NO₂ was dissolved in 5 mg/mL chloroform, and was dropping onto the cleaned glass slide (21.2 mm \times 25.3 mm \times 1.3 mm). **Fig. 40a** shows modified a UV-Vis spectrophotometer to acting a so-called "electronic nose", and **Fig 40b** shows the diagram of the electronic nose system set up [66]. It allows the dynamic measurement

of the absorption change due to the interaction of CuTPP-NO₂ film with flow-in gases. These instruments were supported by Faculty of Medical Technology, Mahidol University. For gas sensing measurement, the CuTPP-NO₂ film was placed perpendicular in front of the light source inside the chamber to interact with the sampled gases. The acquired data can be then analyzed in real-time by in-house software based on Principle Component Analysis (PCA).



Fig. 40a The modified UV-Vis spectrophotometer “electronic nose”

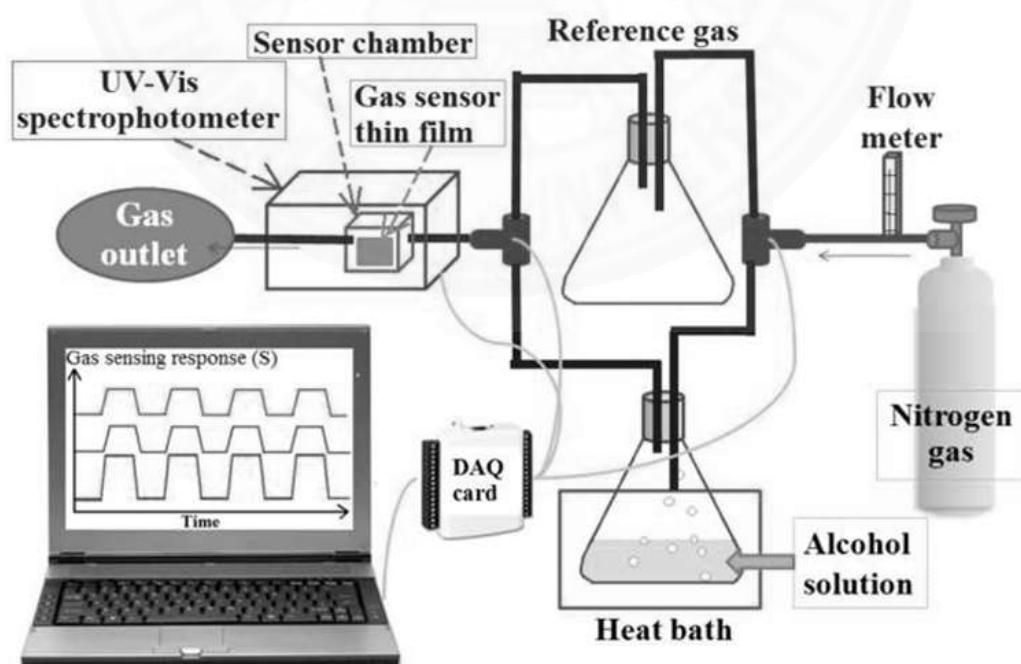


Fig. 40b the diagram of the electronic nose system set up [66]

CHAPTER 4

RESULTS AND DISCUSSION

4.1 Aldehyde synthesis and characterization

The aldehyde with long chain alkane, including butyloxybenzaldehyde **1**, octyloxybenzaldehyde **2** and decyloxybenzaldehyde **3** (**Fig. 42**) were obtained as a yellow oil by refluxing 4-hydroxybenzaldehyde, K_2CO_3 and various alkylbromide in DMF. The reaction was heated at 353 K for 2 hours. The butyloxybenzaldehyde **1** was obtained about 51 - 54% while, both of octyloxybenzaldehyde **2** and decyloxybenzaldehyde **3** were obtained over 70%. The characterization data of aldehydes were displayed in **Table. 2**

Table. 2 Characteristic data of aldehydes 1-3

Compounds	Empirical formula	Yield (%)	Formula weight	MS (m/z) [M+H] ⁺
Butyloxybenzaldehyde 1	$C_{11}H_{14}O_2$	60	178.2	178.8
Octyloxybenzaldehyde 2	$C_{15}H_{22}O_2$	71	234.3	235.3
Decyloxybenzaldehyde 3	$C_{17}H_{26}O_2$	72	262.3	261.2

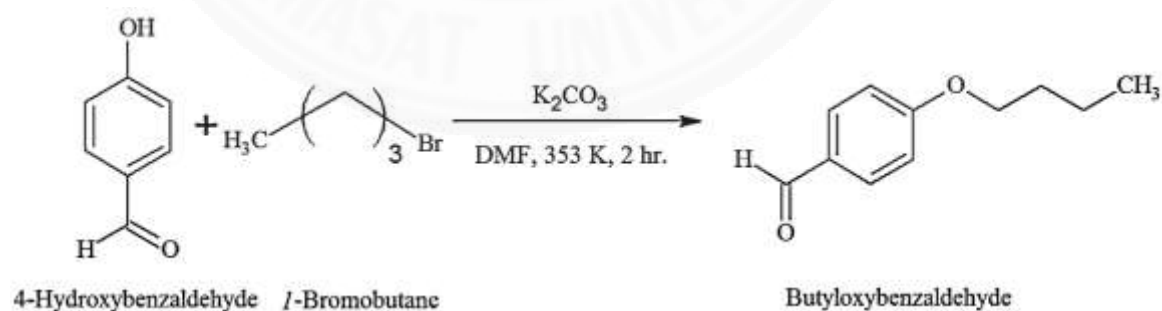


Fig. 41 Synthesis of butyloxybenzaldehyde **1**

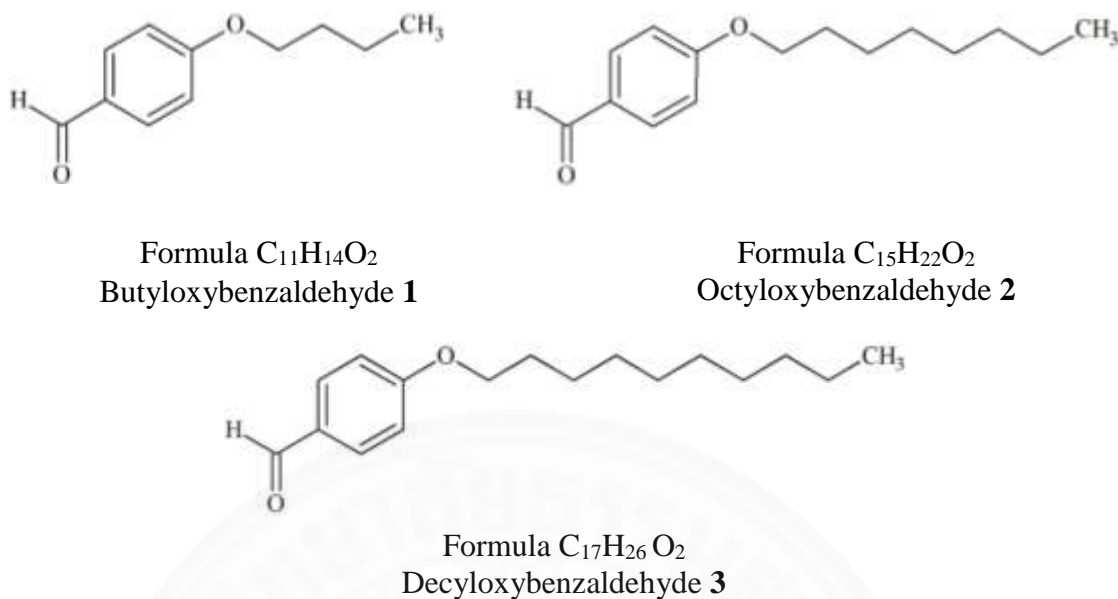


Fig. 42 The structure of aldehyde **1 – 3**

4.1.1 Mass spectrometry

For the synthesis of three benzaldehyde derivatives, mass spectrometry had been used to confirmed the aldehydes structure. **Fig. 43** shows mass spectrum of butyloxybenzaldehyde **1** (without purification). The mass spectrum of butyloxybenzaldehyde **1** shows the strong molecular ion peak $[M+H]^+$ at $m/z = 178.8$. Furthermore, the fragmentation peaks were founded. The fragmentation reaction of butyloxybenzaldehyde **1** is due to the loss of an alkyl group the long chain, similarly to the previous reported by M. Rosario M.D. [71]. The fragment showed peaks at $m/z = 135.0$ and 122.9 , that from the methyl and methylene group loss, and the peak at $m/z = 122.9$ that represent the mass of parent compound (*4*-hydroxybenzaldehyde). In addition the octyloxybenzaldehyde **2** and, decyloxybenzaldehyde **3** were obtained similarly result of butyloxybenzaldehyde **1** due to the loss of methyl and methylene groups from alkyl long chain. The octyloxybenzaldehyde **2** and, decyloxybenzaldehyde **3** show the molecular ion peak $[M+H]^+$ at $m/z = 235.3$ and 216.2 respectively. The mass spectrometry data of all aldehyde were show in **Table. 2**

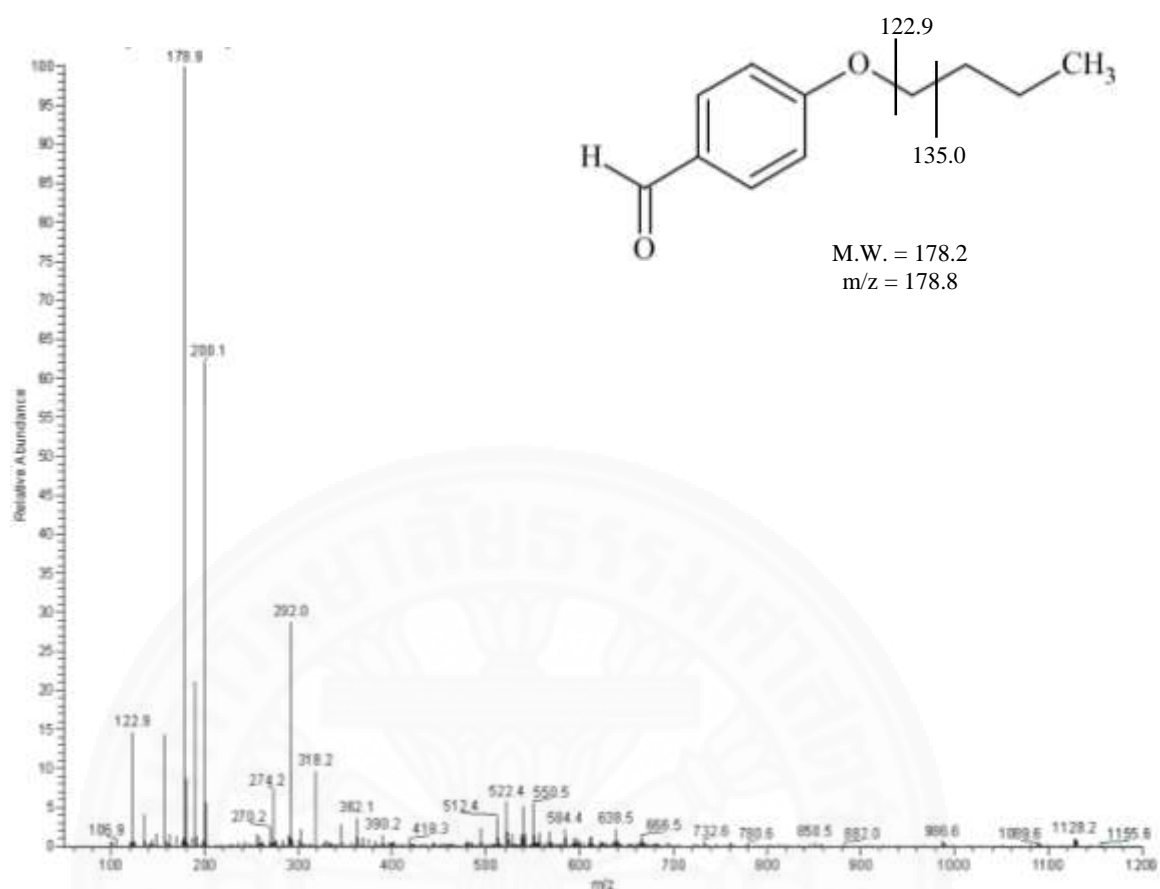


Fig. 43 Mass spectrum of butyloxybenzaldehyde 1

4.1.2 NMR spectroscopy

Both of ^1H NMR and ^{13}C NMR study of all benzaldehyde derivatively (butyloxybenzaldehyde **1**, octyloxybenzaldehyde **2** and, decyloxybenzaldehyde **3**) were studied in CDCl_3 at room temperature.

The ^1H NMR of Butyloxybenzaldehyde **1** exhibits characteristic chemical shift arising from proton at carbonyl group of aldehyde (CHO) at 9.9 ppm, due to the magnetic anisotropy the carbonyl group. The *ortho*- and *para*- proton of phenyl were showed two doublets peaks at 7.8 and 6.9 ppm, respectively. Moreover, the signal of proton from alkyl long chain were observed at 4.0, 1.7, 1.5, and 0.9 ppm. The signal at 4.0 ppm show triplet peak that was assigned to proton of the ether group of alkyl long chain ($-\text{OCH}_2$). The quintet and sextet signal peak at 1.7 and 1.5 ppm were corresponded to methylene proton of alkyl long chain ($-\text{OCH}_2\text{CH}_2-$). The methyl at the end of alkyl long chain show the triplet peak at 0.9 ppm. The ^1H NMR spectrum of butyloxybenzaldehyde **1** show at **Fig. 44** Other benzaldehyde derivatively (octyloxybenzaldehyde **2** and, decyloxybenzaldehyde **3**) exhibited the ^1H NMR signal similarly the butyloxybenzaldehyde **1**. However, the signal of methylene proton of octyloxybenzaldehyde **2** and, decyloxybenzaldehyde **3** that were observed the multiplet peak around 1.3 – 1.1 ppm.

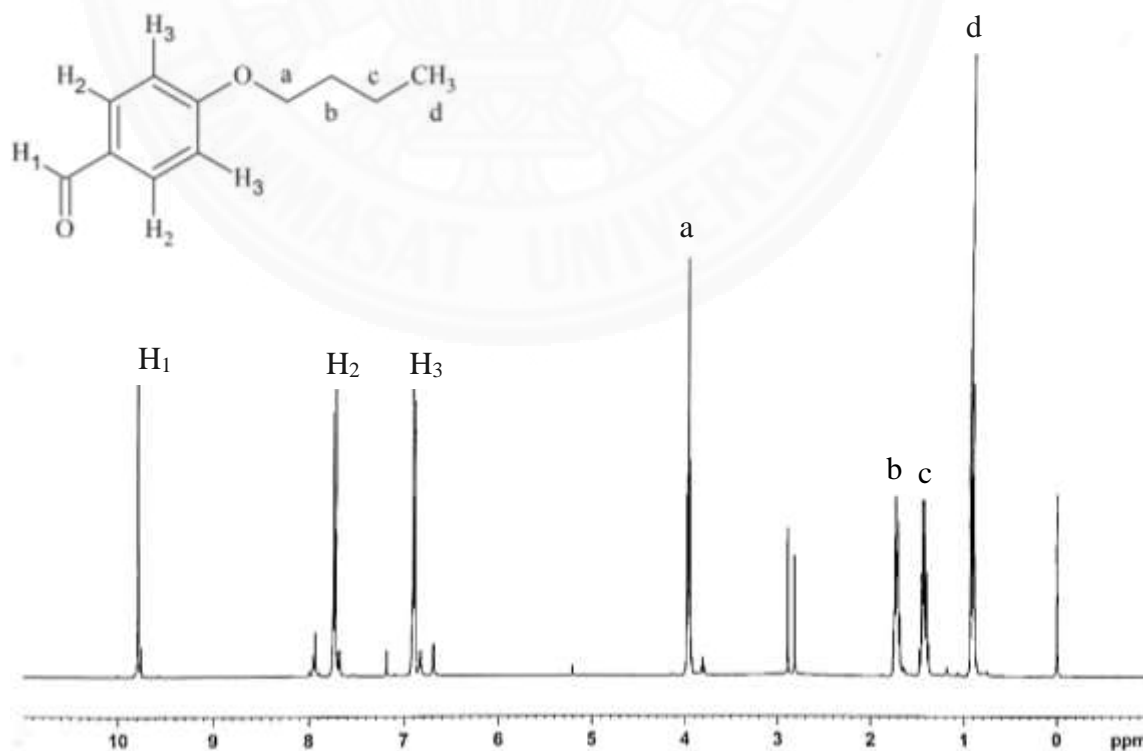


Fig. 44 ^1H NMR spectrum of butyloxybenzaldehyde **1**.

The ^{13}C NMR spectrum of butyloxybenzaldehyde **1** was shown in **Fig. 45**. The signal peak at 190.76 ppm was assigned to carbonyl carbon (CHO) at C_1 position. The carbon of phenyl ring showed four peaks at the chemical shift between 144.46 – 169.62 ppm. Next, the signal peak methylene carbon that near the oxygen atom (C_2) was show at 68.14 ppm, due to the deshielded effect of oxygen atom the similar result was reported by Iannis D.K. [33]. While, the methylene carbon at C_3 and C_4 position were founded the signal at 31.25 and 19.20 ppm respectively. Finally, the methyl carbon at the end of alkyl long chain (C_5 position) was shown signal at 13.66 ppm. The similar result were observed in octyloxybenzaldehyde **2** and, decyloxybenzaldehyde **3**, and the data were summarized in **Table. 3**. The NMR result are in agreement with the previous reported by Debora S.S.C. [72]. The ^1H and ^{13}C NMR were successfully confirmed the corresponding structure of all the benzaldehyde derivative.

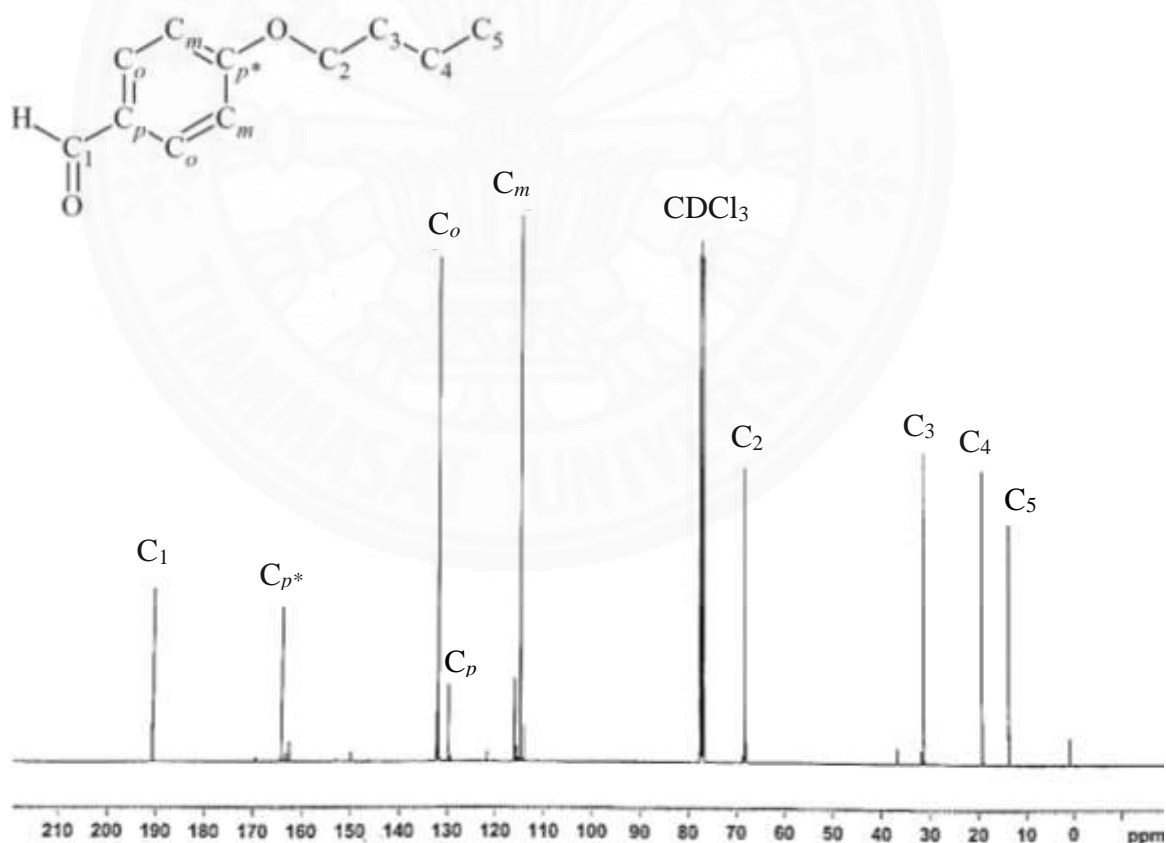


Fig. 45 ^{13}C NMR spectrum of butyloxybenzaldehyde **1**.

Table. 3 ^1H and ^{13}C NMR spectroscopic data for aldehydes **1-3**.

Aldehyde	^1H NMR (ppm), proton							
	<i>CHO</i>	Phenyl, <i>o-H</i>	Phenyl, <i>m-H</i>	<i>OCH</i> ₂	<i>OCH</i> ₂ <i>CH</i> ₂	<i>CH</i> ₂ <i>CH</i> ₃	<i>CH</i> ₂ <i>CH</i> ₂ <i>CH</i> ₂	<i>CH</i> ₃
Butyloxybenzaldehyde 1	9.9 (1H)	7.8 (2H)	6.9 (2H)	4.0 (2H)	1.7 (2H)	1.5 (2H)	-	0.9 (3H)
Octyloxybenzaldehyde 2	9.9 (1H)	7.8 (2H)	6.9 (2H)	4.0 (2H)	1.8 (2H)	1.4 (2H)	1.2 (8H)	0.8 (3H)
Decyloxybenzaldehyde 3	9.8 (1H)	7.7 (2H)	6.9 (2H)	3.9 (2H)	1.8 (2H)	1.4 (2H)	1.2 (12H)	0.9 (3H)

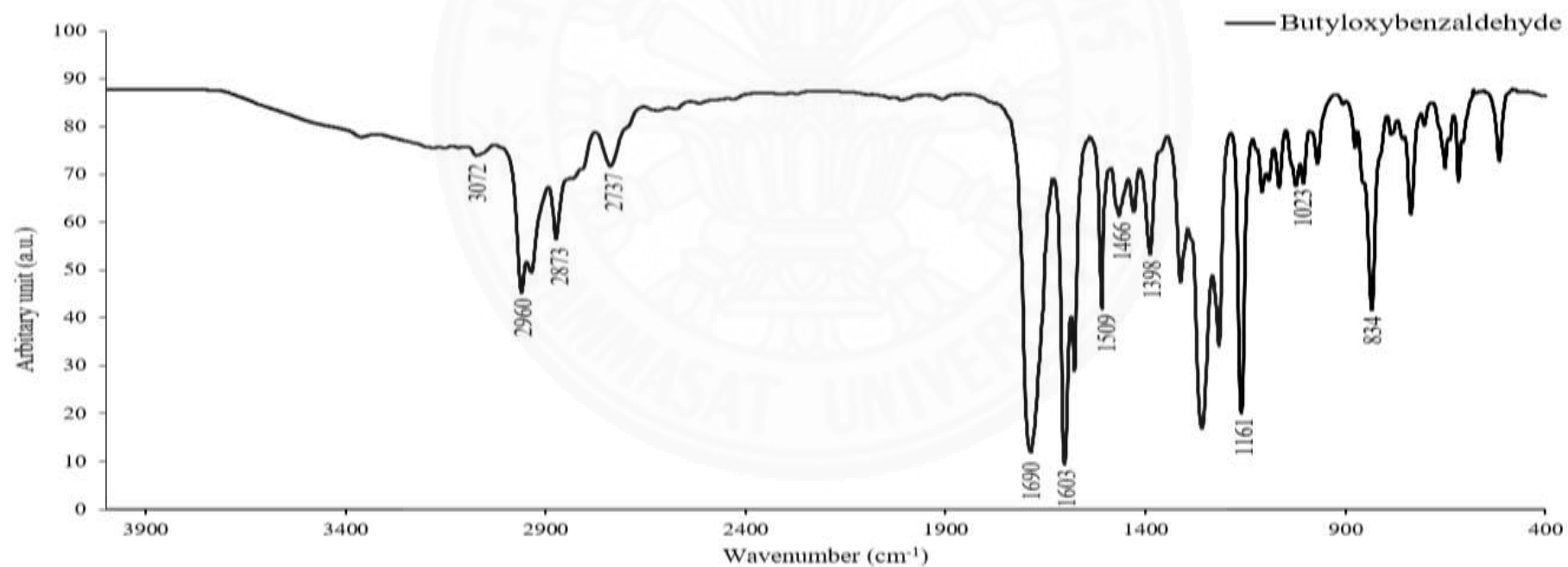
Aldehyde	^{13}C NMR (ppm), carbon								
	<i>CHO</i>	Phenyl, <i>p-C</i>	Phenyl, <i>o-C</i>	Phenyl, <i>m-C</i>	<i>OCH</i> ₂	<i>OCH</i> ₂ <i>CH</i> ₂	<i>CH</i> ₂ <i>CH</i> ₂ <i>CH</i> ₂	<i>CH</i> ₂ <i>CH</i> ₃	<i>CH</i> ₃
Butyloxybenzaldehyde 1	190 (1C)	164 (1C)	133 (1C)	115 (1C)	68 (1C)	32 (1C)	-	20 (1C)	14 (1C)
Octyloxybenzaldehyde 2	190 (1C)	164 (1C)	133 (1C)	114 (1C)	68 (1C)	32 (1C)	29 (4C)	23 (1C)	14 (1C)
Decyloxybenzaldehyde 3	190 (1C)	164 (2C)	132 (1C)	115 (1C)	68 (1C)	32 (1C)	30 (6C)	23 (1C)	14 (1C)

4.1.3 Infrared spectroscopy

The functional group of alkyloxybenzaldehydes were confirmed by IR spectroscopy technique. That was recorded by nujol in NaCl discs. The data were collected in the 4000 – 400 cm^{-1} region. The summarized data of all aldehyde were show in **Table. 4**. All aldehyde show the similarly wavenumber with a little peak shift, due to the effect of alkyl long chain group. **Fig. 47** show the IR spectra of butyloxybenzaldehyde **1** as a representative. The characteristic peak of aldehyde functional group were show two peak of C-H stretching at 2873 and 2757 cm^{-1} including C=O stretching at 1690 cm^{-1} . Other aldehyde show the characteristic peak at the similarly wavenumber, but the signal of aldehyde C-H stretching of octyloxybenzaldehyde **2** and, decyloxybenzaldehyde **3** were decreased when the number of carbon in alkyl chain were increased. Next, the signal at 3072 cm^{-1} were assigned to the C-H sp^2 stretching of phenyl ring and two signals at 1603 and 1509 cm^{-1} , represented the C=C stretching in the phenyl ring. Moreover, the IR spectra of butyloxybenzaldehyde **1** show a C-H sp^3 stretching band of alkyl long chain at 2960 cm^{-1} . The decreasing of wavenumber were observed in octyloxybenzaldehyde **2** and, decyloxybenzaldehyde **3**. The peaks at 1466 and 1389 cm^{-1} were assigned to CH_3 bend in alkyl long chain group. The position of alkyl long chain substitution was confirmed by signal at wavenumber 834 cm^{-1} . This signal was in agreement with the out of plane in the *para* disubstitution. Finally, the signals of ether group were show two peak at 1161 and 1023 cm^{-1} , and the wavenumber was decreased when the alkyl chain was the longest. The result of this studies are in agreement with the previous reports [50, 56].

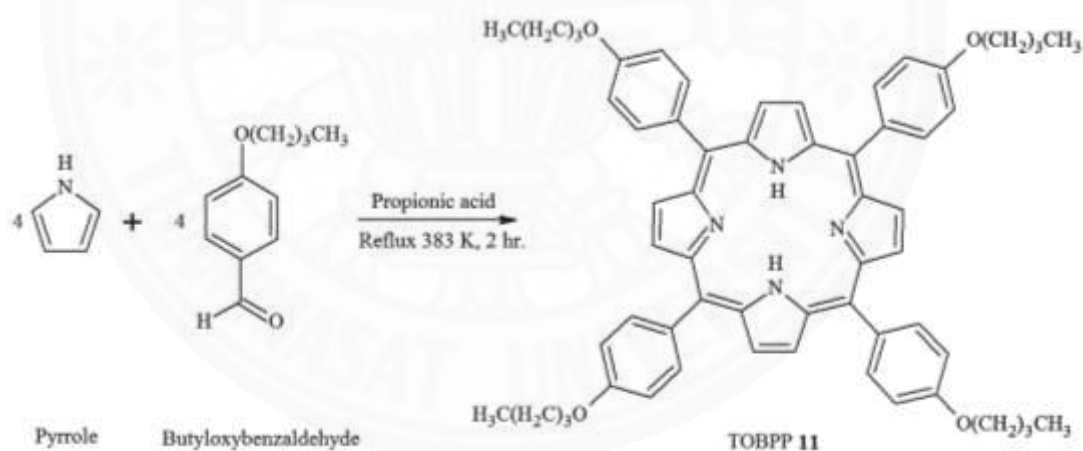
Table. 4 The IR data of aldehydes **1 - 3**

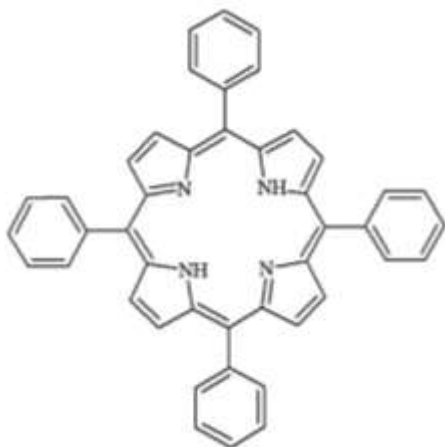
Aldehyde	C-H sp^2 str. in phenyl	C-H sp^3 str. in long chain	C-H str. in aldehyde	C=O str. in aldehyde	C=C str. in phenyl	CH ₃ bend	C-O-C ether	Oop, para disubt.
Butyloxybenzaldehyde 1	3072	2960	2873, 2737	1690	1603, 1509	1466, 1389	1161, 1023	834
Octyloxybenzaldehyde 2	3073	2927	2856, 2732	1691	1602, 1509	1467, 1395	1160, 1020	833
Decyloxybenzaldehyde 3	3074	2926	2855, 2732	1693	1602, 1509	1467, 1393	1160, 1017	833

**Fig. 46** IR spectrum of butyloxybenzaldehyde **1**

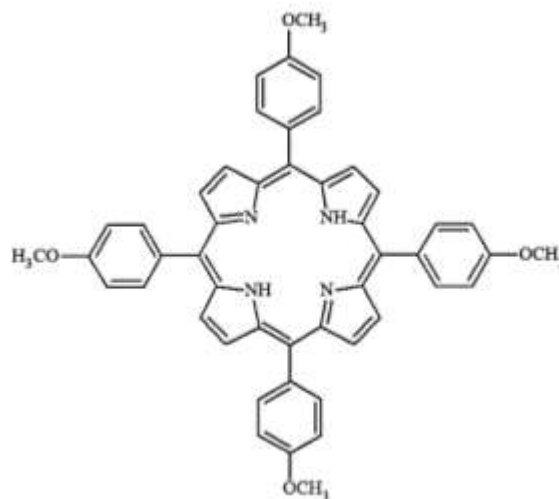
4.2 Porphyrins, copper(II) porphyrins, and β -nitro substituted porphyrin complexes synthesis and characterization

The free base porphyrins, TPP **4** was synthesized by Alder-Longo method [22]. Then other free base porphyrins including TOMPP **5**, TOBPP **6**, TOOPP **7**, and TODPP **8** were synthesized by a modification of Alder-Longo method [31, 32, 50, 65]. Start with, heating aldehyde in propionic acid followed by adding the same amount of pyrrole. The reaction were magnetically refluxed for 2 hours. Then, the ethanol was added, and kept in the refrigerator overnight. The purple crystal were obtained in dark solution, and the products were purified. This process was applied by using longer reaction time. The synthesized products were obtained in range 9 to 36% yield. The long chain derivative porphyrins (TOBPP **6**, TOOPP **7**, and TODPP **8**) gave the lower yield than 10%, due to the steric hindrance and the donating group on *para*-position of alkyl long chain derivative. The characterization data of free base porphyrins showed in **Table. 5**, and the **Fig. 48** shows the structure of all porphyrin. Lastly, the representative example scheme of TOBPP **6** was shown in **Fig. 47**

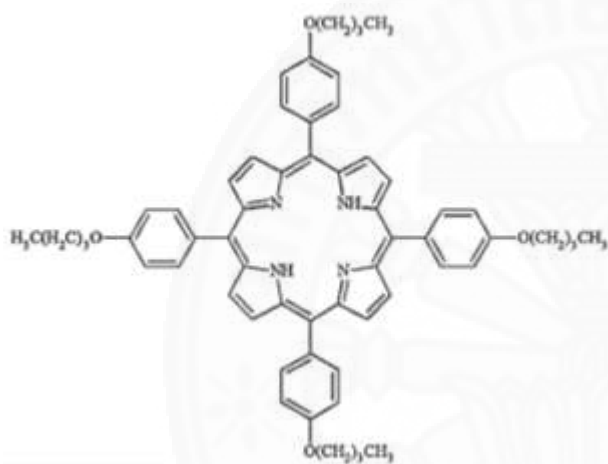




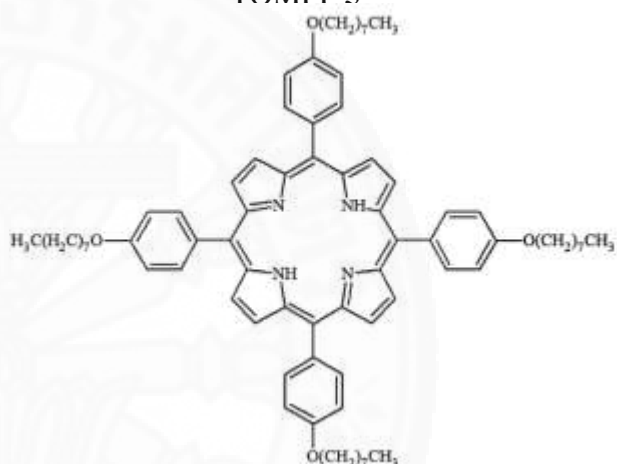
Formula $C_{44}H_{30}N_4$
Tetraphenylporphyrin
TPP 4



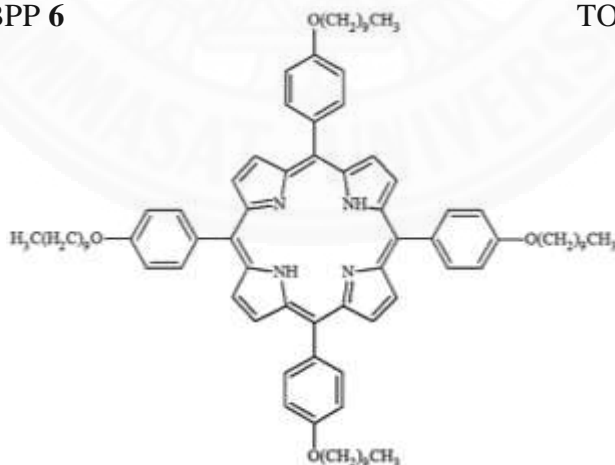
Formula $C_{48}H_{38}N_4O_4$
Tetrakis(4-methoxyphenyl)phenylporphyrin
TOMPP 5



Formula $C_{60}H_{62}N_4O_4$
Tetrakis(4-butyloxyphenyl)phenylporphyrin
TOBPP 6



Formula $C_{76}H_{94}N_4O_4$
Tetrakis(4-octyloxyphenyl)phenylporphyrin
TOOPP 7



Formula $C_{84}H_{110}N_4O_4$
Tetrakis(4-decyloxyphenyl)phenylporphyrin
TODPP 8

Fig. 48 The structure of TPP 4, TOMPP 5, TOBPP 6, TOOPP 7, and TODPP 8

Currently, the metalloporphyrin, copper(II) complexes have been interested. All copper porphyrin complexes including CuTPP **9**, CuTOMPP **10**, CuTOBPP **11**, CuTOOPP **12**, and CuTODPP **13** were prepared by a modified procedure from the previous method [42, 63]. Firstly, various free base porphyrin have been dissolved in mixed solvent of *N,N*-dimethylformamide and dichloromethane (1:1). Then excess copper acetate was added, and heated by refluxing for 5 hours. Next, the distilled water was added for removing the surplus copper acetate. Then, kept it in refrigerator overnight the purple products were obtained, and finally purified by silica gel column chromatography (**Fig. 49**). The result show that the synthetic products were obtained in higher yield than free base porphyrin, due to the size of copper(II) ion that fitted in to the central hole of porphyrin, the similarly result was reported by Hongshan H. for CuTPP [60]. The successful synthesis was obtained due to the long time reaction, more copper acetate, and the reaction driving forward. However, The CuTODPP **13** was received in the lowest yield, while other products were observed moer than 70% yield, suggesting the influence of steric hindrance of *para* substituent. The characteristic data of copper complezes showed in **Table. 5**, and the structure of all compound were illustrated in **Fig. 50**

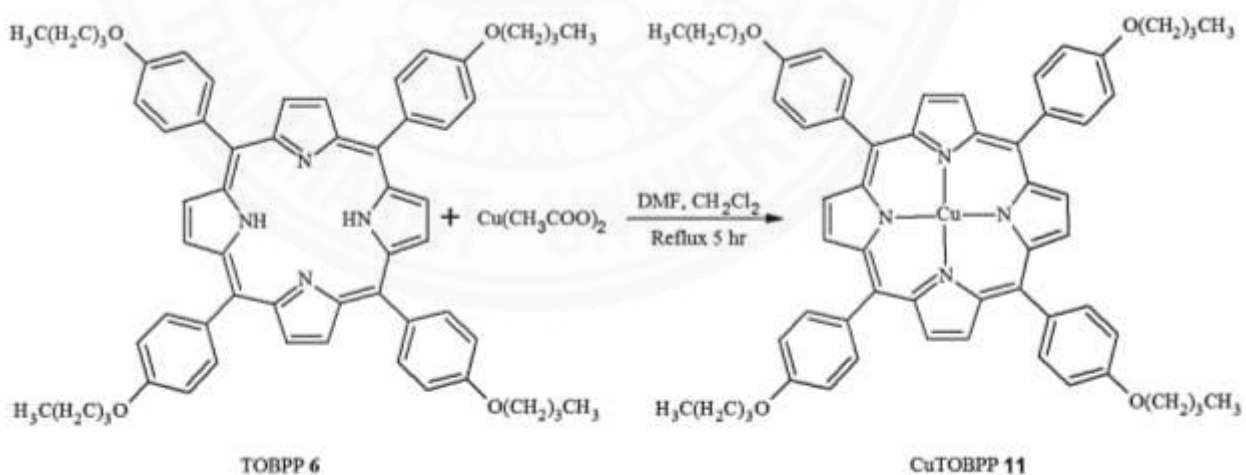
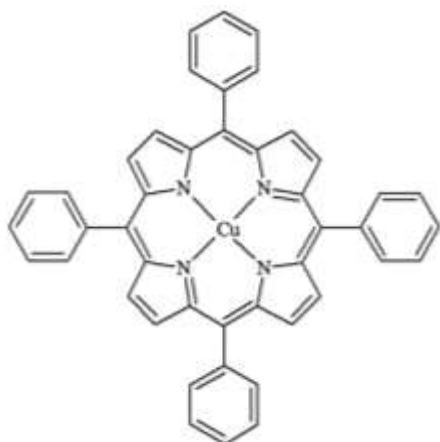
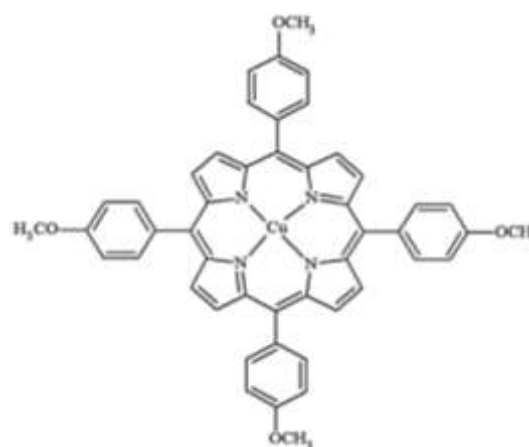


Fig. 49 Synthesis of Tetrakis(4-butyloxyphenyl)phenylporphyrinatocopper(II) (CuTOBPP **11**)



Formula $\text{CuC}_{44}\text{H}_{28}\text{N}_4$
Tetraphenylporphyrinatocopper(II)
CuTPP 9

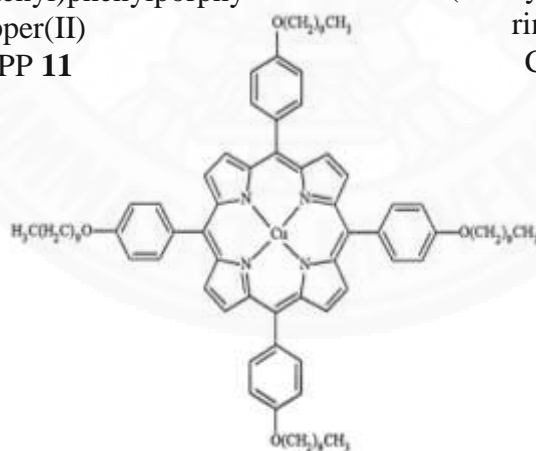


Formula $\text{CuC}_{48}\text{H}_{36}\text{N}_4\text{O}_4$
Tetrakis(4-methoxyphenyl)phenylporphyrinatocopper(II)
CuTOMPP 10



Formula $\text{CuC}_{60}\text{H}_{60}\text{N}_4\text{O}_4$
Tetrakis(4-butoxyphenyl)phenylporphyrinatocopper(II)
CuTOBPP 11

Formula $\text{CuC}_{76}\text{H}_{92}\text{N}_4\text{O}_4$
Tetrakis(4-octyloxyphenyl)phenylporphyrinatocopper(II)
CuTOOPP 12



Formula $\text{CuC}_{84}\text{H}_{108}\text{N}_4\text{O}_4$
Tetrakis(4-decyloxyphenyl)phenylporphyrinatocopper(II)
CuTODPP 13

Fig. 50 The structure of CuTPP 9, CuTOMPP 10, CuTOBPP 11, CuTOOPP 12, and CuTODPP 13

The β -functionalized porphyrins were investigated. The nitro (NO_2) functional group have been inserted into the β -position of copper porphyrin complexes followed the reported by Hongshan H. [60]. For the synthetic method, copper porphyrin derivative were dissolved in chloroform. The copper nitrate and acetic anhydride were added, the mixture were magnetically stirred for 48 hours at room temperature. The reaction mixture was extracted by distilled water and purified by silica gel column chromatography before removed solvent by evaporator. The β - functionalized porphyrin product were collected in a second portion from column. The synthetic products (CuTPP-NO_2 **14**, CuTOMPP-NO_2 **15**, CuTOBPP-NO_2 **16**, CuTOOPP-NO_2 **17**, and CuTODPP-NO_2 **18**) have been obtained in the lowest yield (less than 30%), due to ten steric of substituted group on *para* position, and the aromatic effect of porphyrin ring. The synthetic route of representative CuTOBPP-NO_2 **16** show in **Fig. 51** The structure of all compound show in **Fig. 52**, and the summarized characteristic data were show in **Table. 5**.

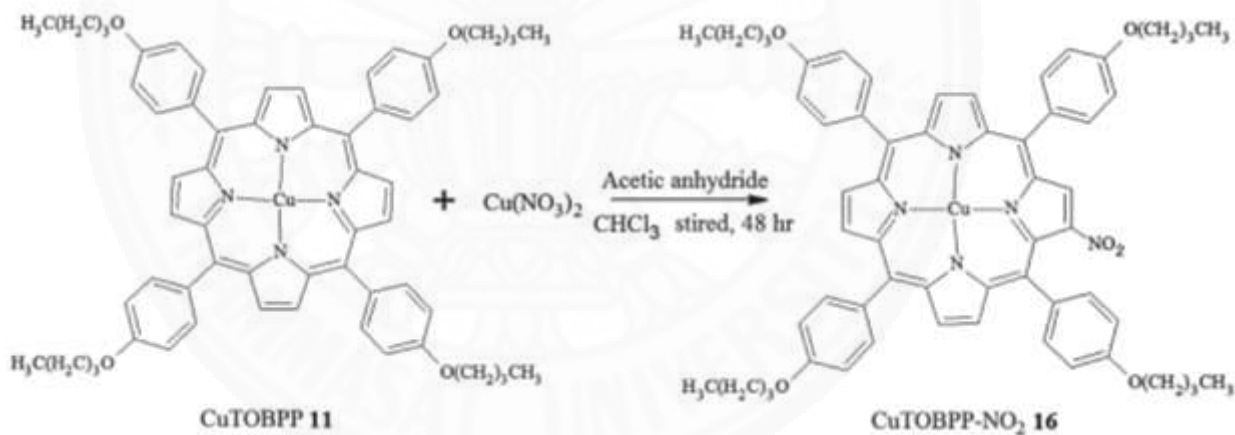
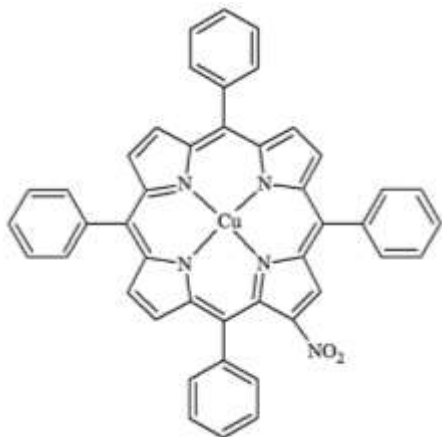
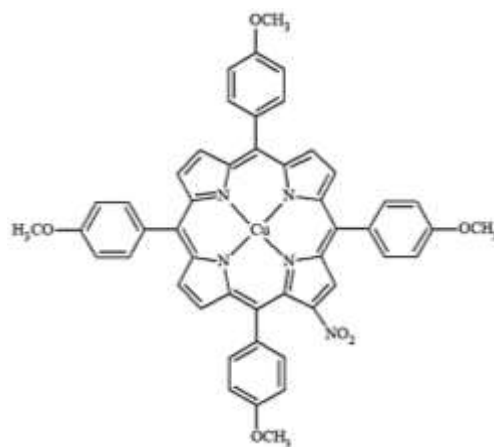


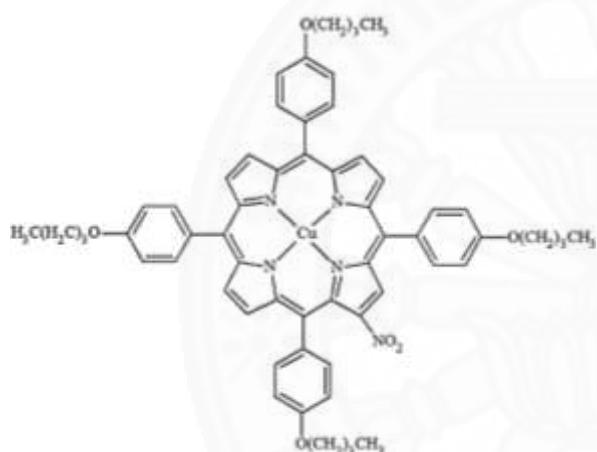
Fig. 51 The synthesis of 2-nitro-tetrakis(4-butoxyphenyl)phenylporphyrinatocopper(II) (CuTOBPP-NO_2 **16**)



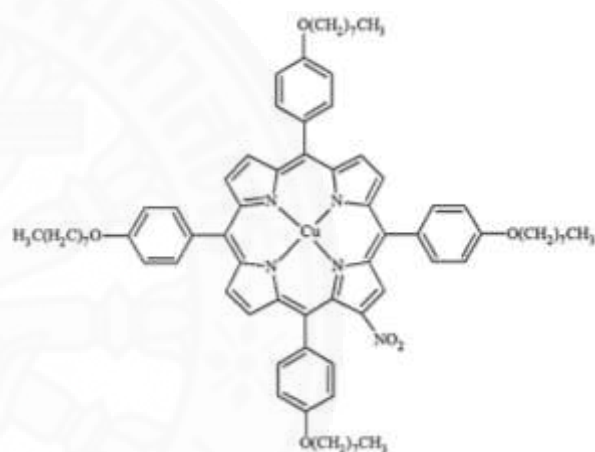
Formula $\text{CuC}_{44}\text{H}_{27}\text{N}_5\text{O}_2$
2-nitro-tetraphenylporphyrinatocopper(II)
CuTPP-NO₂ **14**



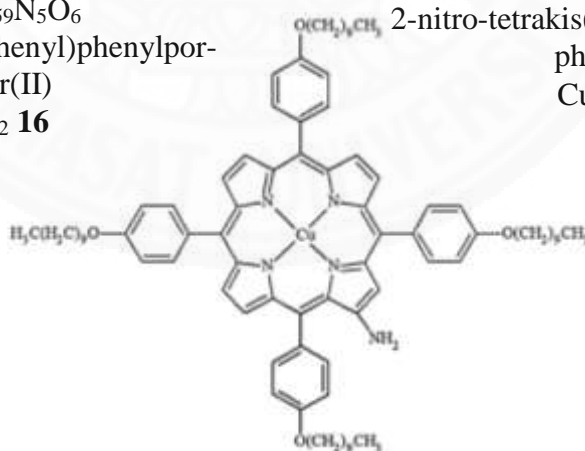
Formula $\text{CuC}_{48}\text{H}_{35}\text{N}_5\text{O}_6$
2-nitro-tetrakis(4-methoxyphenyl)phenylporphyrinatocopper(II)
CuTOMPP-NO₂ **15**



Formula $\text{CuC}_{60}\text{H}_{59}\text{N}_5\text{O}_6$
2-nitro-tetrakis(4-butyloxyphenyl)phenylporphyrinatocopper(II)
CuTOBPP-NO₂ **16**



Formula $\text{CuC}_{76}\text{H}_{91}\text{N}_5\text{O}_6$
2-nitro-tetrakis(4-octyloxyphenyl)phenylporphyrinatocopper(II)
CuTOOPP-NO₂ **17**



Formula $\text{CuC}_{84}\text{H}_{107}\text{N}_5\text{O}_6$
2-nitro-tetrakis(4-decyloxyphenyl)phenylporphyrinatocopper(II)
CuTODPP-NO₂ **18**

Fig. 52 The structure of CuTPP-NO₂ **14**, CuTOMPP-NO₂ **15**, CuTOBPP-NO₂ **16**, CuTOOPP-NO₂ **17**, and CuTODPP-NO₂ **18**

Table. 5 The characteristic data for free base porphyrins, copper(II) porphyrin, and β -nitro substituted porphyrin

Compounds	Empirical formula	Yield (%)	Formula weight ^a	Elemental analysis (^b) %			MS (m/z)
				C	H	N	
TPP 4	C ₄₄ H ₃₀ N ₄	22	614.7	85.9 (86.0)	4.9 (4.9)	9.1 (9.1)	615.0
TOMPP 5	C ₄₈ H ₃₈ N ₄ O ₄	26	734.84	76.42 (78.45)	5.75 (5.21)	7.42 (7.62)	735.4
TOBPP 6	C ₆₀ H ₆₂ N ₄ O ₄	9	903.16	79.44 (79.79)	6.55 (6.92)	5.83 (6.20)	903.6
TOOPP 7	C ₇₆ H ₉₄ N ₄ O ₄	12	1127.57	81.10 (80.95)	8.25 (8.40)	4.93 (4.97)	1127.9
TODPP 8	C ₈₄ H ₁₁₀ N ₄ O ₄	9	1239.78	81.24 (81.37)	8.99 (8.94)	4.58 (4.52)	1239.0
CuTPP 9	CuC ₄₄ H ₂₈ N ₄	93	676.27	76.90 (78.15)	3.94 (4.17)	8.18 (8.28)	677.0
CuTOMPP 10	CuC ₄₈ H ₃₆ N ₄ O ₄ ·2.5 CH ₂ Cl ₂	92	796.38	60.42 (60.14)	4.17 (4.07)	6.22 (5.55)	797.4
CuTOBPP 11	CuC ₆₀ H ₆₀ N ₄ O ₄	71	964.70	74.51 (74.77)	6.25 (6.23)	5.76 (5.82)	965.6
CuTOOPP 12	CuC ₇₆ H ₉₂ N ₄ O ₄ ·2.5 CH ₂ Cl ₂	96	1189.11	68.65 (67.31)	6.95 (6.93)	4.40 (4.00)	1187.0
CuTODPP 13	CuC ₈₄ H ₁₀₈ N ₄ O ₄ ·3 CH ₂ Cl ₂	63	1301.32	66.91 (67.18)	7.30 (7.34)	3.80 (3.60)	1303.7
CuTPP-NO ₂ 14	CuC ₄₄ H ₂₇ N ₅ O ₂	31	721.27	73.30 (73.33)	3.81 (3.75)	9.46 (9.72)	722.3
CuTOMPP-NO ₂ 15	CuC ₄₈ H ₃₅ N ₅ O ₆ ·0.5 CH ₂ Cl ₂	13	841.38	66.04 (65.93)	4.17 (4.07)	7.68 (7.92)	841.8
CuTOBPP-NO ₂ 16	CuC ₆₀ H ₅₉ N ₅ O ₆ ·0.5CH ₂ Cl ₂ ·3.5C ₆ H ₁₄	8	1009.7	72.79 (72.36)	8.27 (8.07)	4.38 (5.18)	1009.6
CuTOOPP-NO ₂ 17	CuC ₇₆ H ₉₁ N ₅ O ₆	14	1232.11	74.12 (74.03)	7.28 (7.39)	5.54 (5.68)	1234.2
CuTODPP-NO ₂ 18	CuC ₈₄ H ₁₀₇ N ₅ O ₆	28	1344.32	74.95 (75.00)	7.95 (7.96)	5.10 (5.21)	1344.8

^a Calculated without solvent^b Theoretical values are given in parentheses.

4.2.1 CHN elemental analysis

Porphyrin, copper(II) porphyrin, and β -nitro substituted porphyrin have been characterized by CHN elemental analysis. The analyst data of all compounds are summarize in **Table. 5**. The elemental analysis data of all synthesized compounds were confirmed the expected structure of all compounds, and were agreed with theoretical value. However, some synthesized compound i.e. CuTOMPP **5**, CuTOOPP **7**, CuTODPP **8** etc. were afforded to difference theoretical composition, due to the trace of solvent (CH_2Cl_2) in their molecule.

4.2.2 Mass spectrometry

Mass spectrometry have been used to confirm the expected structure of free base porphyrin. The **Fig. 53** show the representative mass spectrum example of TOMPP **5**. The mass spectrum displayed the molecular ion peak $[\text{M}+\text{H}]^+$ at $m/z = 735.4$ as main peak. In addition, other free base porphyrin exhibited similar result with TOMPP **5**. The mass spectrum of all free base porphyrin show the characteristic of aromatic compound mass spectra that show very intense molecular ion peak. The fragmentation of free base porphyrin requires a great deal of energy. Therefore, such fragmentation is not observed to any significant extent [73].

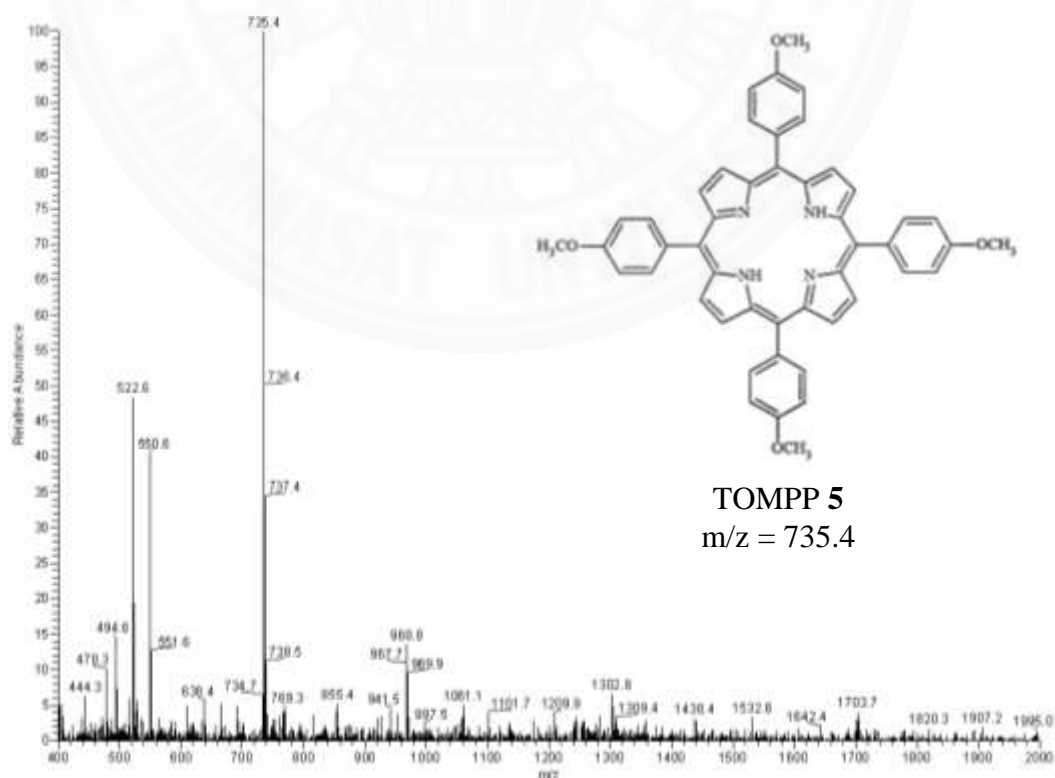


Fig. 53 The mass spectrum of TOMPP **5**

Moreover, the mass spectrum data of all free base porphyrins, copper(II) porphyrins and β -nitro substituted porphyrins were displayed in **Table 5**. The CuTOMPP **10** have been used as a representative example of mass spectrum of copper(II) porphyrins (**Fig. 54**) This copper(II) porphyrin complex exhibits molecular ion peak $[M+H]^+$ at $m/z = 797.4$. The mass spectra of all copper(II) porphyrins were obtained similarly result in free base porphyrin, However, mass spectra of CuTOMPP **10** was showed the strong fragmentation peak at $m/z = 735.4$ as main peak that represented the lossing of copper(II) ion from metal porphyrin structure.

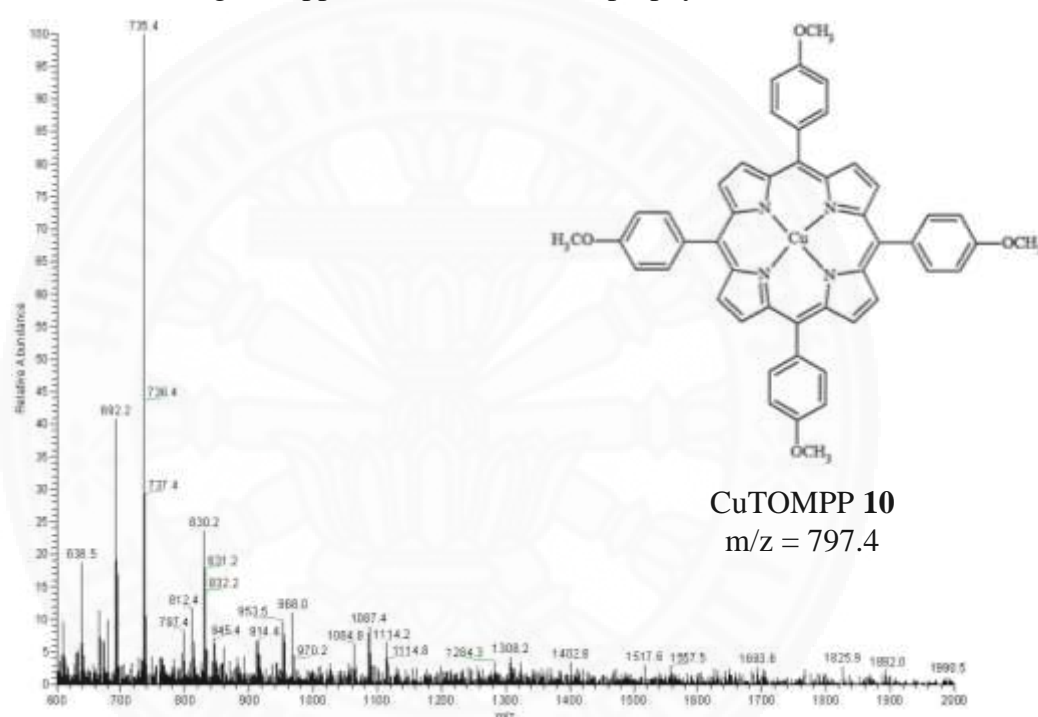


Fig. 54 The mass spectrum of CuTOMPP **10**

In addition, the representative example mass spectra of β -nitro substituted porphyrin is CuTOMPP-NO₂ **15** shown in **Fig. 55**. The CuTOMPP-NO₂ mass spectra was showed the main molecular ion peak $[M+H]^+$ at $m/z = 841.8$. The mass spectra of all β -nitro substituted porphyrin were resembled with free base porphyrin and copper(II) porphyrin, showed very intense molecular ion peaks because they had high energy from the delocalization in molecule. Other β -substituted porphyrins complexes show the similarly result with CuTOMPP-NO₂. The studied of mass spectroscopy were successfully received to confirmed the expected corresponding

TPP. The substituted porphyrin derivative show the up field shift of chemical shift value, as a result of *para*- substituent group on the phenyl ring. The substituent groups including $-\text{OCH}_3$, $-\text{O}(\text{CH}_2)_3\text{CH}_3$, $-\text{O}(\text{CH}_2)_7\text{CH}_3$ and $-\text{O}(\text{CH}_2)_9\text{CH}_3$ are electron donating groups, cause the phenyl proton displayed up field chemical shift, due to the shielding effect. From **Table. 6** the shielding effect of methoxy group are the lowest, when compered with other long chain alkyloxy group. While, increased number of carbon in long alkyl chain, the shielding effect was increased too. The effect of electron donating groups were reported by Hossein D. et al. [75]. In addition, the *para*- proton of phenyl ring in TPP had a chemical shift at 7.52 ppm.

The proton of *para*-substituent group in TOMPP ($-\text{OCH}_3$) was assigned at 4.10 ppm. The alkyl proton in long chain (TOOPP and TODPP) were found to be shielded than TOBPP, due to the inductive effect and electron donating of ether group is side chain. The result found in alkyloxybenzaldehyde.

The signal of N-H proton were observed in very high field (-2.90 ppm), due to the more shielding effect of porphyrin ring. The spectrum of TOMPP showed in **Fig. 56** as a representative example.

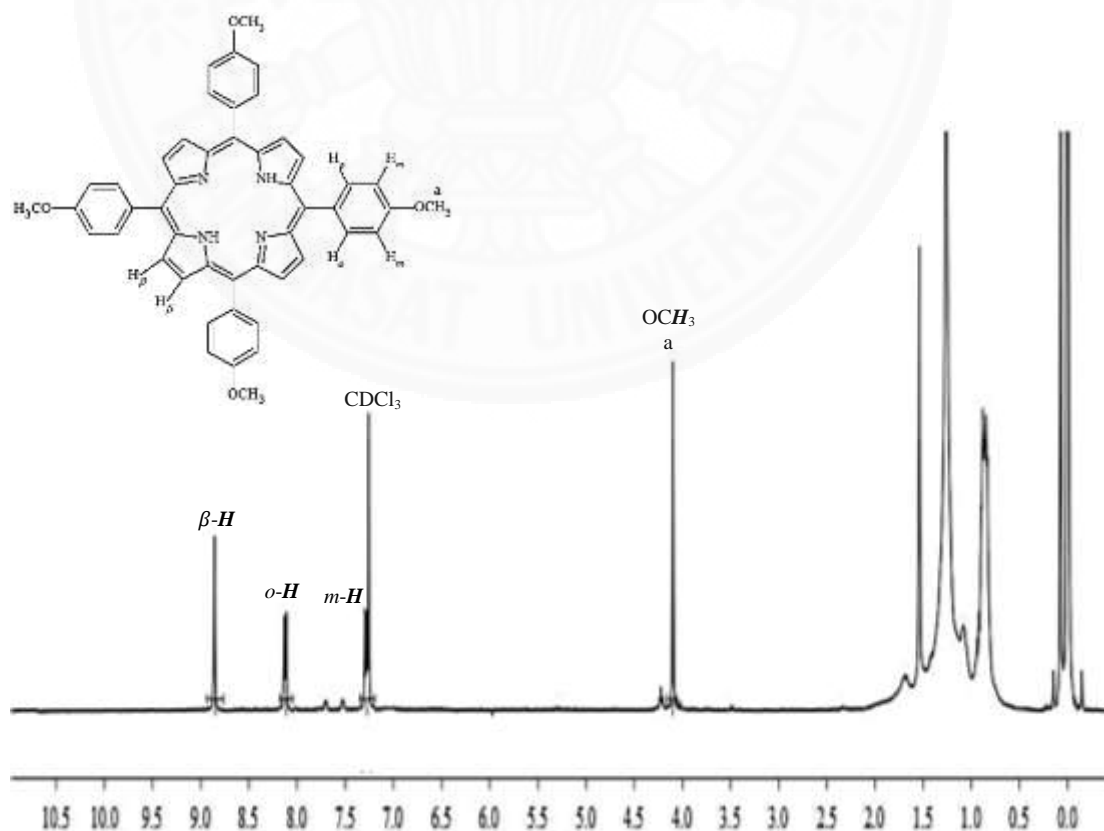


Fig. 56 The ^1H NMR spectrum of TOMPP 5

The ^{13}C NMR spectrum of TOMPP was shown in **Fig. 57** as a representative example, analyzed by using chloroform as solvent. The ^{13}C NMR spectrum of TOMPP was assigned the signal of $\alpha\text{-C}$, pyrrole at 134.68 ppm, $\beta\text{-C}$, pyrrole at 129.97 ppm and *meso*-C, methanebridge at 118.83 ppm. The carbon of phenyl ring was obtained the signal at 158.75 ($p^*\text{-C}$), 133.99 (*o*-C), 127.89 (*p*-C) and 111.44 (*m*-C) ppm. In addition, the signal of carbon in alkyl long chain group was displayed in the same range of aldehyde. The similarly result was observed in other free base porphyrin. The data of ^{13}C NMR of all synthesized porphyrins were concluded in **Table. 6**.

In complexes of porphyrins with copper(II) ions, and the β -nitro substituted porphyrin complexes the chemical shifts was observed the broad peaks related with ligands information only. The copper(II) porphyrins were unsuccessful identified due to the paramagnetic copper porphyrin. Further analysis, including ESR spectroscopy, may be required for studying the information inside into the complexes.

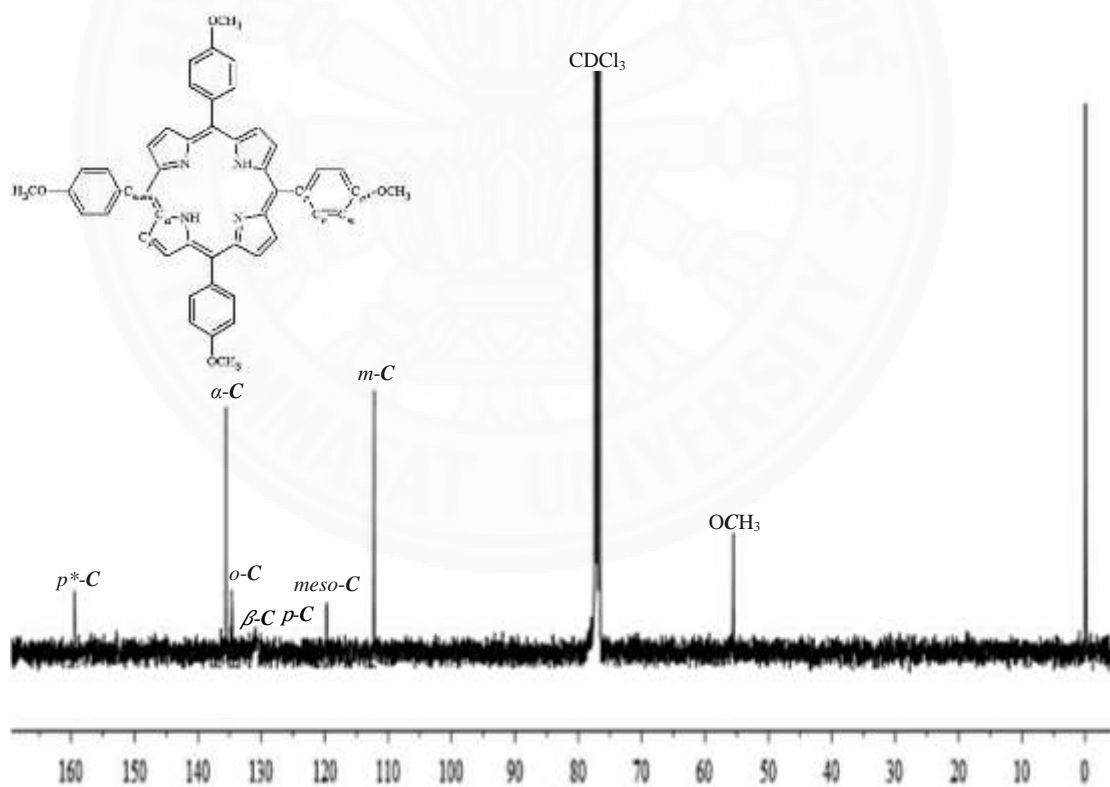


Fig. 57 The ^{13}C NMR spectrum of TOMPP 5

Table. 6 ^1H and ^{13}C NMR spectroscopic data for free base porphyrins

Porphyrins	^1H NMR (ppm), proton												
	Pyrrole, $\beta\text{-H}$	Phenyl, <i>o</i> - H	Phenyl, <i>m</i> - H	Phenyl, <i>p</i> - H	OCH_3	OCH_2	OCH_2CH_2	CH_2CH_3	$\text{CH}_2\text{CH}_2\text{CH}_2$	CH_3			
TPP 4	8.85	8.20	7.77	7.52	-	-	-	-	-	-			
TOMPP 5	8.86	8.12	7.29	-	4.10	-	-	-	-	-			
TOBPP 6	8.86	8.11	7.28	-	-	4.24	1.98	1.30	-	0.90			
TOOPP 7	8.86	8.08	7.21	-	-	4.22	1.98	1.30	1.26	0.88			
TODPP 8	8.86	8.08	7.22	-	-	4.22	1.98	1.30	1.26	0.87			
Porphyrins	^{13}C NMR (ppm), carbon												
	Phenyl, <i>p</i> *- C	$\alpha\text{-C}$	Phenyl, <i>o</i> - C	$\beta\text{-C}$	Phenyl, <i>p</i> - C	<i>Meso</i> - C	Phenyl, <i>m</i> - C	OCH_3	OCH_2	OCH_2CH_2	$\text{CH}_2\text{CH}_2\text{CH}_2$	CH_2CH_3	CH_3
TPP 4	127.70	-	134.56	131.12	142.22	120.15	126.67	-	-	-	-	-	-
TOMPP 5	158.75	134.68	133.99	129.97	127.89	118.83	111.44	54.65	-	-	-	-	-
TOBPP 6	159.09	135.32	134.74	130.70	128.76	119.7	112.84	-	68.14	31.49	-	23.98	13.84
TOOPP 7	159.07	135.54	134.57	131.78	128.74	119.79	112.82	-	68.45	31.84	29.64, 29.53, 29.45, 26.22, 22.64	-	14.00
TODPP 8	159.10	135.51	134.51	130.68	128.76	119.77	112.86	-	68.48	31.88	29.60, 29.55, 29.53, 29.46, 29.28, 26.20, 22.60	-	13.93
Cu(II) porphyrin 9–13 , and β -nitro substituted porphyrin 14–18								- ^a					

^aUnable to identify due to paramagnetic character in ^1H and ^{13}C NMR data.

4.2.4 Infrared spectroscopy

All synthesized porphyrin complexes were confirmed the functional group by IR spectroscopy, that record in KBr disc. The data were collected in the 4000-400 cm^{-1} region. The result were conclude in **Table. 7**. All free base porphyrin exhibited the important signal peak of N-H bending vibration in range from 3,310-3320 cm^{-1} , and 965-967 cm^{-1} , respectively. While, the IR spectrum of copper(II)porphyrins and β -substituted porphyrin, both of this signal were disappeared. That can confirmed, the copper (II) ion was inserted into the porphyrin ring and replace of hydrogen in pyrrole ring. Moreover, the β -nitro substituted porphyrin have been displayed the important signal peak in IR spectrum, this peak were represent the nitro ($-\text{NO}_2$) vibration (N=O) at frequency 1,509-1,521, and 1,340-1,342 cm^{-1} , denote that the nitro group was substituted in porphyrin ring. The comparison IR spectra of TOMPP **5** CuTOMPP **10** and CuTOMPP- NO_2 **15** were show in **Fig. 58**. As mention above, the free base porphyrin TOMPP **5** exhibits the characteristic signal peak of N-H stretching and N-H bending at 3316 and 966 cm^{-1} . While, those of two peak were disappeared in spectrum of CuTOMPP **10** and CuTOMPP- NO_2 **15**. The similar results were reported by Zhijie X. [50]. Moreover, the β -substituted porphyrin complexes CuTOMPP- NO_2 **15** was observed the signal peak of N=O stretching at 1510 and 1340 cm^{-1} while, TOMPP **5** and CuTOMPP **10** weren't displayed this signal. The similar result was reported by Hu J. [56]

Furthermore, the signal peak of C-H stretching (long chain) and C-N stretching in porphyrin ring were showed. The similarly character was found in free base porphyrins, copper(II) porphyrins, and β -nitro substituted porphyrin complexes. When the number of carbon atom in long chain were increased, the frequency of both signals found to be slightly decreased due to the electronic effect of long chain substituent. However the signal peak including C=C stretching in phenyl, C-O stretching in alkyl chain and C-H bending in porphyrin of all synthesized porphyrin complexes displayed a small peak shift in IR spectra.

Table. 7 The IR data of free base porphyrins

Compounds	N-H str. in porphyrin	C-H str. in phenyl and long chain	C=C str. in phenyl	C-N str. in porphyrin	C-O str. in long chain	N-H bend in porphyrin	C-H bend in porphyrin	N=O str.
TPP 4	3310	-	1597, 1469	1212	-	966	794	-
TOMPP 5	3316	2931, 2834	1607, 1509	1248	1174	966	804	-
TOBPP 6	3320	2931, 2868	1607, 1509	1245	1174	966	802	-
TOOPP 7	3318	2927, 2852	1607, 1509	1243	1174	965	804	-
TODPP 8	3317	2924, 2852	1607, 1509	1244	1174	967	803	-
CuTPP 9	-	-	1600, 1441	1345	-	-	793	-
CuTOMPP 10	-	2929, 2835	1607, 1499	1248	1173	-	804	-
CuTOBPP 11	-	2930, 2869	1607, 1502	1246	1174	-	799	-
CuTOOPP 12	-	2926, 2852	1607, 1506	1244	1174	-	804	-
CuTODPP 13	-	2923, 2852	1607, 1504	1246	1174	-	800	-
CuTPP-NO ₂ 14	-	-	1618, 1442	1328	-	-	799	1516, 1342
CuTOMPP-NO ₂ 15	-	2928, 2830	1607, 1502	1249	1174	-	801	1510, 1340
CuTOBPP-NO ₂ 16	-	2927, 2870	1607, 1506	1256	1174	-	800	1521, 1340
CuTOOPP-NO ₂ 17	-	2927, 2855	1607, 1505	1247	1174	-	800	1509, 1341
CuTODPP-NO ₂ 18	-	2923, 2853	1606, 1506	1247	1173	-	800	1509, 1341

Unit Cm⁻¹

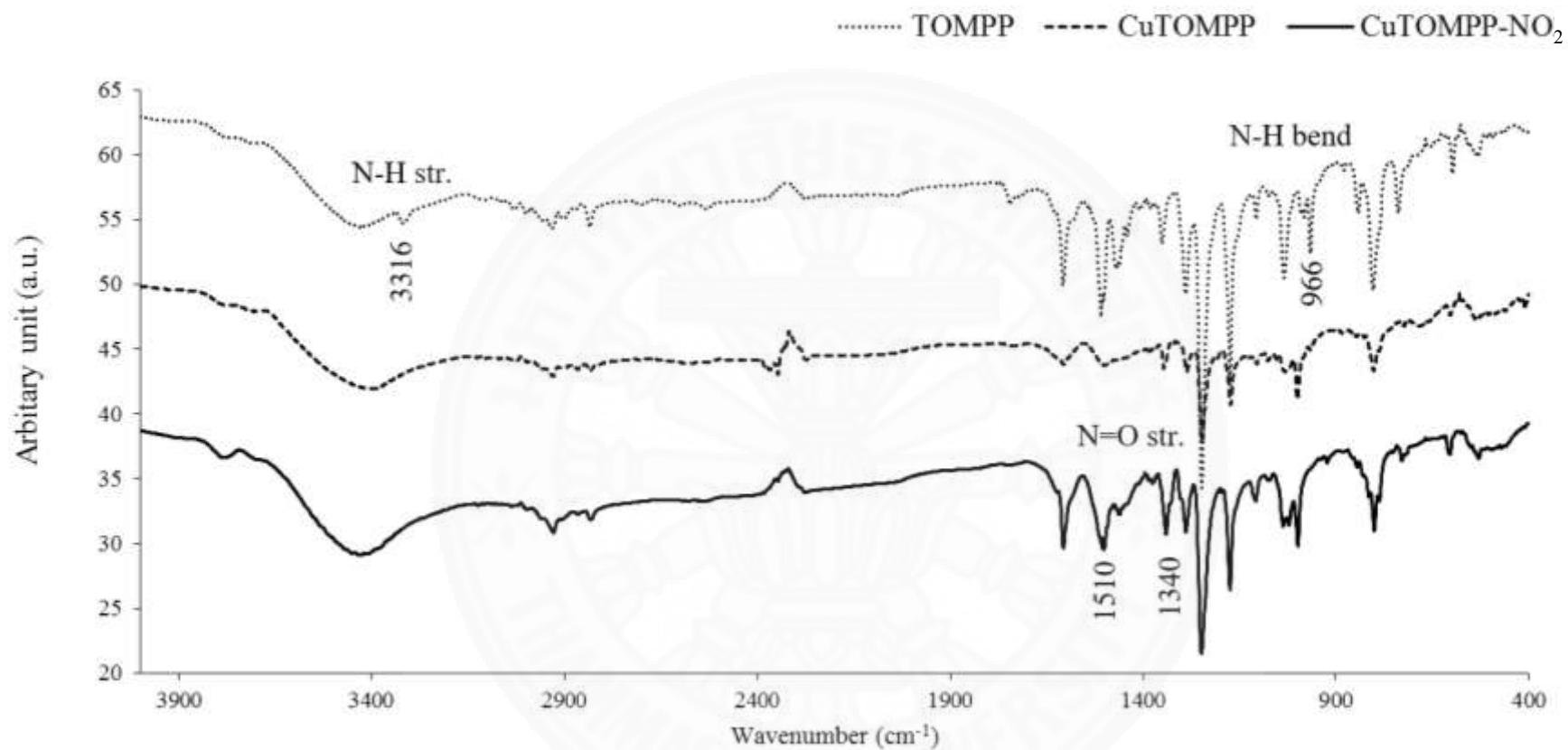


Fig. 58 IR spectrum of TOMPP 5, CuTOMPP 10, and CuTOMPP-NO₂ 15

4.2.5 UV-vis spectroscopy

The absorption spectra of all free base porphyrin were recorded in dichloromethane at room temperature. The absorption data and molar extinction coefficient (ϵ) of all synthesized porphyrins are summarized in **Table. 8**. The absorption spectra of all free base porphyrins exhibited a strong absorption (Soret band) at 417-422 nm and four weak adsorptions (Q band) around 500-700 nm, which can be assigned to $\pi \rightarrow \pi^*$ electronic transitions. The very intense Soret band assigned to the $S_0 \rightarrow S_2$ transition that can be found in shorter wavelength. On the other hand, the Q bands assigned to the $S_0 \rightarrow S_1$ transitions, appear in longer-wavelength [50]. According to UV-Vis spectroscopy data, the Soret band and Q band of the *para*-substituted porphyrin more to a small red shift when compared with TPP. **Fig. 59** show the absorption spectra of all porphyrin.

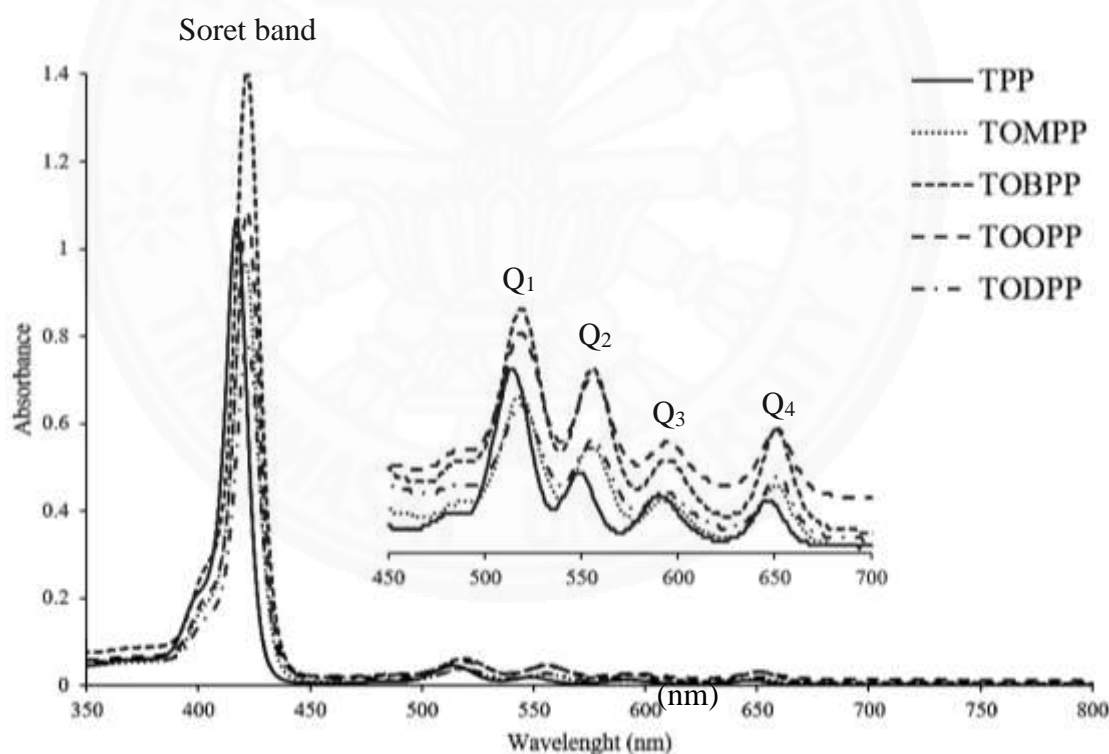


Fig. 59 UV-Vis absorption spectra of all free base porphyrin in CH_2Cl_2

In **Fig. 60**, the absorption spectrum of TOMPP **5**, CuTOMPP **10** and CuTOMPP- NO_2 **15** are shown for comparison. The TOMPP displays a strong Soret-band at 421 nm and four Q band at 518, 555, 595 and 650 nm. After coordination with

copper (II) ion in porphyrin ring. The absorption at 541 nm is identified for Q band of CuTOMPP, the signature of an effective intramolecular charge transfer [53] with red shift. Although, the Soret-band moved to small blue shift. This result were observed in all copper(II) porphyrin, However, when inserted the nitro (-NO₂) group in copper(II) porphyrin the absorption spectra were changed. The Soret-band of β -nitro substituted porphyrin was moved to red shift when compared with copper (II) porphyrin, the similar result was reported by Ravi K. and Muniappan S. [4]. Thus the energy gap (HOMO and LUMO) of β -nitro substituted porphyrin are less than other synthesized complexes. The introduction of nitro (-NO₂) group at β -position does not alter the absorbance spectra.

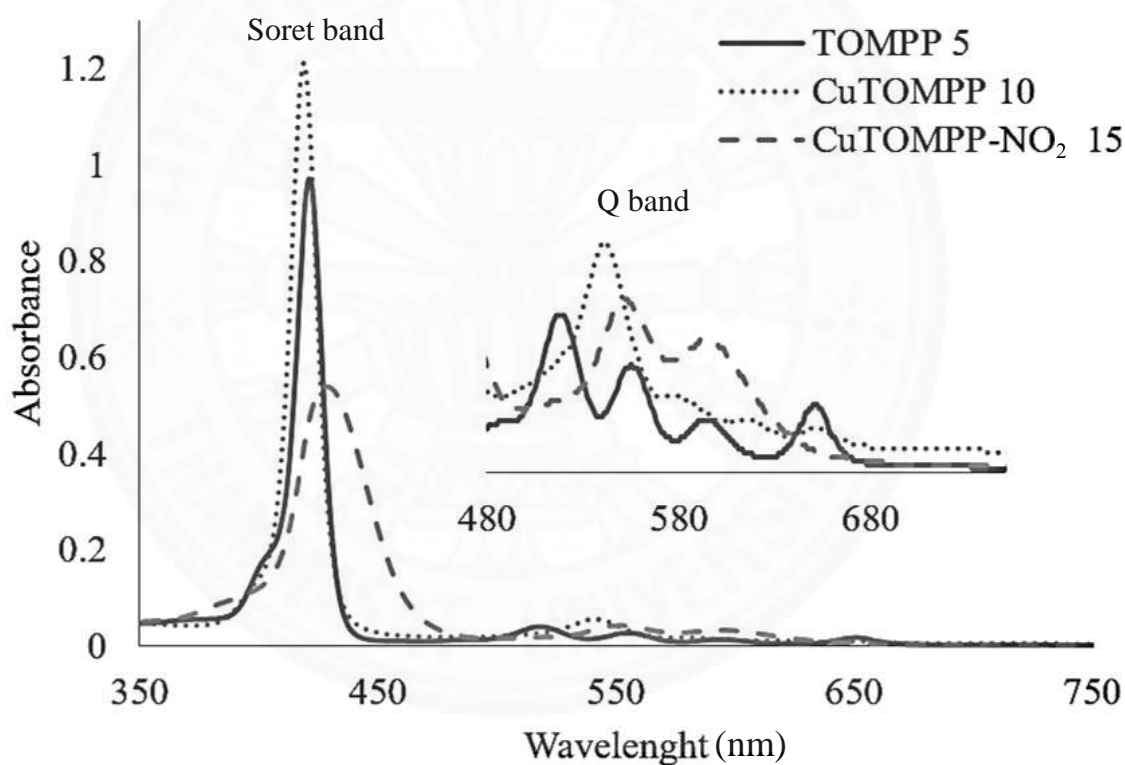


Fig. 60 The UV-Vis absorption spectra of TOMPP **5**, CuTOMPP **10** and CuTOMPP-NO₂ **15** in CH₂Cl₂

Table. 8 The absorption data of all compounds

Porphyrin	Dichloromethane ^a				
	S band (nm)	Q band (nm), $\epsilon(\text{M}^{-1}\text{cm}^{-1})$			
		Q ₁	Q ₂	Q ₃	Q ₄
TPP 4	417	514, 14122	548, 6140	590, 4605	649, 3991
TOMPP 5	421	518, 11941	555, 8266	595, 3980	650, 5205
TOBPP 6	422	519, 22955	556, 17310	595, 8655	651, 11665
TOOPP 7	422	519, 30953	556, 24762	595, 15757	651, 17446
TODPP 8	422	519, 20817	556, 15758	595, 8439	652, 10689
CuTPP 9	415	-	540, 13863	-	-
CuTOMPP 10	419	-	541, 18914	-	-
CuTOBPP 11	419	-	541, 24599	-	-
CuTOOPP 12	419	-	541, 29084	-	-
CuTODPP 13	419	-	541, 14292	-	-
CuTPP-NO ₂ 14	422	-	548, 23277	590, 15408	-
CuTOMPP-NO ₂ 15	428	-	551, 15074	594, 11568	-
CuTOBPP-NO ₂ 16	429	-	552, 20652	596, 16522	-
CuTOOPP-NO ₂ 17	430	-	554, 24082	595, 19041	-
CuTODPP-NO ₂ 18	430	-	552, 28230	596, 21509	-

^a All solution were prepared in the concentration of 1×10^{-4} mol/L, in CH₂Cl₂(n =3, %RSD \leq 1.6) and measured in the wavelength range of 200-800 nm.

4.2.6 Fluorescence spectroscopy

The emission spectra of the free base porphyrins, copper(II) porphyrins, and β -nitro substituted porphyrin complexes were recorded in dichloromethane by the fluorescence spectroscopy. The spectra of all free base porphyrins are shown in **Fig. 61**. All free base porphyrins exhibited the emission characteristic at the emission wavelength from 654 nm, when excited at 534 nm except the TPP 4. The TPP exhibited fluorescence band at 649 nm. The same values of λ_{em} were obtained by exciting the sample at the wavelength of maximum absorption of the Q band (first Q band) [30].

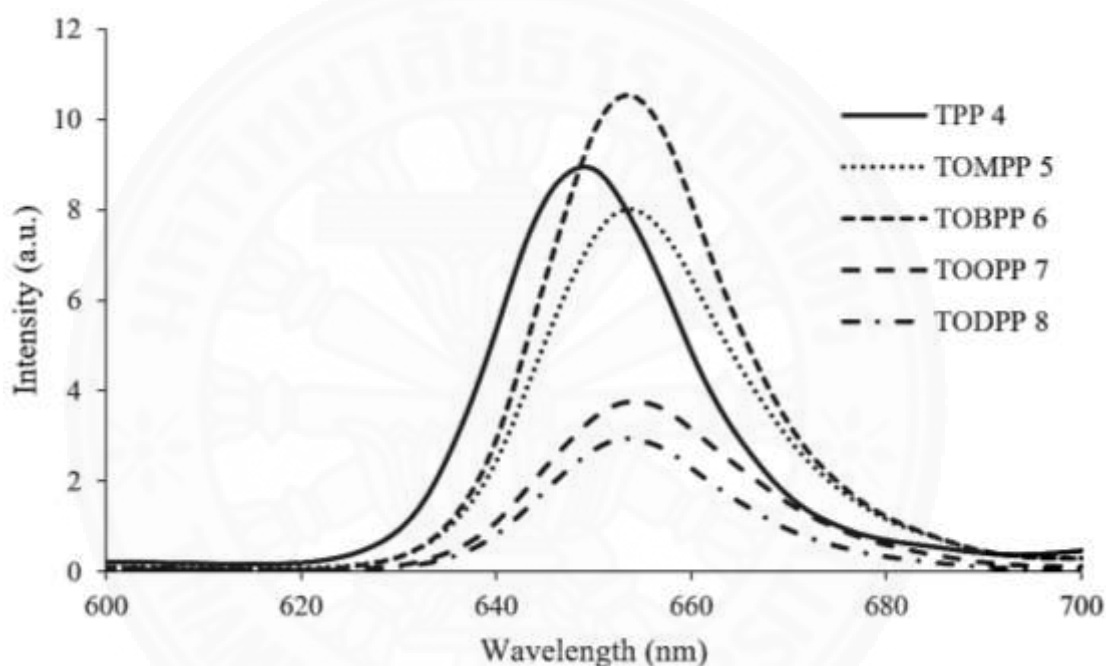


Fig. 61 The emission spectra of free base ligands in dichloromethane

The emission spectra of copper(II) porphyrin and β -nitro substituted porphyrin complexes have been observed. The fluorescence of all copper(II) porphyrins have been obtained at 605 nm when excited at 556 nm, except CuTOMPP (exhibit fluorescence spectra at 654 nm). While the β -nitro substituted porphyrin complexes were excited at 566 nm, the emission spectra were shown between 613 – 620 nm. All synthesized porphyrins compound exhibited an interesting trend in the blue shift of their corresponding emission band in the following order: free base porphyrins, > β -nitro substituted porphyrin complexes > copper(II) porphyrins. The emission data of all compound were summarized in **Table 9**

The difference energy between HOMO (highest occupied molecular orbital) and LUMO (lowest unoccupied molecular orbital) have been calculated in term of energy gap (E_{gap}) The estimated energy gap determined from intersection of UV-vis absorption (Q_4 band) and fluorescence emission spectra follow the equation $E_{\text{gap}} = hc/\lambda$ when h = Planks constant = 6.626×10^{-34} J·s, c = speed of light = 3.0×10^8 m/s, and $1 \text{ eV} = 1.602 \times 10^{-19}$ J. [76]. However, the estimated energy gap of copper(II) porphyrin and β -nitro substituted porphyrin complexes can't be calculated because of the absorption spectra of both compound didn't showed those Q_4 band. The estimated energy gap of all free base porphyrins were summarized in **Table 9**. The long chain substituted free base porphyrin compounds **4 – 8** exhibited lower energy gap at 1.90 eV that related to the donating electron of long chain substituent group at *para*- position.

Table 9 The absorption-emission wavelength and the estimated energy gap of free base porphyrins in dichloromethane

porphyrin	Dichloromethane		
	Absorption wavelength (nm)	Emission wavelength (nm)	E_{gap} (ev)
TPP 4	529	649	1.92 [76]
TOMPP 5	534	654	1.90
TOBPP 6	534	654	1.90
TOOPP 7	534	654	1.90
TODPP 8	534	654	1.90
CuTPP 9	556	605	2.17 ^a
CuTOMPP 10	556	654	2.16 ^a
CuTOBPP 11	556	604	2.17 ^a
CuTOOPP 12	556	605	2.17 ^a
CuTODPP 13	556	605	2.17 ^a
CuTPP-NO ₂ 14	563	613	2.06 ^a
CuTOMPP-NO ₂ 15	566	618	2.05 ^a
CuTOBPP-NO ₂ 16	566	619	2.04 ^a
CuTOOPP-NO ₂ 17	566	620	2.04 ^a
CuTODPP-NO ₂ 18	566	618	2.05 ^a

^a Calculate by using average of wavelength between Q-band and emission band

4.2.7 Thermal gravimetric analysis (TGA)

The free base porphyrins, copper(II) porphyrins, and β -nitro substituted porphyrin complexes were determined the decomposition temperature by using the thermalgravimetric measurement (TGA) under nitrogen atmosphere in range for 308 – 1,173 K. The TGA curve of TOBPP **6**, CuTOBPP **11**, and CuTOBPP-NO₂ **16** are shown Fig. 62. The first derivative curve showed the initial at temperature weight loss ranged from 680 to 699 K for free base porphyrin **5** – **8** while, TPP show weight loss at 671 K. The second state of the weight loss founded in both of copper(II) porphyrins, and β -nitro substituted porphyrin complexes excepted complexes **11** and **12** were show one step, while complexes **15** and **16** exhibited three step decomposition. The decomposition temperature at weight loss occurred between the initial temperature and the temperature at loss a half of the initial weight [77]

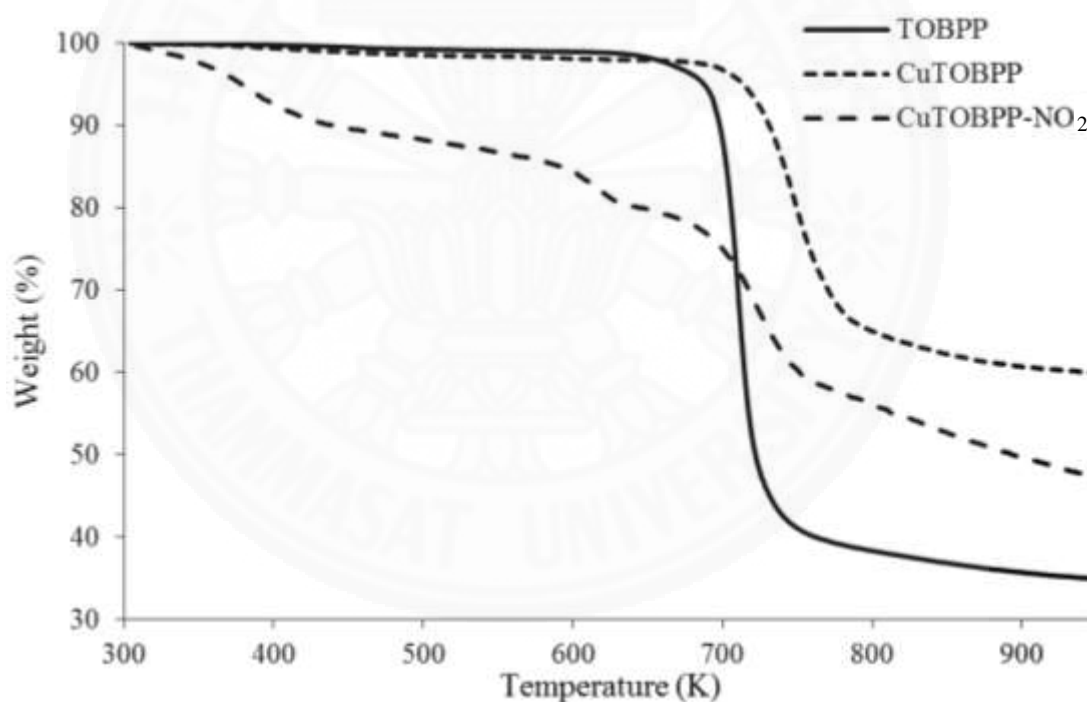


Fig. 62 Thermal gravimetric analysis (TGA) curves of TOBPP **6**, CuTOBPP **11**, and CuTOBPP-NO₂ **16**

The representative example TGA curve of TOBPP **6** show that the process initiated to change curve of TOBPP occurred in the decomposition temperature (state I) at 688 K, while CuTOBPP **11** and CuTOBPP-NO₂ **16** show the main stage decomposition temperature at 748 K and 722 K, respectively. The CuTOBPP showed

the higher thermal decomposition than TOBPP and CuTOBPP-NO₂ due to the strong bond of Cu-N in CuTOBPP structure. The result of the decomposition temperature and weight loss with corresponding temperature were summarized in **Table 10**.

Table 10 Temperatures of decomposition of free base porphyrins copper(II) porphyrins and β -nitro substituted porphyrin complexes

Compounds	Stage I		Stage II	
	T _{decomp} /K	Weight loss/% (Tf/K)	T _{decomp} /K	Weight loss/% (Tf/K)
TPP 4 [77]	671	74.4 (680)	-	-
TOMPP 5 [78]	680	18.7 (738)	738	81.6 (973)
TOBPP 6	688	60.1 (763)	-	-
TOOPP 7	697	71.5 (783)	-	-
TODPP 8	699	72.1 (763)	-	-
CuTPP 9	808	88.2 (859)	-	-
CuTOMPP 10	732	49.2 (773)	-	-
CuTOBPP 11	748	42.7 (777)	-	-
CuTOOPP 12	742	54.6 (789)	-	-
CuTODPP 13	740	49.3 (777)	-	-
CuTPP-NO ₂ 14	654	6.2 (778)	778	14.8 (801)
CuTOMPP-NO ₂ 15	614	5.3 (714)	714	21.9 (853)
CuTOBPP-NO ₂ 16	610	8.21 (722)	722	44.4 (753)
CuTOOPP-NO ₂ 17	611	7.0 (727)	727	45.2 (765)
CuTODPP-NO ₂ 18	613	6.3 (726)	736	50.2 (773)

From **Table 10** the free base porphyrins show the weight loss higher than 60%, copper(II) porphyrins show the weight loss in the same trend of free base porphyrins, while the β -nitro substituted porphyrin complexes show weight loss lower than 50%. The copper(II) porphyrin CuTPP exhibited the thermal stability more than other copper(II) porphyrins. The similarly result was observed in the β -nitro substituted porphyrin complexes series. In addition, all free base porphyrin show one step weight loss, while the major weight loss of TOMPP **5** occurred in two step due to loss the methoxy group in first step. The TGA curve of all free base porphyrins had highly

weight loss due to removed the decomposition of long chain alkyl group on methane bridged and phenyl group of porphyrin. In the case of copper(II) porphyrin complexes **9 – 13** show the greatest thermal stability more than 700 K due to the copper(II) ion in porphyrin ring was obtained that a shorter of the bond distance between the diametrically opposed carbon atom in *meso*-position than pure ligand included the bond distance between copper(II) ion and nitrogen in complexes structure and the copper(II) ion fitted for the free base porphyrin. However, some copper(II) porphyrins (CuTPP, CuTOMPP, and CuTODPP) show two step weight loss. The first thermal process in the 400 – 500 K range, which corresponds to weight loss of 5 – 9 % is referred to the elimination of small molecular impurity. The similar result was found in TGA curve of the β -nitro substituted porphyrin complexes (CuTOMPP-NO₂ and CuTOBPP-NO₂) [63].

Moreover, the β -nitro substituted porphyrin complexes were found to be more thermally stable than free base porphyrins, but lower than copper(II) porphyrin. The weight loss of 6 – 10 % in range for 610 – 650 K were referred to the elimination of nitro group in the structure of β -nitro substituted porphyrin complexes. The major state of decomposition of all copper(II) porphyrin and the β -nitro substituted porphyrin complexes were concluded in **Table 10**.

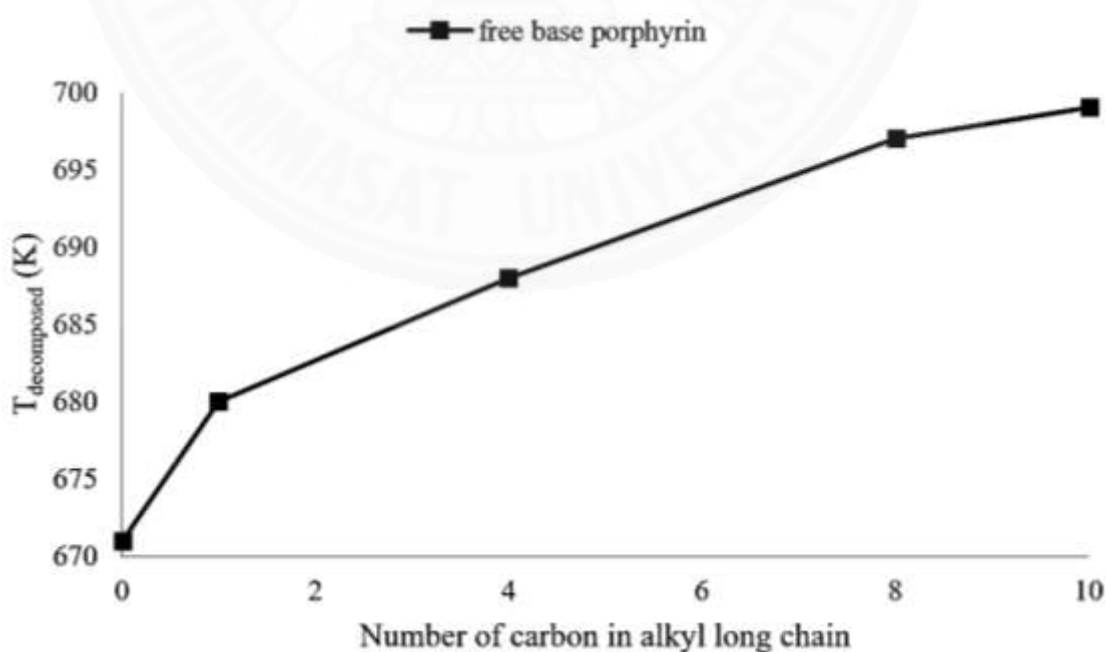


Fig. 63 Correlation between decomposition temperatures with number of carbon in alkyl chain porphyrins

The observation decomposition temperature of the free base porphyrin showed highly thermal stability in rang for 671 – 699 K due to the condensation of pyrrole with alkyl chain aldehyde will afforded the remarkable stability to porphyrin. The trend of decomposition temperature of free base porphyrin found in the range of: TODPP > TOOPP > TOBPP > TOMPP > TPP, related with the increasing number of carbon in alkyl long chain on the *para*- position of phenyl ring. The copper(II) porphyrins show the decomposition temperature higher than free base porphyrins and β -nitro substituted porphyrin complexes. The thermal stability of copper(II) porphyrins can be ranked as the similarly result of free base porphyrin except the CuTPP show the highest thermal stability than other copper complexes. The TGA result of β -nitro substituted porphyrin complexes were founded in same way of copper(II) porphyrin complexes. Consider with TGA, all of synthesized compound can be able to use in alternative energy application.

4.2.8 Biological activity

The current study, the free base porphyrin, copper(II) porphyrin and β -nitro substituted porphyrin complexes were evaluated for their antibacterial activity against *Staphylococcus aureus* (ATCC 25923) and *Escherichia coli* (ATCC 25922) by disc diffusion method at concentration 1 mg/mL. The antibacterial screening data (**Table. 11**) show that all free base porphyrin, copper(II) porphyrin and β -nitro substituted porphyrin complexes were found to be sensitive against both *Staphylococcus aureus* (ATCC 25923) and *Escherichia coli* (ATCC 25922) the inhibition zone was greater than control solvent (DMSO). In addition the commercially available standard drug penicillin was used as a positive control the zone of inhibition against are show in **Fig. 64**.

Table 11 Antibacterial screening data for the synthesized porphyrins **4 – 18**

Complex	<i>Staphylococcus aureus</i>	<i>Bacillus Subtilis</i>
	Inhibition zone (mm)	Inhibition zone (mm)
TPP 4	7.5	6.5
TOMPP 5	8.0	6.5
TOBPP 6	6.8	6.5
TOOPP 7	7.5	6.5
TODPP 8	7.3	6.5
CuTPP 9	13.0	6.5
CuTOMPP 10	14.0	8.0
CuTOBPP 11	8.0	6.5
CuTOOPP 12	10.5	7.3
CuTODPP 13	9.0	8.5
CuTPP-NO ₂ 14	9.0	8.0
CuTOMPP-NO ₂ 15	11.5	8.0
CuTOBPP-NO ₂ 16	9.0	6.5
CuTOOPP-NO ₂ 17	7.0	6.5
CuTODPP-NO ₂ 18	7.0	6.5
DMSO	6.8	6.5
Penicilin	12.5	8.0

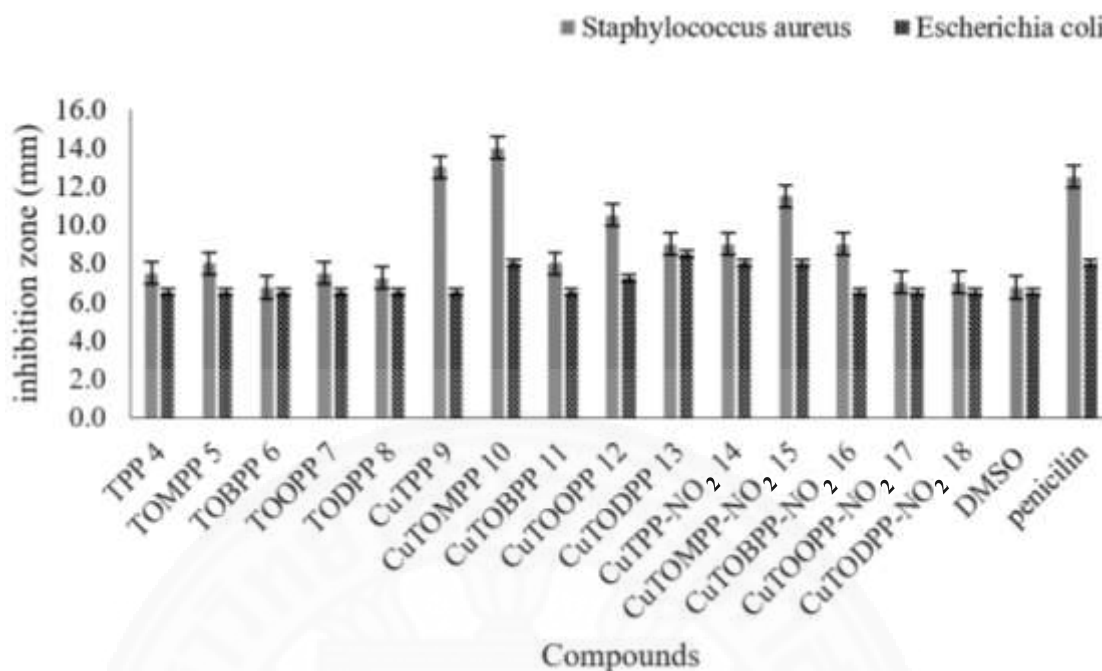


Fig. 64 Comparison of the antimicrobial activities of the synthesized porphyrins 4 – 18

The antibacterial screening data indicate that the copper(II) porphyrin complexes are more potent antibacterial against than β -nitro substituted porphyrin complexes and free base porphyrin. In free base porphyrin, the TOMPP shown the greatest zone of inhibition of 8.0 mm against *S. aureus*, while the inhibition zone of *E. coli* was observed at 6.5 mm. Among all of free base porphyrin, the antibacterial activity of the free base porphyrin showed the maximum zone of inhibition in the order as follow: TOMPP > TPP \geq TOOPP \geq TOBPP \geq TODPP. The similarly trend were observed in both of against *S. aureus*, and *E. coli*. The CuTOMPP and CuTOMPP-NO₂ show the maximum zone of inhibition of *S. aureus*, at 14.0 and 12.5 mm, respectively. In the other hand both of complexes show 8.0 mm of inhibition zone of against *E. coli*. The trend of zone of inhibition were founded similarly in free base porphyrin.

The minimum inhibitory concentration (MIC) and the minimum bactericidal concentration (MBC) the copper(II) porphyrin complexes were summarized in **Table 12**. The minimum inhibitory concentration (MIC) of all copper(II) porphyrin was determined against both of *Staphylococcus aureus* (ATCC 25923) and *Escherichia coli* (ATCC 25922). All copper(II) porphyrin complexes show MIC value at concentration 320 ppm for bacterial strain *S. aureus*, and 160 ppm for bacterial strain *E. coli*. Furthermore, the minimum bactericidal concentration (MBC) value of all copper(II)

porphyrin were founded in the same concentration for both of tested bacterial at 640 ppm. Whereas the CuTPP founded MBC value at 320 ppm for *E. coli* against.

Table 12 The MIC and MBC value of copper(II) porphyrin complexes **9 – 13**

Copper(II) porphyrin	minimum inhibitory concentration (MIC/ppm)		minimum bactericidal concentration (MBC/ppm)	
	<i>S. aureus</i>	<i>E. coli</i>	<i>S. aureus</i>	<i>E. coli</i>
	CuTPP 9	320	160	640
CuTOMPP 10	320	160	640	640
CuTOBPP 11	320	160	640	640
CuTOOPP 12	320	160	640	640
CuTODPP 13	320	160	640	640

4.2.9 Gases sensing application

The gases sensing application of 2-nitro-tetraphenylporphyrinato-copper (II) (CuTPP-NO₂) have been tested, by prepared a film on glass slide. This CuTPP-NO₂ film was prepared by dropped solution of CuTPP-NO₂ in dichloromethane solvent onto substrate glass slide. The SEM image of CuTPP-NO₂ thick film was showed in **Fig. 65**, which CuTPP-NO₂ was dissolved homogeneously, and smoothly coated on substrates show in **Fig. 65b**.

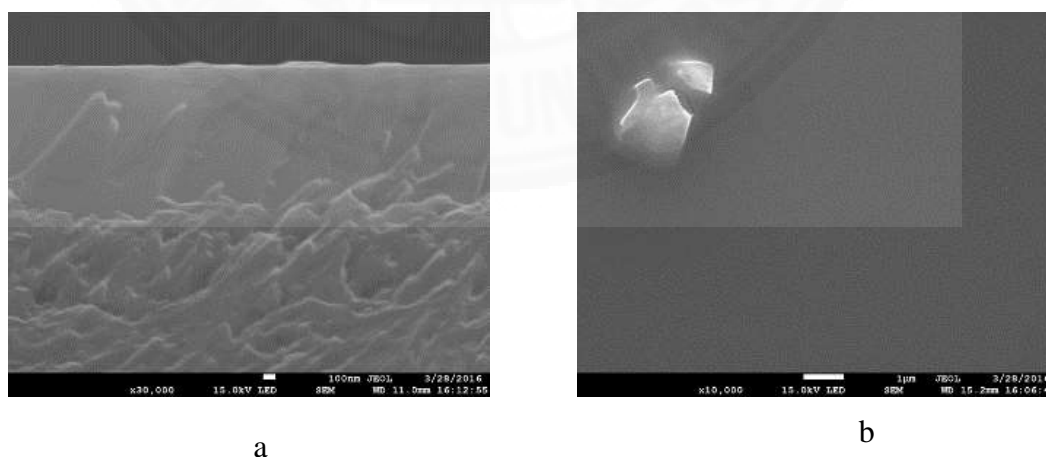


Fig. 65 SEM images of **a** cross section of CuTPP-NO₂ film ($\times 30,000$), and **b** surface of CuTPP-NO₂ film ($\times 10,000$)



Fig. 66 The CuTPP-NO₂ film

For the preliminary test, the alcohol vapors including methanol and ethanol were used to gas sensing tested sample. The gas sensing response of CuTPP-NO₂ film was analyzed from the change in its optical property. The gas sensing response properties of the CuTPP-NO₂ films to 100% methanol were displayed in **Fig. 67**. The similarly results have been reported by Sumance K. [67]. Results have been observed that the CuTPP-NO₂ film was able to act as gas sensor.

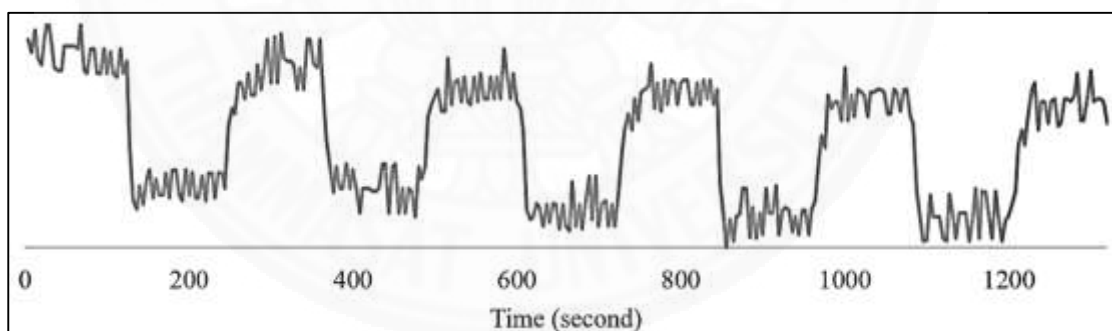


Fig. 67 The dynamic responses of CuTPP-NO₂ film of UV-vis spectra under exposure to methanol (red LED)

Finally, the CuTPP-NO₂ film has been used to sensing alcohol vapors, i.e. 100% methanol, 100% ethanol and mixed sample of methanol and ethanol (1:1) by using electronic nose (e-nose). PCA was used as a pattern recognition method to analyze the data set produced from an UV-Vis spectrophotometer. **Fig. 68a** shows the clear separation of methanol, and ethanol vapors base on the PC1 and PC2 axis. Thus, only

the first two PCs, namely PC1 (58.3%) and PC2 (24.7%), already account for 83% of the information. Results confirm that CuTPP-NO₂ has the capability of performing as an alcohol sensor. In addition, this sensor can be used to identify contamination of the alcohol content as shown in **Fig. 68b** in which the data plot of the methanol (50%) mixed with ethanol (50%). The mixture is located separately between the data plots of pure methanol and ethanol.

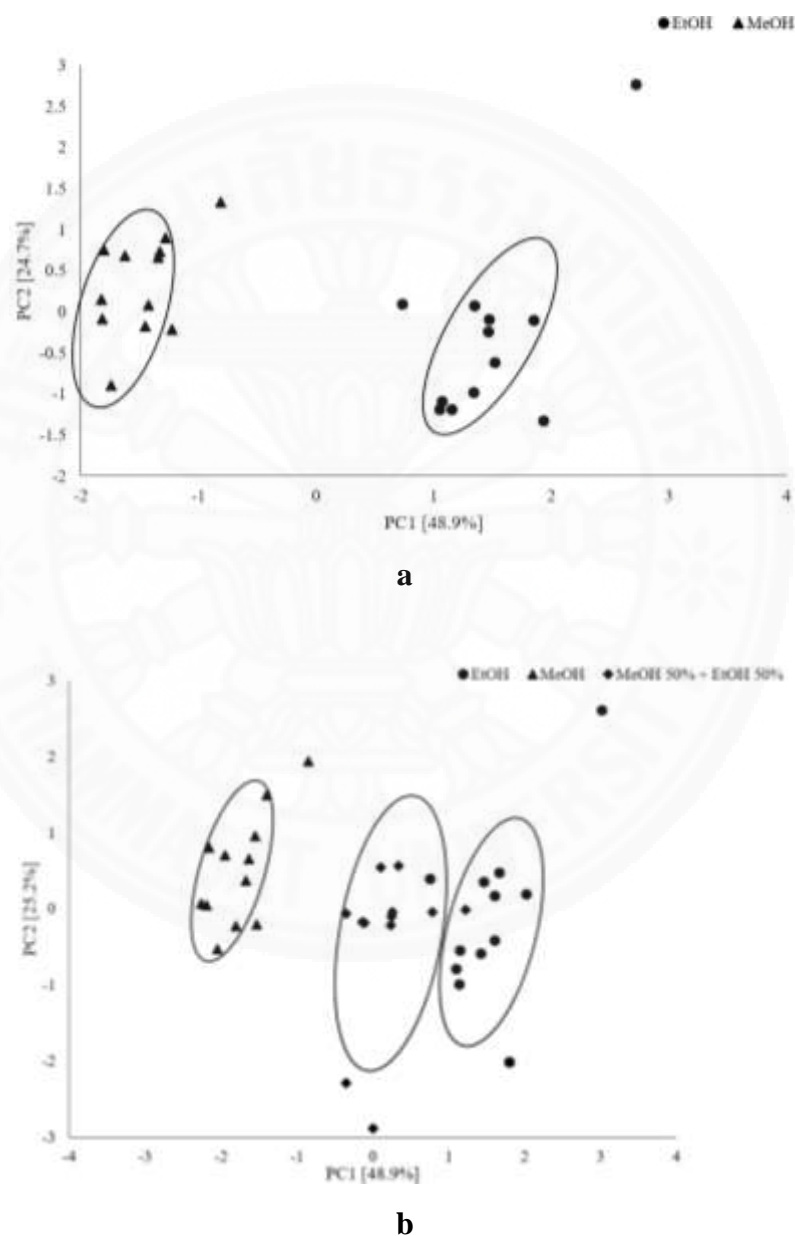


Fig. 68 PCA plot of the optical response of the CuTPP-NO₂ film to alcohol: (a) methanol (100%), and ethanol (100%), and (b) methanol (100%), ethanol (100%), and methanol/ethanol (1:1)

CHAPTER 5

CONCLUSIONS AND RECOMMENDATIONS

The benzaldehyde derivative with alkyl long chain (n=4, 8, and 10) were prepared from a modification previously reported by Jeannis D.K. The alkyloxybenzaldehyde products were confirmed the structure by mass spectrometry (MS), ¹H NMR, ¹³C NMR, and IR spectroscopy. The synthetic aldehyde (compound **1-3**) have been obtained in high reaction yield as over 60%

The *meso*-aryl long chain porphyrins were synthesized by a modification of Alder-Longo method. The optimized condition (refluxed in propionic acid) have been used to synthesized free base porphyrin including TPP **4**, TOMPP **5**, TOBPP **6**, TOOPP **7**, and TODPP **8**. Follow the modified method all free base porphyrin were obtained in range 9-26% yield. Moreover, the copper(II) porphyrin complexes have been prepared by refluxing each free base porphyrin with copper(II)acetate in mixed solvent of dichloromethane and *N,N*-dimethylformamide. The reaction of ligand and copper(II) acetate provided CuTPP **9**, CuTOMPP **10**, CuTOBPP **11**, CuTOOP **12** and CuTODPP **13** in 93%, 92%, 71%, 96% and 63% yield, respectively. The copper(II) porphyrin gave the high yield due to the copper(II) ion size, that fitted into the porphyrin control hole. In addition, all copper(II) porphyrin complexes were inserted the nitro (-NO₂) group into the β -position. The nitration reaction between copper(II) porphyrin complexes with copper(II) nitrate and acetic anhydride in chloroform have been used to synthesized the β -nitro substituted porphyrin including CuTPP-NO₂ **14**, CuTOMPP-NO₂ **15**, CuTOBPP- NO₂ **16**, CuTOOPP- NO₂ **17** and CuTODPP- NO₂ **18**. All β -nitro substituted porphyrin complexes were gave in low reaction yield, less than 30% yield, due to the steric of alkyl long chain and nitro group at β -position. The free base porphyrins, copper(II) porphyrin complexes and β -nitro substituted porphyrin complexes were confirmed the expected synthesized structure by CHN elemental analysis (CHN), mass spectrometry (MS), ¹H and ¹³C NMR, and IR spectroscopy.

The UV-vis absorption spectra of free base porphyrin exhibited a strong absorption (soret band) with four weak absorption (Q band), copper(II) porphyrin complexes displayed a single. Soret band with only one Q band, while the β -nitro

substituted porphyrin show one Soret band with two Q band in dichloromethane solution. The absorption spectra of copper(II) porphyrin moved to a small blue shift, while the absorption of β -nitro substituted porphyrin moved to small red shift when compared with free base porphyrin. When excited the free base porphyrin at 530 nm, the synthesized porphyrin exhibited fluorescence spectra at 654 nm. The calculated energy gap of all free base porphyrin were observed at 1.90 eV. For the fluorescence studied of copper(II) porphyrin and β -nitro substituted porphyrin complexes were show the low intensity fluorescence at 605 and 613 – 620 nm, respectively when excited at the maximum absorption of the Q band. The thermal stability of all synthesized compounds were measured by thermal gravimetric analysis (TGA). The heating process were studied at 308 – 1,173 K. All of synthesized compounds were found to be highly thermal stability as over 600 K. The trend of thermal stability was follow: TODPP > TOOPP > TOBPP > TOMPP > TPP. Although, CuTPP and CuTPP-NO₂ show the thermal stability than other copper(II) porphyrin and β -nitro substituted porphyrin complexes. The copper(II) porphyrin complexes were found to be the highly thermal stability than pure ligand and β -nitro substituted porphyrin complexes.

The antibacterial activity indicates that the synthesized compounds is found to be sensitive against both of *Staphylococcus aureus* (ATCC 25923) and *Escherichia coli* (ATCC 25922). The TOMPP, CuTOMPP, and CuTOMPP-NO₂ show higher zone of inhibition than other compound in each series. The minimum inhibitory concentration (MIC) and the minimum bactericidal concentration (MBC) of the copper(II) porphyrin complexes were investigated. All copper(II) porphyrin found the MIC value of *S. aureus* and *E. coli* at 320 and 160 ppm, respectively. While the MBC value of all complexes were found at 640 ppm for both of bacterial strain. Furthermore, the gas sensing properties of CuTPP-NO₂ have been observed. The CuTPP-NO₂ film was shown to be very effective in the discrimination of alcohol.

REFERENCES

1. Porphyrin-http://shodhganga.inflibnet.ac.in/bitstream/10603/323/3/06_chapter1.pdf. Retrieved October 07, 2015.
2. Milgrom L. R. (1997). The colours of life: an introduction to the chemistry of porphyrins and related compounds. *Oxford University Press, Oxford*.
3. Vicente, M.G.H. and Smith, K.M. (2000) Porphyrins and Derivatives: Synthetic Strategies and Reactivity Profiles. *Current Organic Chemistry* 4, 139 - 174.
4. Kumar, R. and Sankar, M. (2014) Synthesis, Spectral, and Electrochemical Studies of Electronically Tunable β -Substituted Porphyrins with Mixed Substituent Pattern. *Inorganic Chemistry* 53(24), 12706-12719.
5. Collman J.P., Hallbert T.R. and Suslick K.S. (1980). Metal ion activation of dioxygen. *In Metal Ions in Biology*, 2.
6. Lu-Lin L., Eric Wei-Guang D. (2013). Porphyrin-sensitized solar cell. *Chemical Society Reviews* 42, 297 – 304.
7. Heme-<http://en.wikipedia.org/wiki/Heme>. Retrieved October 22, 2015.
8. Heme-www.chemistry.wustl.edu/~edudev/LabTutorials/Hemoglobin/MetalComplexinBlood.html. Retrieved October 22, 2015.
9. Chlorophyll-<http://en.wikipedia.org/wiki/Chlorophyll>. Retrieved October 22, 2015.
10. Chlorophyll-scifun.chem.wisc.edu/chemweek/chlrphyl/chlrphyl.html. Retrieved October 22, 2015.
11. Vitamin B12-http://en.wikipedia.org/wiki/Vitamin_B12. Retrieved October 22, 2015.
12. Vitamin B12-<http://www.nlm.nih.gov/medlineplus/ency/article/002403.html>. Retrieved October 22, 2015.
13. Enzyme-<http://en.wikipedia.org/wiki/Enzyme>. Retrieved October 22, 2015.
14. Paul R. (1935), Formation of porphyrin from pyrrole and aldehyde. *Journal of the American Chemical Society* 57, 2010 – 2011.

15. Jonathan R. S. (2010). Synthesis and photophysical characterization of π -extended platinum porphyrins for application in high efficiency near-IR light emitting diodes. Doctor of philosophy. *University of Florida*.
16. Kevin M. S. *et al.*(1989). *Reu. Port. Quim.*, 31, 29 – 41.
17. Kavin, M. S., and Vicent M.G.H. (2014). Synthesis and functionalizations of porphyrin macrocycles. *Current. Organic. Synthesis* 11(1), 3 – 28.
18. Dolmans, D.E., Dai, F., Rakesh, K.J. (2003) Photodynamic therapy for cancer. *Nature Reviews Cancer* 3, 380 – 387
19. Banfi, S., Caruso, E., Buccafurni, L., Battini, V., Zazzaron, S., Barbieri, P. and Orlandi, V. (2006) Antibacterial activity of tetraaryl-porphyrin photosensitizers: an in vitro study on Gram negative and Gram positive bacteria. *J Photochem Photobiol B* 85(1), 28-38.
20. Timm, R.A., Falla, M.P.H., Huila, M.F.G., Peres, H.E.M., Ramirez-Fernandez, F.J., Araki, K. and Toma, H.E. (2010) Vanadium oxide-porphyrin nanocomposites as gas sensor interfaces for probing low water content in ethanol. *Sensors and Actuators B: Chemical* 146(1), 61-68.
21. Rothmund, P. (1936) A New Porphyrin Synthesis. The Synthesis of Porphin. *Journal of the American Chemical Society* 58, 625 - 627.
22. Alan D. Adler, Longo, F.R. and Shergalis, W. (1964) Mechanistic Investigations of Porphyrin Syntheses. I. Preliminary Studies on *meso*-Tetraphenylporphin. *Journal of the American Chemical Society* 86, 3145 - 3149.
23. Lindsey, J.S., Hsu, H.C. and Schreiman, I.C. (1986) Synthesis of Tetraphenylporphyrin Under Very Mild Condition *Tetrahedron Letters* 27, 4969 - 4970.
24. Temelli, B. and Unaleroglu, C. (2009) Synthesis of *meso*-tetraphenyl porphyrins via condensation of dipyrromethanes with N-tosyl imines. *Tetrahedron* 65(10), 2043-2050.
25. Hombrecher, H.K. and Ohm, S. (1993) An Efficient Synthesis of Tetraaryl Porphyrins Substituted with Ester Groups Bearing Long Alkyl Chains *Tetrahedron* 49, 2447 - 2456.

26. Wang, M.-C., Sue, L.-S., Liao, B.-C., Ko, B.-T., Elango, S. and Chen, J.-H. (2001) Mercury Complexes of *meso*-Tetra-(*p*-cyanophenyl)porphyrin and *N*-methylporphyrin: *meso*-Tetra(*p*-cyanophenyl)porphyrinato-mercury(II) and Chloro(*N*-methyl-mesotetraphenylporphyrinato)mercury(II). *Inorganic Chemistry* 40, 6064 - 6048.
27. Lee, Y.-Y., Chen, J.-H. and Hsieh, H.-Y. (2003) Metal complexes of *meso*-tetra-(*p*-chlorophenyl)porphyrin and *meso*-tetra-(*p*-bromophenyl)porphyrin: Tl[(*p*-Cl)4tpp](OAc) and In[(*p*-X)4tpp](OAc) [X=Cl, Br, tpp=5,10,15,20-tetraphenylporphyrinate]. *Polyhedron* 22(13), 1633-1639.
28. Gupta, I. and Ravikanth, M. (2003) Synthesis of *meso*-furyl porphyrins with N₄, N₃S, N₂S₂ and N₃O porphyrin cores. *Tetrahedron* 59(32), 6131-6139.
29. Luguya, R., Jaquinod, L., Fronczek, F.R., Vicente, M.G.H. and Smith, K.M. (2004) Synthesis and reactions of *meso*-(*p*-nitrophenyl)porphyrins. *Tetrahedron* 60(12), 2757-2763.
30. Maestrin, A.P.J., Tedesco, A.C., Neri, C.R., Gandini, M.E.F., Serra, O.A. and Iamamoto, Y. (2004) Synthesis, Spectroscopy and Photosensitizing Properties of Hydroxynitrophenylporphyrins. *Journal of The Brazilian Chemical Society* 15, 708 - 713.
31. Fedulova, I.N., Bragina, N.A., Novikov, N.V., Ugol'nikova, O.A. and Mironov, A.F. (2007) Synthesis of lipophilic tetraphenylporphyrins to design lipid-porphyrin ensembles. *Russian Journal of Bioorganic Chemistry* 33(6), 589-593.
32. Ghosh, A., Selvamani, T., Jose, D.A., Das, A. and Mukhopadhyay, I. (2007) Generation of Nanostructures by the Aggregation of Porphyrin Derivatives with Long Alkane Chain in Mix-Solvent. *Journal of Nanomaterials* 2007, 1-8.
33. Kostas, I.D., Coutsolelos, A.G., Charalambidis, G. and Skondra, A. (2007) The first use of porphyrins as catalysts in cross-coupling reactions: a water-soluble palladium complex with a porphyrin ligand as an efficient

- catalyst precursor for the Suzuki–Miyaura reaction in aqueous media under aerobic conditions. *Tetrahedron Letters* 48(38), 6688-6691.
34. Li, J., Tang, T., Li, F. and Li, M. (2008) The synthesis and characterization of novel liquid crystalline, *meso*-tetra[4-(3,4,5- trialkoxybenzoate)phenyl] porphyrins. *Dyes and Pigments* 77(2), 395- 401.
35. Wang, C., Yang, G., Li, J., Mele, G., Slota, R., Broda, M., Duan, M., Vasapollo, G., Zhang, X. and Zhang, F. (2009) Novel *meso*-substituted porphyrins: Synthesis, characterization and photocatalytic activity of their TiO₂-based composites. *Dyes and Pigments* 80(3), 321-328.
36. Sun, E., Sun, Z., Yuan, M., Wang, D. and Shi, T. (2009) The synthesis and properties of *meso*-tetra(4-alkylamidophenyl)porphyrin liquid crystals and their Zn complexes. *Dyes and Pigments* 81(2), 124-130
37. Xue, Z., Lee, P.P.S., Wang, Y., Kwong, D.W.J., Li, J., Xin, J.H., Wong, W.-K. and Cheuk, K.K.L. (2011) Further insight into aryl nitration of tetraphenylporphyrin. *Tetrahedron* 67(33), 6030-6035.
38. Moonsin, P., Sirithip, K., Jungsuttiwong, S., Keawin, T., Sudyoasuk, T. and Promarak, V. (2011) *meso*-Multi(iodophenyl) porphyrins: synthesis, isolation, and identification. *Tetrahedron Letters* 52(37), 4795-4798.
39. Liao, J.X., Zhao, H.B., Yang, D.L., Chen, L. and Wang, B.Y. (2011) {*meso*-Tetra-kis[p-(hept-yloxy)phen-yl]-porphyrinato}silver(II). *Acta Crystallogr Sect E Struct Rep Online* 67(Pt 9), m1316.
40. Zieba, G., Rojkiewicz, M., Kozik, V., Jarzembek, K., Jarczyk, A., Sochanik, A. and Kus, P. (2012) The synthesis of new potential photosensitizers. 1. Mono-carboxylic acid derivatives of tetraphenylporphyrin. *Monatsh Chem* 143(1), 153-159.
41. Thomas, A.P., Saneesh Babu, P.S., Asha Nair, S., Ramakrishnan, S., Ramaiah, D., Chandrashekar, T.K., Srinivasan, A. and Radhakrishna Pillai, M. (2012) *Meso*-tetrakis(p-sulfonatophenyl)N-confused porphyrin tetrasodium salt: a potential sensitizer for photodynamic therapy. *J Med Chem* 55(11), 5110-5120.

42. Taesch, J., Dang, T.T. and Heitz, V. (2012) Efficient synthesis and Suzuki cross-coupling reactions of *meso*-tetrakis(2,6-dimethyl-4-triflyloxyphenyl)porphyrin. *Tetrahedron Letters* 53(3), 333-337.
43. Wu, Y.-h., Chen, L., Yu, J., Tong, S.-l. and Yan, Y. (2013) Synthesis and spectroscopic characterization of *meso*-tetra (Schiff-base substituted phenyl) porphyrins and their zinc complexes. *Dyes and Pigments* 97(3), 423-428.
44. Zhang, Y.J., Shi, J., Liu, W. and Yu, M. (2013) 5, 10, 15, 20-Tetra (N-Long Chain-Alkyl Carbazole) Porphyrin and Their Lanthanide Complexes. *Synthesis and Reactivity in Inorganic, Metal-Organic, and Nano-Metal Chemistry* 43(5), 640-646.
45. Pinto, V.H., Carvalhoda-Silva, D., Santos, J.L., Weitner, T., Fonseca, M.G., Yoshida, M.I., Idemori, Y.M., Batinic-Haberle, I. and Reboucas, J.S. (2013) Thermal stability of the prototypical Mn porphyrin-based superoxide dismutase mimic and potent oxidative-stress redox modulator Mn(III) *meso*-tetrakis(N-ethylpyridinium-2-yl)porphyrin chloride, MnTE-2-PyP(5+). *J Pharm Biomed Anal* 73, 29-34.
46. Nandi, G. and Sarkar, S. (2014) High yield synthesis of oxo-tungsten(V) porphyrin: Structural characterization of the hydrolyzed products. *Inorganica Chimica Acta* 410, 106-110.
47. Xu, Z., Mei, Q., Weng, J. and Huang, W. (2014) Synthesis, characterization and properties of covalently linked porphyrin–naphthalimide pentamer and its metal complexes. *Journal of Molecular Structure* 1074, 687-694.
48. Zhang, Z., Duan, Y., Zhang, L., Yu, M. and Li, J. (2015) Synthesis, crystal structure of two new Zn(II), Cu(II) porphyrins and their catalytic activities to ethylbenzene oxidation. *Inorganic Chemistry Communications* 58, 53-56.
49. Jiblaoui, A., Leroy-Lhez, S., Ouk, T.S., Grenier, K. and Sol, V. (2015) Novel polycarboxylate porphyrins: synthesis, characterization, photophysical properties and preliminary antimicrobial study against Gram-positive bacteria. *Bioorg. Med. Chem. Lett.* 25(2), 355-362.

50. Xu, Z., Mei, Q., Hua, Q., Tian, R., Weng, J., Shi, Y. and Huang, W. (2015) Synthesis, characterization, energy transfer and photophysical properties of ethynyl bridge linked porphyrin–naphthalimide pentamer and its metal complexes. *Journal of Molecular Structure* 1094, 1-8.
51. Misra, R. and Gautam, P. (2015) *Meso*-tetrakis(ferrocenylethynylphenyl) porphyrins: Synthesis and properties. *Journal of Organometallic Chemistry* 776, 83-88.
52. Huang, G., Mo, L.-Q., Cai, J.-L., Cao, X., Peng, Y., Guo, Y.-A. and Wei, S.-J. (2015) Environmentally friendly and efficient catalysis of cyclohexane oxidation by iron *meso*-tetrakis(pentafluorophenyl)porphyrin immobilized on zinc oxide. *Applied Catalysis B: Environmental* 162, 364-371.
53. Siri, O., Jaquinod, L. and Smith, K.M. (2000) Coplanar conjugated β -nitroporphyrins and some aspects of nitration of porphyrins with N_2O_4 *Tetrahedron Letters* 41, 3583 - 3587.
54. Domingues, M.R.r.M., S.-Marques, M.G.a.O., Domingues, P., Neves, M.G.a., Cavaleiro, J.A.S. and Ferrer-Correia, A.J. (2000) Differentiation of Positional Isomers of Nitro *Meso*-Tetraphenylporphyrins by Tandem Mass Spectrometry. *American Society for Mass Spectrometry* 12, 381 - 384.
55. Terazono, Y., Patrick, B.O. and Dolphin, D.H. (2002) Synthesis, Crystal Structures, and Redox Potentials of 2,3,12,13-Tetrasubstituted 5,10,15,20-Tetraphenylporphyrin Zinc(II) Complexes. *Inorganic Chemistry* 41, 6703 - 6710.
56. Hu, J., Pavel, I., Moigno, D., Wumaier, M., Kiefer, W., Chen, Z., Ye, Y., Wu, Q., Huang, Q., Chen, S., Niu, F. and Gu, Y. (2003) Fourier-transform Raman and infrared spectroscopic analysis of 2-nitro-tetraphenylporphyrin and metallo-2-nitro-tetraphenylporphyrins. *Spectrochimica Acta Part A: Molecular and Biomolecular Spectroscopy* 59(9), 1929-1935.
57. Ostrowski, S. and Grzyb, S. (2012) Direct β -amination reaction in porphyrin systems—a simple route to compounds containing two nitrogen

- substituents at both β -positions of the same pyrrole unit. *Tetrahedron Letters* 53(47), 6355-6357.
58. Sirithip, K., Morada, S., Namuangruk, S., Keawin, T., Jungsuttiwong, S., Sudyoasuk, T. and Promarak, V. (2013) Synthesis and characterization of β -pyrrolic functionalized porphyrins as sensitizers for dye-sensitized solar cells. *Tetrahedron Letters* 54(19), 2435-2439.
59. Campbell, W.M., Jolley, K.W., Wagner, P., Wagner, K., Walsh, P.J., Gordon, K.C., Schmidt-Mende, L., Nazeeruddin, M.K., Wang, Q., Gratzel, M. and Officer, D.L. (2007) Highly Efficient Porphyrin Sensitizers for Dye-Sensitized Solar Cells. *The Journal of Physical Chemistry C* 111, 11760 - 11762.
60. He, H., Dubey, M., Zhong, Y., Shrestha, M. and Sykes, A.G. (2011) 2-(1-Acetyl-2-oxopropyl)-5,10,15,20-tetraphenylporphyrin and Its Transition-Metal Complexes. *European Journal of Inorganic Chemistry*, 3731 - 3738 .
61. Tan, Q., Zhang, X., Mao, L., Xin, G. and Zhang, S. (2013) Novel zinc porphyrin sensitizers for dye-sensitized solar cells: Synthesis and spectral, electrochemical, and photovoltaic properties. *Journal of Molecular Structure* 1035, 400-406.
62. Chitpakdee, C., Namuangruk, S., Suttisintong, K., Jungsuttiwong, S., Keawin, T., Sudyoasuk, T., Sirithip, K., Promarak, V. and Kungwan, N. (2015) Effects of π -linker, anchoring group and capped carbazole at *meso*-substituted zinc-porphyrins on conversion efficiency of DSSCs. *Dyes and Pigments* 118, 64-75.
63. Kooriyaden, F.R., Sujatha, S. and Arunkumar, C. (2015) Synthesis, spectral, structural and antimicrobial studies of fluorinated porphyrins. *Polyhedron* 97, 66-74.
64. Xu, X.-J., Xue, Z., Qi, Z.-D., Hou, A.-X., Li, C.-H. and Liu, Y. (2008) Antibacterial activities of manganese(II) ebselen-porphyrin conjugate and its free components on *Staphylococcus aureus* investigated by microcalorimetry. *Thermochimica Acta* 476(1-2), 33-38.

65. Rojkiewicz, M., Kuś, P., Kozub, P. and Kempa, M. (2013) The synthesis of new potential photosensitizers [1]. Part 2. Tetrakis-(hydroxyphenyl)porphyrins with long alkyl chain in the molecule. *Dyes and Pigments* 99(3), 627-635.
66. Roales, J., Pedrosa, J.M., Castellero, P., Cano, M. and Richardson, T.H. (2011) Optimization of mixed Langmuir–Blodgett films of a water insoluble porphyrin in a calixarene matrix for optical gas sensing. *Thin Solid Films* 519(6), 2025-2030.
67. Kladsomboon, S. and Kerdcharoen, T. (2012) A method for the detection of alcohol vapours based on optical sensing of magnesium 5,10,15,20-tetraphenyl porphyrin thin film by an optical spectrometer and principal component analysis. *Anal Chim Acta* 757, 75-82.
68. Esteves, C.H.A., Iglesias, B.A., Li, R.W.C., Ogawa, T., Araki, K. and Gruber, J. (2014) New composite porphyrin-conductive polymer gas sensors for application in electronic noses. *Sensors and Actuators B: Chemical* 193, 136-141.
69. Song, F., Ma, P., Chen, C., Jia, J., Wang, Y. and Zhu, P. (2016) Room temperature NO₂ sensor based on highly ordered porphyrin nanotubes. *J Colloid Interface Sci* 474, 51-57.
70. Zhao, L., Li, M., Liu, M., Zhang, Y., Wu, C. and Zhang, Y. (2016) Porphyrin-functionalized porous polysulfone membrane towards an optical sensor membrane for sorption and detection of cadmium(II). *J Hazard Mater* 301, 233-241.
71. Domingues, M.R.M., S.-Marques, M.G.a.O., Vale, C.A.M., Neves, M.G.a., Cavaleiro, J.A.S. and Ferrer-Correia, A.J. (1998) Do Charge-Remote Fragmentations Occur under Matrix-Assisted Laser Desorption Ionization Post-Source Decompositions and Matrix-Assisted Laser Desorption Ionization Collisionally Activated Decompositions? *American Society for Mass Spectrometry* 10, 217 - 223.
72. Costa, D.S., Martino, T., Magalhaes, F.C., Justo, G., Coelho, M.G., Barcellos, J.C., Moura, V.B., Costa, P.R., Sabino, K.C. and Dias, A.G. (2015) Synthesis of N-methylarylnitrones derived from alkyloxybenzaldehydes

- and antineoplastic effect on human cancer cell lines. *Bioorg Med Chem* 23(9), 2053-2061.
73. Gary M.L., Donald L.P., George S.K., James R.V. (2010) *Spectroscopy 4th edition*. USA.
74. Meng, S., Xu, Z., Hong, G., Zhao, L., Zhao, Z., Guo, J., Ji, H. and Liu, T. (2015) Synthesis, characterization and in vitro photodynamic antimicrobial activity of basic amino acid-porphyrin conjugates. *Eur J Med Chem* 92, 35-48.
75. Dehghani, H. and Shaterian, M. (2009) New Cationic Sandwich-type Intermediate Sitting-atop Complexation between *meso*-Tetraarylporphyrins and Tantalum(V) Chloride: Synthesis, Spectroscopic Characterization and Photoluminescence Study. *Bulletin of the Korean Chemical Society* 30, 2792 -2794.
76. Barbara V., Lucia F.G.M., Fabio L. and David L.O. (2008). Extending the porphyrin core: synthesis and photophysical characterization of porphyrins with ρ -conjugated β -substituents. *New Journal of Chemistry*, 32, 166-178.
77. Gamboa M. and Campos M. (2010). Study of the stability of 5,10,15,20-tetraphenylporphine (TPP) and metalloporphyrins NiTPP, CoTPP, CuTPP, and ZnTPP by differential scanning calorimetry and thermogravimetry. *The Journal of Chemical Thermodynamics*, 42, 666-674.
78. Xiuhua W., Xiuhong D., Donghua C. and Zhangping C. (2006). Thermal analysis study of 5,10,15,20-tetrakis (methoxyphenyl) porphyrins and their nickel complexes. *Thermochimica Acta*, 440, 181-187.



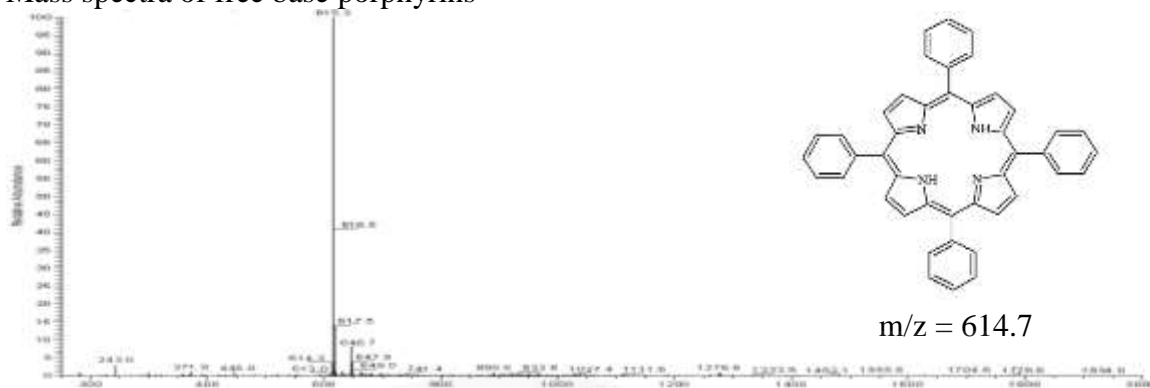
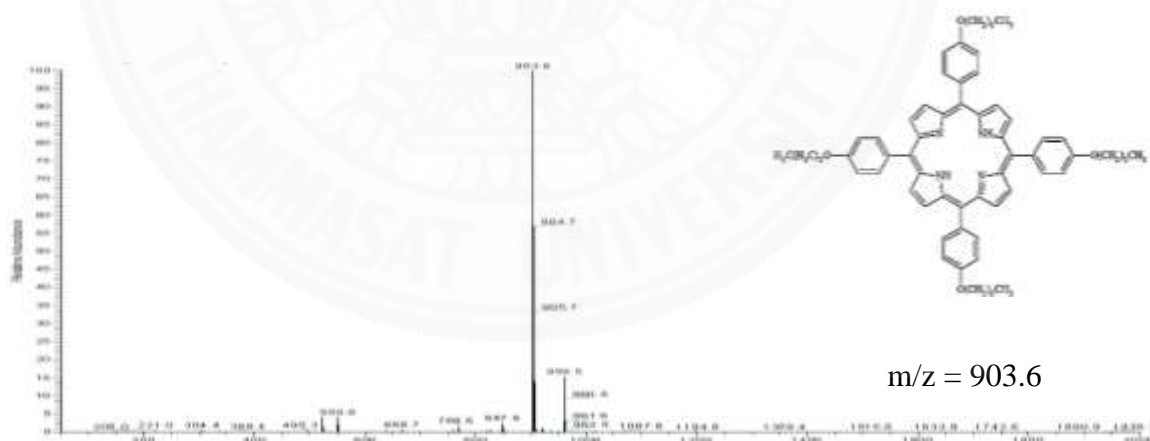
APPENDICES

APPENDIX A MASS SPECTRA

Mass spectra of aldehyde



Mass spectra of free base porphyrins

Fig. A4 The mass spectrum of TPP 4 in CH_2Cl_2 Fig. A5 The mass spectrum of TOMPP 5 in CH_2Cl_2 Fig. A6 The mass spectrum of TOBPP 6 in CH_2Cl_2

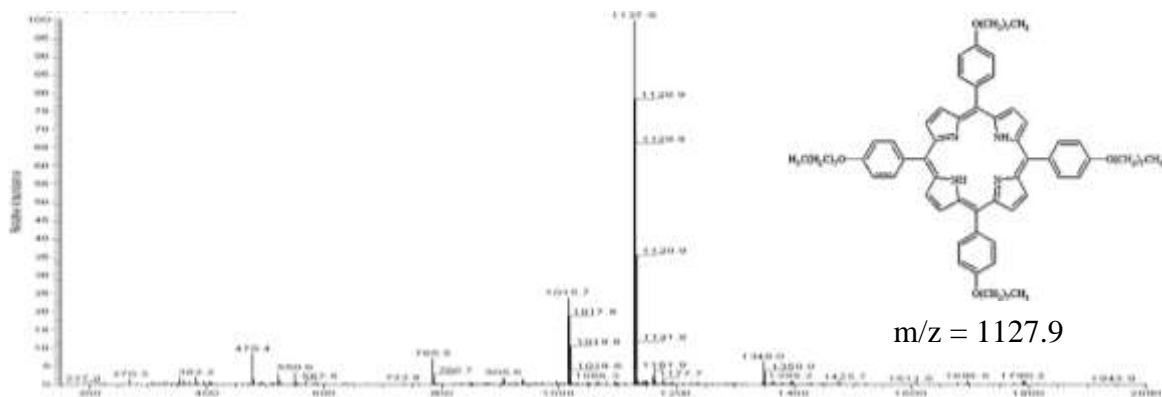


Fig. A7 The mass spectrum of TOOPP **7** in CH_2Cl_2

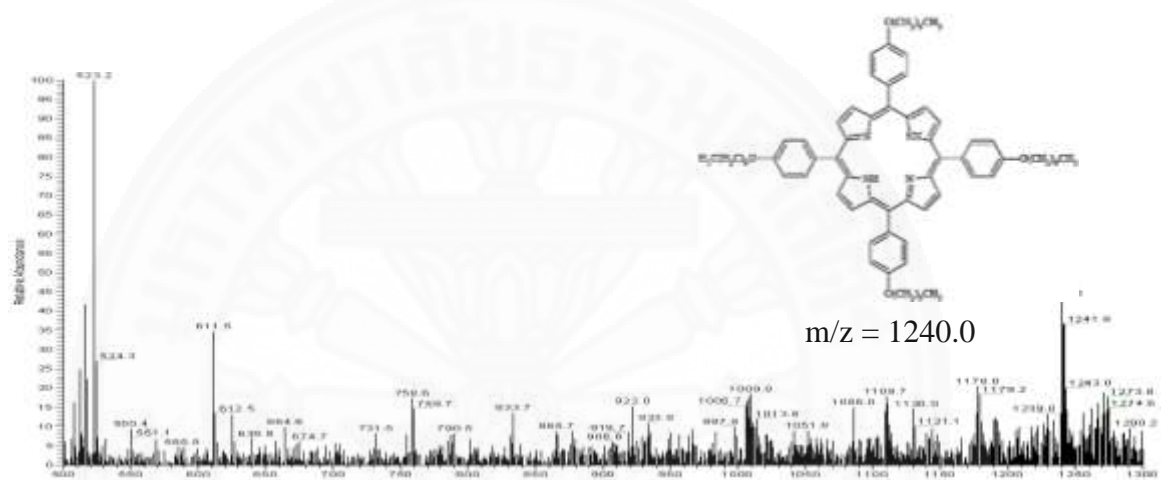


Fig. A8 The mass spectrum of TODPP **8** in CH_2Cl_2

Mass spectra of copper(II) porphyrins

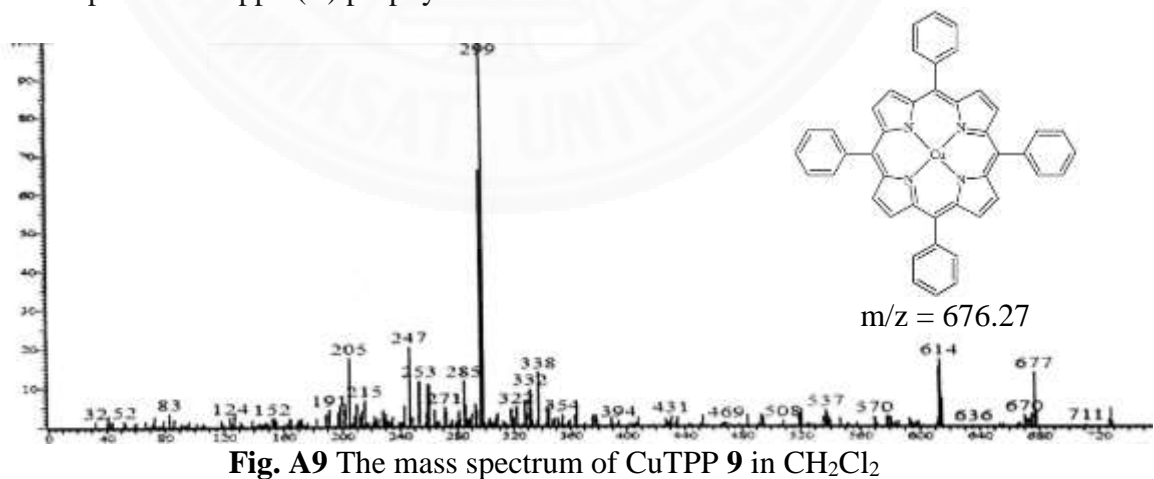


Fig. A9 The mass spectrum of CuTPP **9** in CH_2Cl_2

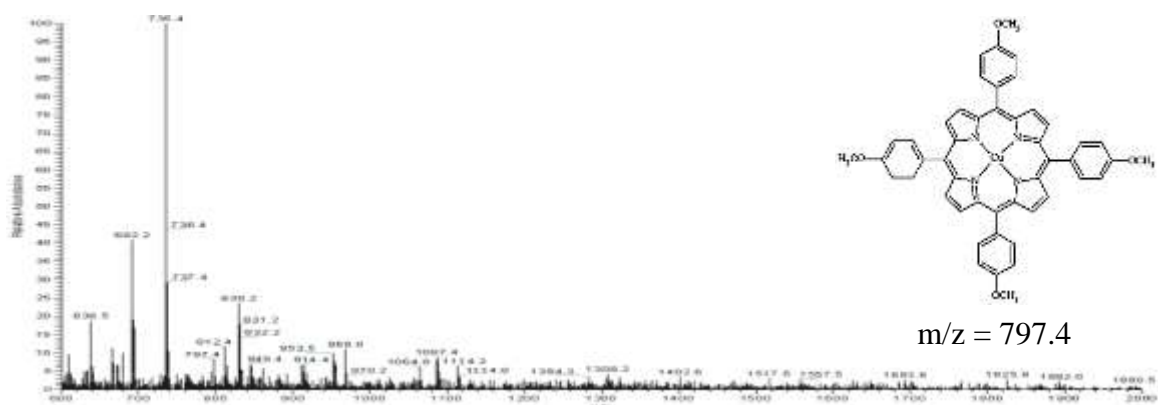


Fig. A10 The mass spectrum of CuTOMPP 10 in CH₂Cl₂

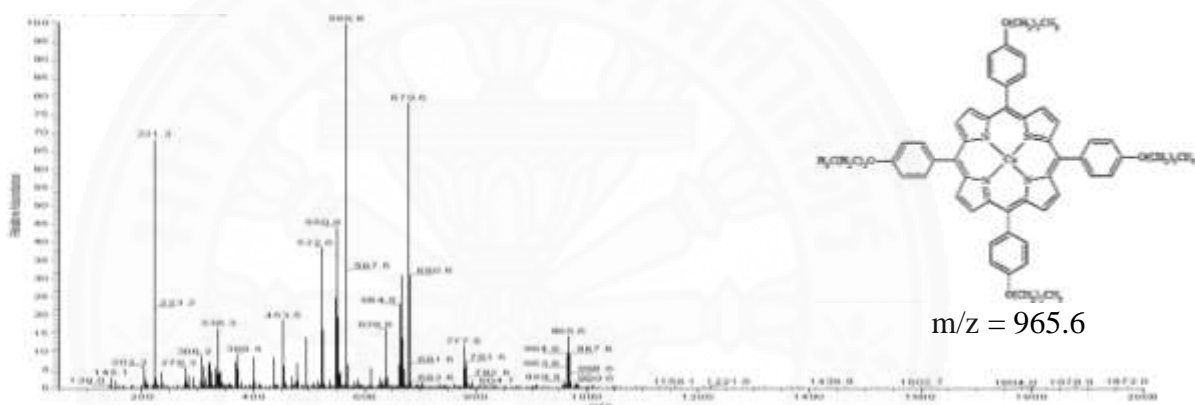


Fig. A11 The mass spectrum of CuTOBPP 11 in CH₂Cl₂

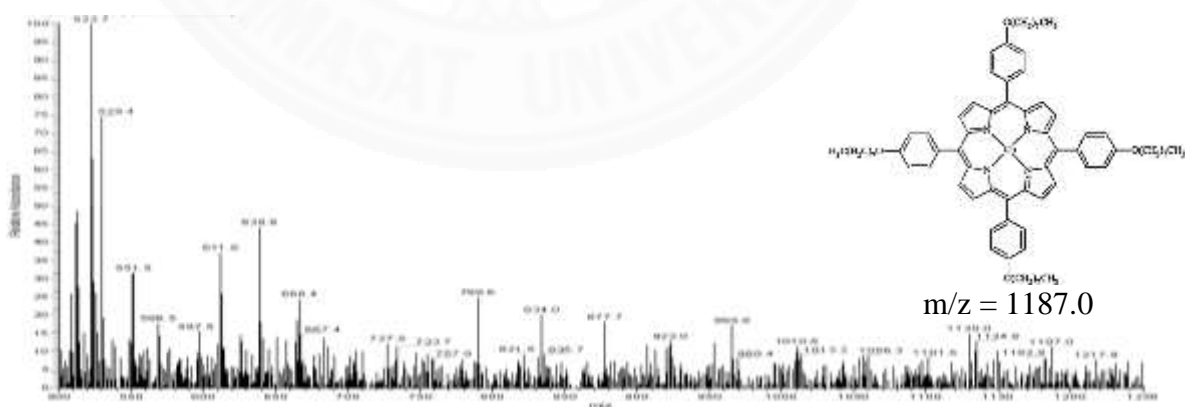


Fig. A12 The mass spectrum of CuTOOPP 12 in CH₂Cl₂

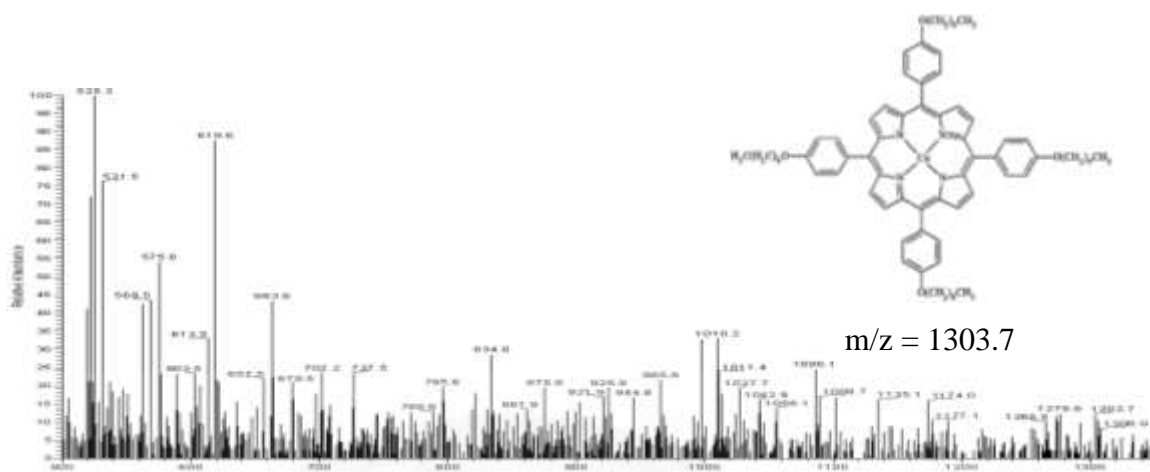


Fig. A13 The mass spectrum of CuTODPP 13 in CH₂Cl₂

Mass spectra of β -nitro substituted porphyrin complexes

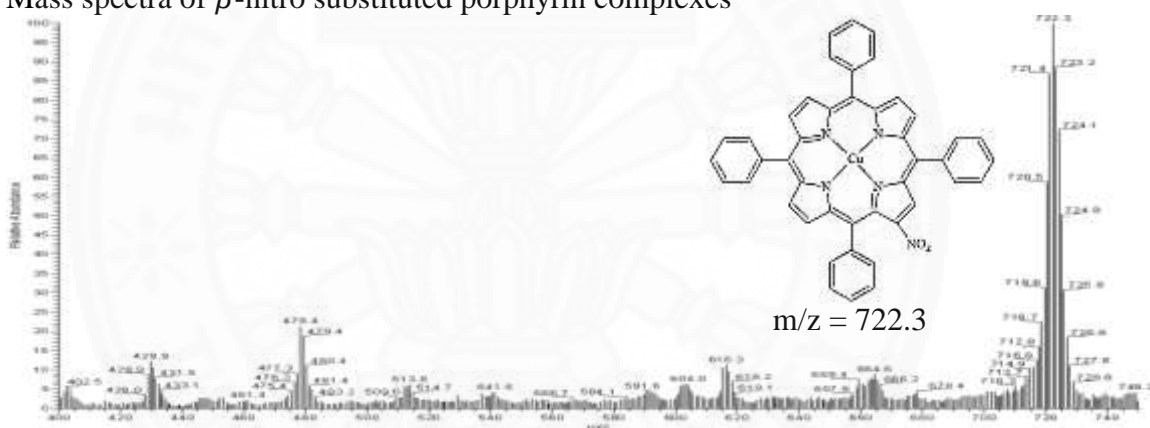


Fig. A14 The mass spectrum of CuTPP-NO₂ 14 in CH₂Cl₂

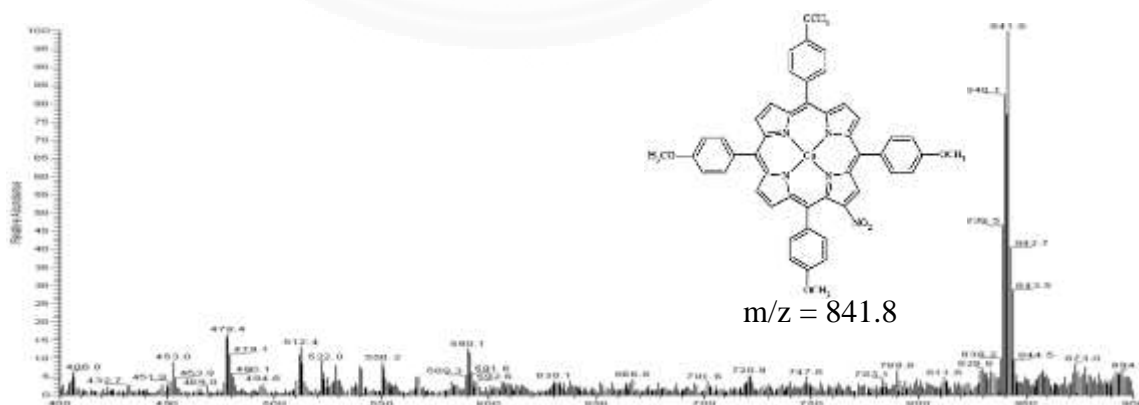
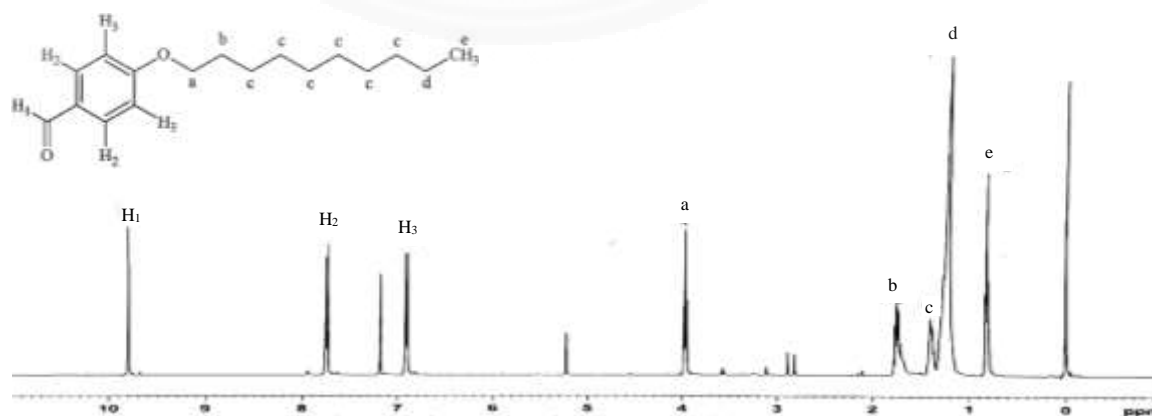
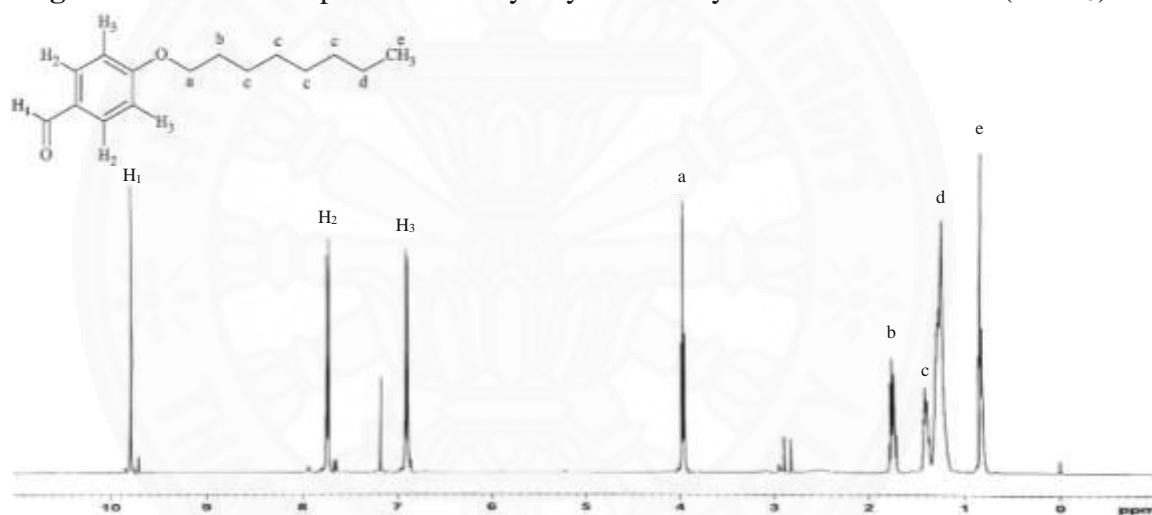
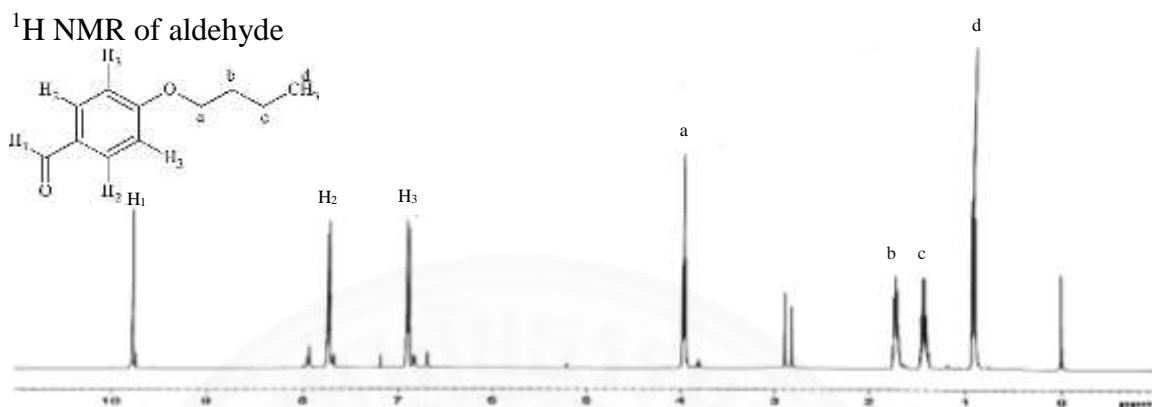


Fig. A15 The mass spectrum of CuTOMPP-NO₂ 15 in CH₂Cl₂

APPENDIX B

NMR SPECTRA



^1H NMR of free base porphyrin:

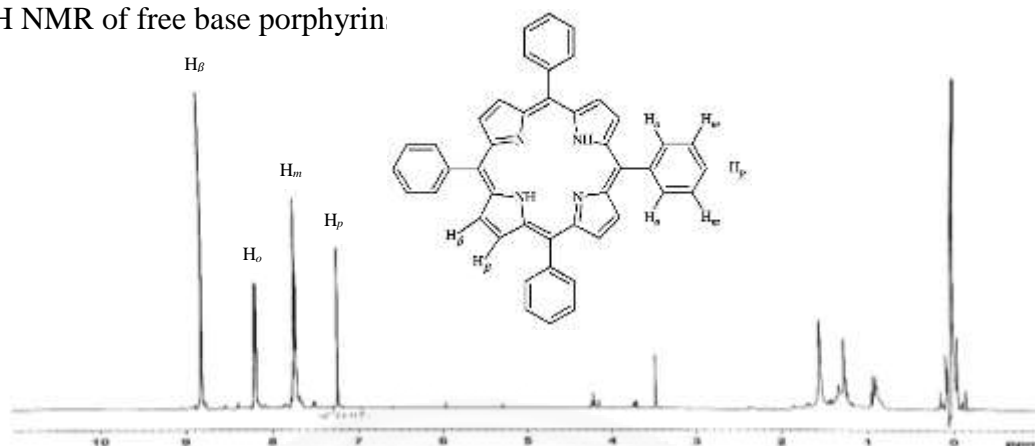


Fig. B4 The ^1H NMR spectrum of TPP 4 in chloroform-d (CDCl_3)

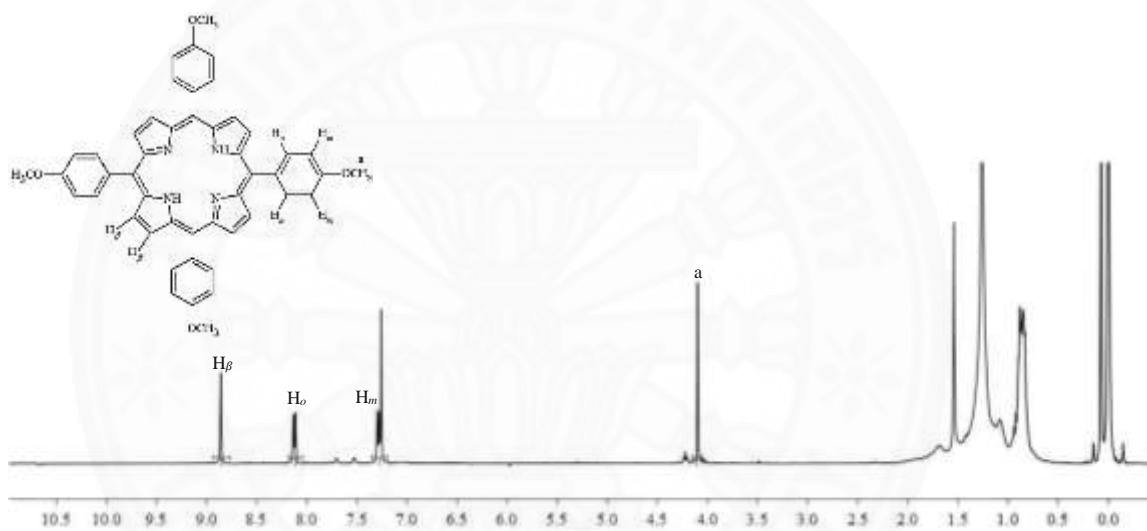


Fig. B5 The ^1H NMR spectrum of TOMPP 5 in chloroform-d (CDCl_3)

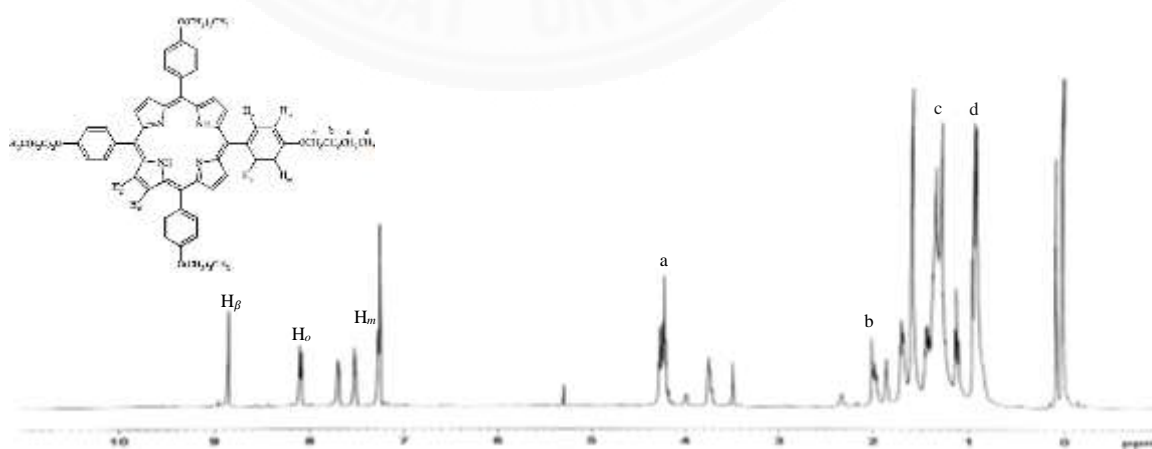


Fig. B6 The ^1H NMR spectrum of TOBPP 6 in chloroform-d (CDCl_3)

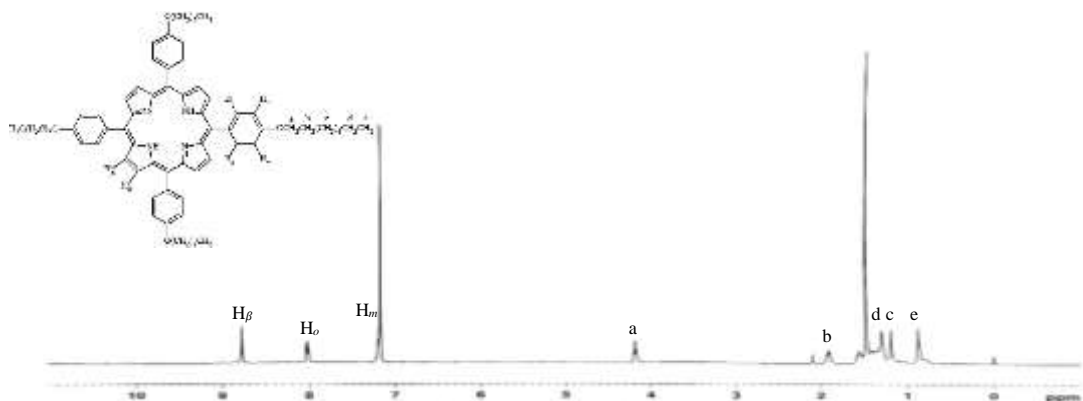


Fig. B7 The ^1H NMR spectrum of TOOPP **7** in chloroform-d (CDCl_3)

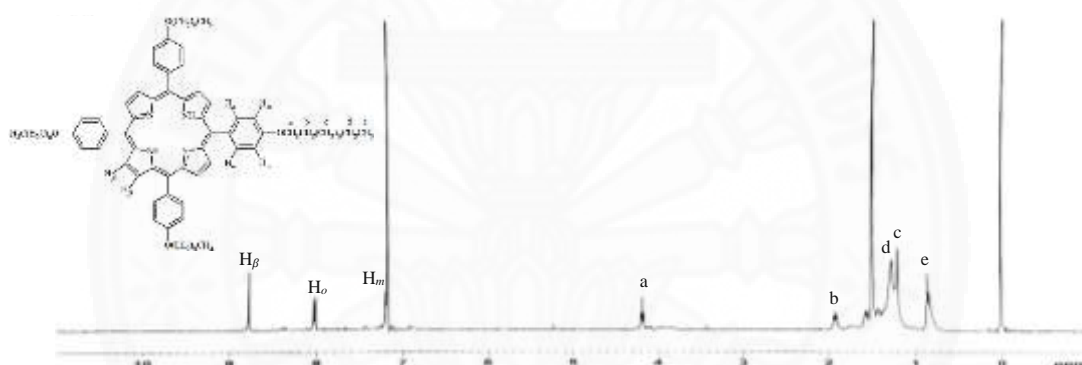


Fig. B8 The ^1H NMR spectrum of TODPP **8** in chloroform-d (CDCl_3)

^{13}C NMR spectra of aldehyde

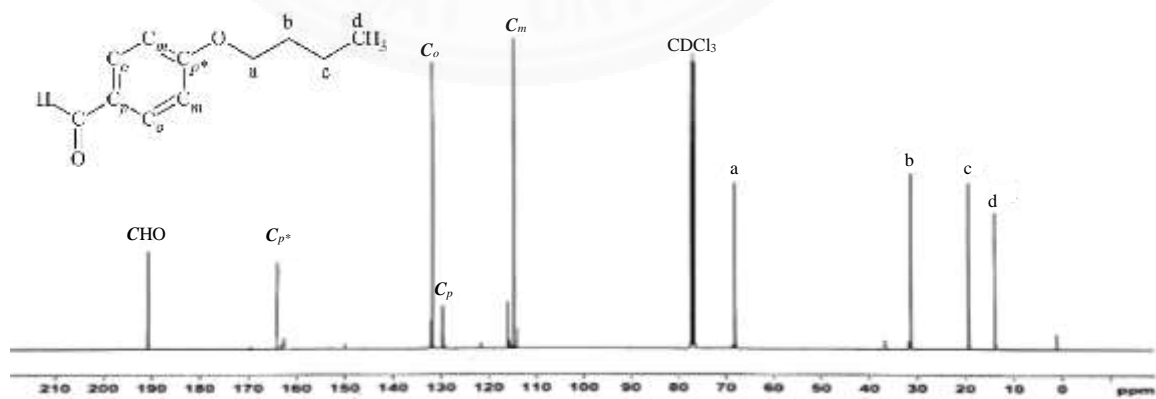


Fig. B9 The ^{13}C NMR spectrum of butyloxybenzaldehyde **1** in chloroform-d (CDCl_3)

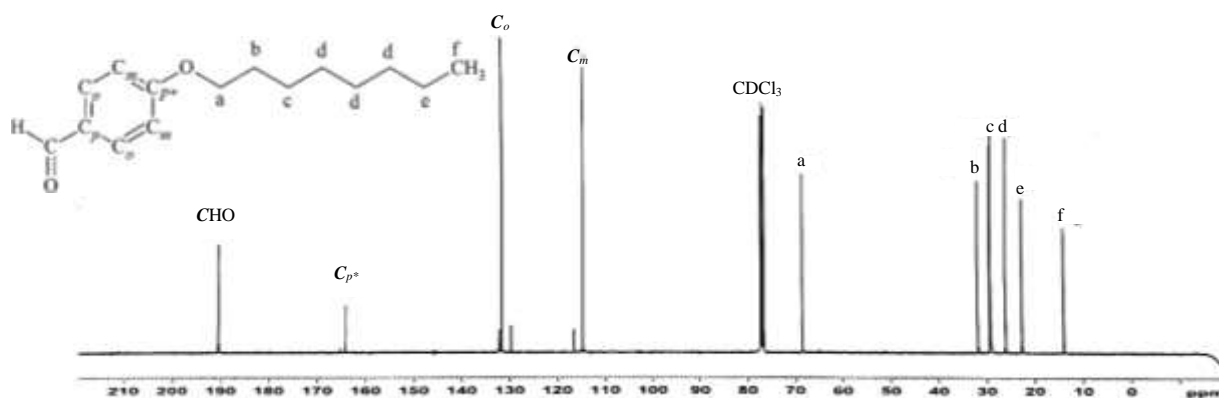


Fig. B10 The ^{13}C NMR spectrum of octyloxybenzaldehyde **2** in chloroform-d (CDCl_3)

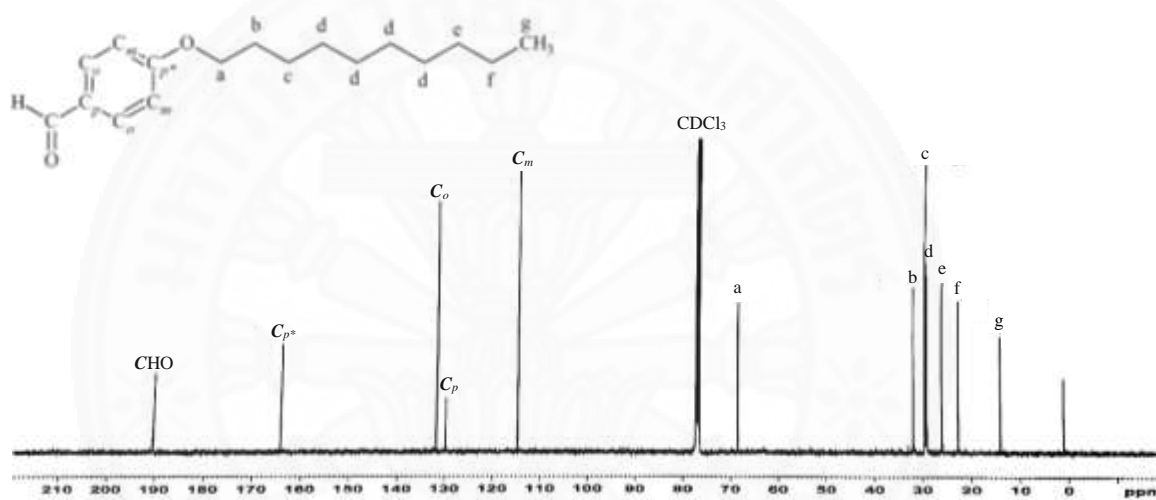


Fig. B11 The ^{13}C NMR spectrum of dectyloxybenzaldehyde **3** in chloroform-d (CDCl_3)

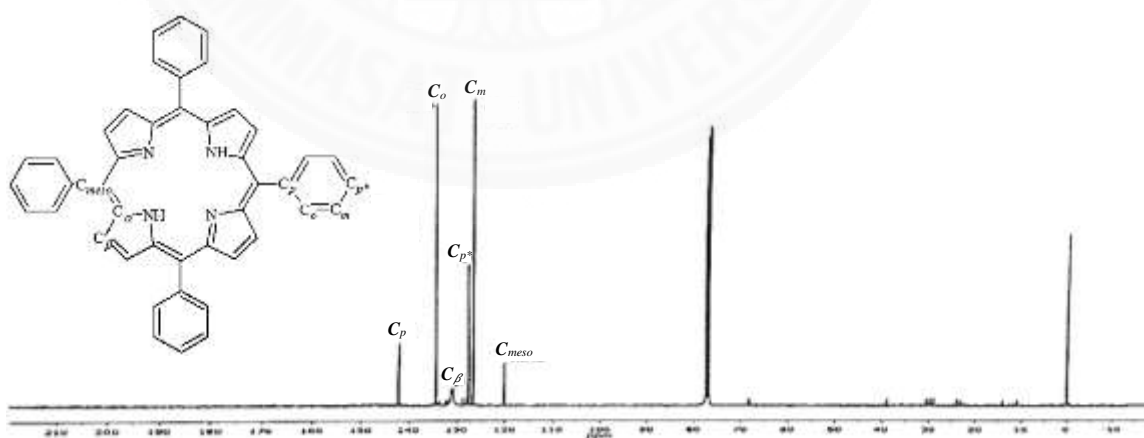


Fig. B12 The ^{13}C NMR spectrum of TPP **4** in chloroform-d (CDCl_3)

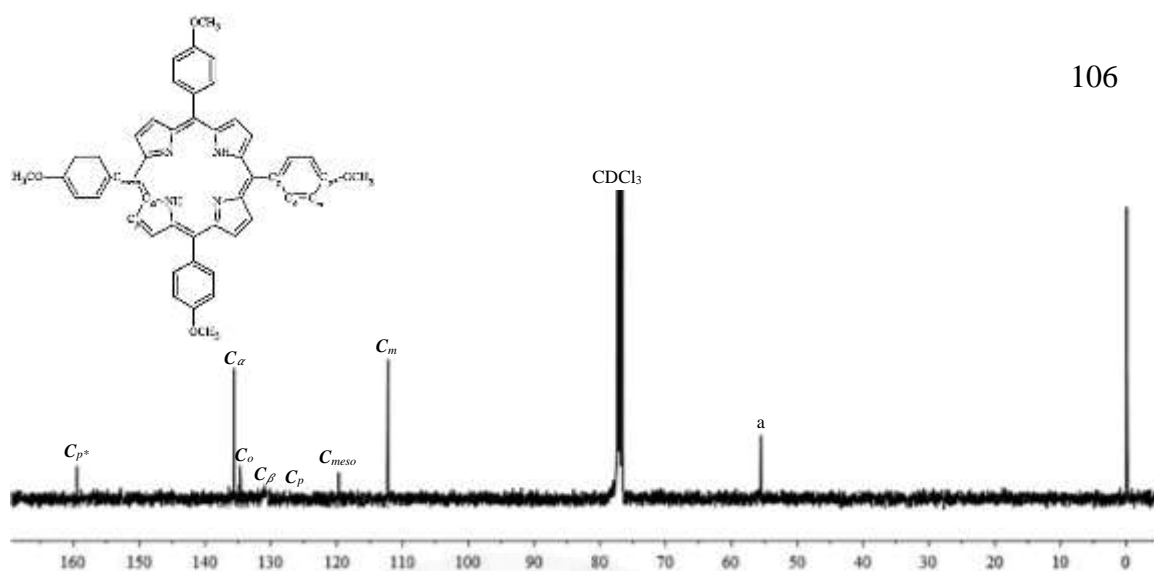


Fig. B13 The ^{13}C NMR spectrum of TOMPP **5** in chloroform-d (CDCl_3)

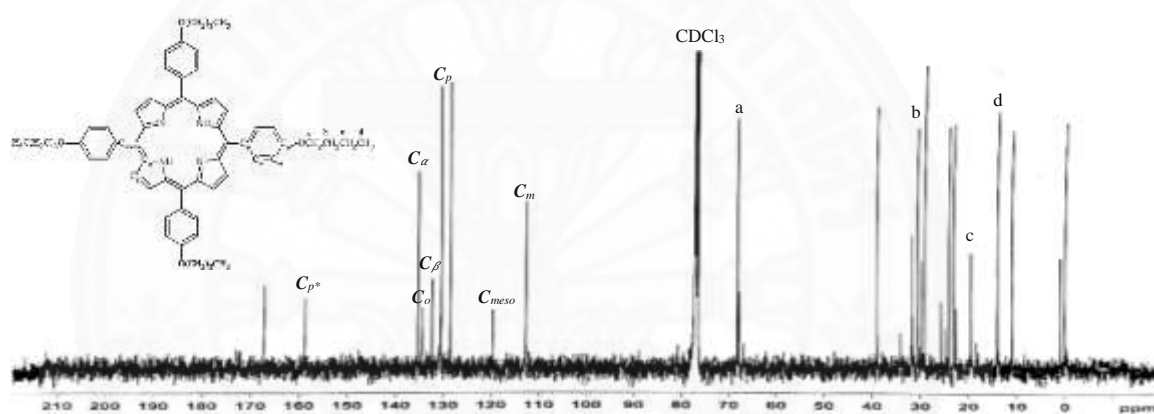


Fig. B14 The ^{13}C NMR spectrum of TOBPP **6** in chloroform-d (CDCl_3)

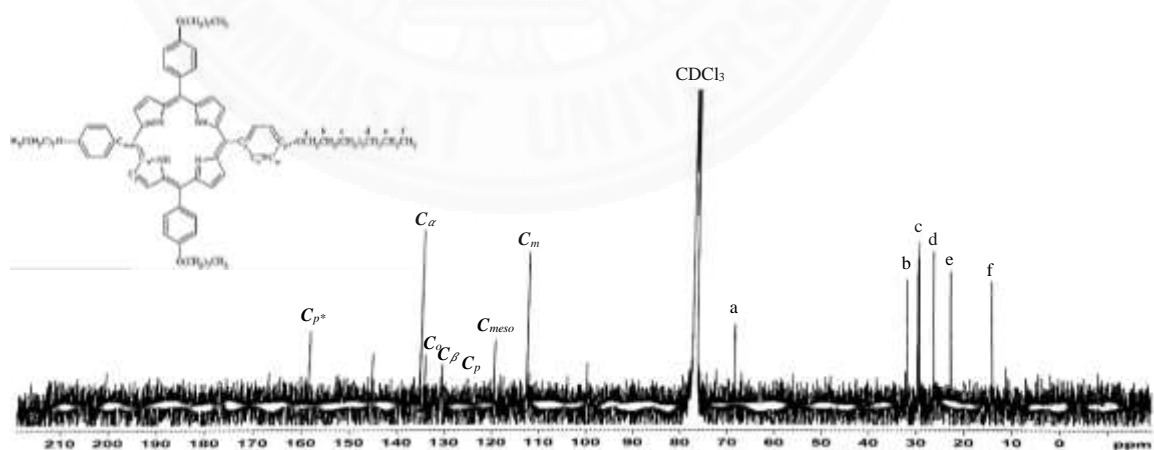


Fig. B15 The ^{13}C NMR spectrum of TOOPP **7** in chloroform-d (CDCl_3)

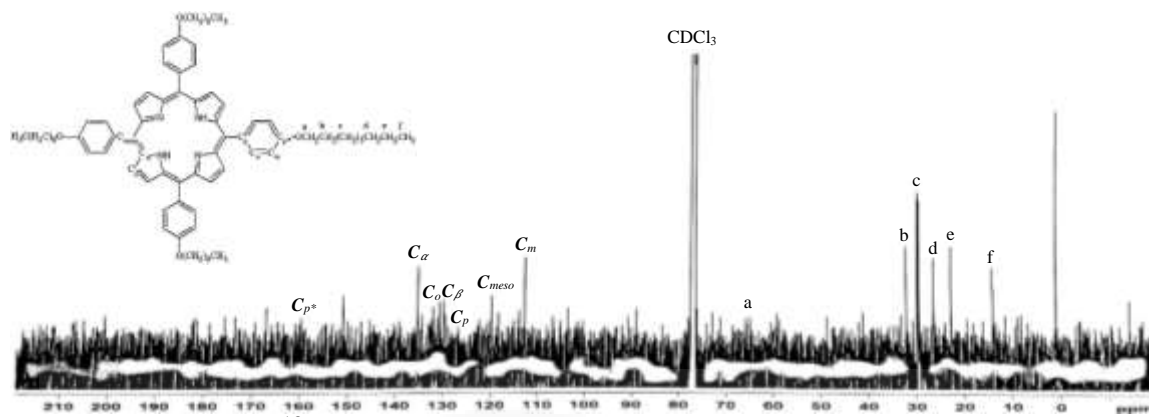


Fig. B16 The ^{13}C NMR spectrum of TODPP **8** in chloroform-d (CDCl_3)

APPENDIX C

IR SPECTRA

IR spectra of aldehyde

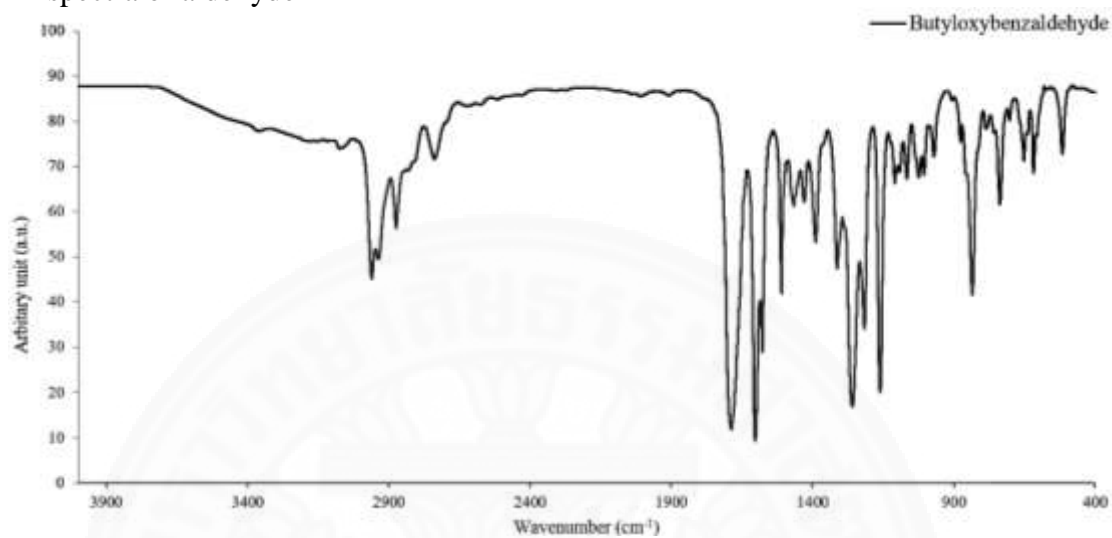


Fig. C1 The IR spectrum of butyloxybenzaldehyde

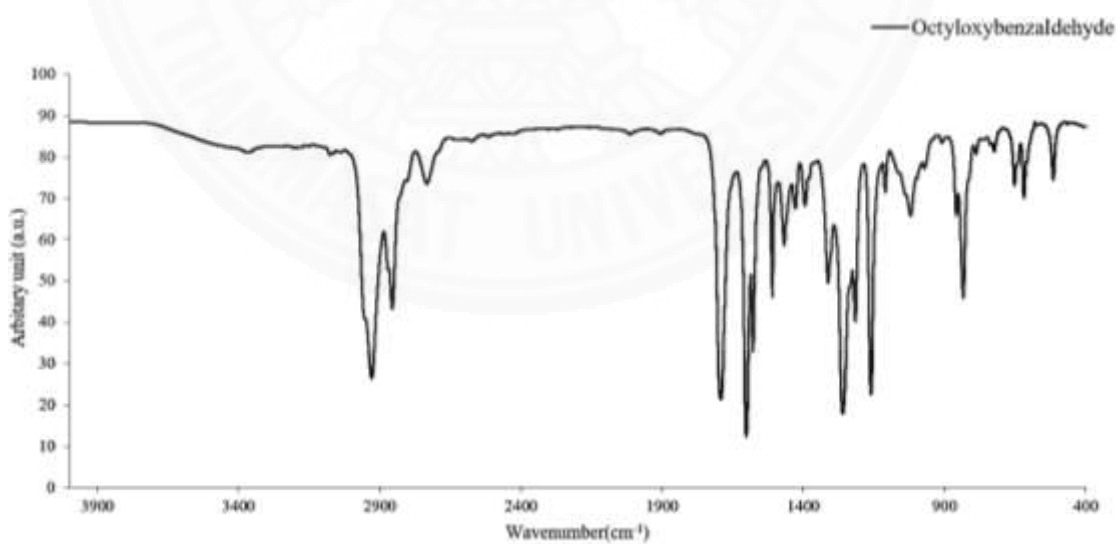


Fig. C2 The IR spectrum of Octyloxybenzaldehyde

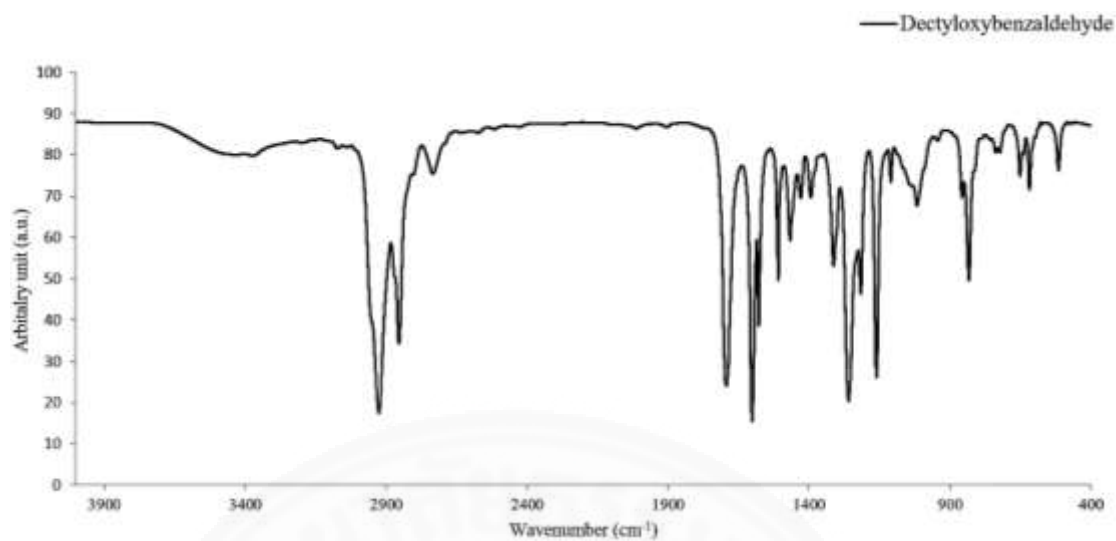


Fig. C3 The IR spectrum of dectyloxybenzaldehyde
IR spectra of free base porphyrins, copper(II) porphyrin, and β -nitro substituted porphyrin complexes

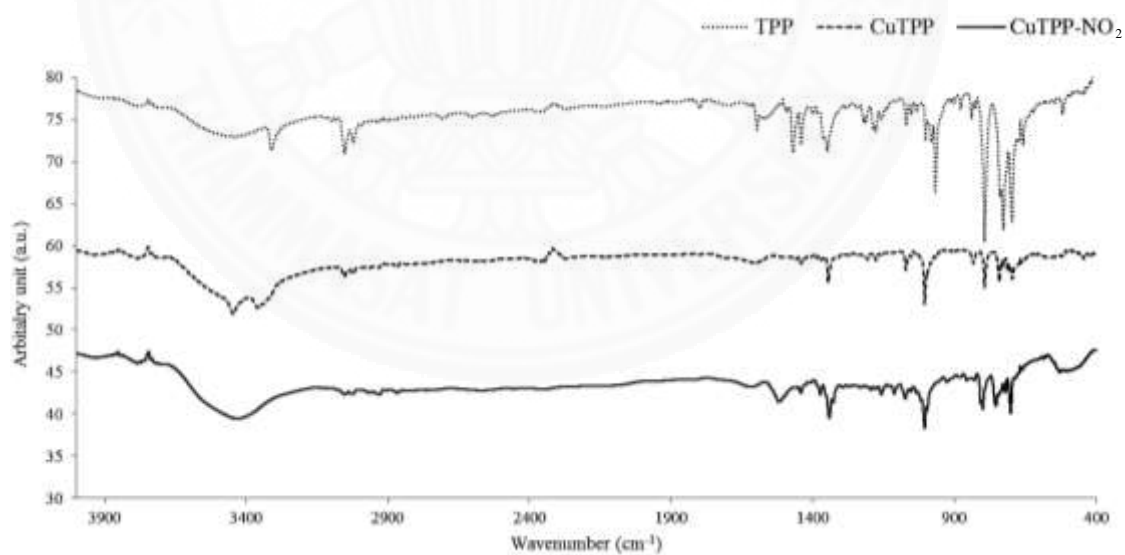


Fig. C4 The IR spectrum of TPP 4, CuTPP 9, and CuTPP-NO₂ 14

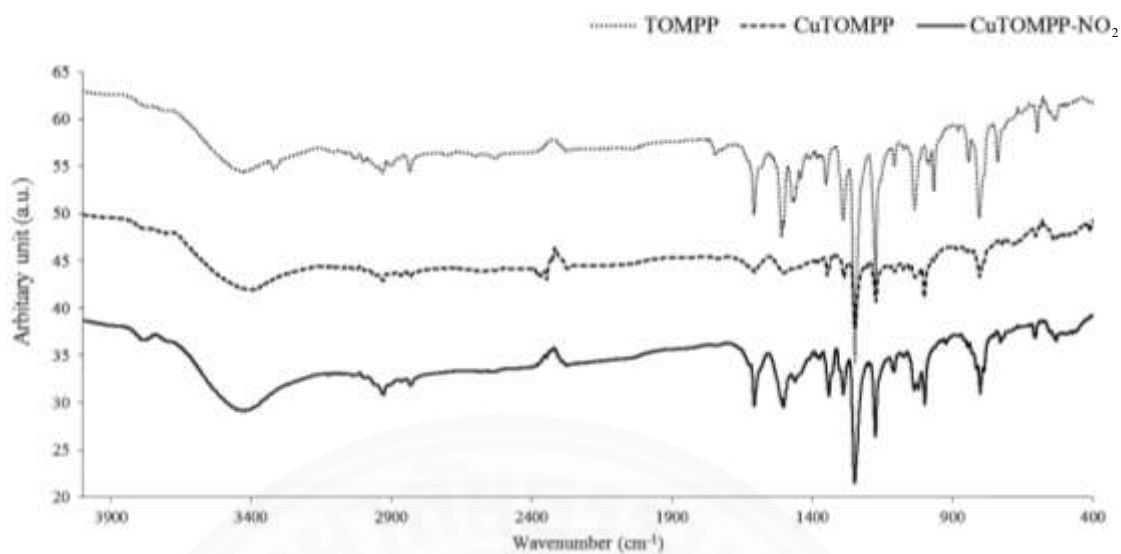


Fig. C5 The IR spectrum of TOMPP **5**, CuTOMPP **10**, and CuTOMPP-NO₂ **15**

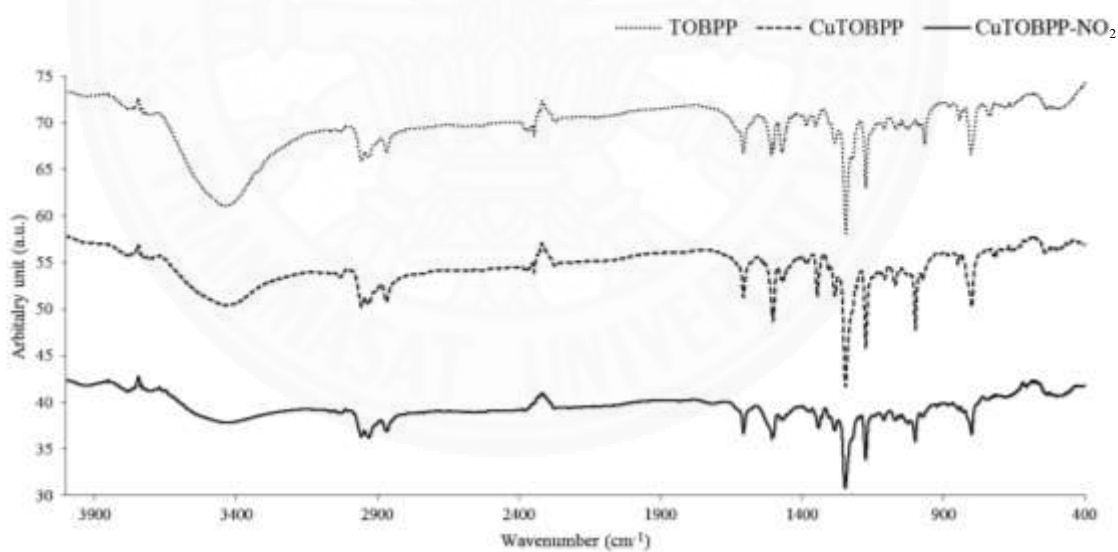


Fig. C6 The IR spectrum of TOBPP **6**, CuTOBPP **11**, and CuTOBPP-NO₂ **16**

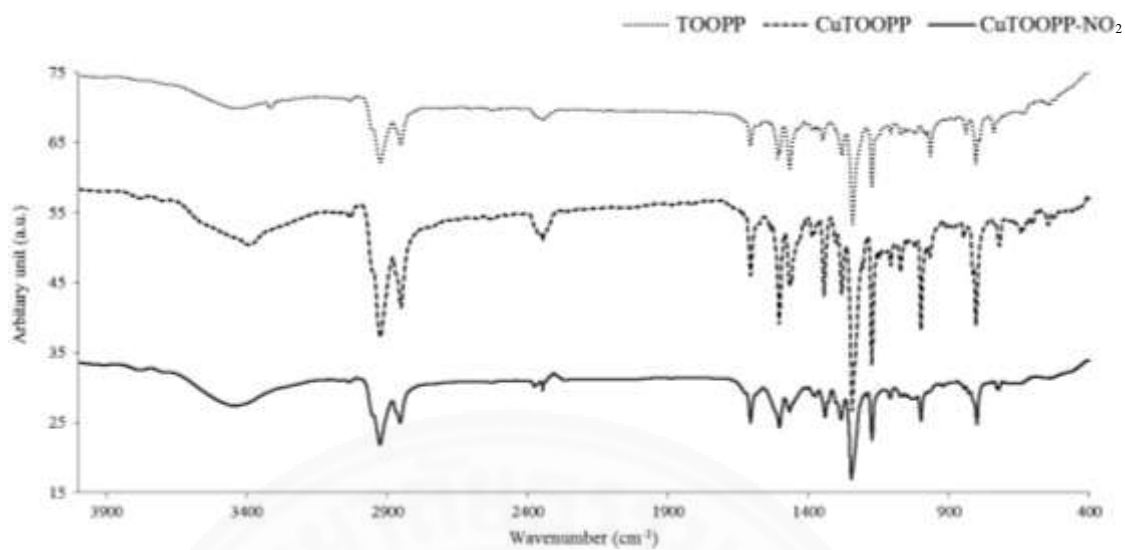


Fig. C7 The IR spectrum of TOOPP **7**, CuTOOPP **12**, and CuTOOPP-NO₂ **17**

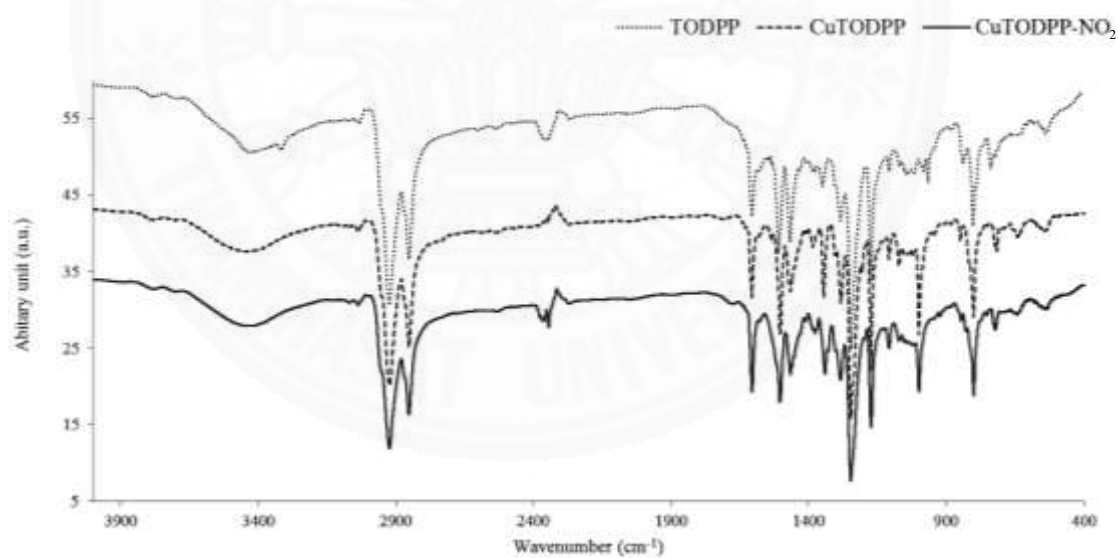
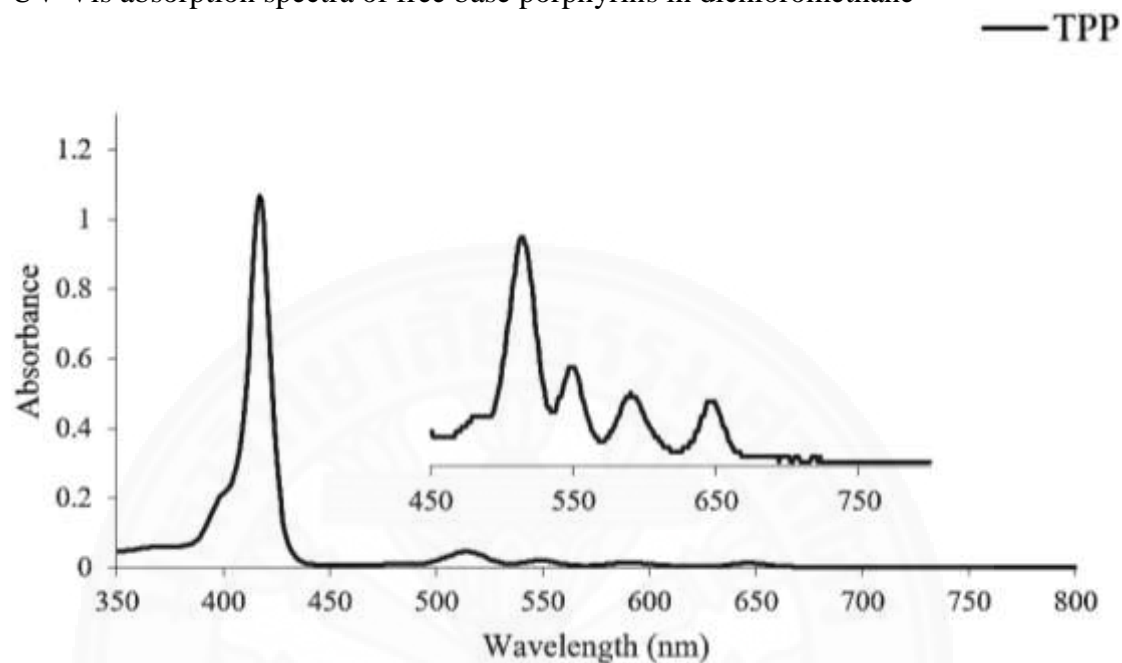
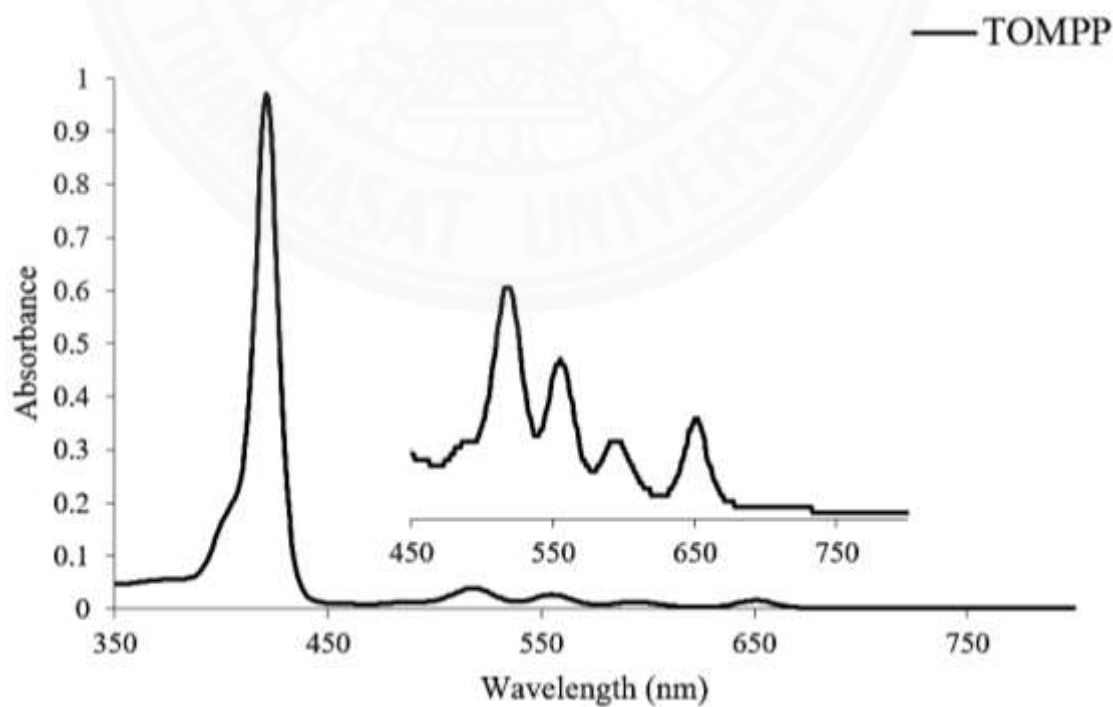


Fig. C8 The IR spectrum of TODPP **8**, CuTODPP **13**, and CuTODPP-NO₂ **18**

APPENDIX D

UV-vis ABSORPTION SPECTRA

UV-Vis absorption spectra of free base porphyrins in dichloromethane

**Fig. D1** UV-Vis absorption spectra of TPP 4**Fig. D2** UV-Vis absorption spectra of TOMPP 5

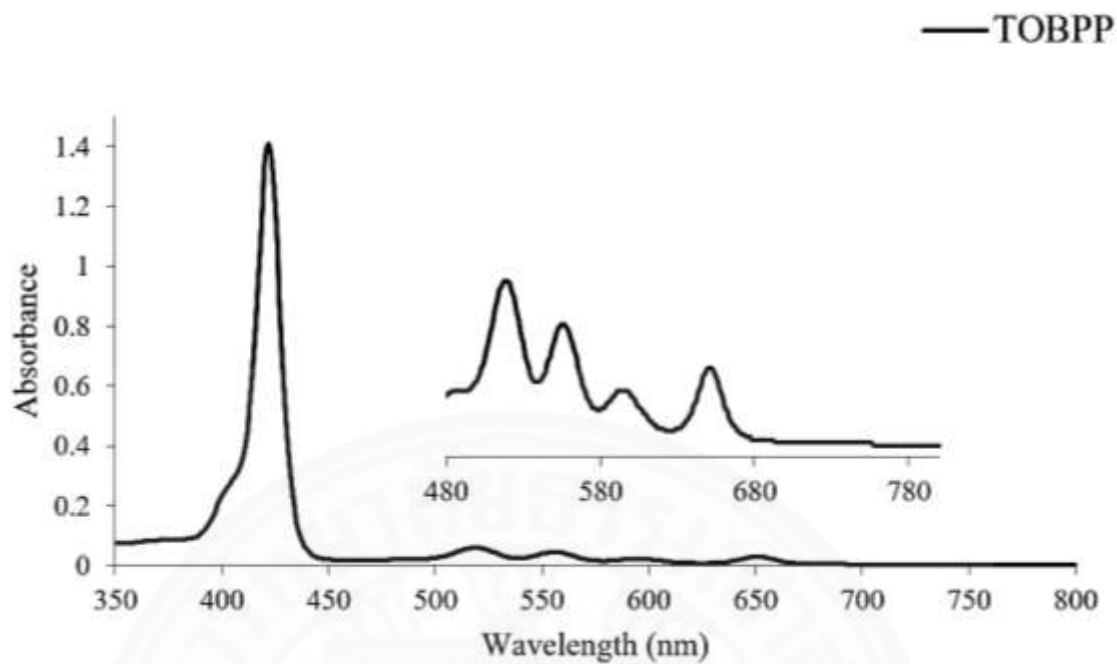


Fig. D3 UV-Vis absorption spectra of TOBPP 6

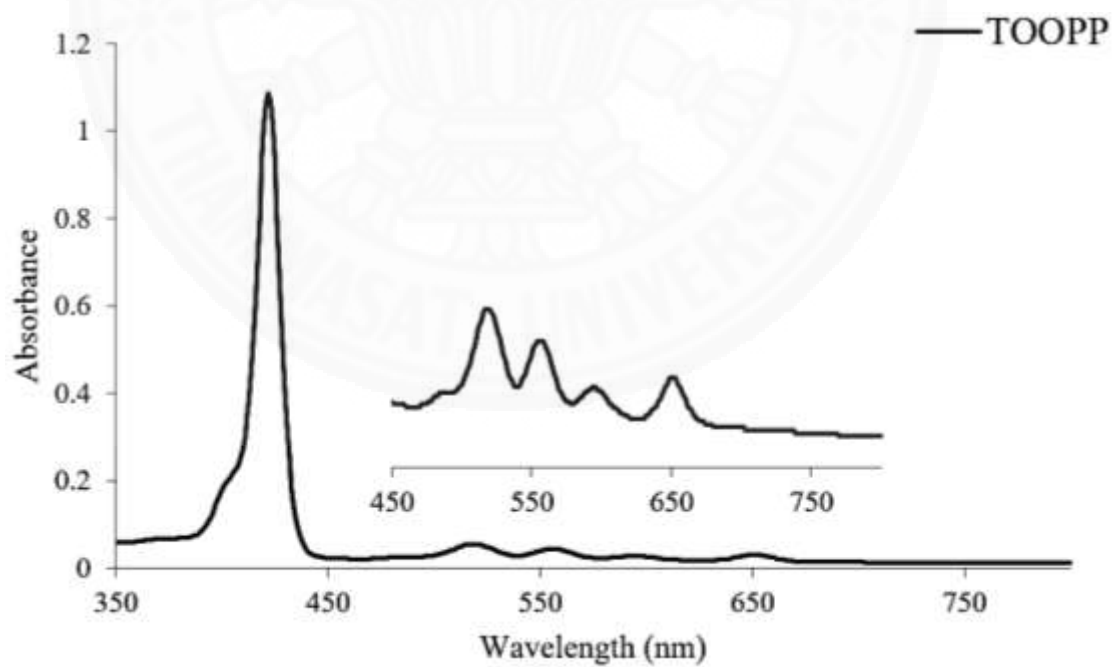


Fig. D4 UV-Vis absorption spectra of TOOPP 7

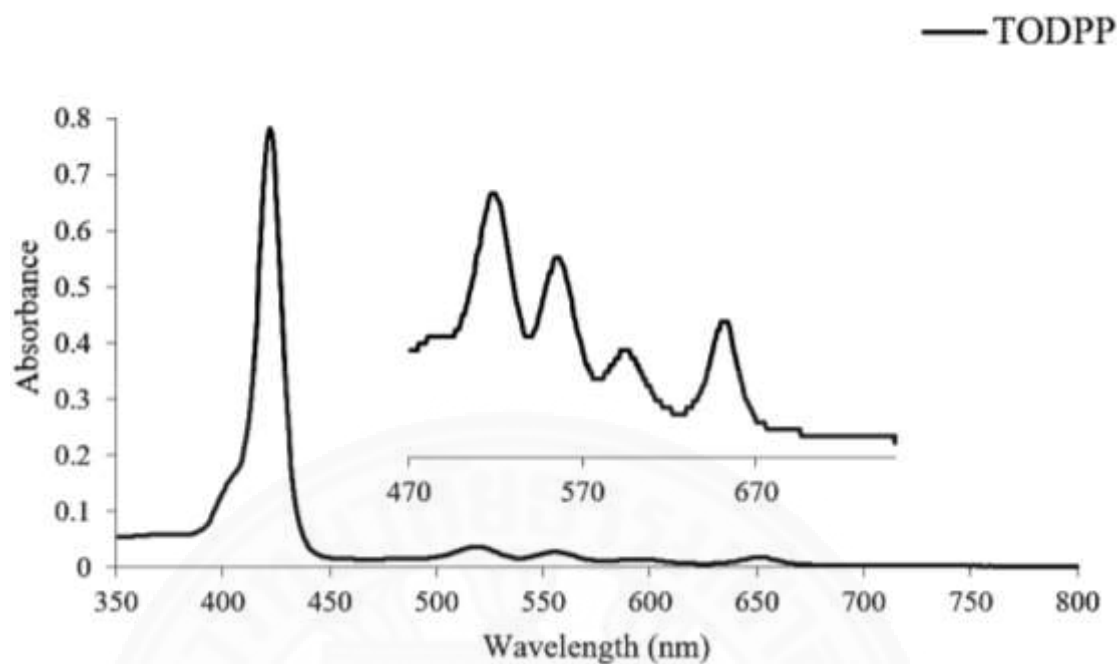


Fig. D5 UV-Vis absorption spectra of TODPP 8

UV-Vis absorption spectra of copper(II) porphyrins in dichloromethane

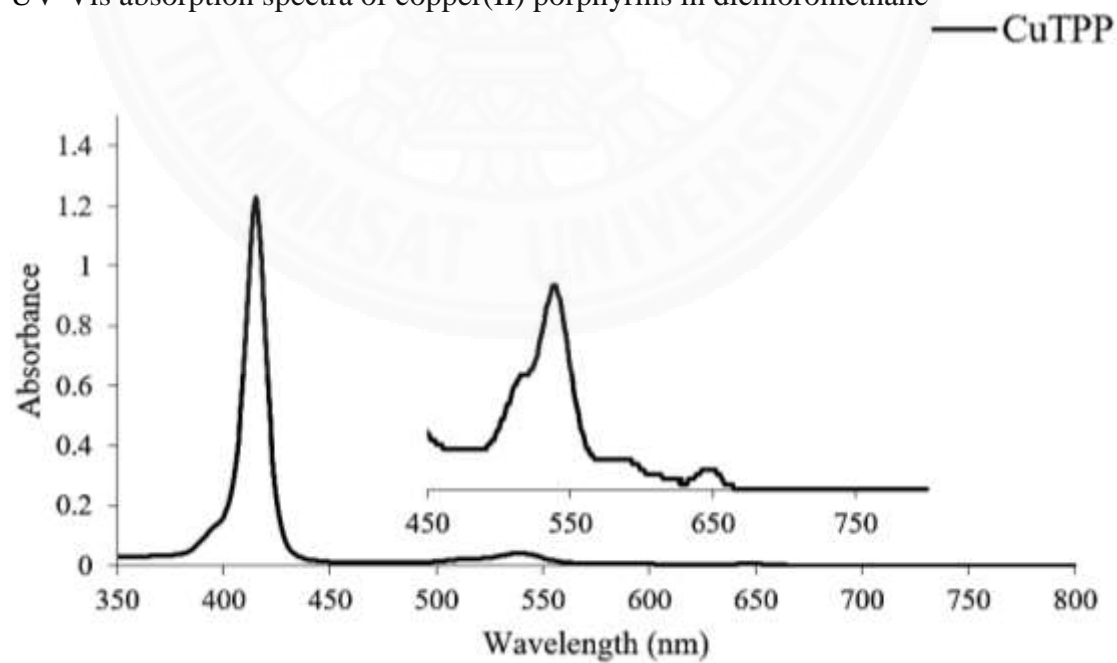


Fig. D6 UV-Vis absorption spectra of CuTPP 9

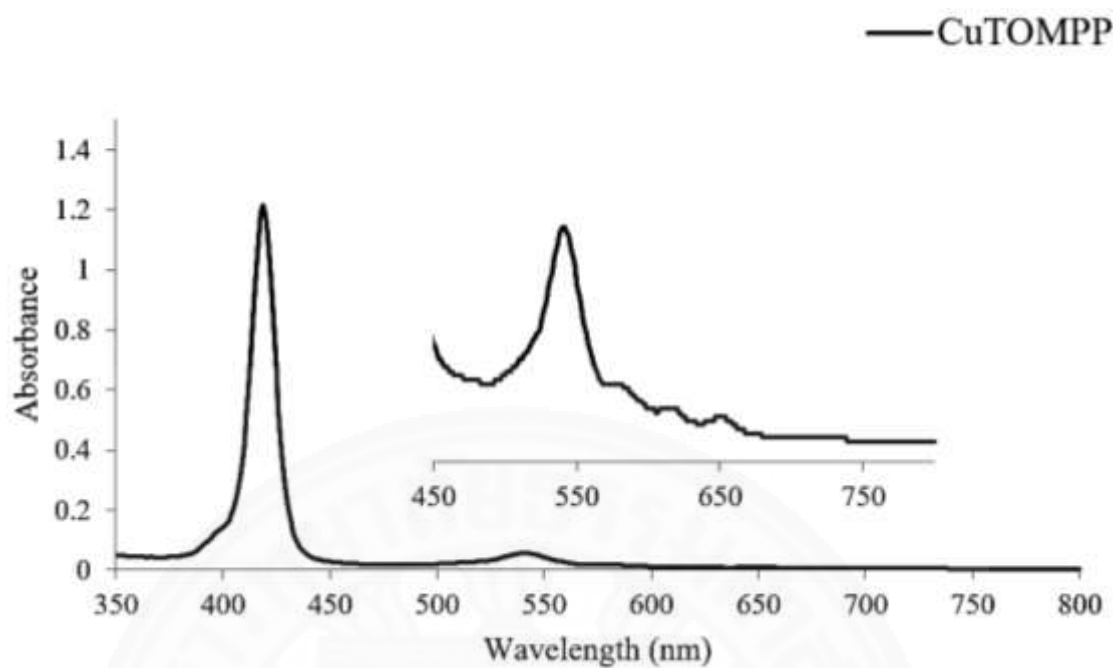


Fig. D7 UV-Vis absorption spectra of CuTOMPP 10

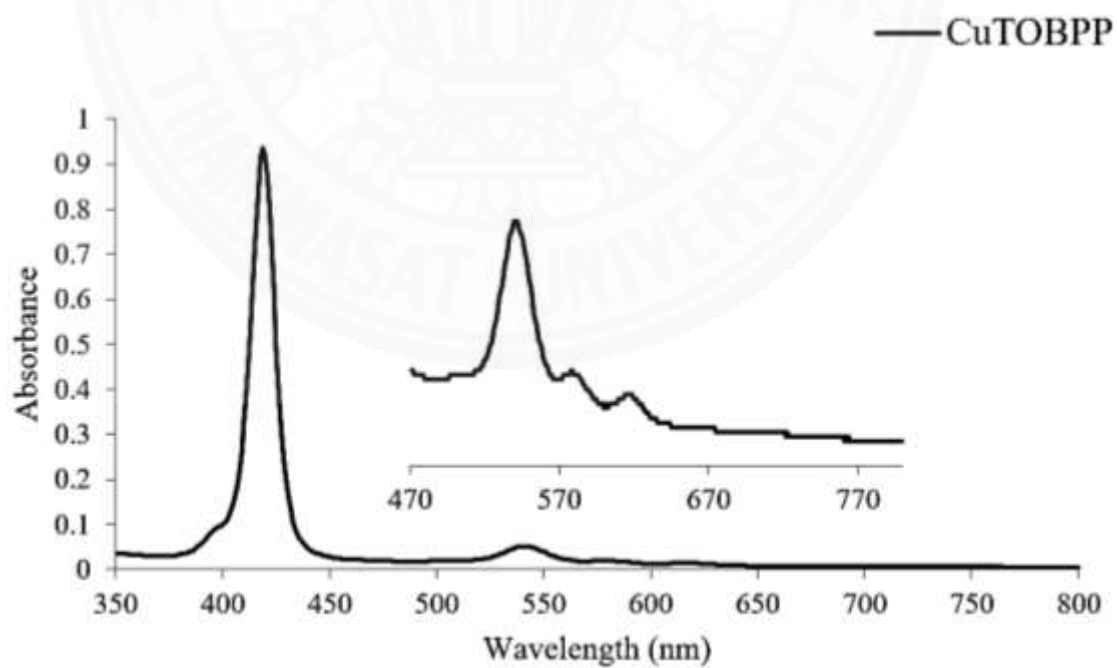


Fig. D8 UV-Vis absorption spectra of CuTOBPP 11

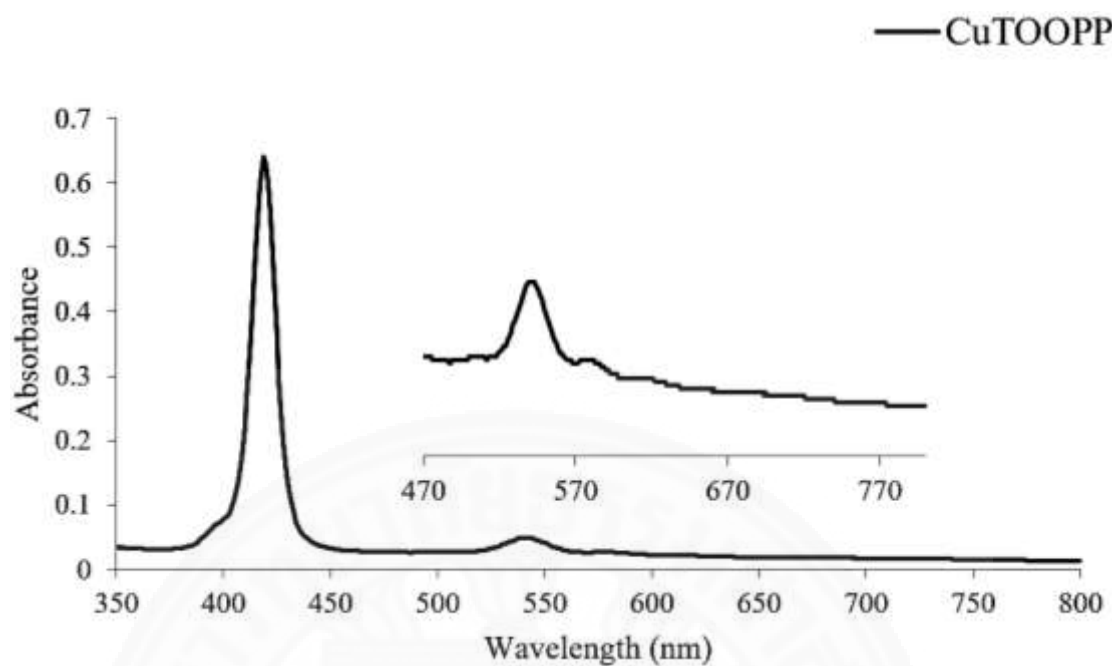


Fig. D9 UV-Vis absorption spectra of CuTOOPP 12

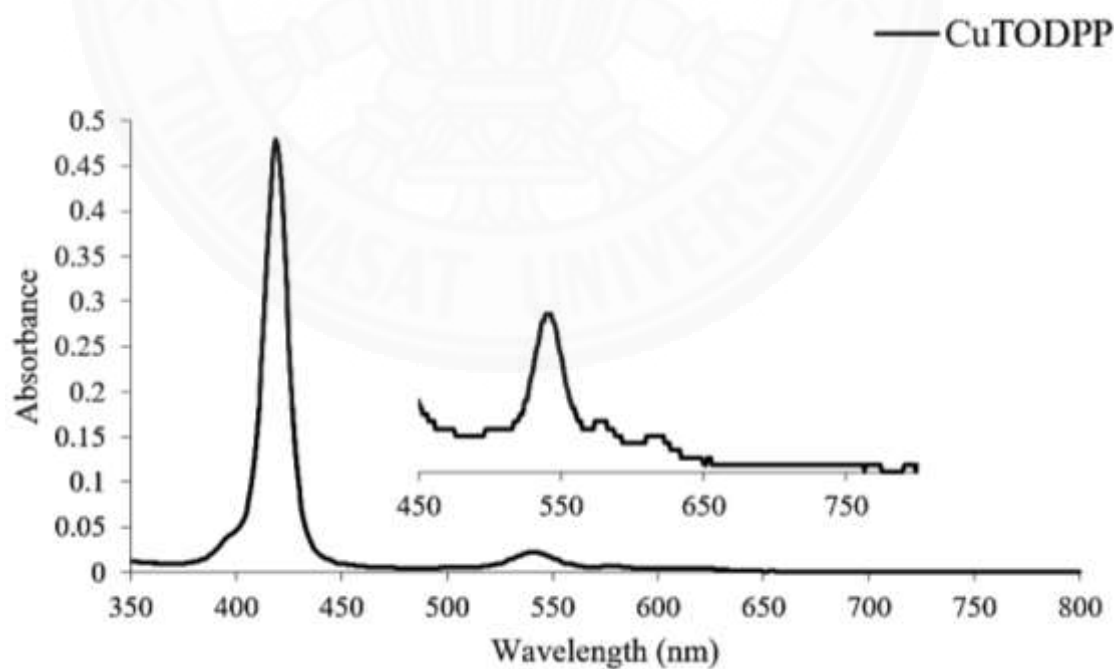


Fig. D10 UV-Vis absorption spectra of CuTODPP 13

UV-Vis absorption spectra of β -nitro substituted porphyrin complexes in dichloromethane

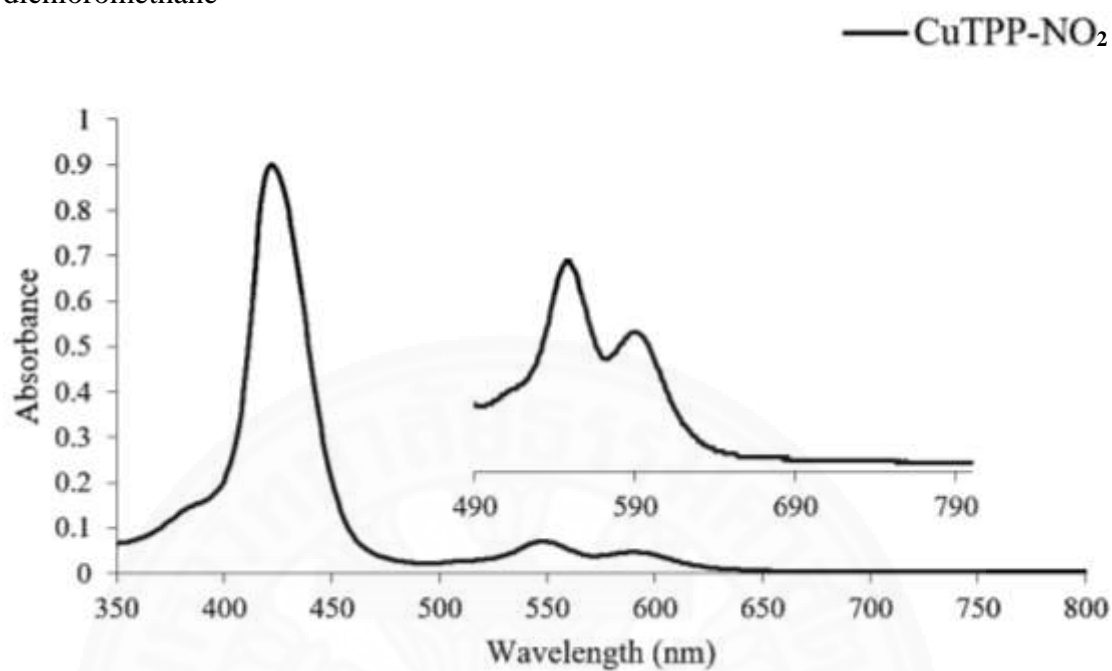


Fig. D11 UV-Vis absorption spectra of CuTPP-NO₂ 14

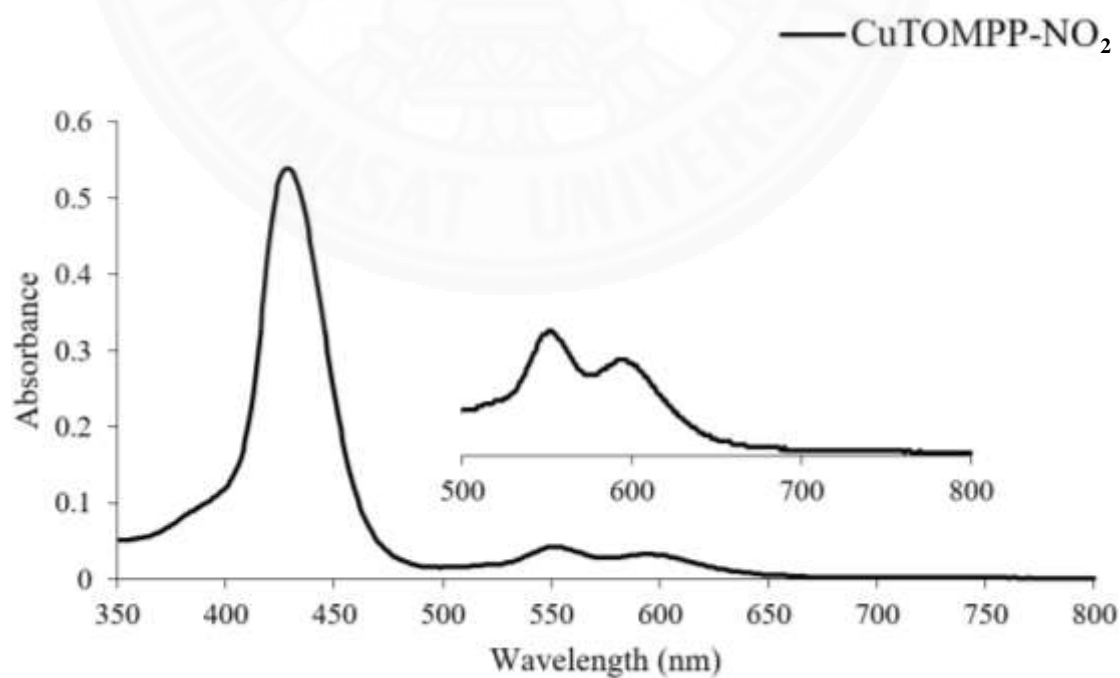


Fig. D12 UV-Vis absorption spectra of CuTOMPP-NO₂ 15

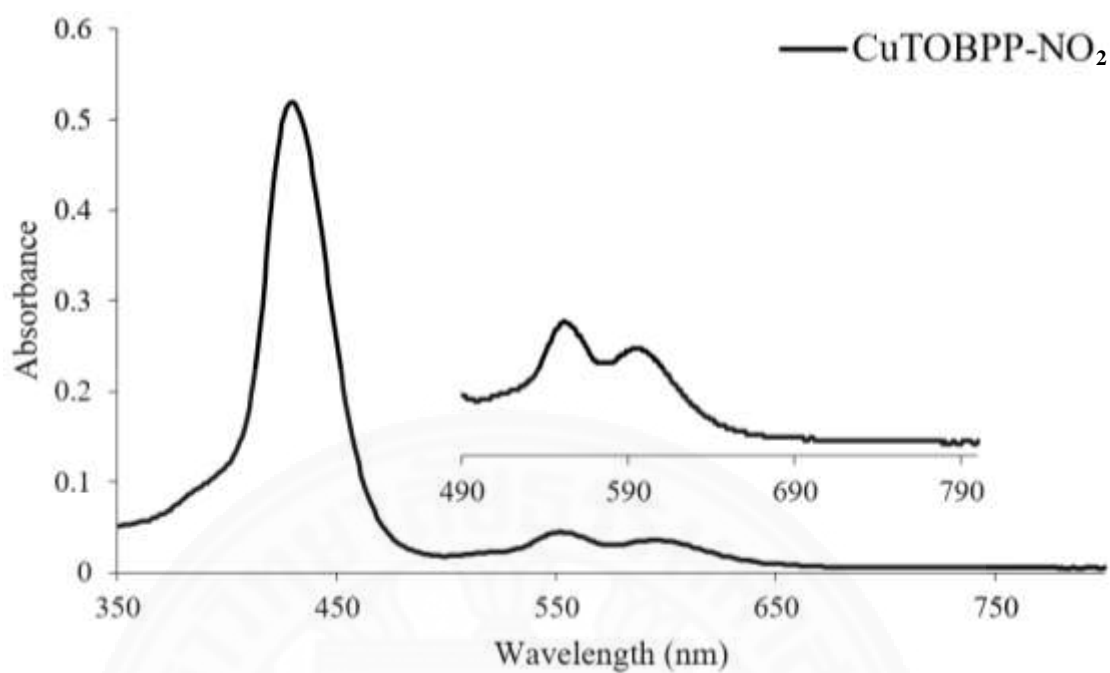


Fig. D13 UV-Vis absorption spectra of CuTOBPP-NO₂ 16

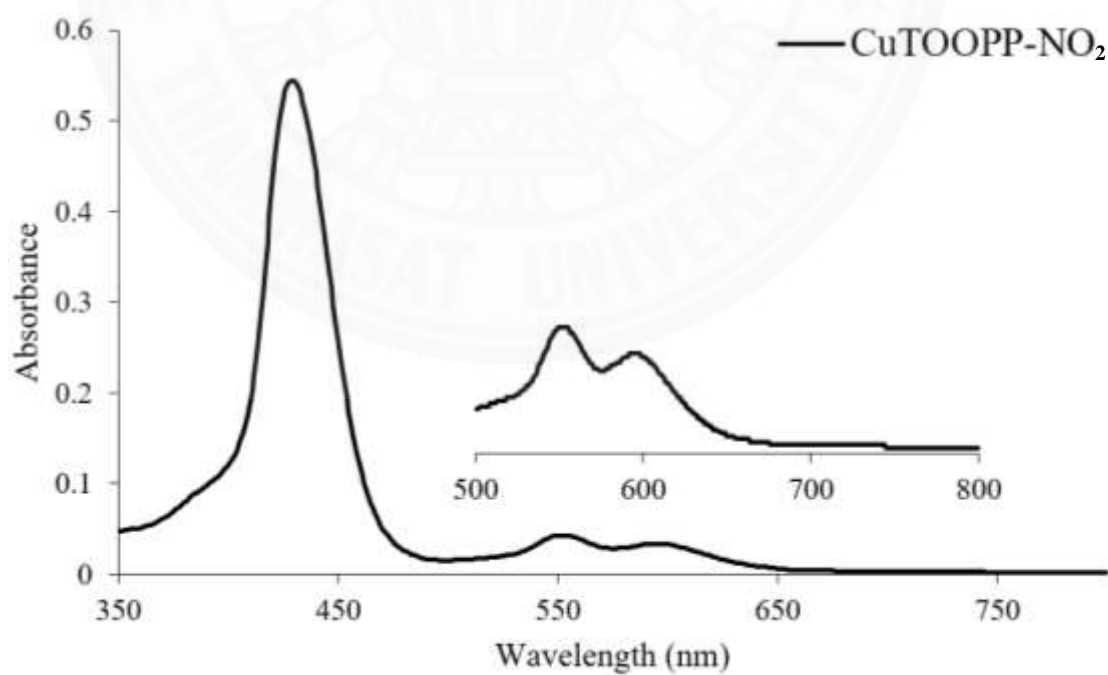


Fig. D14 UV-Vis absorption spectra of CuTOOPP-NO₂ 17

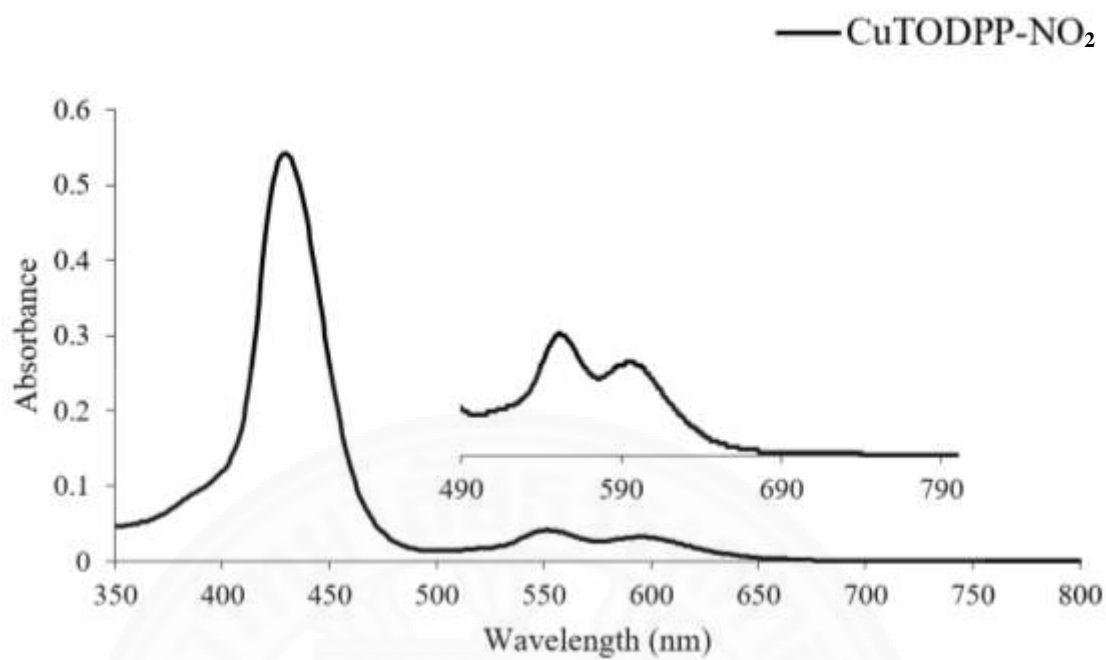


Fig. D15 UV-Vis absorption spectra of CuTODPP-NO₂ **18**

APPENDIX E
FLUORESCENCE SPECTRA

Fluorescence spectra of free base porphyrins

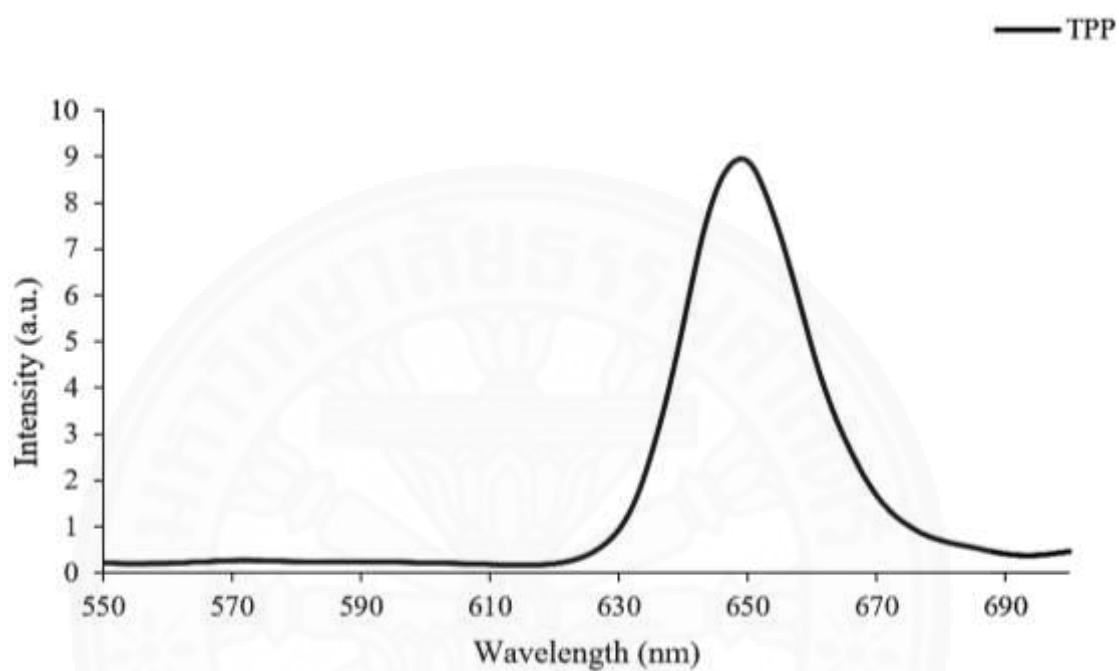


Fig. E1 Fluorescence spectra of TPP 4

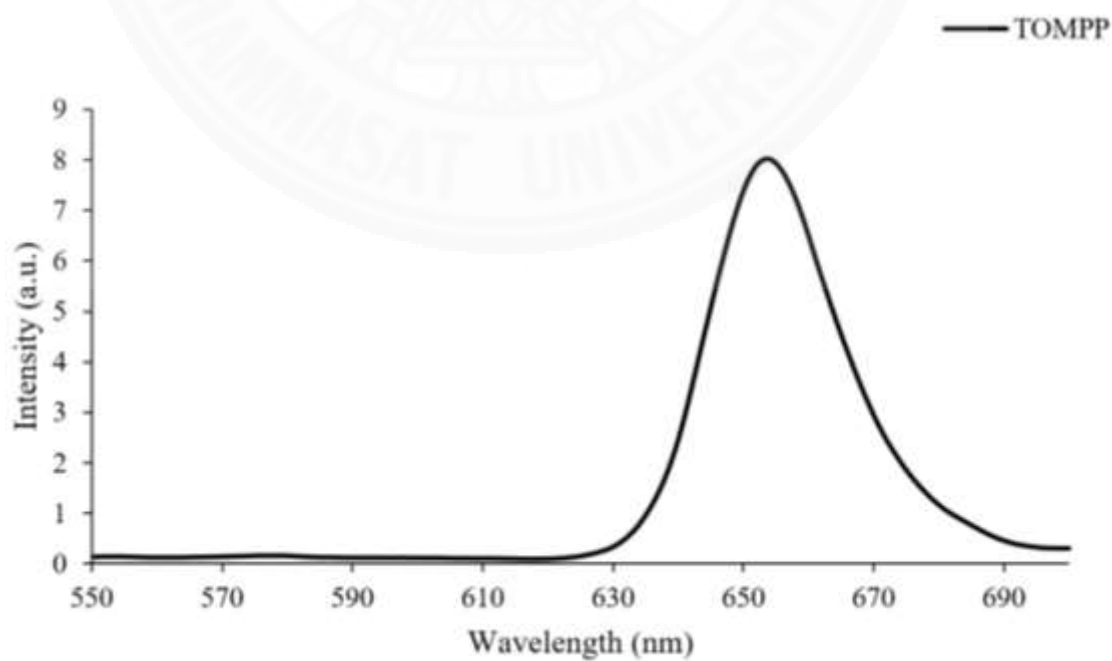


Fig. E2 Fluorescence spectra of TOMPP 5

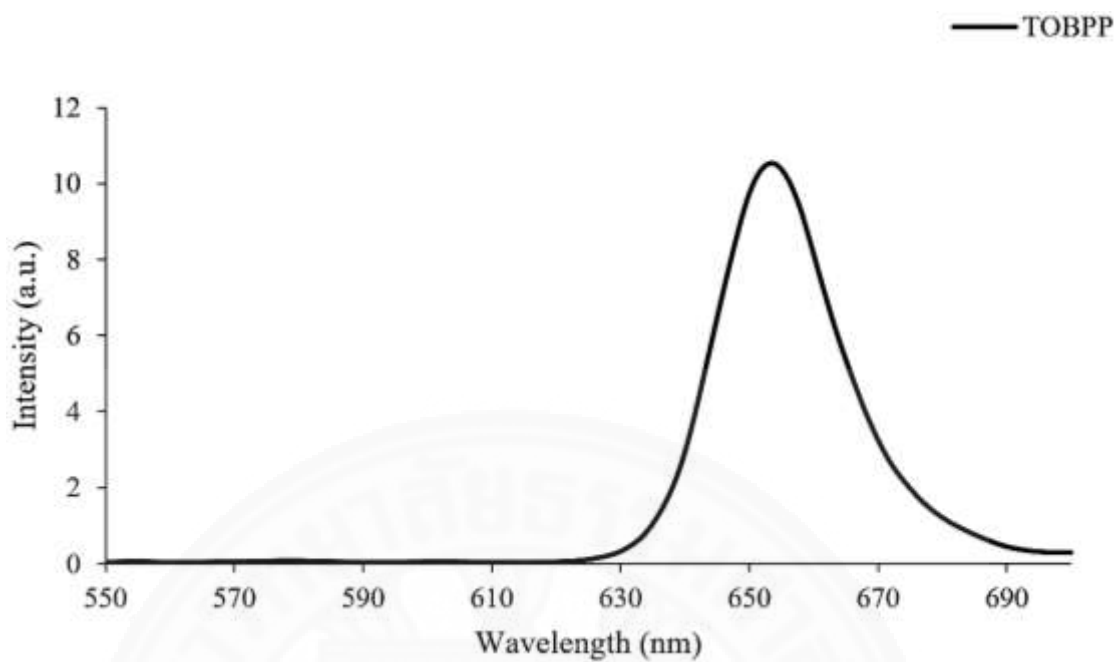


Fig. E3 Fluorescence spectra of TOBPP 6

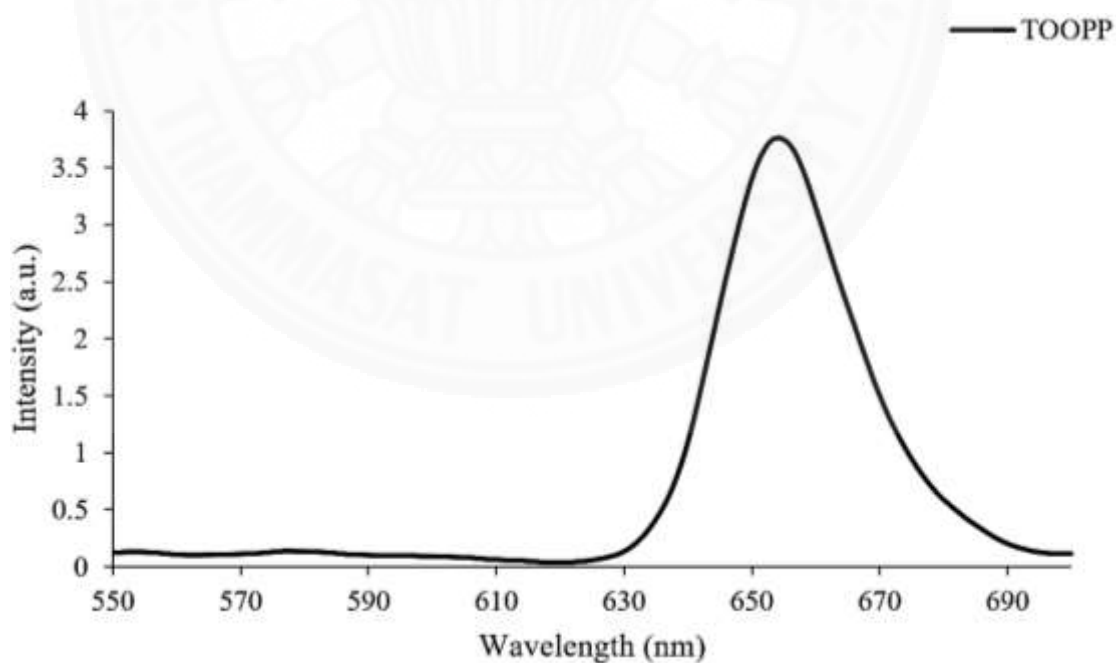


Fig. E4 Fluorescence spectra of TOOPP 7

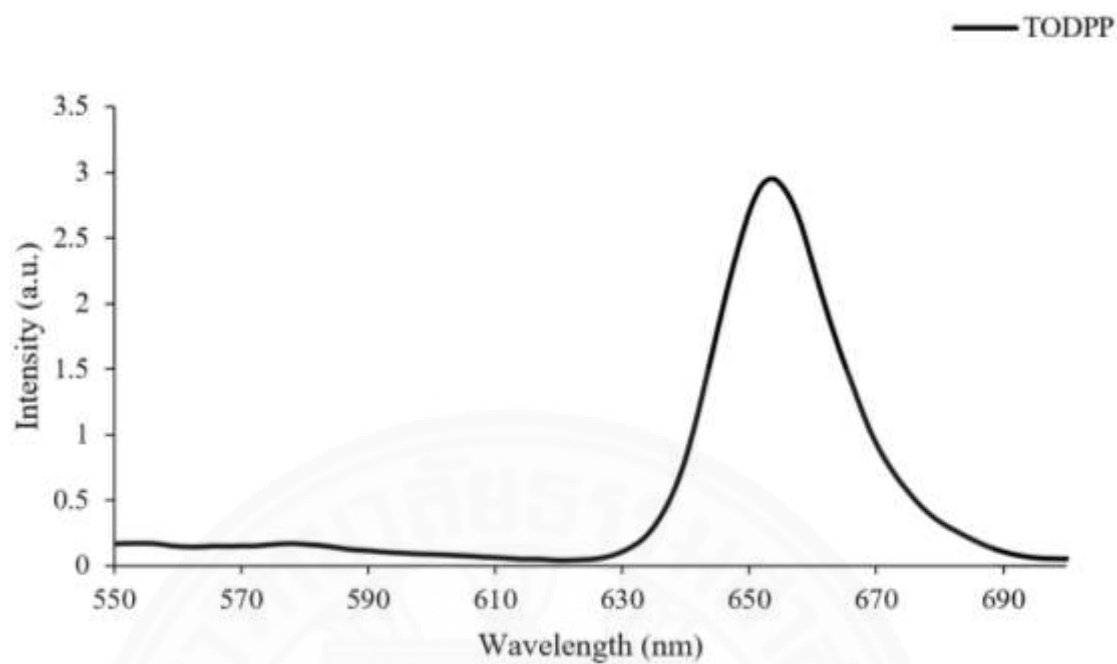


Fig. E5 Fluorescence spectra of TODPP 8

Fluorescence spectra of copper(II) porphyrins

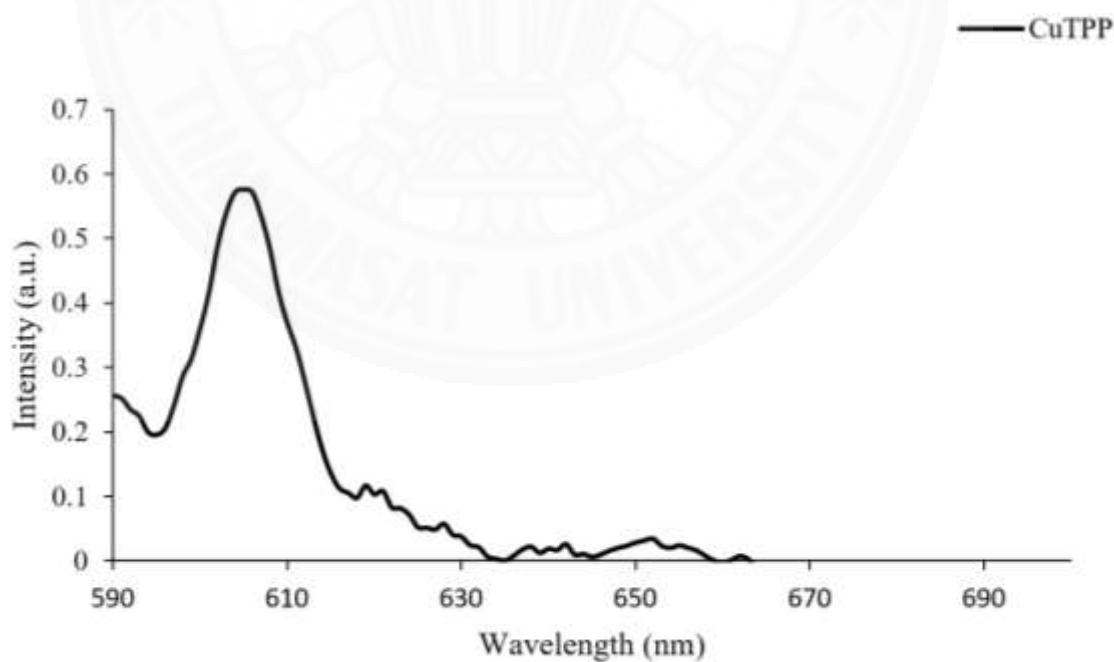


Fig. E6 Fluorescence spectra of CuTPP 9

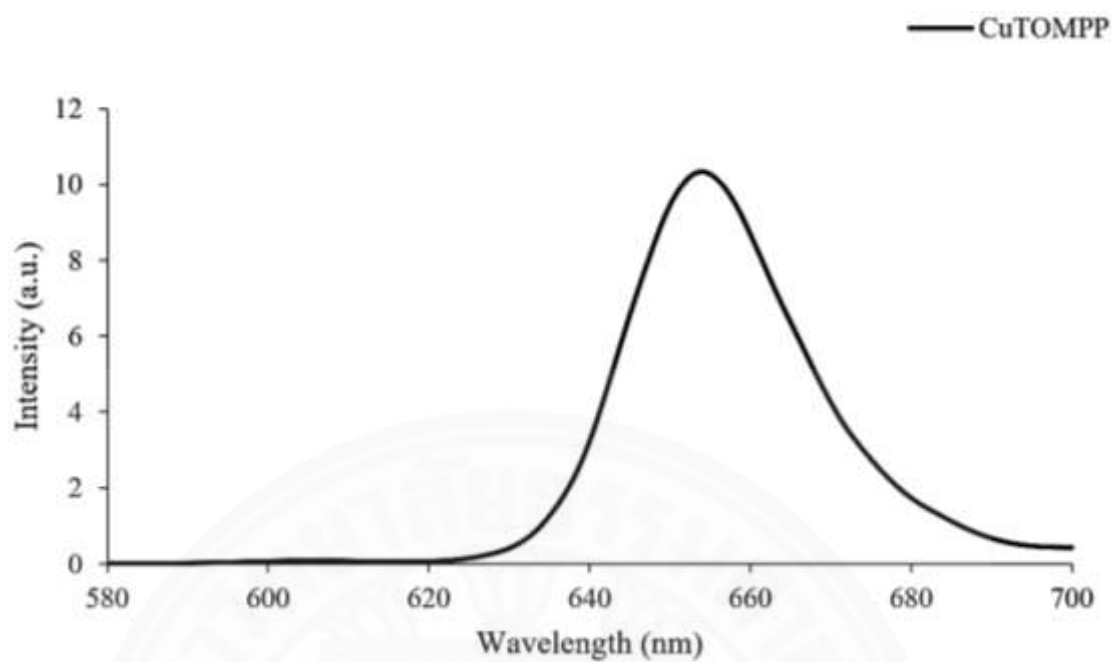


Fig. E7 Fluorescence spectra of CuTOMPP **10**

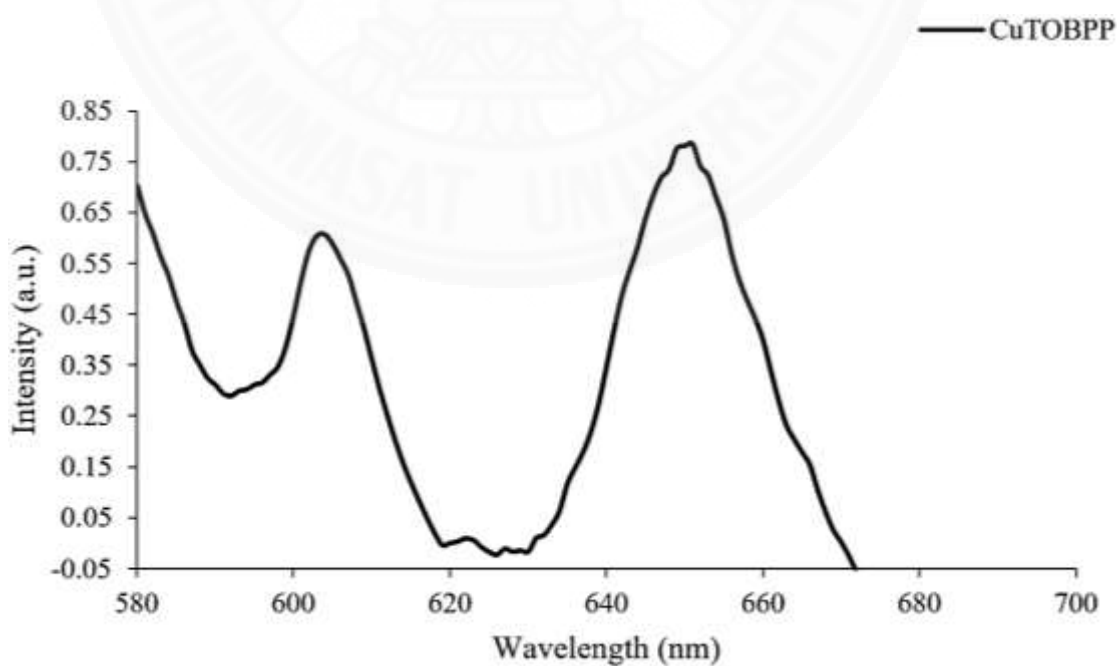


Fig. E8 Fluorescence spectra of CuTOBPP **11**

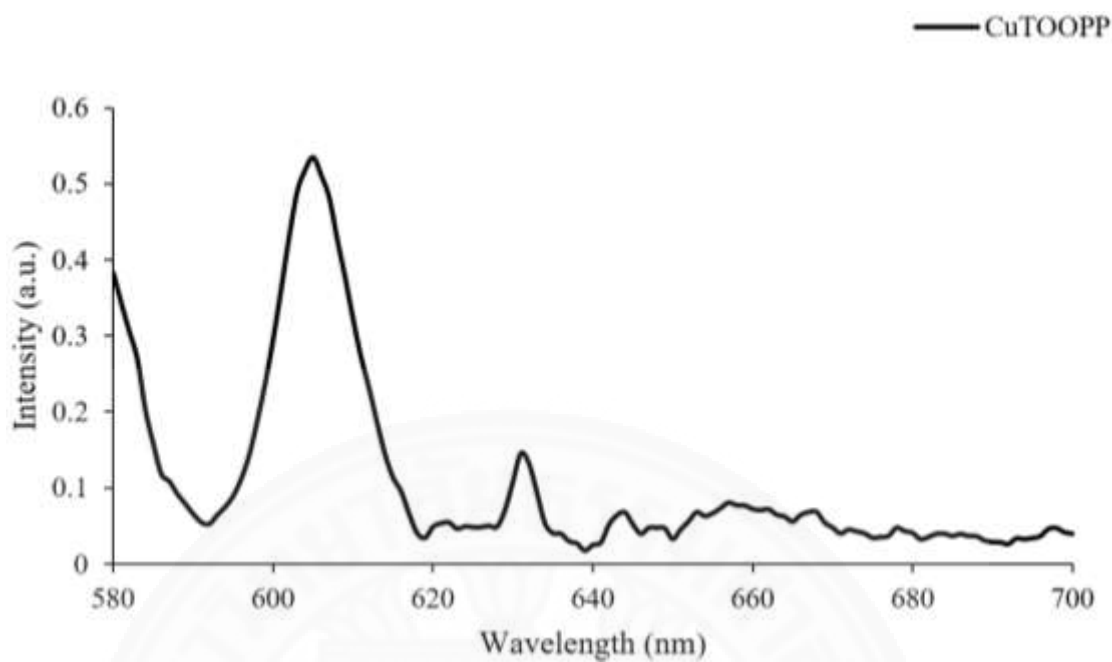


Fig. E9 Fluorescence spectra of CuTOOPP 12

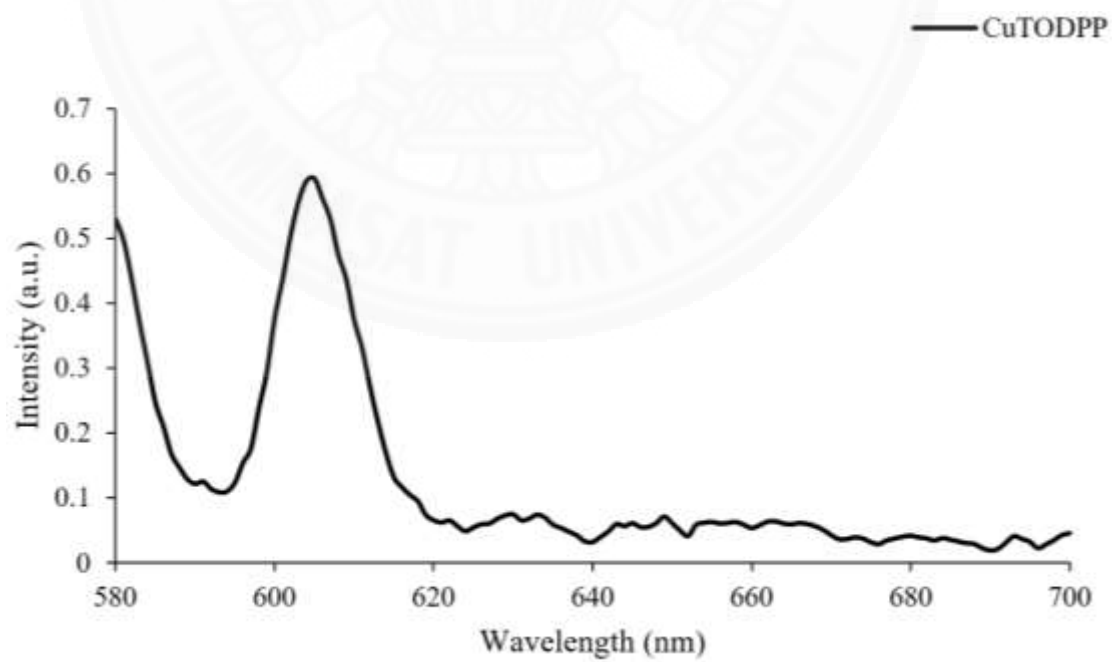


Fig. E10 Fluorescence spectra of CuTODPP 13

Fluorescence spectra of β -nitro substituted porphyrins complexes

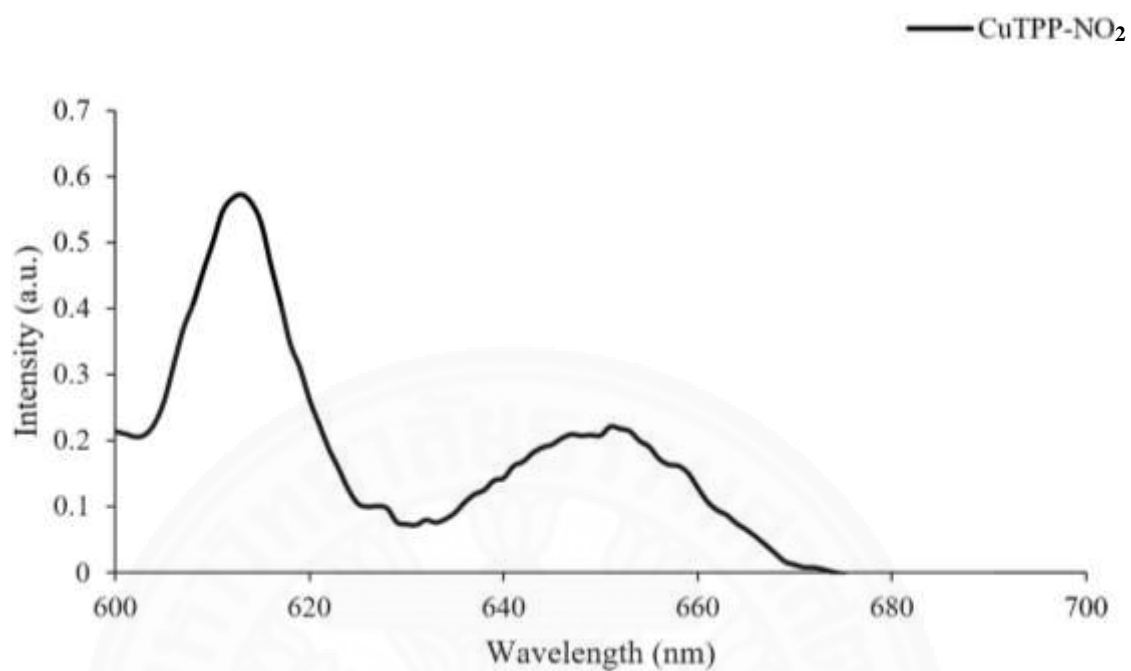


Fig. E11 Fluorescence spectra of CuTPP-NO₂ 14

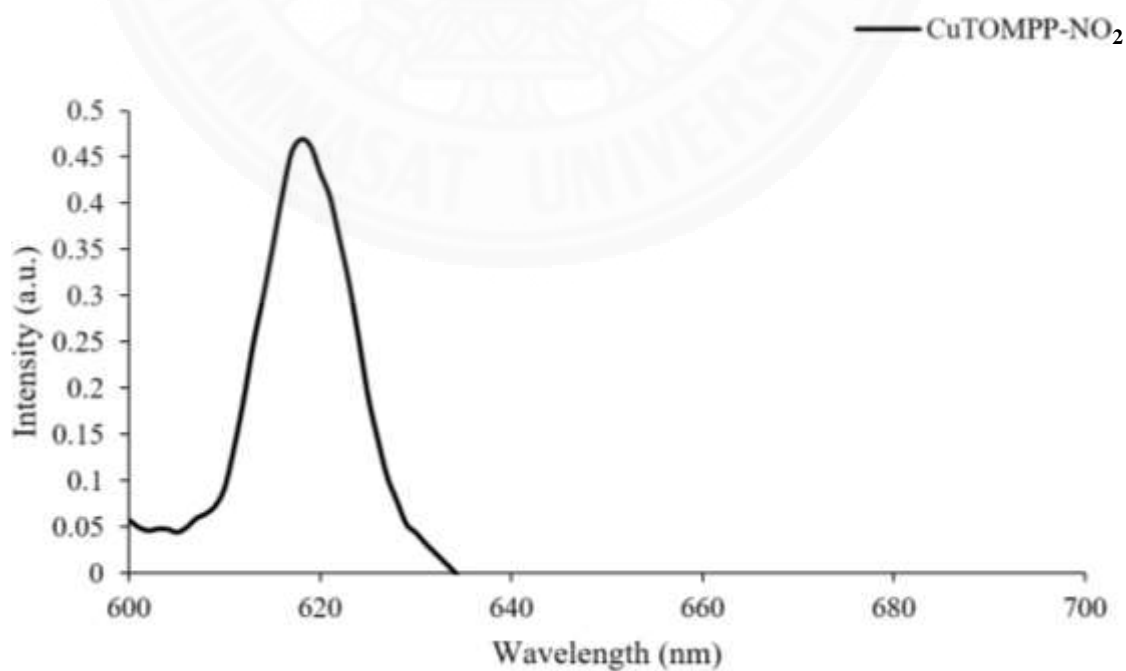


Fig. E12 Fluorescence spectra of CuTOMPP-NO₂ 15

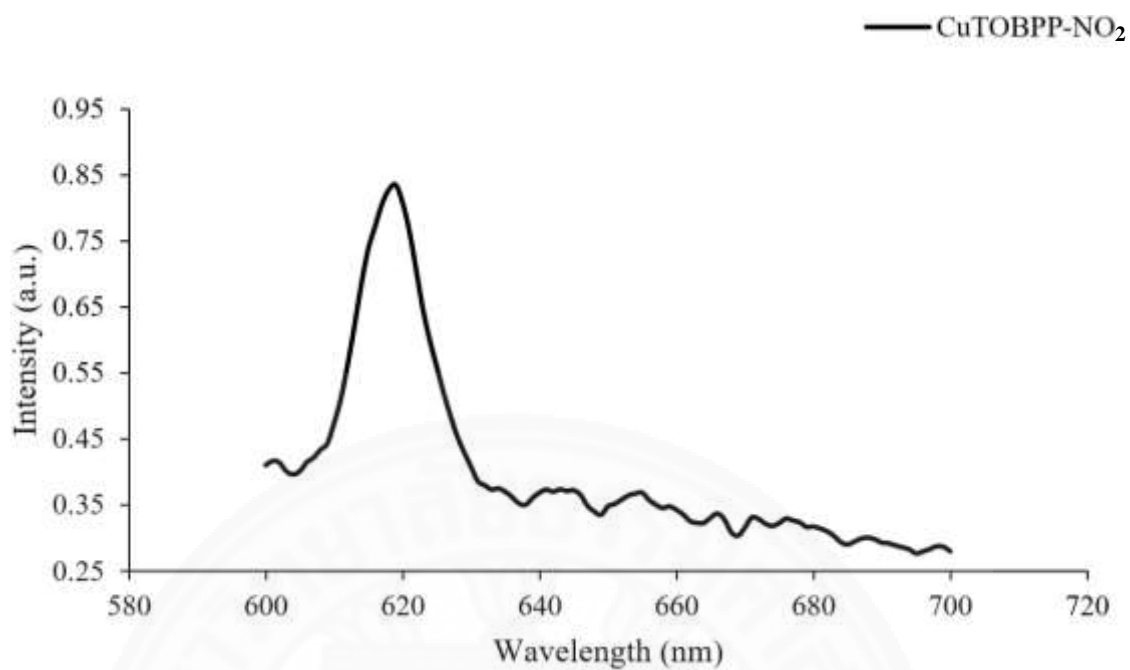


Fig. E13 Fluorescence spectra of CuTOBPP-NO₂ 16

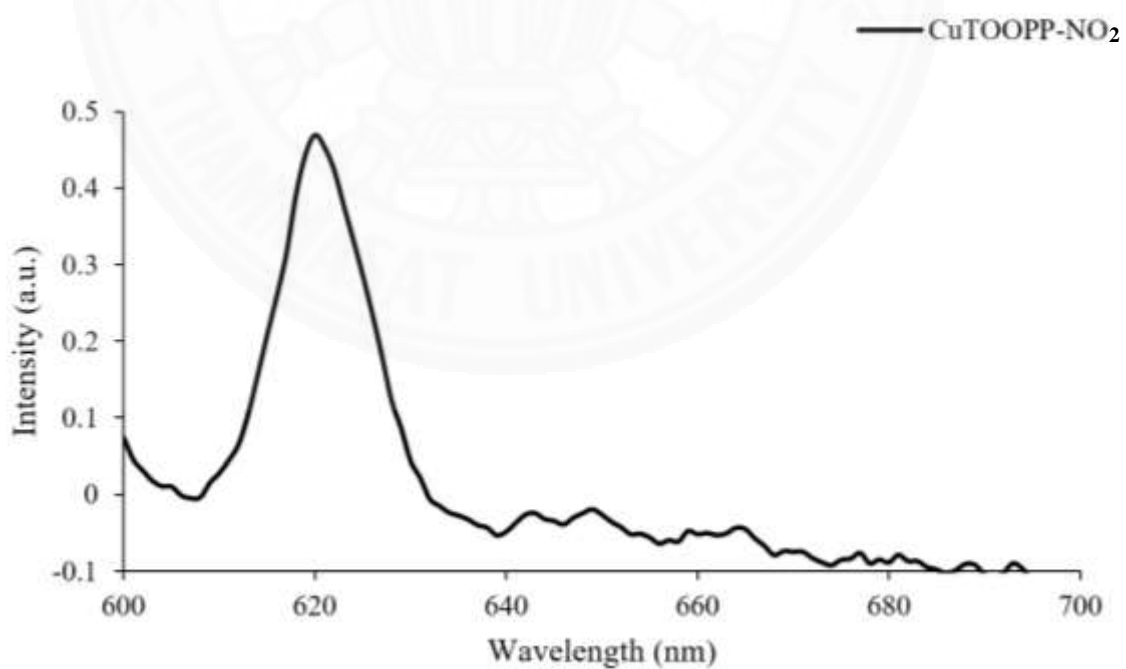


Fig. E14 Fluorescence spectra of CuTOOPP-NO₂ 17

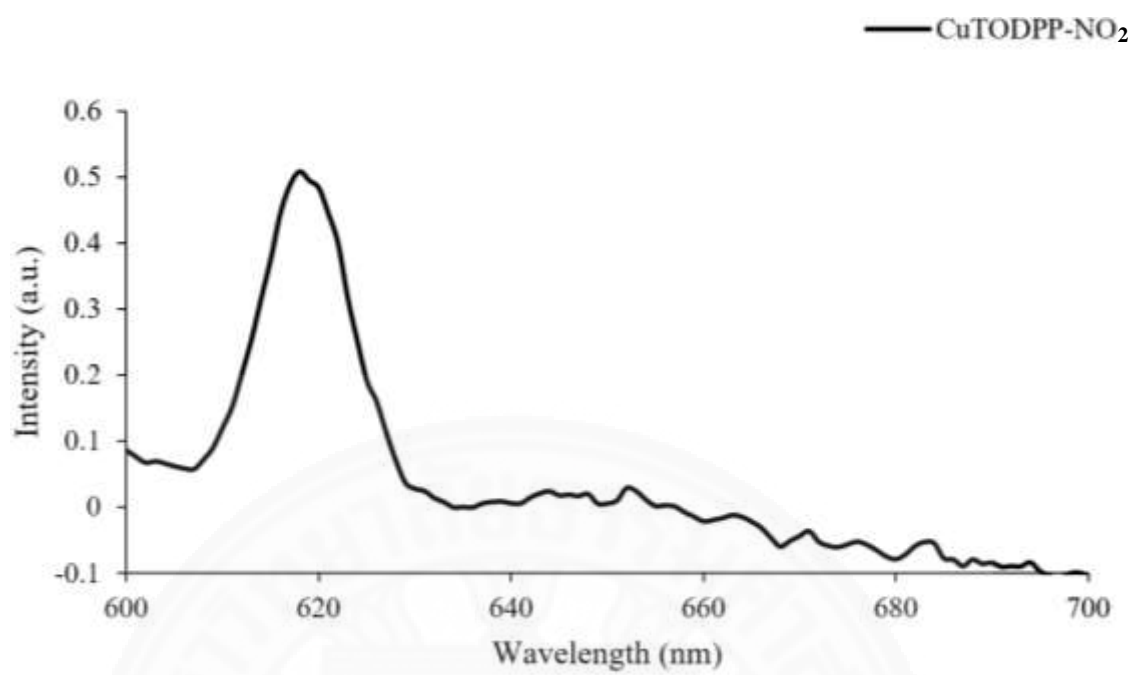


Fig. E15 Fluorescence spectra of CuTODPP-NO₂ **18**

APPENDIX F

THERMOGRAVIMETRIC ANALYSIS (TGA)

Thermogravimetric analysis (TGA) curves for free base porphyrins

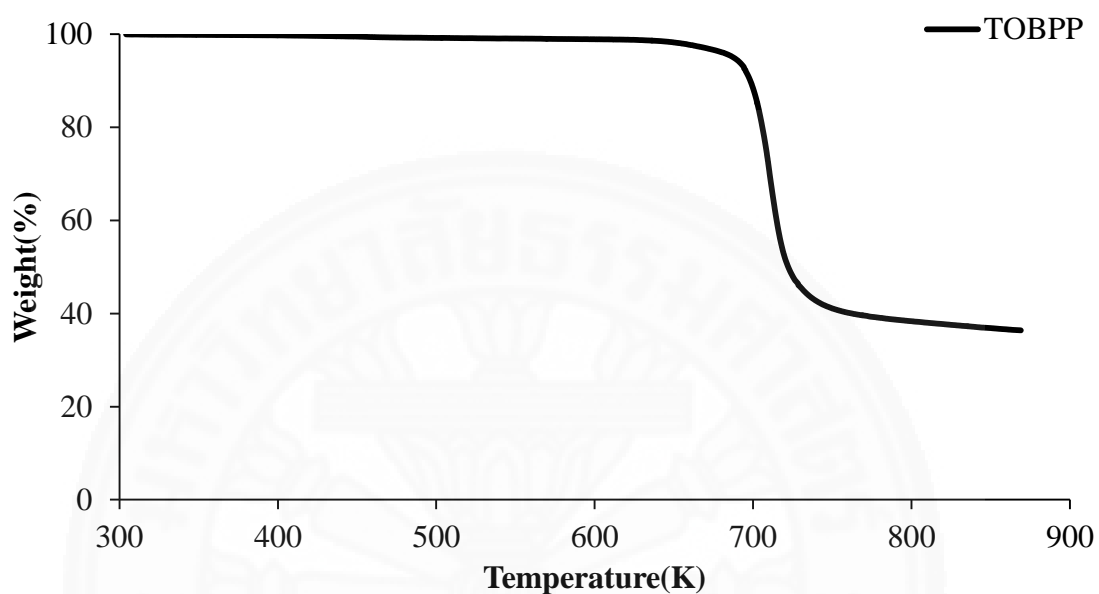


Fig. F1 Thermogravimetric analysis (TGA) curves of TOBPP 6

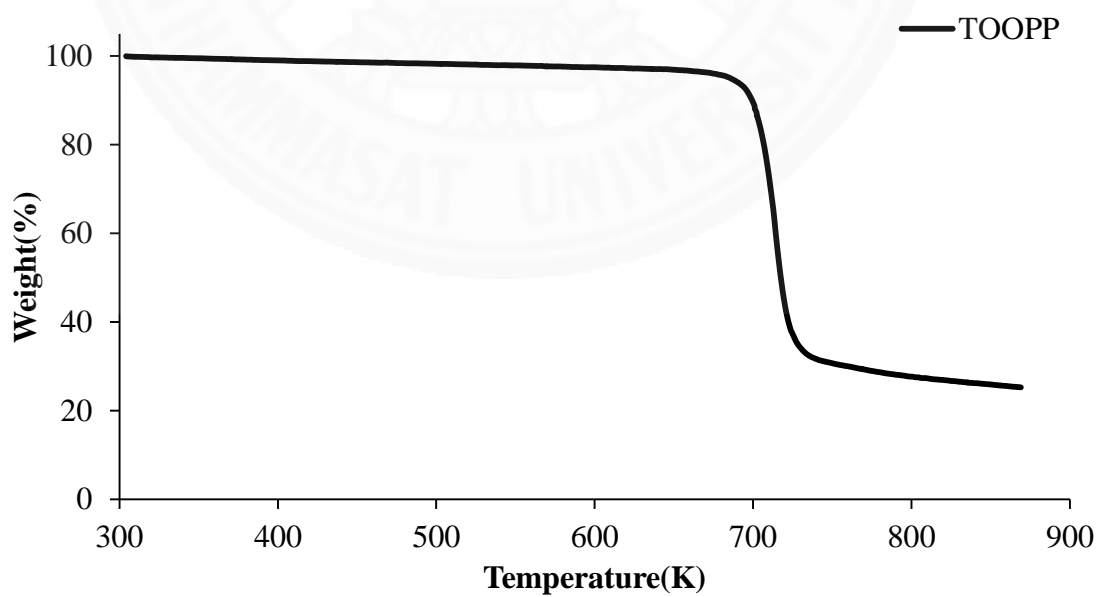


Fig. F2 Thermogravimetric analysis (TGA) curves of TOOPP 7

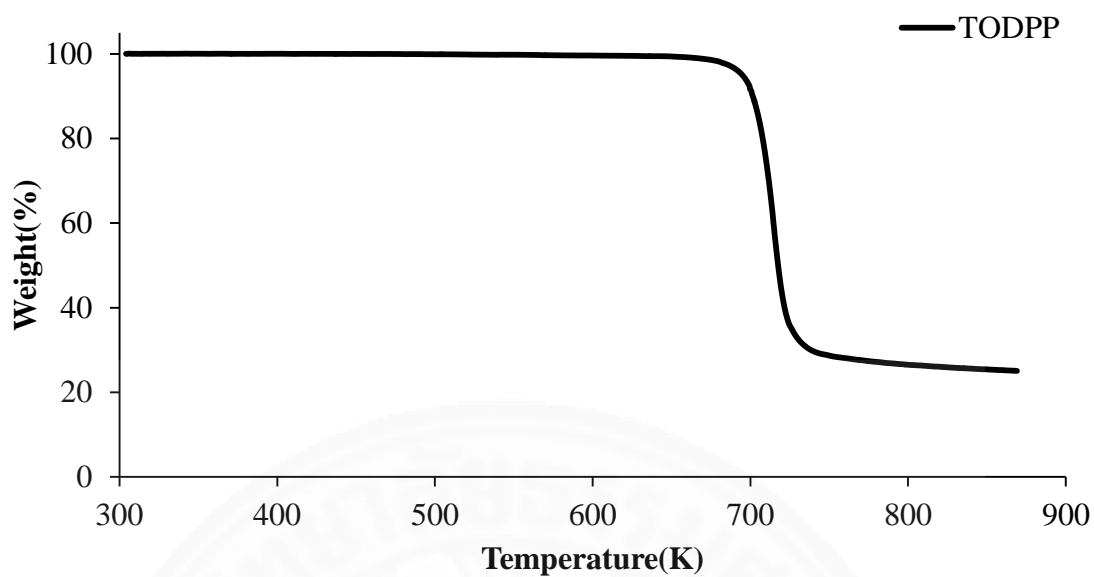


Fig. F3 Thermogravimetric analysis (TGA) curves of TODPP 8

Thermogravimetric analysis curve of copper(II) porphyrins

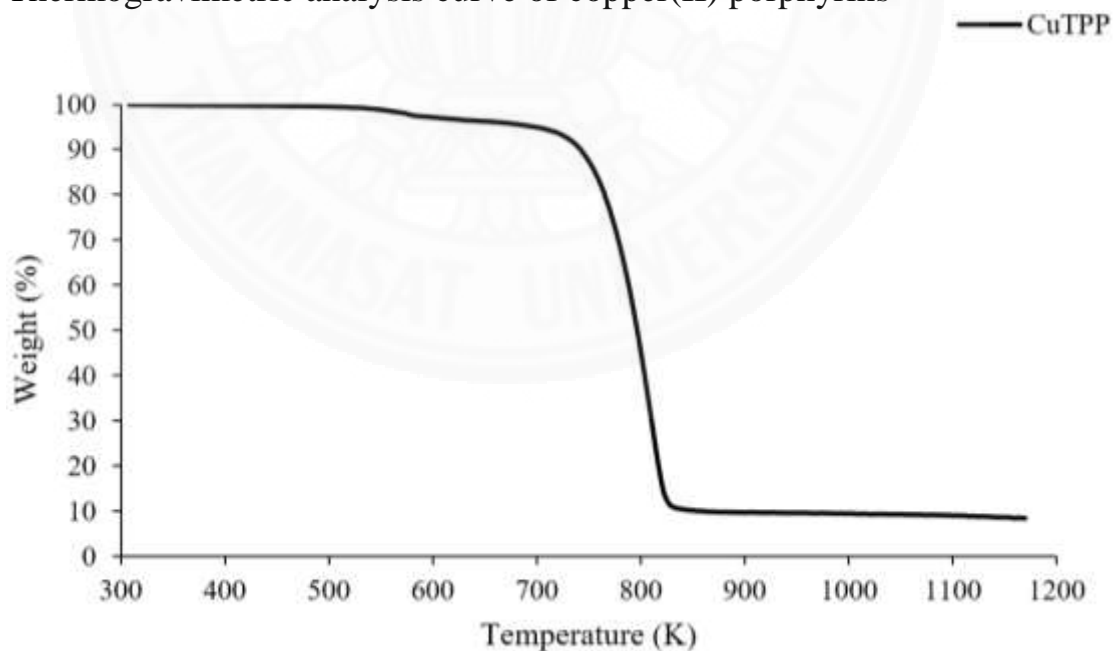


Fig. F4 Thermogravimetric analysis (TGA) curves of CuTPP 9

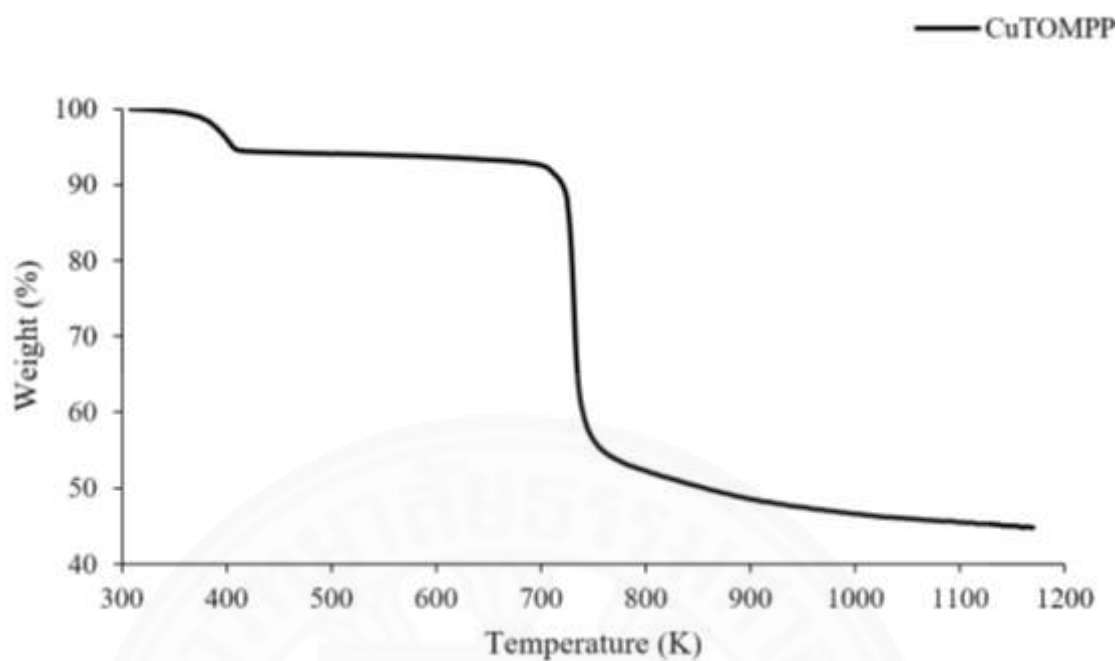


Fig. F5 Thermogravimetric analysis (TGA) curves of CuTOMPP 10

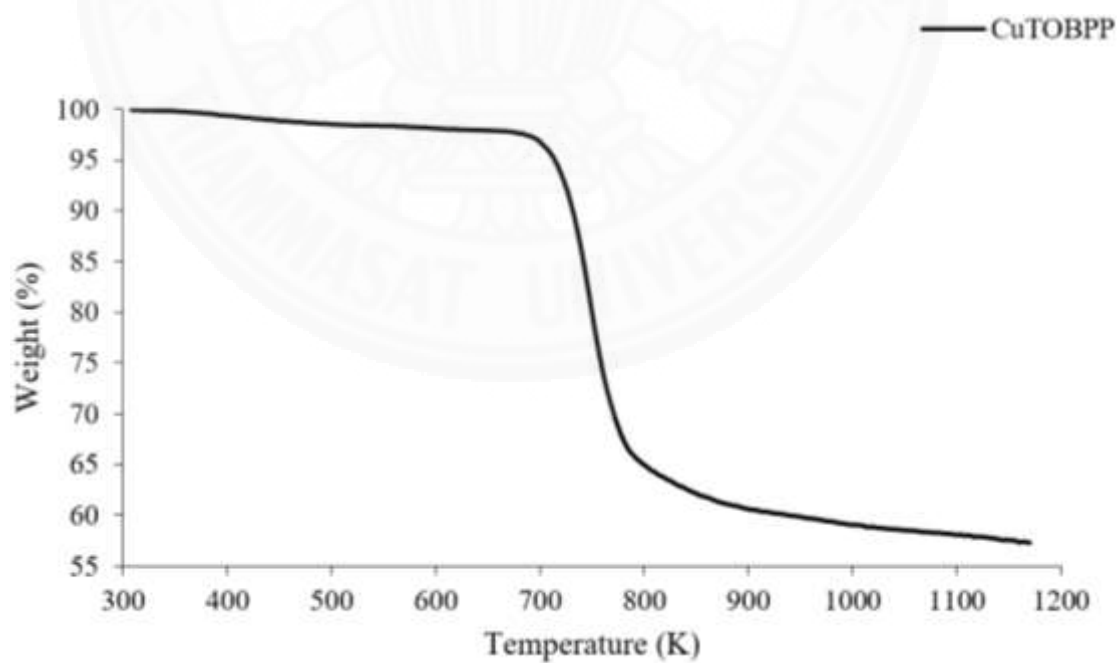


Fig. F6 Thermogravimetric analysis (TGA) curves of CuTOBPP 11

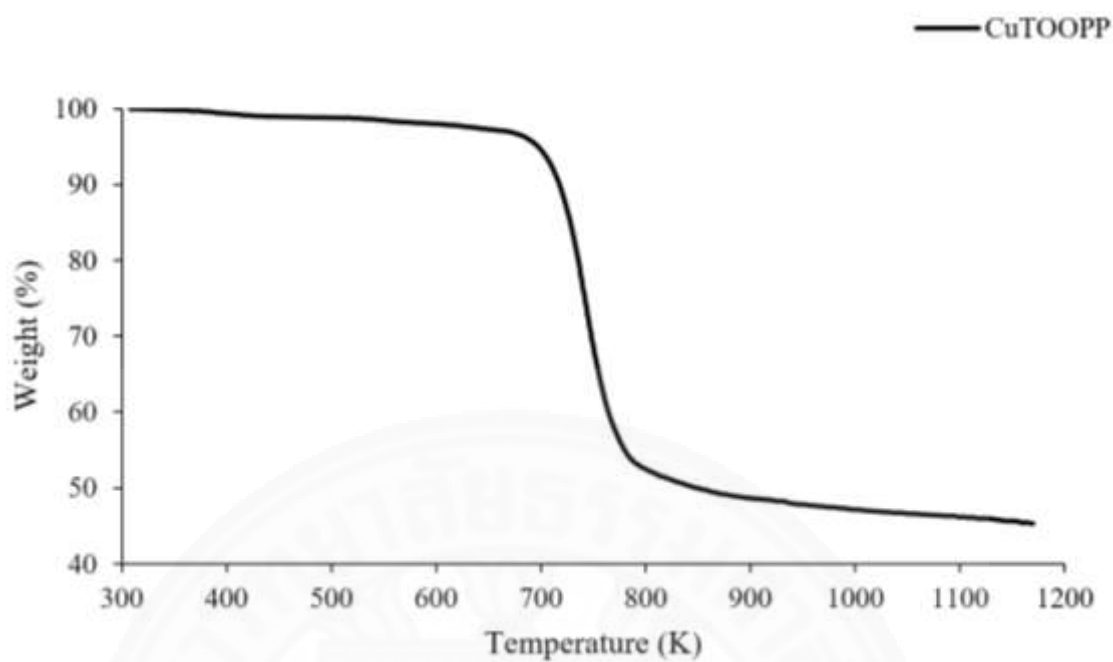


Fig. F7 Thermogravimetric analysis (TGA) curves of CuTOOPP 12

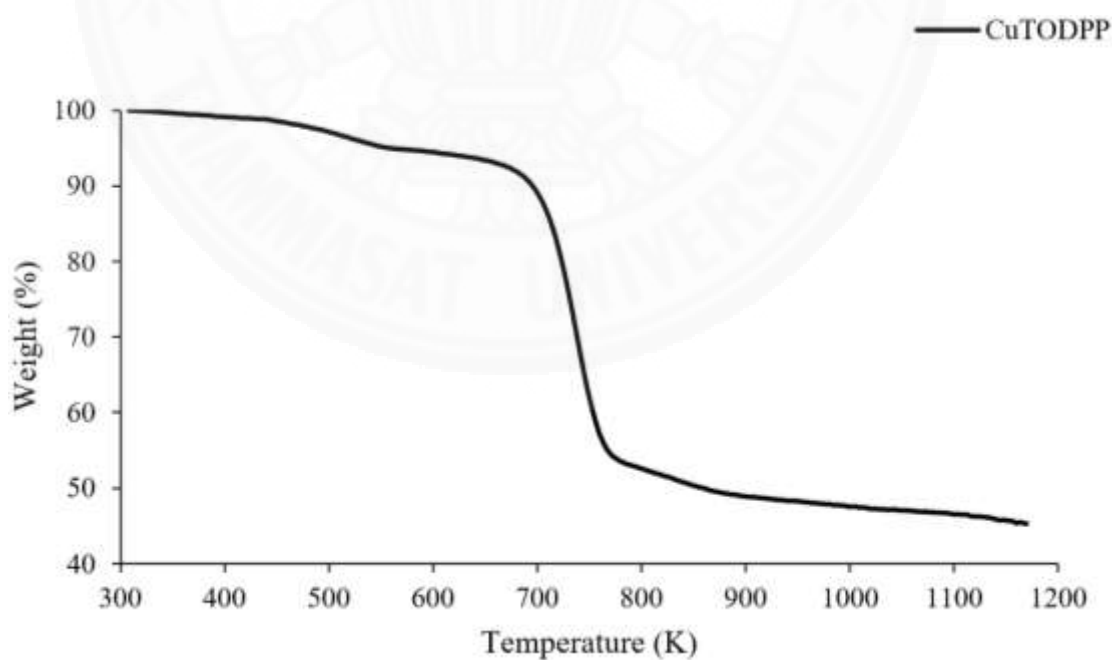


Fig. F8 Thermogravimetric analysis (TGA) curves of CuTODPP 13

Thermogravimetric analysis (TGA) curve of β -nitro substituted porphyrins

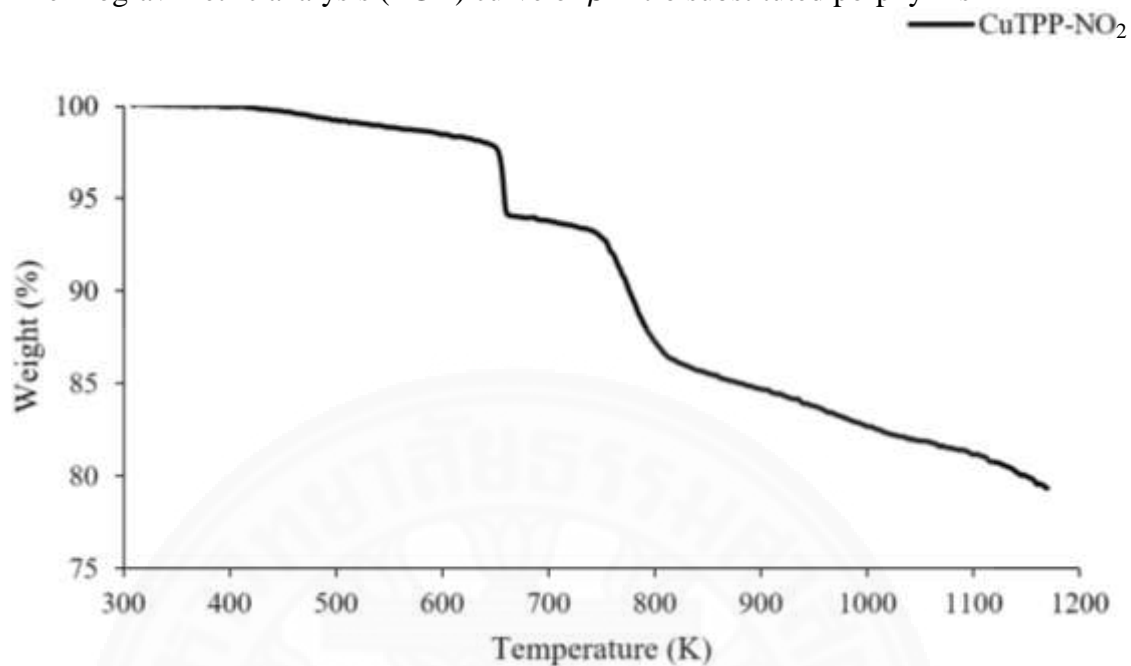


Fig. F9 Thermogravimetric analysis (TGA) curves of CuTPP-NO₂ 14

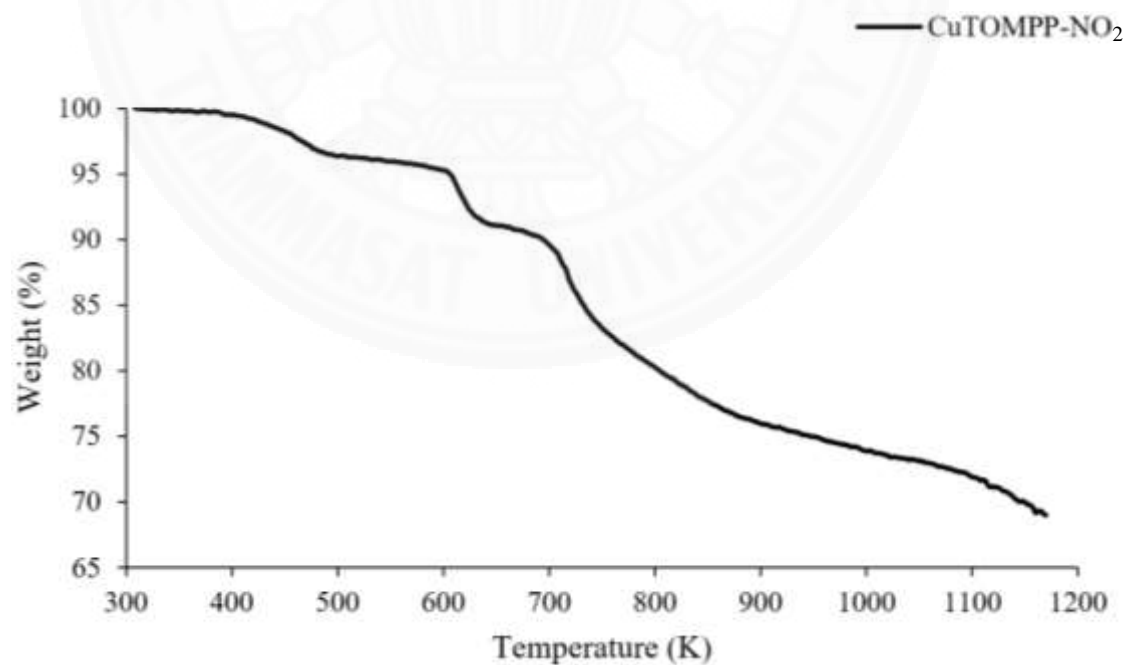


Fig. F10 Thermogravimetric analysis (TGA) curves of CuTOMPP-NO₂ 15

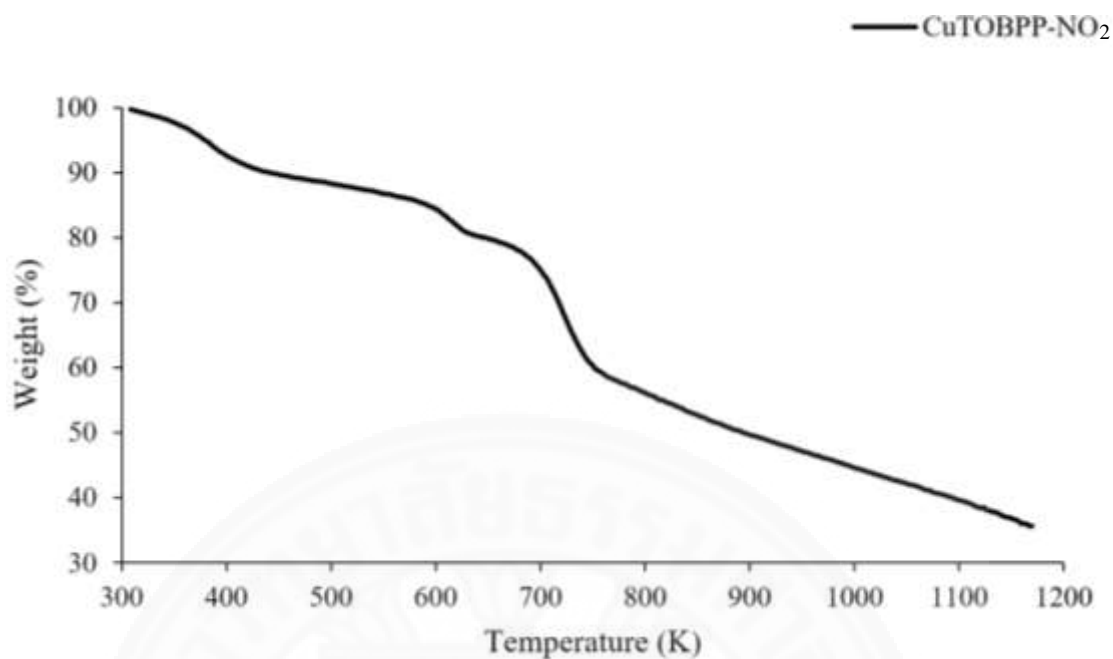


Fig. F11 Thermogravimetric analysis (TGA) curves of CuTOBPP-NO₂ 16

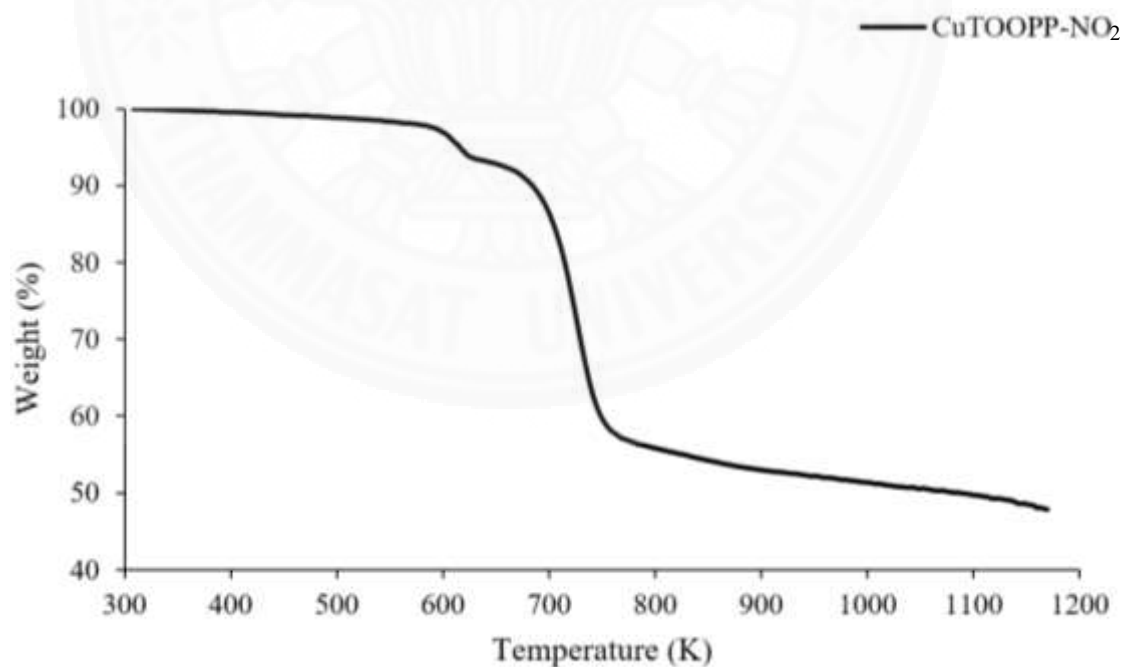


Fig. F12 Thermogravimetric analysis (TGA) curves of CuTOOPP-NO₂ 17

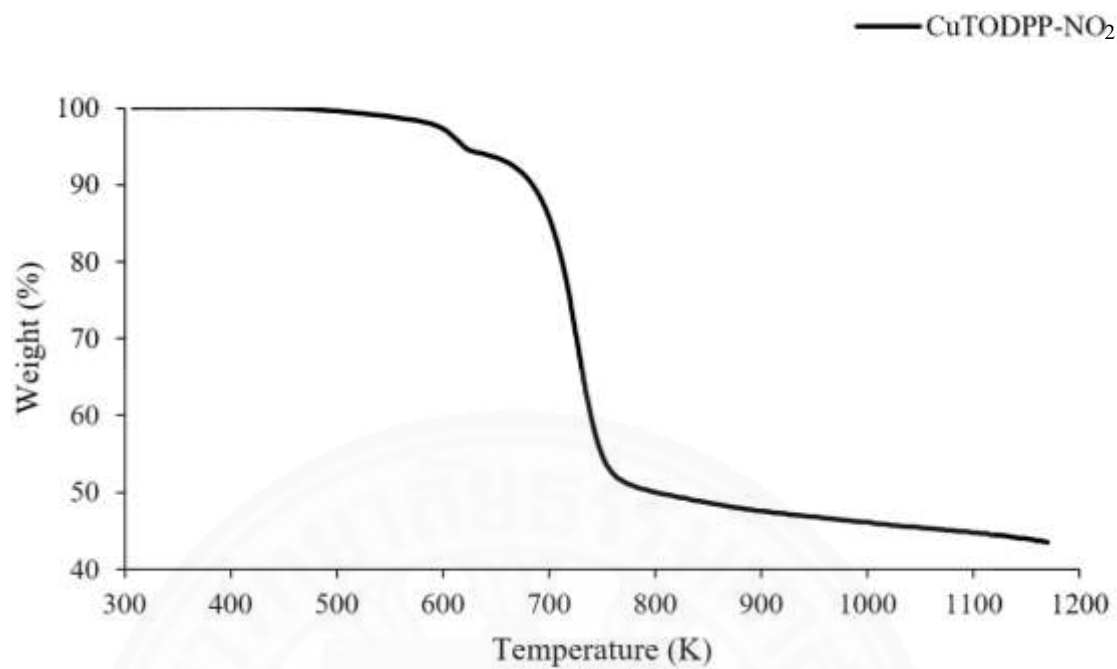


Fig. F13 Thermogravimetric analysis (TGA) curves of CuTODPP-NO₂ **18**

BIOGRAPHY

Name	Mr. Tossapon Phromsatit
Date of Birth	September 30, 1991
Educational Attainment	2013: Bachelor of Science in Chemistry, Thammasat University
Scholarship	2010: Science Achievement Scholarship of Thailand

Publications

Poster presentation at The 40th Congress on Science and Technology of Thailand (STT 40)

Paper publishing in Thai Journal of Science and Technology 3 (1) January – April (2014)

Poster presentation at Pure and Applied Chemistry International Conference (PACCON 2015)

Poster presentation at The 41st Congress on Science and Technology of Thailand (STT 41)

Poster presentation at The 5th TIChE International Conference 2015 (ITIChE2015)

Poster presentation at Pure and Applied Chemistry International Conference (PACCON 2016)

Oral presentation at 2016 5th International Conference on Chemical and Process Engineering (ICCPE 2016)